Photo-mediated Oxygen Atom Transfer and light-induced Organocatalytic and Transition metal-catalyzed Amination Reactions

Monography

in partial fulfillment of the requirements for the degree of

doctor rerum naturalium (Dr. rer. nat.)

at the University of Rostock

Faculty for Mathematics and Natural Sciences

submitted by

Tobias Täufer

Born June 06st 1989

in Crivitz, Germany.

Leibniz Institute for Catalysis

at the University of Rostock

2021

https://doi.org/10.18453/rosdok_id00003467

Selbstständigkeitserklärung

Ich versichere hiermit an Eides statt, dass ich die vorliegende Arbeit selbständig angefertigt und ohne fremde Hilfe verfasst habe, keine außer die von mir angegebenen Hilfsmittel und Quellen dazu verwendet habe und die den benutzten Werken inhaltliche und wörtlich entnommenen Stellen als solche kenntlich gemacht habe.

Rostock, den 26.01.2022

…….

Name

Die vorliegende Dissertation wurde vom 02.01.2017 bis 31.04.2021 am Leibniz-Institut für Katalyse e.V. an der Universität Rostock unter Anleitung von Dr. Jola Pospech erstellt.

1. Gutachter: Johannes Gerardus DeVries
2. Gutachter: Olga Garcia Mancheño
3. Gutachter: Jola Pospech

Tag der mündlichen Prüfung: 26.10.2021

Acknowledgements

Ich möchte mich hier bei allen Menschen bedanken, die mich zu der Person gemacht haben, die ich heute bin.

Zuallererst möchte ich mich bei meinen Eltern bedanken. In meiner Kindheit gabt ihr mir alle Freiheiten und ich konnte mich komplett entfalten. Meine Weltvorstellung und Ansichten habe ich von euch vermittelt bekommen und ihr habt die Entscheidungen in meinem Leben stets akzeptiert und mir meine Ausbildung ermöglicht.

Elisa, mein Schwesterchen, auch dir gilt mein besonderer Dank. Du warst immer eine tolle große Schwester und wir sind zusammen durch dick und dünn gegangen. Ok… du hattest mich mal im Wäschetrockner eingesperrt und ich hatte dir einmal Mehl in den Föhn gemacht, aber sonst lief unsere gemeinsame Kindheit und Jugend doch sehr harmonisch ab. Danke Schwesterchen!

Freunde kommen und gehen und im Laufe meines Lebens habe ich viele Freundschaften geschlossen. Viele davon sind auch leider wieder auseinander gegangen, jedoch nie in Vergessenheit geraten. Wir haben gelacht, geweint und standen immer zueinander. Durch euch alle war ich in meinem Leben niemals einsam. Für die unvergesslichen Momente danke ich euch von Herzen; vor allem Taube, Martin, Markus und Mölli, díe schon lange an meiner Seite sind und hoffentlich noch lange dort bleiben.

Auch bei meinen Ausbildern, sowohl in der Schule als auch im Studium, möchte ich mich bedanken. Besonders hervorheben möchte ich meine Chemielehrerin Frau Zaddach sowie Prof. Schulz und Prof. Langer, die mit ihrem bahnbrechenden Enthusiasmus meine Begeisterung für diese Fachrichtung entfachten und schließlich auch festigten. Des Weiteren bedanke ich mich bei Dr. Alexander Villinger. Wir haben zwar nie Seite an Seite im Labor gearbeitet, doch konnte er mir in vielen Gesprächen und fachlichen Diskussionen sehr gut vermitteln, wie man das Beste aus einer präparativen Synthese rausholt.

Jola, ich weiß gar nicht ob du weißt, wie glücklich ich bin hier in deiner Arbeitsgruppe zu sein. In der dunkelsten Stunde meines Studiums, als ich die Chemie beinahe aufgegeben hätte, gabst du mir eine Chance. Bis heute versteh ich nicht, warum du das getan hast und möchte mich alleine schon deswegen in höchster Form bedanken. Ich habe so viele unterschiedliche Methodiken und Praktiken kennengelernt und du hast mich stets unterstützt und gefördert. Durch dich habe ich neue Grenzen kennen gelernt und das meine ich positiv! Für all das, die sehr produktiven Diskussionen und deinen wissenschaftlichen Rat bin ich dir überaus dankbar.

Ebenfalls bedanken möchte ich mich bei Prof. Hans DeVries, sowohl für die Aufnahme in seinen Arbeitskreis, als auch die wertvollen Hinweise während der Seminare.

Zusätzlich möchte ich mich bei den Arbeitsgruppen bedanken, die mich während meiner Arbeit unterstützt haben. Besonders hervorheben möchte ich dabei Dr. Jabor Rabeah, für die Realisierung der vielen EPR-Experimente und Dr. Ralf Jackstell, für die Unterstützung bei der Buchwald-Hartwig-Aminierung. Des Weiteren möchte ich Prof. Haijun Jiao, für die Durchführung der Computersimulationen und Dr. Annette-Enrica Surkus, für die Unterstützung im Bereich der Elektrochemie danken. Bei Andreas Hutter bedanke ich mich für die vielen zeitnahen Reparaturen der unterschiedlichsten Geräte. Außerdem möchte ich mich bei meinen Laborkollegen Richy und Firas bedanken. Die Zeit mit euch war einfach toll und ich werde unsere RoHan-Reise nach Vietnam niemals vergessen.

Der größte Dank allerdings gebührt meiner Ehefrau Amely. Du schaffst es, mich immer wieder aufs Neue zu überraschen und ich fühle mich, egal wo ich bin, bei dir zuhause. Du hast unseren beiden Söhnen das Leben geschenkt und ich kann es jetzt schon kaum erwarten, was uns die Zukunft noch bringt. Bei der Fertigstellung dieser Arbeit hast du mich trotz deiner Schwangerschaft mit unserem zweiten Sohn in allen erdenklichen Belangen bestmöglich unterstützt und entlastet, damit ich mich vollkommen auf diese fokussieren konnte. Dir allein widme ich diese Arbeit.

Abstract

The first chapter of this thesis introduces the interplay of light and matter as well as a short overview of the different modi operandi in photoredox catalysis. A protocol for the deoxygenation of various pyrimidopteridine *N*-oxide derivatives and the photochemical and electrochemical characterization corresponding plain heterocycles is discussed. In addition, the employment of the deoxygenated pyrimidopteridine-*N*-oxides as organic photoredox catalysts is exemplified.

The second chapter describes the mechanistic study of the light-mediated hydroamination of stilbenes with primary amines catalyzed by the previously introduced pyrimidopteridine-based photoredox catalysts. Classical and competitive fluorescence quenching, NMR and EPR experiments are investigated, leading to the postulate of a plausible reaction mechanism, which is further supported by quantum chemical calculations.

The third chapter outlines the investigation towards synthetically valuable photo-mediated oxygen atom transfer reaction from simple pyridine *N*-oxide derivatives. For this purpose, the photophysical and electrochemical properties of a variety of heteroaromatic *N*-oxides were determined and suitable candidates were selected for test reactions. Furthermore, the synthesis of (methylsulfonyloxy)pyridinium methanesulfonate and its use in photocatalytic reactions is described which let to a photo-mediated dehydrogenation of alkyl arenes.

In the fourth chapter of this thesis, the synthesis of *N*,*N*-dimethylaniline derivatives from dimethylamine and aryl triflates is discussed. The palladium-catalyzed C−N bond formation proceeds in excellent yields using a simple catalytic system, a mild base, and triflates as electrophiles which are readily available from inexpensive and abundant phenols. *N*,*N*-dimethylanilines are multifunctional reactants and represent useful but underutilized building blocks in organic synthesis.

Table of contents

List of abbreviations

$[M^+]$	molecular ion peak
OAc	acetate
MeCN	acetonitrile
Ac	acetyl
Alk	alkyl
aq.	aqueous
Ar	aryl
Bn	benzyl
calcd.	calculated
cat.	catalytic
Δ	chemical shift
J	coupling constant
DFT	density function theory
DCM	dichloromethane
DMSO	dimethylsulfoxide
Ed.	Editor
EI	electron ionization
EI-MS	electron ionization mass spectroscopy
eV	electron volt
EPR	electron paramagnetic resonance
EDG	electron-donating group
EWG	electron-withdrawing group
ESI	electrospray ionization
equiv.	equivalent
OEt	ethoxy
Et	ethyl
e.g.	for example
GC	gas chromatography
X	halide
Hz	Hertz
HRMS	high resolution mass spectroscopy
HOMO	highest occupied molecular orbital
HOMO	highest occupied molecular orbital
HPLC	high-performance liquid chromatography
H	hours
IR	infrared spectroscopy
isol.	isolated
*i*Pr	isopropyl
L	ligand
LUMO	lowest unoccupied molecular orbital
MS	mass spectrometry
m/*z*	mass-to-charge ratio
m.p.	melting point
Mes	mesityl
M	*meta*
m-CPBA	*meta*-chloroperbenzoic acid
[M]	metal
MeOH	methanol
MeO	methoxy
Me	methyl
mL	milliliter
Mmol	millimol
Min	minute
M	multiplet
DMF	*N*,*N*-dimethylacetamide
Bu	*n*-butyl
NMR	nuclear magnetic resonance spectroscopy
O	*ortho*
P	*para*
ppm	parts per million
PPT	pyrimidopteridine
PPTNO	pyrimidopteridine *N*-oxide
Ph	phenyl

R	rest
Rt	room temperature
sat.	saturated
SCE	saturated calomel electrode
solv	solved
T	temperature
Boc	*tert*-butyloxycarbonyl
t-Bu	*tert*-butyl
TBS	*tert*-butyldimethylsilyl
THF	tetrahydrofuran
TLC	thin layer chromatography
t	time
PhMe	toluene
TFA	trifluoroacetic acid
TFAA	trifluoroacetic acid anhydride
TMS	trimethylsilyl
TPA	triphenylacetate

1 Pyrimidopteridines as organic photoredox catalysts

1.1 Introduction

A fundamental property of nature is the interaction of matter with electromagnetic radiation. This property is used, among other things, to elucidate the structure of chemical compounds and to characterize their properties.[1] Depending on the wavelength and the type of particle to interact with, different processes are initiated. Figure 1.1 schematically shows an electromagnetic wave with increasing wavelength. The energy of the photons is inversely proportional to the wavelength. In the case of low-energy microwaves (10^{-1}-10^{-3} m), the molecules are excited to rotate or twist. Infrared rays (10^{-3}-10^{-6} m) excite characteristic atomic vibrations. Shorter wavelength (10^{-6}-10^{-8} m) fall into the regions of visible light and ultraviolet radiation. This is the zone in which molecules can enter excited states. The absorption of this radiation enhances an electron from the highest occupied molecular orbital (HOMO) to the lowest unoccupied molecular orbital (LUMO). Energetically higher radiation (<10^{-8} m), such as gamma radiation, promotes electrons from lower molecular into antibonding orbitals, which often results in bond cleavage. The ground state is regained by emitting radiation known as fluorescence.

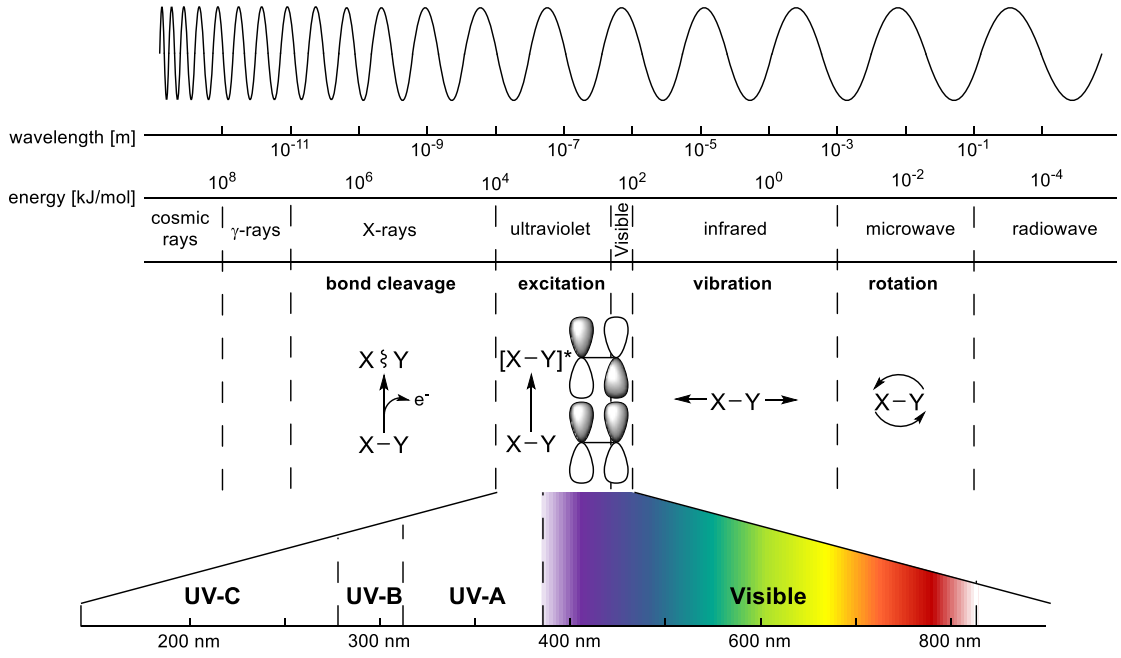

Figure 1.1: Interaction of electromagnetic radiation with chemical compounds.

The emitted radiation has a lower energy than the absorbed photon. According to quantum mechanics, the energy of a molecule can only attain certain states with discrete energy levels which are described as wave functions.[2] In the electronic ground state and in the excited state,

different vibrational states can be entered. The photo-chemists Franck and Condon postulated that electronic excitations occurs via a vertical transition. The probability of a vibronic transition is proportional to the overlap integral of the wavefunctions of the two states that are involved in the transition (Figure 1.2).[3]

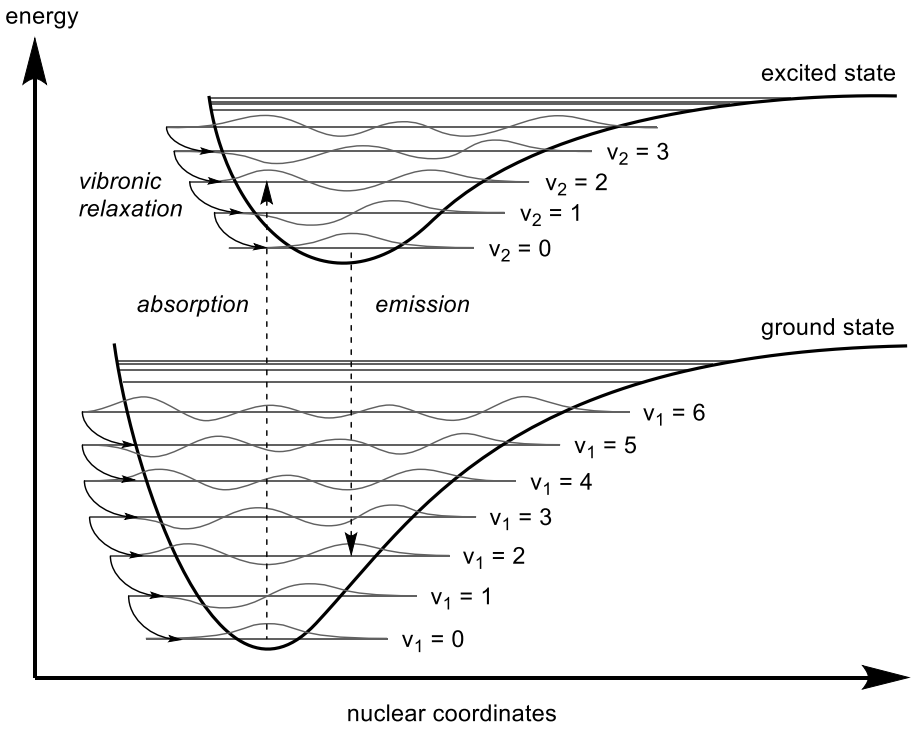

Figure 1.2: Schematic illustration of the Franck–Condon principle.

By absorbing light, different vibrational states of the excited state ($v_2 \geq 0$) can be reached. However, the excited electrons quickly relax to the lowest excited state ($v_2 = 0$). The spontaneous emission of a photon or a chemical reaction always occurs from the lowest electronically excited state. Thus, the emission wavelength of a photon is independent of the excitation wavelength. This relationship was postulated by Michael Kasha in 1950 and is referred to as the Kasha's rule.[4] However, vertical emission may again enter different vibrational states of the electronic ground state according to the Franck-Condon principle.

The excitation of the electron occurs from the HOMO to the LUMO, resulting in two half-occupied molecular orbitals (SOMO) (Figure 1.3). Sufficient persistence of the excited state allows the molecule to engage in a chemical reaction with another molecule.[5] On the one hand, the excited electron is more facile to remove as compared to the ground state molecule. On the other hand, the electron whole in the low-lying former HOMO is a thermodynamically attractive electron acceptor, resulting in an electronic state equaling the reduced ground state. Thus, both oxidation and reduction are facilitated in the excited state.

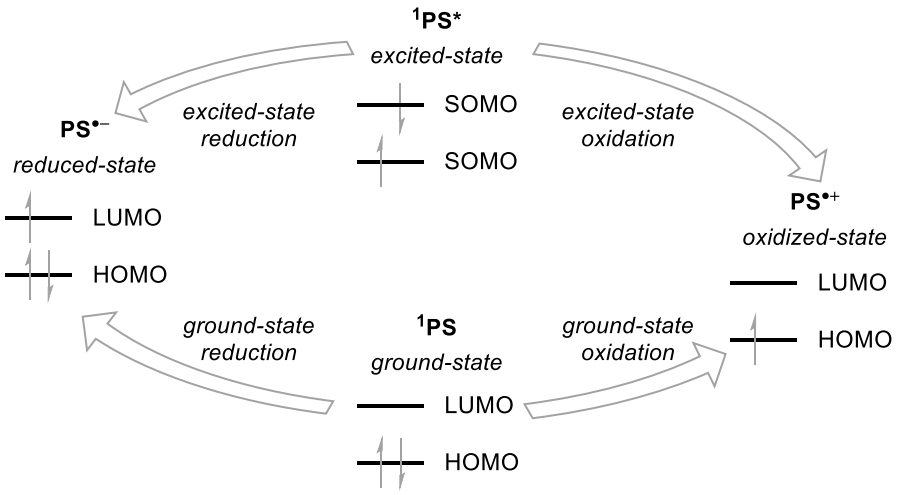

Figure 1.3: Access of redox states from ground state and excited state molecules.

Depending on the electronic nature of the reactants, the excited molecule can either accept or donate an electron, resulting in its reduced or oxidized state, respectively. The prerequisite of a molecule qualifying as photoredox catalyst is the ability to reenter its ground state after reductive or oxidative quenching (Figure 1.4).

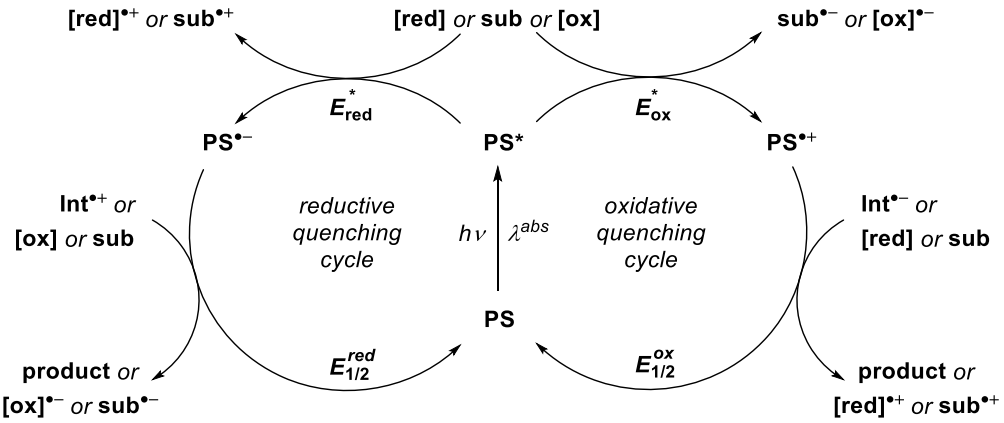

Figure 1.4: Reductive and oxidative quenching cycles of photoredoxcatalysts.

Depending on the properties of the photocatalysts, a reductive or oxidative quenching cycle can occur. If the excited-state catalyst is an oxidizing agent, a reductive quenching cycle can occur (Figure 1.4, left side). A suitable substrate is oxidized by the excited state photoredox catalyst and may engage in subsequent radical reactions (Figure 1.4, sub → sub$^{\bullet+}$). The catalytic cycle is closed by the oxidation of the reduced catalyst by a suitable reaction intermediate or sacrificial oxidant (Figure 1.4, int$^{\bullet+}$ or [ox] → product or [ox]$^{\bullet-}$). However, chemical reaction can also be provoked by the reduced state of the photocatalyst which was entered through oxidation of a sacrificial reductant ([red] → [red]$^{\bullet+}$). Analogously, an oxidative quenching cycle occurs when the catalyst is a good reducing agent in the excited state (Figure 1.4, right side; PS* → PS$^{\bullet+}$). The catalyst turn-over is achieved by a suitable substrate, intermediate or sacrificial reductant.

To initiate a photochemical reaction, the ground state redox potentials of the substrate and the excited state redox potentials of the photoredox catalyst must match to ensure a thermodynamically favorable single electron transfer (SET). The excited state redox potentials are determined according to a relation between the excited state energy $E_{0,0}$ and the ground state redox potentials $E_{1/2}^{red}$ and $E_{1/2}^{ox}$.[5]

$$\boldsymbol{E_{red}^{*} = E_{0,0} + E_{1/2}^{red}} \qquad \text{(eq. 1)}$$

$$\boldsymbol{E_{ox}^{*} = E_{1/2}^{ox} - E_{0,0}} \qquad \text{(eq. 2)}$$

Organic molecules have oxidation potentials between+0.5 and +2.5 V vs SCE and reduction potentials in a range of −0.5 to (−2.5) V vs SCE (Figure 1.5).[6] To achieve an oxidative quenching of an excited state reductant, its excited state oxidation potential has to be more negative than the ground state reduction potential of the elected substrate. For a reductive quenching of an excited state oxidant, the excited state reduction potential must exceed the ground state oxidation potential of the substrate.

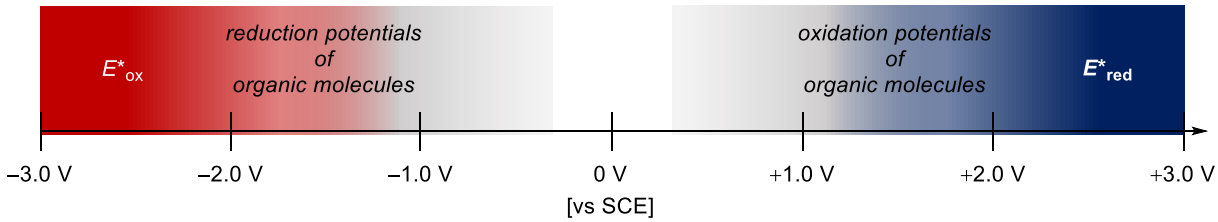

Figure 1.5: Illustration of redox potentials of organic molecules and excited state photoredox catalysts.

The constant advancement and studies of photocatalytic systems renders photochemistry a rapidly growing area of interest.[7] In addition to a multitude of transition metal-based photocatalysts with excellent photophysical-chemical properties, metal-free, organic photo redox catalysts have also been developed and enjoy a widespread applicability (Figure 1.6).[8] Transition metal-based catalysts are particularly appealing due to their tunable absorption and redox properties controlled by the ligands.[9] Metal-ligand complexes provide long excited state lifetimes, which enhances the probability of chemical reactions.[10] Ruthenium and Iridium polypyridyl complexes are the most widespread representatives of this class of catalysts.

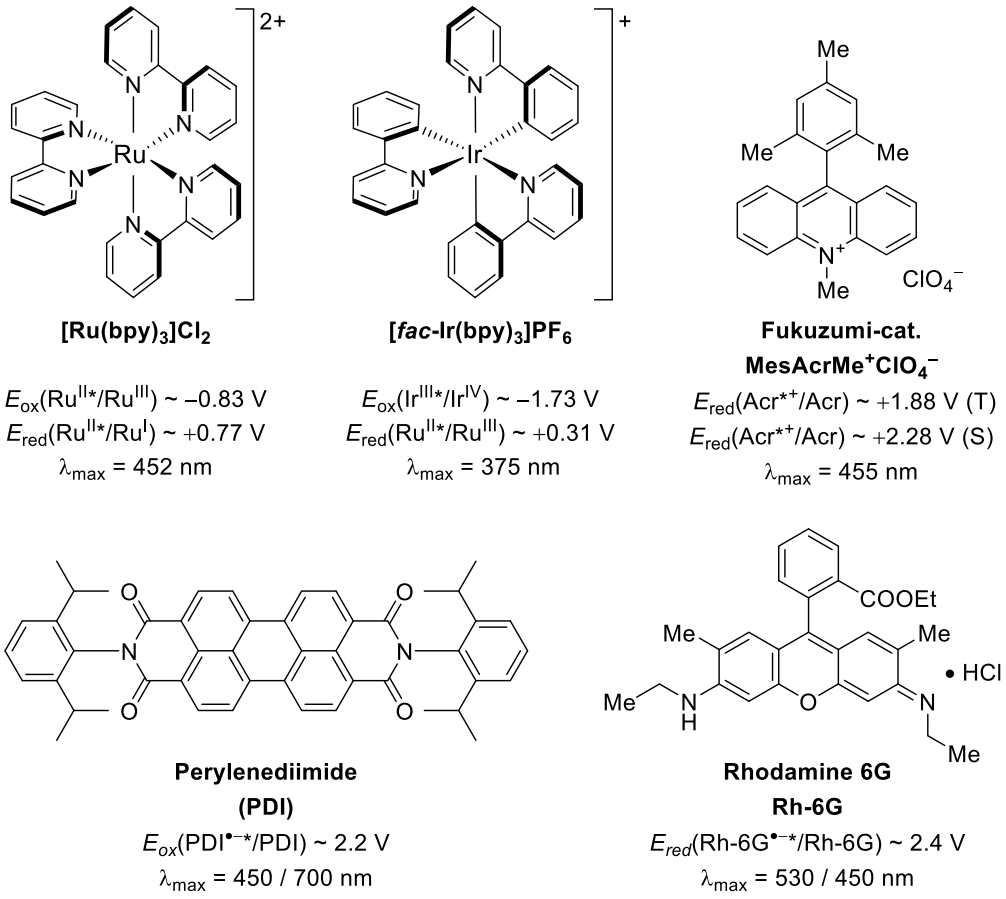

Figure 1.6: Examples for transition metal and organic photoredox catalysts including selected photo-physical properties. All potentials are reported vs SCE.[7a]

Organic photoredox catalysts are diverse in structure and thus exhibit a broad span of excited state redox potentials, exceeding those of transition metal-based photocatalysts.[5] However, organic photocatalysts generally possess lower productivity as compared to ruthenium and iridium catalysts, often due to catalyst degradation or deactivation pathways. These scenarios are compensated by higher catalyst loadings. Nevertheless, organic photoredox catalysts remain attractive due to their low costs and low toxicity.[5]

In 1986, the group of Maki reported a first account on the photochemical behavior of a tetraalkylated pyrimidopteridine *N*-oxide (PPTNO) and its application in photo-mediated oxygen atom transfer (POAT) reactions.[11] Their seminal finding exposed the potential for photochemical oxygen atom transfer in a wide variety of reactions such as *N*-demethylation[11], C–H-oxygenation[12] and C–C bond cleavage[13] (Scheme 1.1).

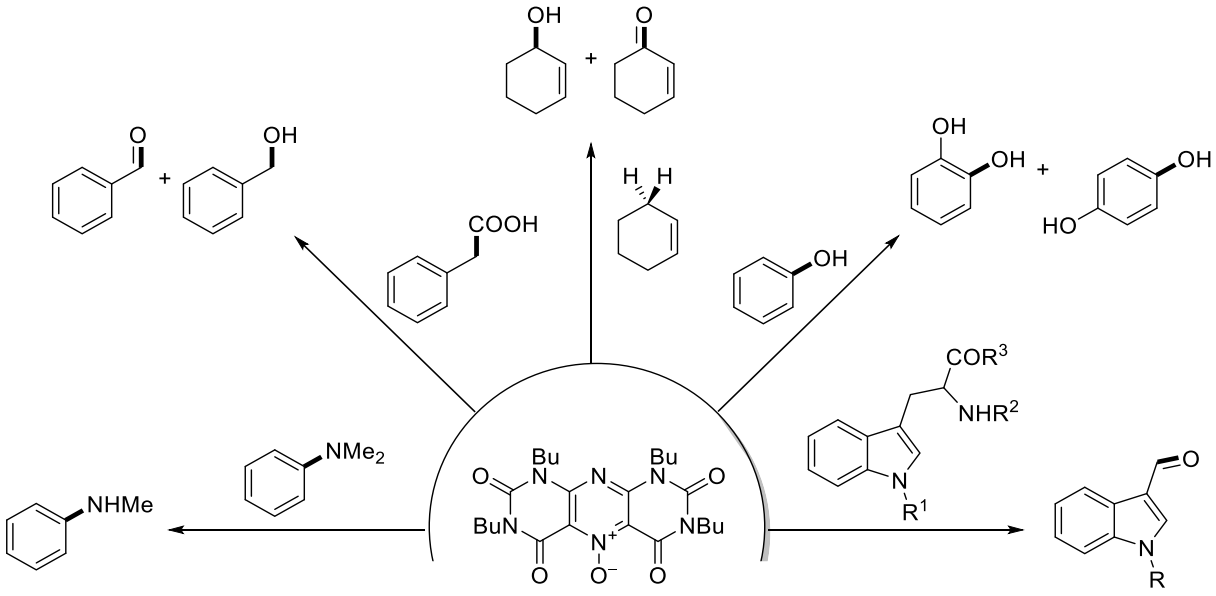

Scheme 1.1: Oxidative photo-mediated transformations utilizing PPTNO.

Previous work of the Pospech group focused on the development of photo-mediated oxygenation reactions using *N*-oxides as oxygen source.[14] At the outset of our studies, an improved approach to access pyrimidopteridine *N*-oxides was described.[15] Pyrimidopteridine *N*-oxides can be synthesized in four steps from *N*,*N*'-disubstituted ureas or in two steps from commercially available 6-amino-1,3-dialkyluracils. The key advance is the replacement of stochiometric lead tetraacetate with the less toxic (diacetoxyiodo)benzene, a hypervalent iodine species allowing for a routine synthesis on gram scale (Scheme 1.2). The major goal of the revised synthesis and derivatization of pyrimidopteridine *N*-oxides aimed to gain a better understanding of the electrochemical and photophysical behavior of these rare OAT reagents.

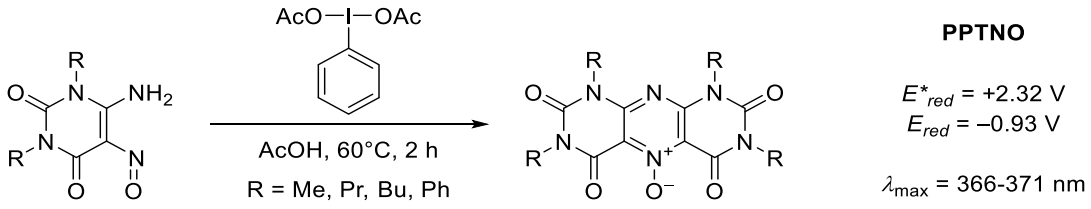

Scheme 1.2: Synthesis of pyrimidopteridine-*N*-oxides derivatives. Potentials are reported vs SCE.

The thorough investigation unraveled the quality of PPTNOs to act as potent organic photocatalyst. The photo-mediated decarboxylative Giese-type reaction for radical alkylation of electron-deficient alkenes demonstrated its potential.[16] Detailed studies revealed that the deoxygenated pyrimidopteridine can also be employed in this reaction (Scheme 1.3).

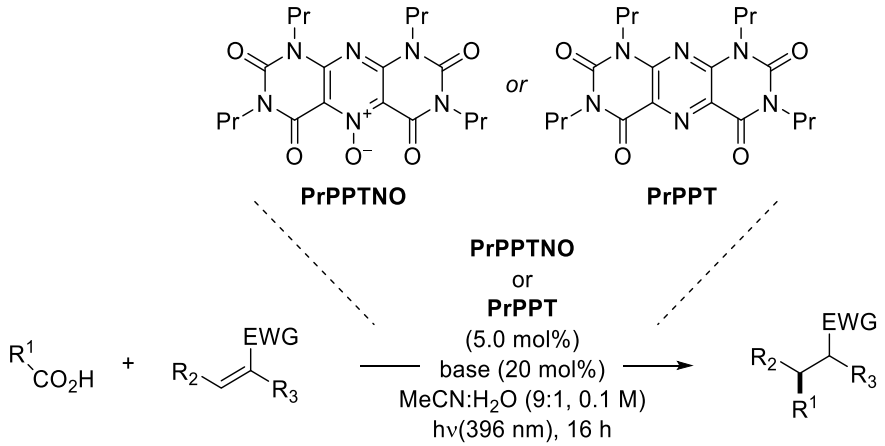

Scheme 1.3: Photo-mediated decarboxylative C–C coupling of electron-deficient alkenes.

The photocatalytic properties of pyrimidopteridine *N*-oxides were further exemplified in the photo-mediated hydroamination of stilbenes with primary amines (see also chapter 2). Also in this case, both the oxygenated PPTNO and deoxygenated pyrimidopteridine (PPT) was capable of providing the desired product (Scheme 1.4).

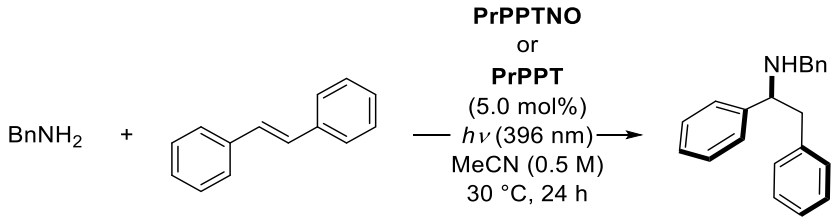

Scheme 1.4: Photo-mediated hydroamination of stilbenes with primary amines.

1.2 Objectives

In previous work of our group, the photophysical properties of pyrimidopteridine *N*-oxides (PPTNO) were characterized[15] and their utilization as photoredox catalyst was exemplified.[16] However due to their tendency to deoxygenate upon irradiation, the identity of the actual catalytically active species became a focal point or interest.

The aim of this project was to grant reliable access to the deoxygenated pyrimidopteridine (PPT) followed by thorough characterization. The compounds are characterized electrochemically by cyclo-voltammetric and differential pulse voltammetric measurements. The photophysical properties are investigated, aiming to determine the excited state potential energy. Finally, catalytic properties of the deoxygenated heteroarenes will be compared with the parent pyrimidopteridine *N*-oxides (Figure 1.7).

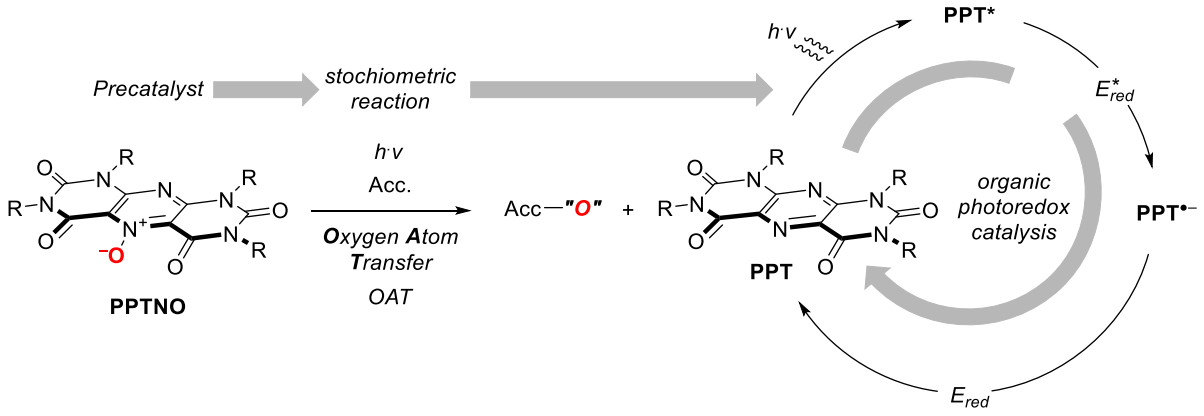

Figure 1.7: Photo-mediated deoxygenation of PPTNO and the photocatalytic properties of PPT.

1.3 Results and discussion

1.3.1 Photo-mediated synthesis of pyrimidopteridines

Initially, access to the deoxygenated pyrimidopteridines must be established by the utilization of a suitable acceptor molecule.[14] From our studies concerning the photo-mediated hydroamination of stilbenes with primary amines, (*E*)-stilbene was chosen as the oxygen atom acceptor.[16b] To ensure complete conversion, the oxygen acceptor was used in slight excess. After irradiation at 396 nm for 16 h, a series of pyrimidopteridine *N*-oxides were successfully deoxygenated (Table 1.1).

Table 1.1: Photochemical deoxygenation of pyrimidopteridines.

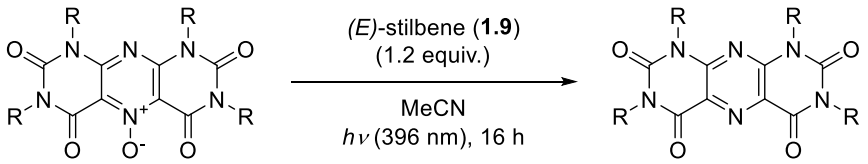

1.1-1.4 **1.5-1.8**

entry	substrate		product		isol. yield
1	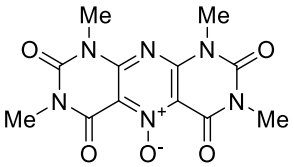	**1.1**	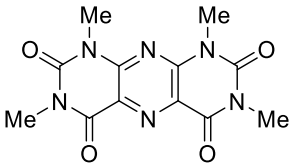	**1.5**	90%
2	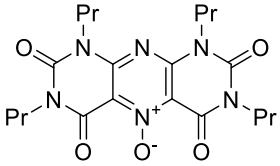	**1.2**	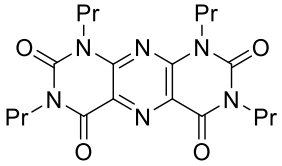	**1.6**	*quant.*
3	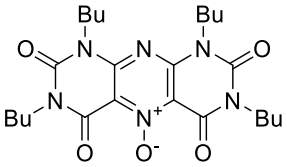	**1.3**	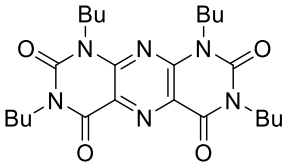	**1.7**	99%
4	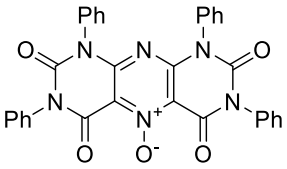	**1.4**	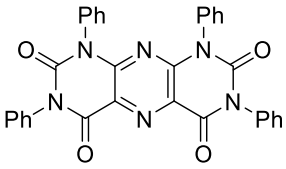	**1.8**	*quant.*

Footnote: substrate (0.5 mmol), **1.9** (1.2 eq.), MeCN (0.1 M), 396 nm, 16 h.

Four different pyrimidopteridine-*N*-oxides were subjected to photochemical deoxygenation. The pyrimidopteridine bearing methyl moieties **1.5** was isolated in a good yield of 90% (Table 1.1, entry 1). Pyrimidopteridine-*N*-oxides with larger alkyl substituents such as propyl or butyl **1.2** and **1.3** furnished the corresponding products **1.6** and **1.7** in quantitative yield (Table 1.1, entries 2-3). The pyrimidopteridine bearing phenyl substituents **1.8** was obtained in 99% isolated yield (Table 1.1, entry 4). Besides routine structural analysis, the identity of the products (**1.5**-**1.8**) was further confirmed by X-ray crystallography (Figure 1.8).

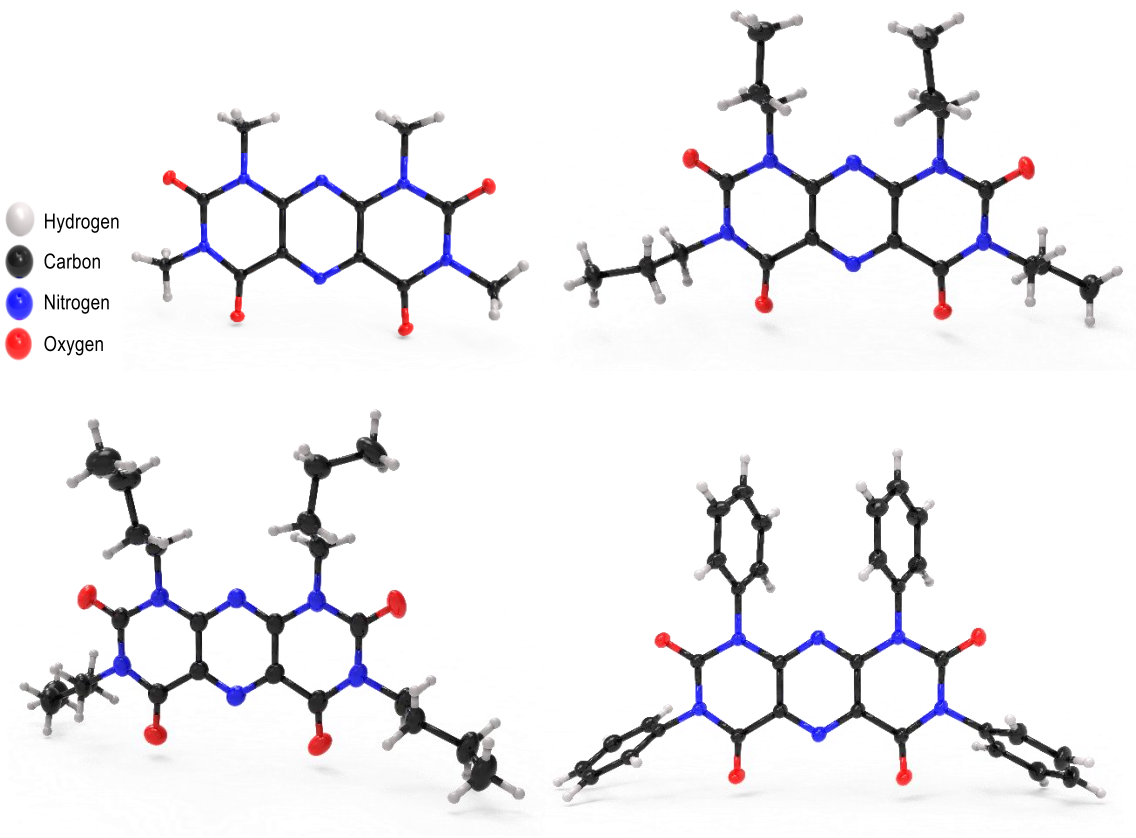

Figure 1.8: X-ray structures of PPTs 1.5-1.8. Displacement ellipsoids correspond to 30% probability.

Crystal structure analysis confirmed the planar pyrazine core structure of the heterocycle. The nitrogen atoms of the amine groups show a trigonal planar geometry corresponding to a sp^2-hybridization. Furthermore, the aromatic core structure is partially shielded by the substituents. Two of the *N*-substituents point in the same direction while the other two protrude at an angle of 120°.

After the successful structural elucidation of the pyrimidopteridines (**1.5**-**1.8**), the reactions were also evaluated with respect to the reaction products of (*E*)-stilbene (Figure 1.9). Initiated by energy transfer from the excited state of the photocatalyst, isomerization of (*E*) and (*Z*)-stilbenes (**1.9** and **1.10**) occurs under photochemical conditions.[17] Both isomers can act as oxygen acceptors leading to the formation of the oxidation products. Trace amounts of deoxybenzoin (**1.13**) and benzaldehyde (**1.14**) were observed as by-products. The main products were identified as *trans*- and *cis*-stilbene oxides (**1.11** and **1.12**) and were separated and isolated by column chromatography (Table 1.2).

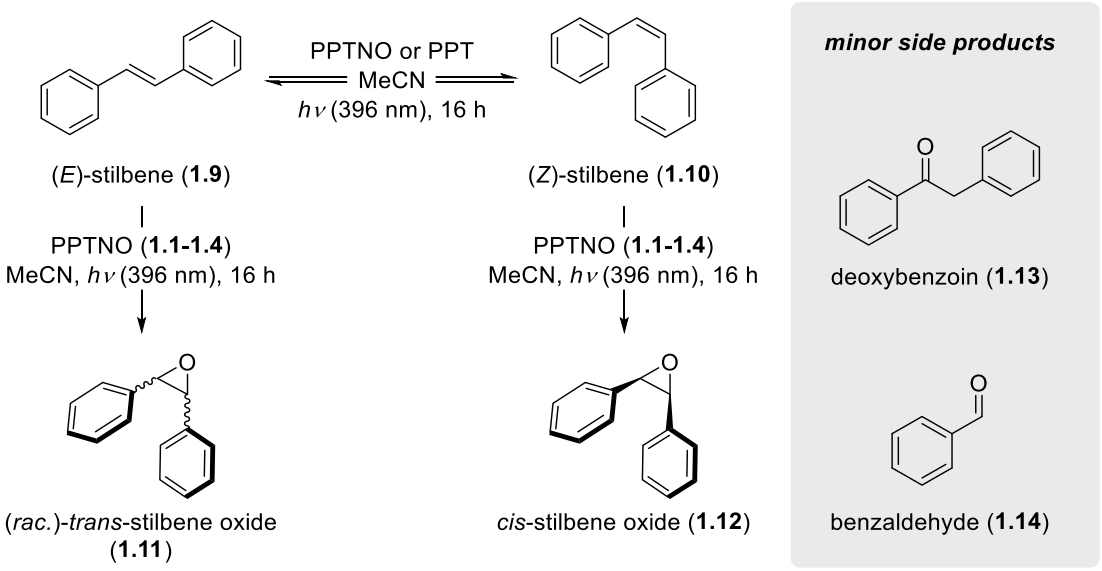

Figure 1.9: Photo-mediated *contra*-thermodynamic isomerization and oxygenation of stilbenes catalyzed by PPTNO.

Table 1.2: Photochemical synthesis of *cis*- and *trans*-stilbene oxide (1-11 and 1.12).

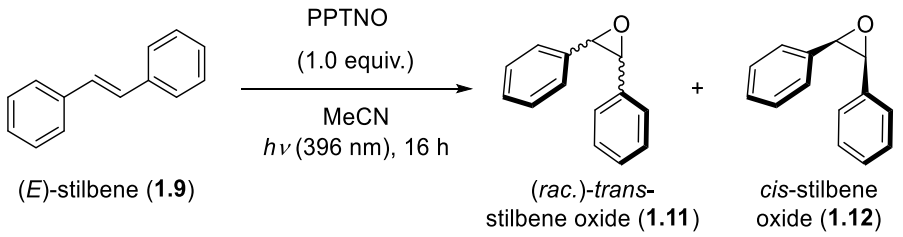

entry	PPTNO	rsm **1.9** [%][a]	*E*/*Z* ratio [**1.9**/**1.10**][a]	yield of **1.11** and **1.12** [%][b]	*trans*/*cis* ratio [**1.11**/**1.12**][b]
1	MePPTNO (**1.1**)	41	58:42	61	64:36
2	PrPPTNO (**1.2**)	26	45:55	64	66:33
3	BuPPTNO (**1.3**)	38	45:55	62	68:32
4	PhPPTNO (**1.4**)	32	52:48	56	52:48

Footnote: PPTNO (0.5 mmol), **1.9** (1.2 eq.), MeCN (0.1 M), 396 nm, 16 h. [a] Isolated yield based on (*E*)-stilbene (**1.9**). [b] Isolated yield based on PPTNO.

After the reaction, 26-41% of the starting material was recovered as mixture of *E*/*Z*-isomers in an even product distribution. The reaction of the methyl-substituted pyrimidopteridine *N*-oxides afforded a slightly higher amount of (*E*)-stilbene (**1.9**) compared to (*Z*)-stilbene (**1.10**) (Table 1.2, entry 1). Pyrimidopteridine *N*-oxides bearing propyl, butyl, phenyl groups exhibited tendentially more (*Z*)-stilbenes (Table 1.2, entries 2-4). The photo-mediated oxygen atom transfer from the pyrimidopteridine *N*-oxides (**1.1**-**1.4**) afforded the desired stilbene oxides **1.11** and **1.12** in 56-64% isolated yield. Alkyl-substituted pyrimidopteridine *N*-oxides resulted in

slightly higher yet comparable product yields (Table 1.2, entries 1-3). The alkyl-substituted pyrimidopteridine *N*-oxides showed a product distribution of *trans*- and *cis*-stilbene oxide (**1.11** and **1.12**) of 2:1. In contrast, the reaction with the pyrimidopteridine *N*-oxide bearing tetraphenyl substituents exhibited a more even distribution of the diastereomeric stilbene oxides (Table 1.2, entry 4). The occurrence of the product mixture can be explained by the fluctuation of the benzylic radicals that can reside on either side of the prochiral intermediate. From the product distribution one can conclude that the radical recombination is faster in the case of alkyl-substituted PPTNOs **1.1**-**1.3** as compared to the phenyl-substituted derivative **1.4**.

The proposed mechanism for the photo-mediated oxygen atom transfer from pyrimidopteridine-N-oxides to stilbene is depicted in Figure 1.10 below.

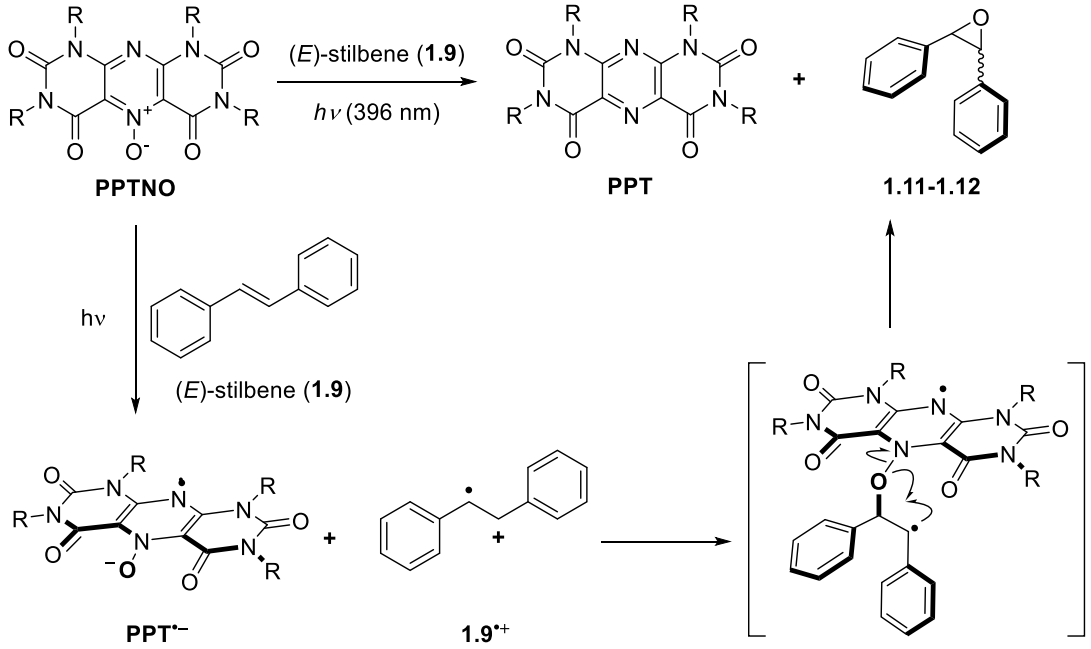

Figure 1.10: Proposed mechanism for the photo-mediated oxygen atom transfer of pyrimidopteridine-*N*-oxide (1.1-1.4) to stilbene (1.9).

The oxidation of (*E*)- and (*Z*)-stilbene (**1.9** and **1.10**) results in a common radical cationic intermediate (**1.9**$^{\bullet+}$). The *cis/trans*-distribution of the stilbene oxides is likely associated with a stepwise oxygen atom transfer mechanism. The reduced pyrimidopteridine-*N*-oxide (**PPS**$^{\bullet-}$) undergoes a nucleophilic attack by the *N*-oxide. Free rotation around the C–C single bond in the pyrimidopteridine-*N*-oxide-stilbene-adduct and fluctuation of the benzylic radical may lead to the stilbene oxide diastereomers **1.11** and **1.12**. Homolytic N–O bond cleavage and radical recombination results in the formation of stilbene oxide and the deoxygenated pyrimidopteridine (PPT).

1.3.2 Electrochemical and photophysical characterization of pyrimidopteridines

To determine the absorption maxima, ground state and excited state redox potentials of the pyrimidopteridines (PPTs, **1.5**-**1.8**), UV-vis absorption, luminescence and cyclicvoltammetry measurements were performed.

UV-vis absorption measurements

UV-vis absorption measurements were conducted to characterize the photophysical absorption properties of the pyrimidopteridine derivatives (**1.5**-**1.8**). This technique allows the determination of the suitable wavelength to enter the excited state. In this process, binding and non-binding electrons absorb the energy of the radiation and undergo excitation into the LUMO. Depending on the type of participating orbitals, different transitions such as σ - σ^* or π - π^* can be observed.[18] The pyrimidopteridine derivatives (**1.5**-**1.8**) were dissolved in acetonitrile (c = 50 µM) and measured in a cuvette (d = 1 cm) using a UV-vis absorption spectrometer (Figure 1.11).

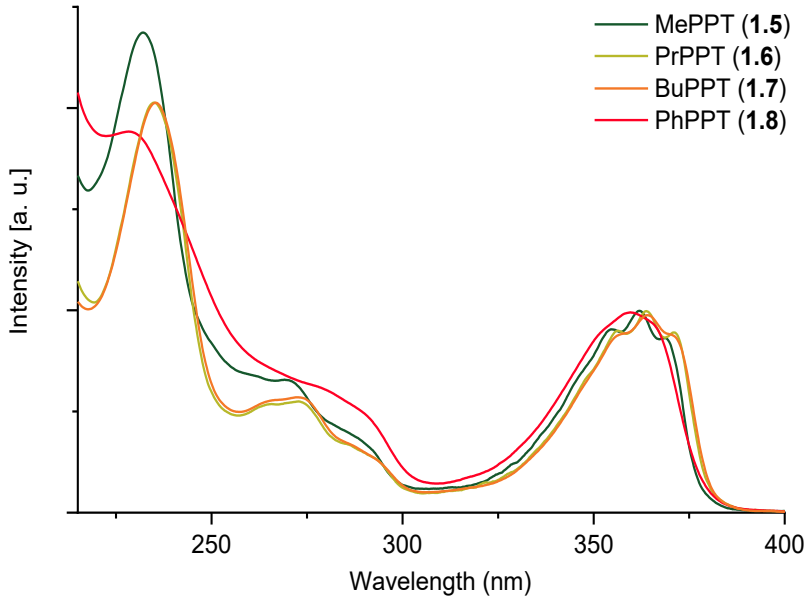

Figure 1.11: UV-vis absorption spectra of pyrimidopteridine derivatives 1.5-1.8 in MeCN.

The methyl substituted pyrimidopteridines shows three local absorption maxima in the UVA region (355 nm, 361 nm and 369 nm). In addition, an absorption maximum at 232 nm was observed in the UVC range (Figure 1.11, green). The pyrimidopteridines carrying propyl and butyl substituents **1.6.** and **1.7** show almost congruent absorption spectra with a slight bathochromic shift to 362 nm as compared to the methyl-substituted PPT **1.5**. In the UVC region, an absorption maximum of 235 nm was observed (Figure 1.11, yellow and orange). The pyrimidopteridine carrying phenyl rings shows a slight hypsochromic shift. The UVA

absorption maximum was detected at 359 nm and the UVC absorption maximum at 228 nm (Figure 1.11, red). The absorption maxima of the pyrimidopteridines in the UVA range (350 nm-370 nm) correspond to the smallest energy gap between the HOMO and the LUMO. This transition can be attributed to the n→π* transition from the lone-pairs of the carbonyl groups.[1, 18] The absorption bands of the UVB and UVC region correspond to a larger energy gap and can be assigned to π→π* transition of the heteroaromatic core structure.[1, 18]

Luminescence of pyrimidopteridines

Another measure to characterize the photophysical properties of the pyrimidopteridine derivatives (**1.4**-**1.8**) is to determine the luminescence characteristics. This involves determining the spontaneous emission of electromagnetic radiation triggered by the relaxation of the excited state to the photophysical ground state. This technique aids to determine the energy of the excited state.[5] The molecule is excited by the absorption of light in the region of the absorption maximum (e.g., λ = 350 nm). The pyrimidopteridine derivatives (**1.4**-**1.8**) were dissolved in acetonitrile (c = 20 µM) and measured in a cuvette (d = 1 cm) using a fluorescence spectrometer (Figure 1.12).

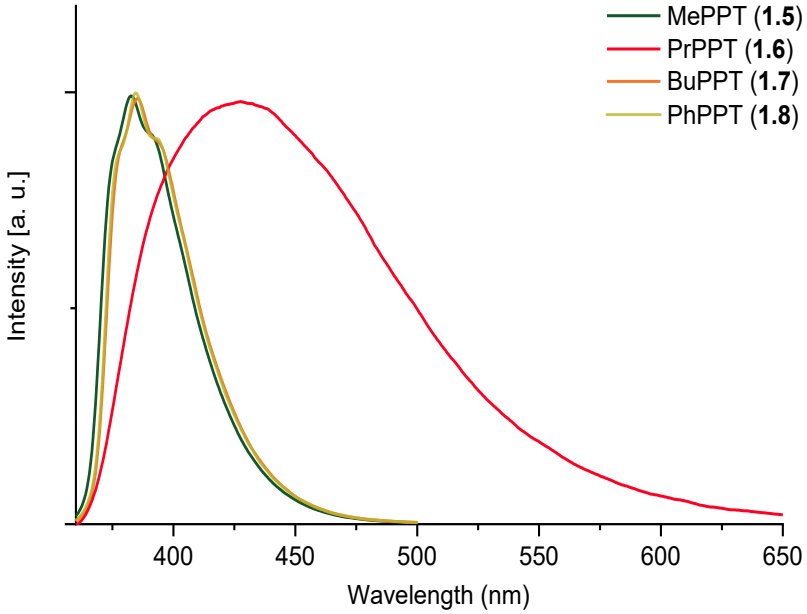

Figure 1.12: Emission spectra of pyrimidopteridine derivatives 1.5-1.8.

The alkylated pyrimidopteridines exhibit very similar emission spectra. The pyrimidopteridine bearing methyl groups **1.5** shows an emission maximum at 383 nm (Figure 1.12, green). Th propyl- and butyl-substituted pyrimidopteridines **1.6** and **1.7** show emission maxima at 385 nm (Figure 1.12, yellow and orange). The emission spectra of all alkyl-substituted pyrimidopteridines exhibit mirror image symmetry with respect to their absorption spectra. In contrast, for the pyrimidopteridine containing the phenyl moieties **1.8** revealed an emission

maximum at 427 nm (Figure 1.12, red). The increased Stokes shift can be attributed electron-vibrational coupling and no-radiative vibrational decay associated with the phenyl-substituents.[19]

Excited state energy of pyrimidopteridines

The potential energy of the excited state ($E_{0,0}$) refers to the transition between the lowest vibrational state of the S_1 (v =0) to the lowest vibrational ground state S_0 (v =0). The excited state energy cannot be measured directly and must be estimated. If the Stokes shift is sufficiently small, the intersection of the normalized absorption and emission spectra is preferably chosen for this purpose. Alternatively, the onset of the emission-spectrum can be chosen which represents an overestimation of the excited state energy or the maximum of the emission spectrum which represents an underestimation of the excited state energy.[5, 20]

The normalized absorption and emission spectra of the alkyl-substituted pyrimidopteridine derivatives (**1.5**-**1.7**) reveals a close to mirror image symmetry with a small Stokes shift of 22 nm (Figure 1.13). Thus, one half of the Stokes shift is an appropriate measure to determine the excited state energy.

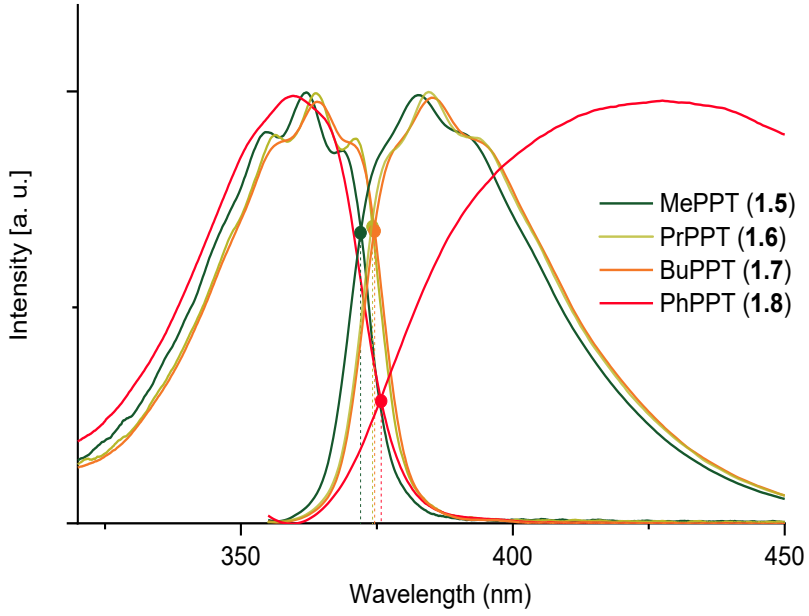

Figure 1.13: Normalized absorption- and emission spectra of pyrimidopteridines 1.5-1.8.

The intercept of the methyl-substituted pyrimidopteridine (**1.5**) is at 372 nm, which corresponds to an energy of 3.33 eV (Figure 1.13, green). Propyl and butyl substituted pyrimidopteridines (**1.6**-**1.7**) show an intercept at 375 nm corresponding to an energy of 3.31 eV (Figure 1.13, yellow and orange). In contrast, the pyrimidopteridine bearing phenyl substituents (**1.8**) shows no mirror symmetry of the normalized absorption and emission

spectra. The intercept is at 376 nm and corresponds to an energy of 3.30 eV (Figure 1.13, red).

Cyclic voltammetry and differential pulse voltammetry

Cyclovoltammetry and differential pulse voltammetry were applied to determine the ground state redox potential of the pyrimidopteridines **1.5**-**1.8**. The potentials were determined in acetonitrile (c = 1 mM) with tetrabutylammonium hexafluorophosphate as electrolyte (c = 0.1 M) against the silver-silver chloride reference electrode. To minimize an error of the reference system and thus ensure comparability with the literature, the oxidation potential of the Fc^+/Fc redox couple was used as reference standard. The voltammograms were referenced to $E_{1/2}^{ox}(Fc^*/Fc) = 0$ V.[21] Most commonly, redox potentials in the literature are discussed against the reference system of the standard calomel electrode (SCE), which is readily convertible by adding 0.38 V to the values referenced to Fc^+/Fc. Consequently, all measured voltammograms are depicted and discussed against the ferrocene reference system (Figure 1.14) and the final potentials are listed against SCE (Table 1.3).

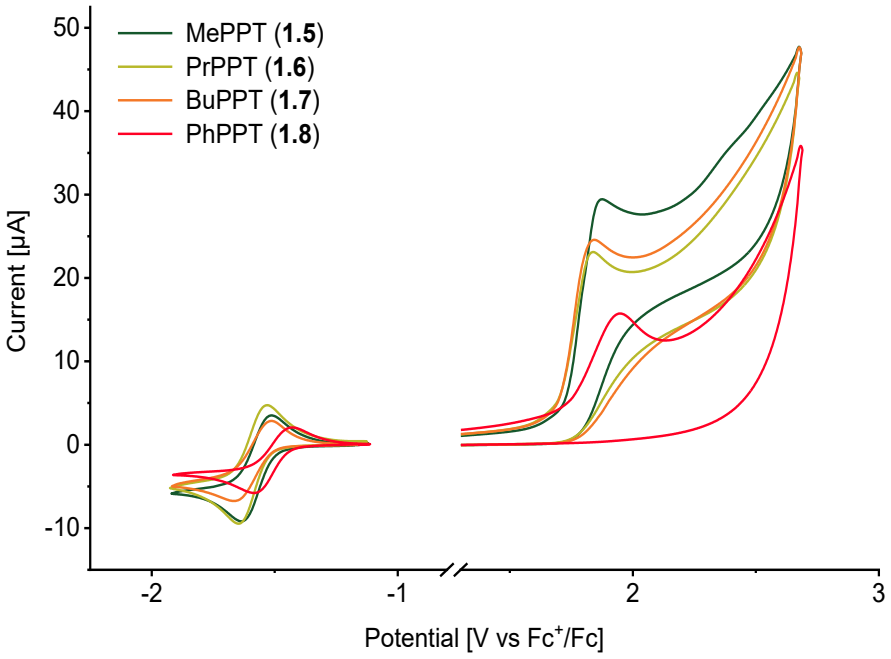

Figure 1.14: Cyclic voltammograms of pyrimidopteridine derivatives 1.5-1.8.

All deoxygenated pyrimidopteridines show an irreversible oxidation response. The anodic peak potential of the alkyl substituted pyrimidopteridines (**1.5**, **1.6** and **1.7**) was observed between +1.83 and +1.86 V vs Fc^+/Fc (Table 1.3, entries 1-3). The pyrimidopteridine bearing phenyl rings (**1.8**) exhibited a slightly elevated peak potential at +1.95 V vs Fc^+/Fc (Table 1.3, entry 4). In contrast, a reversible reduction signal was observed for all pyrimidopteridines, allowing the determination of the reduction potential as the average of the minimum of the reduction and the maximum of the oxidation half-wave. The alkyl substituted

pyrimidopteridines (**1.5**, **1.6** and **1.7**) show a ground state reduction potential at −1.58-(−1.59) V vs Fc^+/Fc (Table 1.3, entries 1-3). The pyrimidopteridine bearing phenyl rings shows a ground state reduction potential at −1.51 V vs Fc^+/Fc (Table 1.3, entry 4).

Subsequently, the deoxygenated pyrimidopteridine-*N*-oxides were analyzed by differential pulse voltammetry.[22] This voltammetry method uses a series of voltage pulses superimposed on the linear sweep potential and the current change is plotted against the potential. The resulting signal maximum is a good approximation of the half-wave $E_{1/2}$ potential and can be determined without the requirement of having defined peaks for the anodic and cathodic currents. The pyrimidopteridines were dissolved in a 0.1 M solution of $TBAPF_6$ in MeCN and measured against the silver-silver chloride reference electrode. The Fc^+/Fc peak was used as internal reference (Figure 1.15).

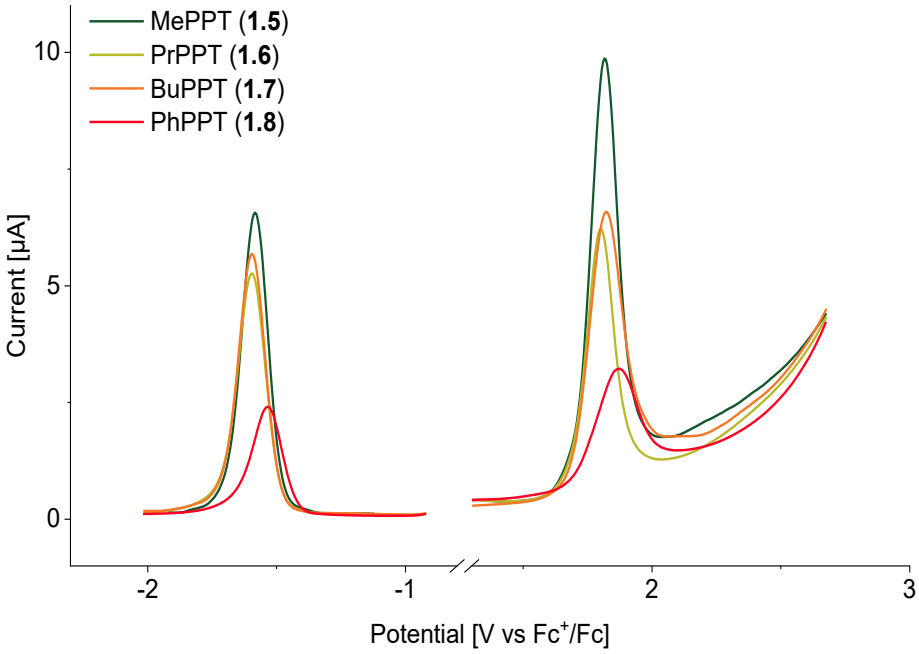

Figure 1.15: Differential pulse voltammogram of pyrimidopteridine derivatives 1.5-1.8.

A summary of the collected data is shown in Table 1.3, below. The alkyl substituted pyrimidopteridines (**1.5**, **1.6** and **1.7**) showed a peak potential between +1.80 V and +1.82 V vs Fc^+/Fc in the anodic region (Table 1.3, entries 1-3). Again, the pyrimidopteridine with phenyl rings **1.8** showed a slightly increased anodic peak signal with +1.87 V vs Fc^+/Fc (Table 1.3, entry 4). In the cathodic region, the alkyl-substituted pyrimidopteridines show a peak potential of −1.58 V to −1.59 V vs Fc^+/Fc which is in perfect agreement with the results of the CV-measurements (Table 1.3, entries 1-3). The pyrimidopteridine bearing phenyl rings **1.8** shows a cathodic peak at −1.54 V vs Fc^+/Fc (Table 1.3, entry 4).

Table 1.3: Data collection of CV and DPV measurements.

entry	substrate	$E_{1/pc}^{red}$	$E_{1/pa}^{red}$	$E_{1/pc}^{ox}$	$E_{1/pa}^{ox}$	$E_{1/2}^{red}$	$E_{1/2}^{ox}$	E_{DPV}^{red}	E_{DPV}^{ox}
		[V vs Fc^+/Fc][a]		[V vs Fc^+/Fc][a]		[V vs SCE][b,c]		[V vs SCE][b,d]	
1	MePPTNO (**1.5**)	–1.64	–1.52	-	+1.87	–1.20	-	–1.20	+2.20
2	PrPPTNO (**1.6**)	–1.65	–1.53	-	+1.84	–1.21	-	–1.21	+2.18
3	BuPPTNO (**1.7**)	–1.66	–1.52	-	+1.84	–1.21	-	–1.21	+2.20
4	PhPPTNO (**1.8**)	–1.59	–1.43	-	+1.95	–1.13	-	–1.16	+2.25

Footnote: [a] Potentials were measured using cyclic voltammetry referenced to Fc^+/Fc redox couple. [b] Referenced to SCE by adding 0.38 V to the value relative to Fc^+/Fc.[21] [c] Average of anodic and cathodic peak potential. [d] Potentials were measured using differential pulse voltammetry referenced to Fc^+/Fc redox couple.

Excited state redox potentials of pyrimidopteridines

After determining the energy of the excited state, the excited state redox potentials were calculated. The combination of the voltammetrically determined redox potentials ($E_{1/2}^{red}$ and $E_{1/2}^{ox}$) and the potential energy of the excited state ($E_{0/0}$) allows to determine an approximation of the excited state redox potentials.[5]

The excited state reduction potential E_{red}^{*} is calculated by

$$\boldsymbol{E_{red}^{*}}(cat^{*}/cat^{\bullet-}) = \boldsymbol{E_{0,0}} + \boldsymbol{E_{1/2}^{red}}(cat/cat^{\bullet-}) \qquad \text{equation 1}$$

The excited state oxidation potential E_{ox}^{*} is calculated by

$$\boldsymbol{E_{ox}^{*}}(cat^{\bullet+}/cat^{*}) = \boldsymbol{E_{1/2}^{ox}}(cat^{\bullet+}/cat) - \boldsymbol{E_{0,0}} \qquad \text{equation 2}$$

A tabular overview is shown below (Table 1.4).

Summary

A tabular overview of the absorption and emission maxima, the excited state potential and redox potentials of the ground state and the excited state are listed below (Table 1.4).

Table 1.4: Photophysical and electrochemical properties of pyrimidopteridines.

compound	λ_{max}^{abs} [nm]	λ_{max}^{em} [nm]	$E_{0,0}^{S1}$ [eV][c]	$E_{1/2}^{red}$ [V vs Fc^+/Fc][a]	$E_{1/2}^{ox}$ [V vs Fc^+/Fc][a]	$E_{1/2}^{red}$ [V vs SCE][b]	$E_{1/2}^{ox}$ [V vs SCE][b]	E_{red}^{*} [V vs Fc^+/Fc][d]	E_{ox}^{*} [V vs Fc^+/Fc][d]	E_{red}^{*} [V vs SCE][d]	E_{ox}^{*} [V vs SCE][d]
MePPT (**1.5**)	361	383	+3.33	–1.58	+1.82	–1.20	+2.20	+1.75	–1.51	+2.13	–1.13
PrPPT (**1.6**)	363	385	+3.31	–1.59	+1.80	–1.21	+2.18	+1.72	–1.51	+2.10	–1.13
BuPPT (**1.7**)	363	385	+3.31	–1.59	+1.82	–1.21	+2.20	+1.72	–1.49	+2.10	–1.11
PhPPT (**1.8**)	359	427	+3.30	–1.54	+1.87	–1.16	+2.25	+1.76	–1.43	+2.14	–1.05

Footnote: [a] Potentials were measured using cyclic voltammetry (CV) and differential pulse voltammetry (DPV) relative to Fc^+/Fc. [b] Referenced to SCE by adding 0.38 V to the value relative to Fc^+/Fc. [c] $E_{0,0}$ values corresponding to the energy at the intersection of the excitation and emission spectra. [d] Calculated by $E_{red}^{*} = E_{0,0} + E_{1/2}^{red}$ and $E_{ox}^{*} = E_{1/2}^{ox} - E_{0,0}$.

All pyrimidopteridine derivatives (**1.5**-**1.8**) described herein show excellent excited state characteristics. In photo-mediated systems, it must be ensured that the correct wavelength is used for the excitation of the molecule. The pyrimidopteridines derivatives (**1.5**-**1.8**) show absorption maxima around 360 nm. Despite the hyposochromic shift of the absorption maxima as compared to the pyrimidopteridine-*N*-oxides (**1.1**-**1.4**), a sufficient overlap with the emission spectra of the utilized UV-A lamps is evident (Figure 1.16).

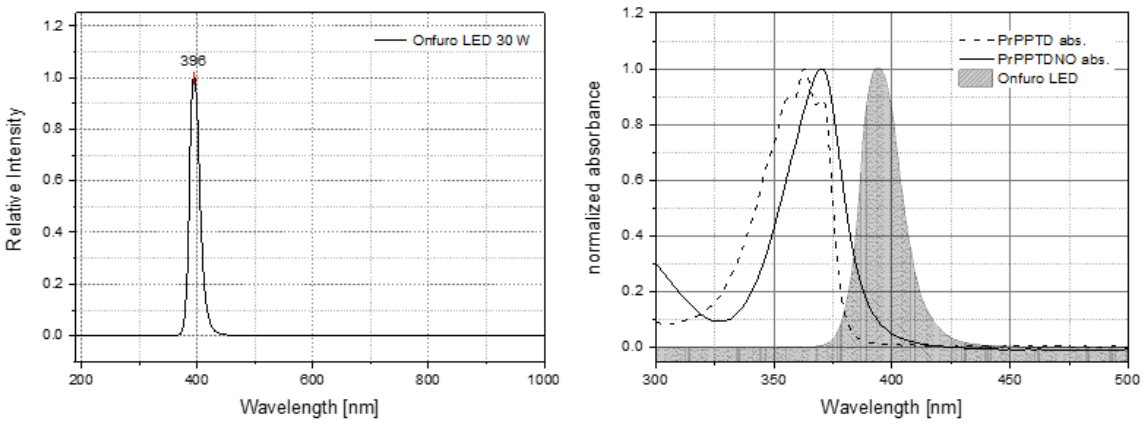

Figure 1.16: Emission spectrum of the utilized LED-lamp ONFURO IP66 (30 W) (left). Absorption spectra of PrPPTNO and PrPPT and emission spectra of ONFURO IP66 LED.

Based on the emission maximum of the utilized black-light LED at 396 nm and the absorption maxima of PPT and PPTNO at 363 nm and 370 nm, respectively.[14] A comparison of the offset of the absorption spectra of the heterocycles at 393 nm and 417 nm, respectively, compared to the onset of the emission spectrum of the light source (373 nm) shows that both compounds can be excited with this light source.

The excited state reduction potential of the pyrimidopteridines (**1.5**-**1.8**) ranges from +2.10 to +2.14 V vs. SCE. These values indicate that the pyrimidopteridines should be suitable for the oxidation of a broad range of organic compounds.[6] The ground state reduction potential is superior to other organic photoredox catalysts and ensures facile catalyst turn-over.[5] The excited state oxidation potential of the pyrimidopteridines ranges from −1.05 V to −1.13 V vs. SCE. Their utilization as an excited state reducing agents is accordingly feasible for readily to moderately reducible compounds. However, the irreversibility of the anodic oxidation raises doubts about the catalyst turn-over in this scenario.

1.3.3 Application of pyrimidopteridines as photoredox catalysts

Oxidative cyclization of 2-phenylbenzoic acid

To test the applicability of the heterocycles (**1.5**-**1.8**) in photoredox catalysis, the pyrimidopteridines were applied in an oxidative cyclization reaction.[23] Due to the high oxidation potential of carboxylates (~1.5 V vs SCE),[6] the cyclization of 2-phenylbenzoic acid (**1.15**) was chosen as the model reaction. The pyrimidopteridines were used at a catalyst loading of 5 mol%. The reaction was irradiated at 396 nm under an oxygen atmosphere for 24 h. The isolated yields of the desired product **1.16** are given in Table 1.5. The reaction was not further optimized.

Table 1.5: Oxidative cyclization of 2-phenyl benzoic acid (1.15).

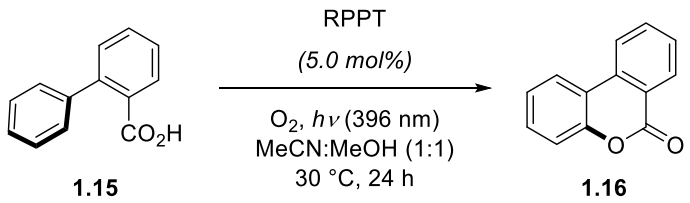

1.15 **1.16**

entry	catalyst	isolated yield
1	MePPT (**1.5**)	80%
2	PrPPT (**1.6**)	66%
3	BuPPT (**1.7**)	66%
4	PhPPT (**1.8**)	85%

Footnote: The reaction was carried out on a 0.5 mmol mass scale (0.1 M) with 5 mol% RPPT.

All pyrimidopteridine derivatives (**1.5**-**1.8**) showed a good performance as photo-redox catalysts. The product **1.16** was isolated in moderate to very good yields. The methyl-substituted pyrimidopteridine (**1.5**) delivered the product in an isolated yield of 80% (Table 1.5, entry 1). The pyrimidopteridines bearing propyl or butyl groups (**1.6** and **1.7**) furnished the

product in a yield of 66% each (Table 1.5, entries 2-3). The phenyl substituted pyrimidopteridine showed the best catalytic activity yielding the desired product **1.16** in 86% isolated yield (Table 1.5, entry 4). The isolated yields follow the trend of the previously calculated excited state reduction potential (Table 1.4).

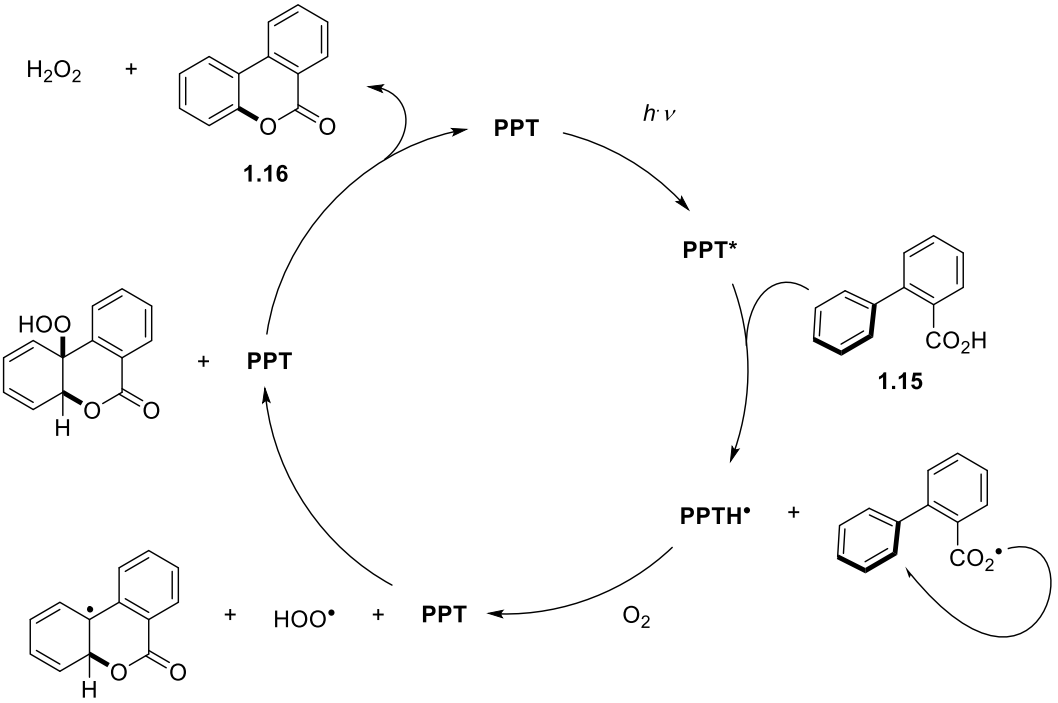

Scheme 1.5: Proposed mechanism for the photo-mediated oxidative cyclization of 2-phenyl benzoic acid (1.15) to 6*H*-benzo[*c*]chromen-6-one (1.16).

The generated active PPT catalyst is excited by irradiation at 396 nm. 2-Phenyl benzoic acid (**1.15**) reacts with the excited state of PPT via a proton-coupled electron transfer. The oxidized cationic carbonate undergoes intramolecular cyclization at the ortho-position in the sense of electrophilic aromatic substitution resulting in the *C*-centered radical. The catalyst is restored by reaction with elemental oxygen, yielding a hydrogen peroxo radical. The radical recombination results in the formation of a hydrogen peroxo intermediate, which leads to the desired product (**1.16**) through the cleavage of hydrogen peroxide.

Comparison of tetrapropylpyrimidopteridine-*N*-oxide and tetrapropylpyrimidopteridine in the photo-mediated hydroamination of *E*-stilbene

The previously investigated pyrimidopteridine *N*-oxides[15] have already been successfully employed as a pre-catalyst in the photo-mediated hydroamination of (*E*)-stilbenes.[16b] Due to the predominant deoxygenation of the pre-catalyst, the stilbene substrate is consumed according to the mechanism discussed in chapter 1.3.1. This trend was investigated in the hydroamination between (*E*)-stilbenes (**1.9**) and benzylamine (**1.17**) at different catalyst

loadings. The propyl-substituted pyrimidopteridine (**1.6**) and the corresponding *N*-oxide (**1.2**) were used as catalyst (Table 1.6).

Table 1.6: Photo-mediated hydroamination of (*E*)-stilbene (1.9) with benzylamine (1.17) with PrPPTNO (1.2) and PrPPT (1.6) at different catalyst loadings.[a]

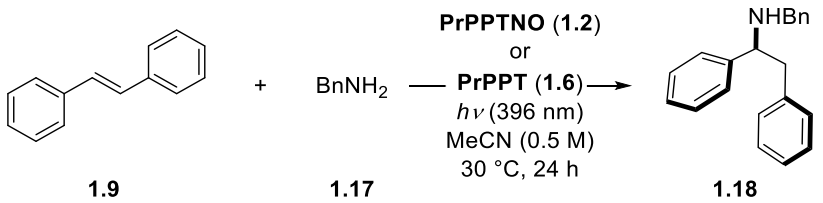

1.9 **1.17** **1.18**

entry	catalyst	catalyst loading [mol%]	yield [%][b]
1	PrPPT (**1.6**)	5	72
2	PrPPTNO (**1.2**)	5	72
3	PrPPT (**1.6**)	10	77
4	PrPPTNO (**1.2**)	10	77
5	PrPPT (**1.6**)	25	86
6	PrPPTNO (**1.2**)	25	71

Footnote: [a] Reactions were performed on a 0.5 mol% scale. [b] Average yield of two experiments.

At a catalyst loading of 5.0 mol% of the PPTNO and PPT catalysts **1.2** and **1.6**, the hydroamination product *N*-benzyl-1,2-diphenylethan-1-amine (**1.18**) was obtained in 72% isolated yield (Table 1.6, entries 1 and 2). Similarly, at a catalyst loading of 10 mol%, no deterioration in the yields of the product was observed (Table 1.6, entries 3-4). At a catalyst loading of 25 mol%, a good yield of 86% was obtained with the deoxygenated photocatalyst (Table 1.6, entry 5). In contrast, the pyrimidopteridine *N*-oxide catalyst gave the product with a yield of 71% (Table 1.6, entry 6).

Based on these results, a good performance of both PPTNO **1.2** and PPT **1.6** in the photo-mediated hydroamination is evident. The yields, recorded after 24 h, reflect the yields at high turnover. Following the reaction trajectory using calibrated GC, revealed the full deoxygenation of the PPTNO within the initial 60 min of the reaction.[16b, 24] Stilbenoxides (**1.11** and **1.12**) were formed besides by several by-products under the applied reaction conditions. However, the overall yield of the reaction was not significantly impaired. Thus, the in-situ generation of the active photoredox catalyst is a viable approach. In more delicate reaction in which product purification becomes an issue, the utilization of unoxygenated pyrimidopteridines is advisable.

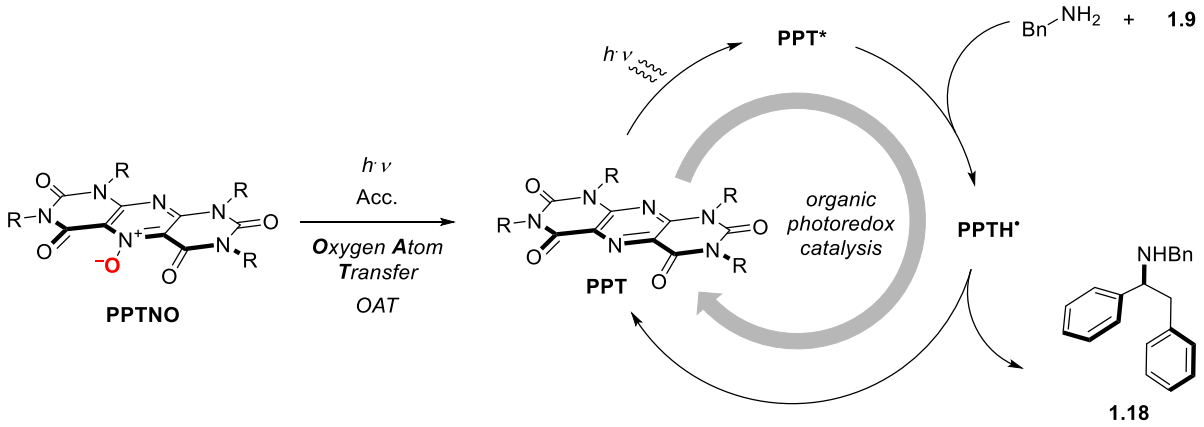

Scheme 1.6: Catalytic cycle for the photo-mediated hydroamination via stilbene activation.

A detailed mechanistic analysis is presented and discussed vide infra (see Chapter 2.3.6).

1.4 Conclusion

In summary, a protocol for the photochemical deoxygenation of pyrimidopteridine *N*-oxides (**1.1**-**1.4**) utilizing (*E*)-stilbene (**1.9**) as an oxygen atom acceptor has been successfully established. The pyrimidopteridine derivatives (**1.5**-**1.8**) have been synthesized in very good to excellent yields and were fully characterized, including X-ray crystallographic analysis. The oxidation products (*E*)- and (*Z*)-stilbene oxide has been identified and were fully characterized and were isolated in yields of 56%-64%.

The ground state redox potential of the pyrimidopteridines was determined by cyclovoltametric and differential pulse voltametric measurements. The photophysical properties of all pyrimidopteridine derivatives was analyzed by UV-vis absorption and fluorescence spectroscopy. In addition, the combination of absorption and emission spectroscopy aided to determine the energy of the excited state. The resulting excited state redox potentials of the pyrimidopteridines suggest a high potency as excited state oxidant. With an excited state reduction potential of over +2.10 V vs SCE in MeCN, these heteroarene-based photosensitizers are capable of oxidizing a wide variety of compounds, such as amines, alcohols, and carboxylic acids.[6] The applicability of pyrimidopteridines as photocatalysts has been demonstrated in the oxidative cyclization of 2-phenyl benzoic acid. Furthermore, it was shown that PPTNO serves as precatalyst to pyrimidopteridine heterocyle. The utilization of unoxygenated PPTs is advantageous under anaerobic conditions, resulting in a cleaner reaction mixture.

2 Mechanistic investigations concerning the hydroamination of stilbenes with primary amines catalyzed by a pyrimidopteridine photoredox catalyst

2.1 Introduction

In nature, alkylamines represent a ubiquitous class of compounds which are importance in many biological processes.[25] Neurotransmitters such as adrenaline, dopamine and serotonin possess crucial functions in the mammalian nervous system (Figure 2.1).[26] Ingestion of such endogenous or xenobiotic substances can induce pharmacological processes, which are used for therapy or treatment of diseases like Alzheimer or the restless legs syndrome.[27] Motivated by the possibility of initiating directed therapeutic effects, the demand for the derivatization and synthesis possibilities of such compounds is increasing.

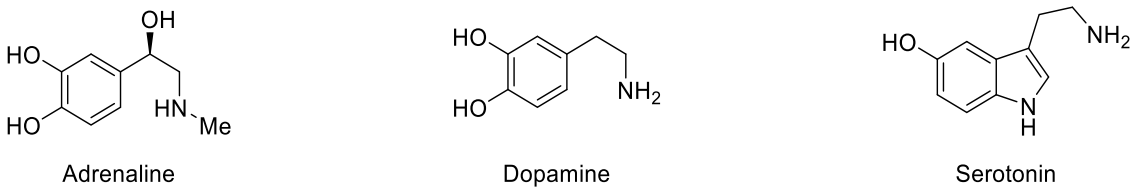

Figure 2.1: Nitrogen containing neurotransmitters.

Photo-mediated hydroamination reactions have become a valuable tool for the construction of omnipresent C−N bonds.[28] Photo mediated reactions were also successfully applied in total synthesis. In 2002, Trost and Trang described an enantioselective strategy for the preparation of (-)-codeine and (-)-morphine.[29] The key step was an intramolecular hydroamination of the secondary amine to the styrene moiety. The authors described the irradiation as necessary and only decomposition products were observed in the dark (Scheme 2.1).

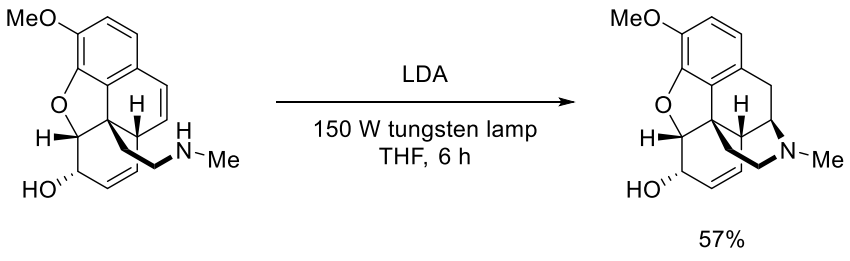

Scheme 2.1: Photo-mediated intramolecular hydroamination in the synthesis of (-)-codeine.

A profound understanding of the fundamental reaction mechanism is essential for the development of viable protocols. Different activation of the photo-mediated formal addition of an amine to an alkene may involve (i) formation of *N*-centered radicals, (ii) the formation of *C*-

centered radicals through the oxidation of the alkene, or (iii) an interconversion from *N*- to *C*-centered radicals through a hydrogen atom transfer (Scheme 2.2).[30]

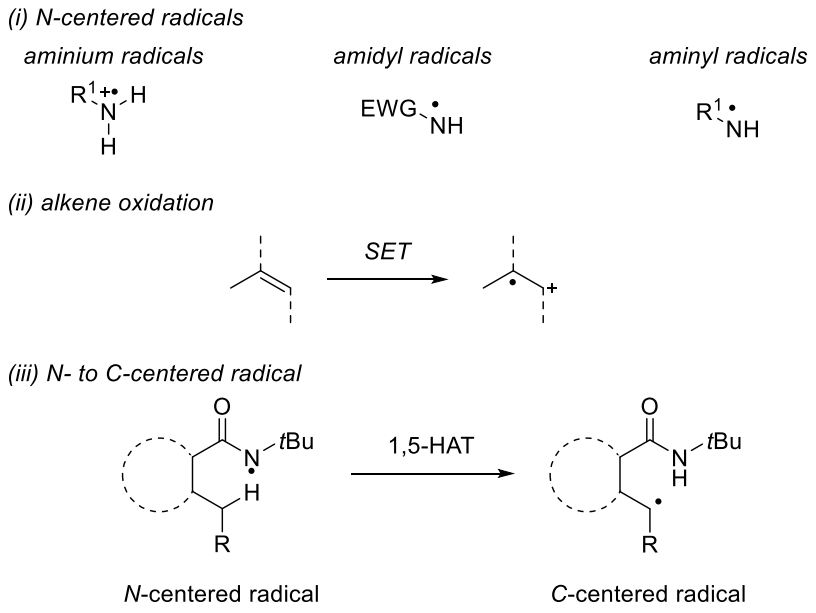

Scheme 2.2: Plausible reaction trajectories and corresponding radical intermediates.[30g]

Aliphatic amines can be oxidized to their corresponding radical cations. The oxidation potential E_{ox} decreases with an increased degree of substitution due to stabilization of the positive charge by additional alkyl substituents. Thus, tertiary amines ($E_{ox} = 0.82\ V$ vs SCE in MeCN for tributylamine) possess lower oxidation potentials as compared to secondary amines ($E_{ox} = 1.13\ V$ vs SCE in MeCN for dibutylamine).[31] Primary amines ($E_{ox} = 1.51\ V$ vs SCE in MeCN for butylamine)[32] and ammonia ($E_{ox} = 1.90\ V$ vs SCE in MeCN)[33] have the highest oxidation potentials. Thus, secondary amines most readily engage in phot-mediated oxidation reactions. In contrast, the number of examples that utilize primary amines is limited. The resulting ammonium radical is an electrophilic species that preferentially reacts with electron-rich alkenes. Thus, the photo-mediated oxidation of amines results in an umpolung of the intrinsic reactivity.

The group of Knowles has extensively studied the intermolecular *anti*-Markovnikov hydroamination of aliphatic, olefins with alkylamines through the intermediacy of ammonium radicals.[30h, 34] Their methodology utilized a iridium metal complexes in conjunction with a thiol-based hydrogen atom transfer (HAT) co-catalyst (Scheme 2.3). In a seminal account published in 2017, Knowles and co-workers developed a phot-mediated hydroamination of aliphatic alkenes with secondary amines, using a mild excited state oxidant ([Ir(dF(Me)ppy)$_2$(dtbbpy)]PF$_6$ (**A**) (E^*_{red} (Ir*^{III}/Ir^{II}) = +0.97 V vs SCE in MeCN). In 2019, the application of a stronger excited state oxidant [Ir(dF(CF$_3$)ppy)$_2$(4,4′-d(CF$_3$)-bpy)]PF$_6$ (**B**) (E^*_{red} (Ir*^{III}/Ir^{II}) = +1.65 V vs SCE in MeCN) enabled the utilization of primary amines.

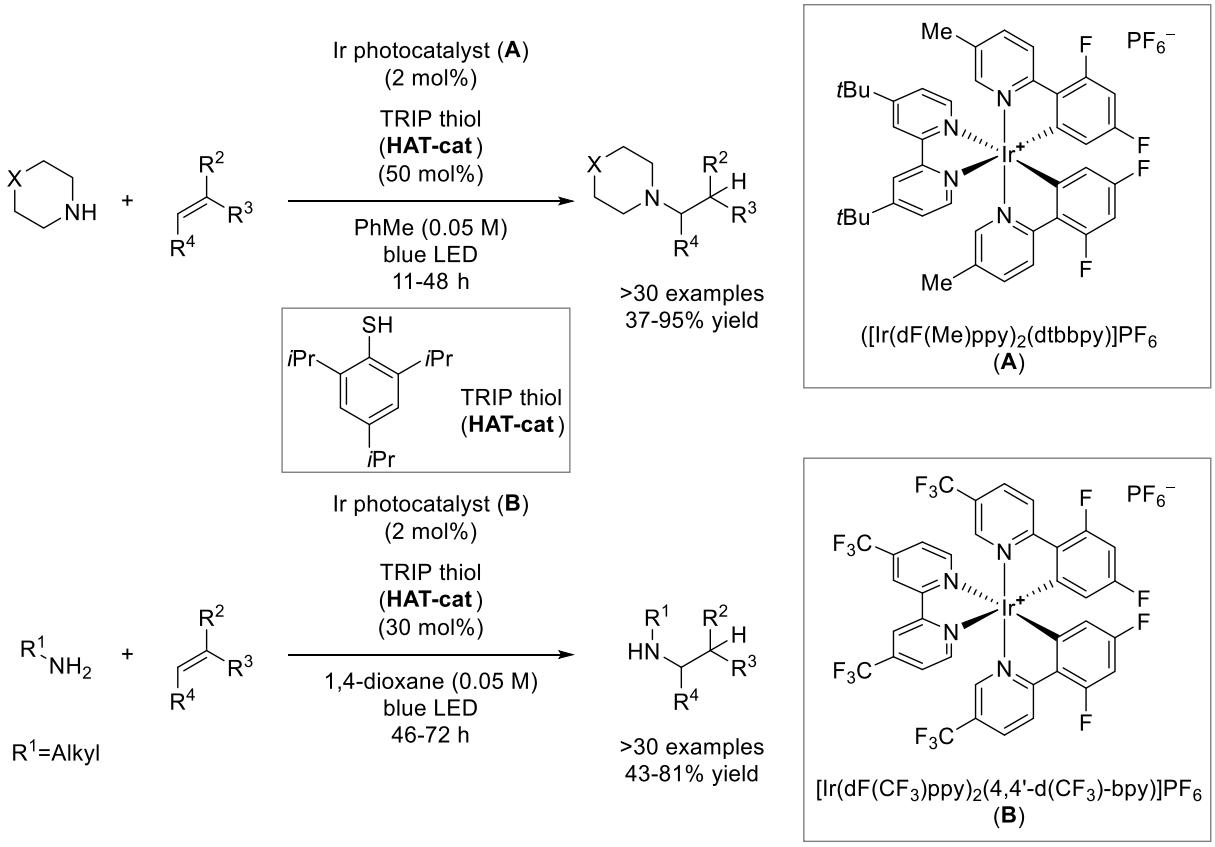

Scheme 2.3: Intermolecular hydroamination of inactivated internal olefins with alkylamines.[34c]

A general mechanism is depicted in Figure 2.2, below.[30h, 34]

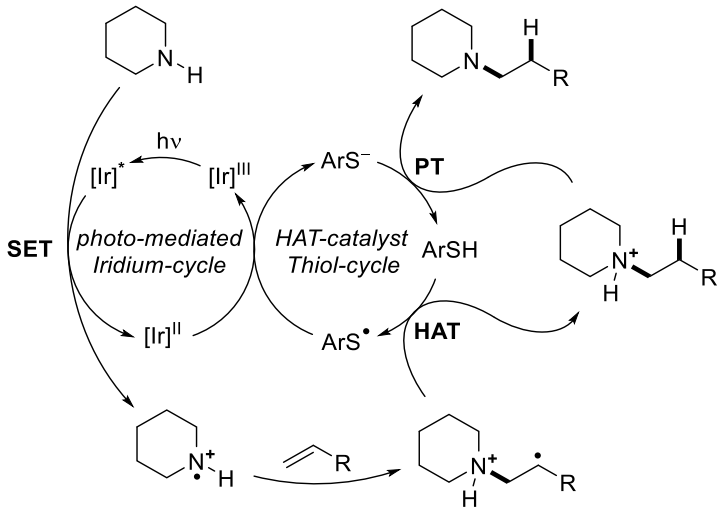

Figure 2.2: Proposed mechanism for the hydroamination of alkenes via an amine oxidation.

The proposed mechanism commences with the excitation of the Ir photoredox catalyst, followed by single electron oxidation of electron-rich amine. The *N*-centered, electrophilic radical is adding to the electron-rich olefin upon formation of a *C*-centered radical. The reduction potentials of the resulting radical intermediate exceeds the reduction potential of the reduced form of the catalyst, prohibiting a direct catalyst turn-over.[35] Thus, an additional thiol or disulfide co-catalyst is required.[36] The co-catalyst operates as HAT catalyst. The resulting

thiyl radical oxidizes the Ir(II) species to generate the active photoredox catalyst. Eventually, the thiolate anion deprotonates the ammonium adduct, yielding the desired product.

Noteworthy contributions in the field of photo-mediated intermolecular hydroamination through alkene oxidation has been reported by the group of Nicewicz among others.[30b, 36a, 37] Their accounts focused on the single electron oxidation of electron-rich olefins. The organic 9-mesityl-10-methylacridinium salt (E^*_{red} (Mes-Acr-Me^{+*}/ Mes-Acr-Me) = +2.18 V vs SCE in MeCN). served as a photocatalyst in cooperation with a disulfide cocatalyst and catalytic amounts of 2,6-lutidine (Scheme 2.4).

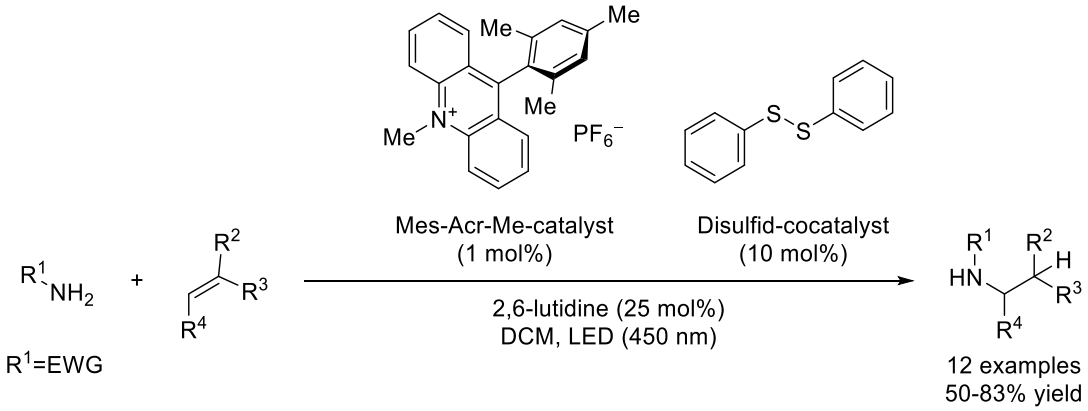

Scheme 2.4: Intermolecular hydroamination of internal olefins with deactivated amines.[36a]

The reaction trajectory proceeds via a *C*-centered radical cation that is scavenged by a nucleophile (Scheme 2.5). This methodology is limited to electron-rich alkene derivatives with relatively low oxidation potentials ($E_{ox} < 1.50\ V$ vs SCE in MeCN).[34a] The scope of amines include carbamates,[37b] sulfonamides,[37a] and *N*-heterocycles[36a] that do not competitively inhibit oxidation between the alkene and the photo redox catalyst. The one-electron oxidation of olefins benefits from the conversion of the alkene to a more electrophilic species.[36a,38] The resulting cationic *C*-centered radical is captured by a nucleophilic amine yielding the olefin-amine adduct. Since the reduction potential of the intermediates (E_{red} (Ethylbenzol$^{\bullet}$/ Ethylbenzol^{-}) = −1.60 V vs SCE in MeCN)[35] also exceeds the capability of the organic photocatalyst (E_{red} (Mes-Acr-Me^{+}/Mes-Acr-Me) = −0.49 V vs SCE in MeCN), a HAT co-catalyst is required.[35, 36d-f] The thiyl radical, readily formed from disulfides, is engaged in the re-oxidation of the acridinium catalyst and HAT to the neutral *C*-centered radical to form the desired hydroamidation product.

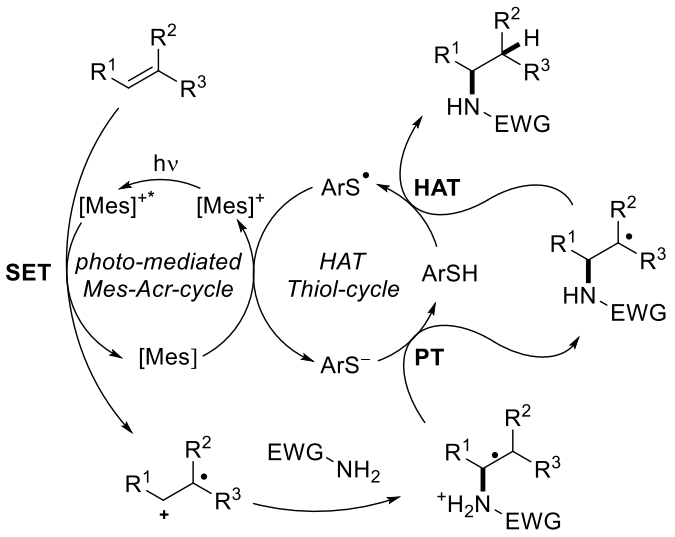

Scheme 2.5: Proposed mechanism for the hydroamination of alkenes via alkene oxidation.

In summary, both approach require an HAT-reagent to ensure the conversion of the amine-alkene adduct and the turn-over of the photoredox catalyst.[36] In previous work, a variety of thiol-based compounds have been successfully employed (Figure 2.3).[39]

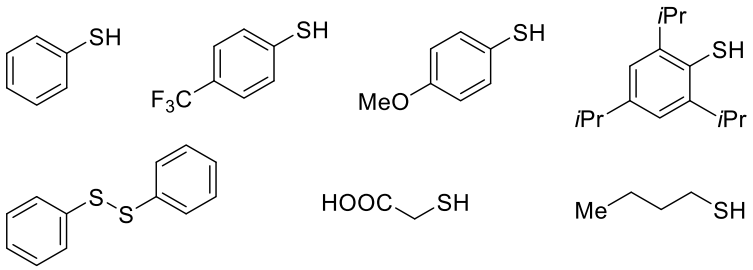

Figure 2.3: A variety of different thiol-based HAT co-catalysts.[39]

Already in 1986, the photoamination of phenanthrene and other polycyclic aromatic hydrocarbons mediated by dicyanobenzenes (DCNBs) was described by the research group of Yasuda.[40] The introduction of catalytic amounts *m*-dicyanobenzene enabled the hydroamination with ammonia and a series of primary amines (Scheme 2.6). Due to the unfavorable photophysical properties of classical cyanobenzenes, high energy mercury lamps are required in this process.

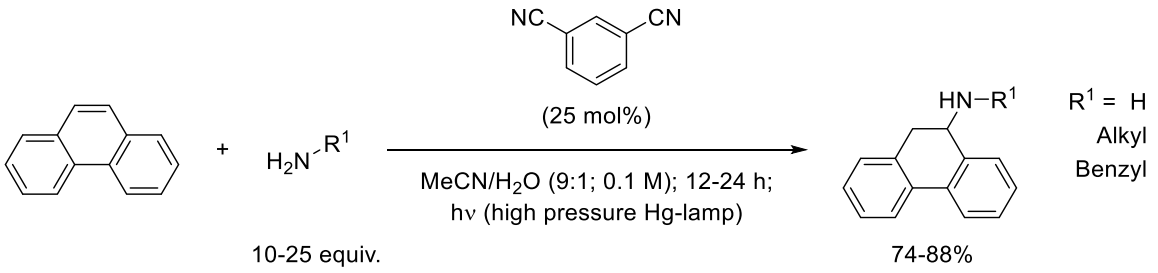

Scheme 2.6: Photo-mediated hydroamination of anthracene catalyzed by *m*-dicyanobenzene.

In the following years, Yasuda and co-workers reported several examples of the photo-mediated hydroamination of (*E*)-stilbenes using stochiometric amounts of *p*-dicyanobenzene as photoinduced electron transfer (PET) reagent (Scheme 2.7).[41] Detailed mechanistic analysis, applying Stern-Vollmer quenching experiments and Taft-Hammett correlations that the excitation of the alkene (λ_{max}((*E*)-stilbene = 295 nm) initiates the photo-mediated hydroamination reaction, followed by fluorescence quenching by the DCNB.[42]

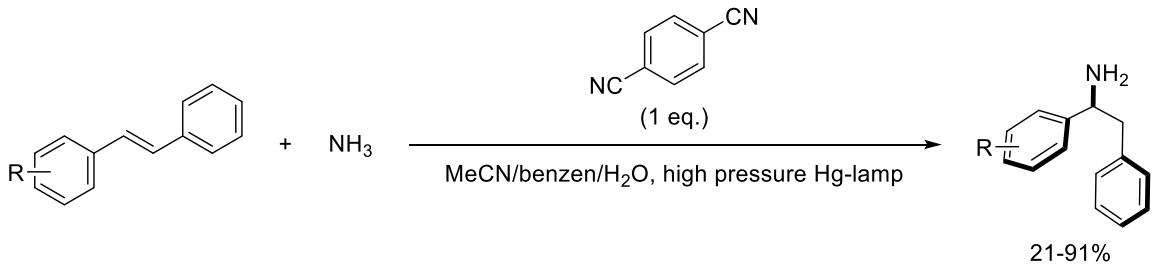

Scheme 2.7: Photo mediated hydroamination of (*E*)-stilbenes with NH_3 using high energy light.[41]

2.2 Objectives

In our research group, the organic photoredox catalyst PrPPT (**1.6**) was identified as optimal catalyst for the photo-mediated hydroamination of stilbenes. Dr. Firas El-Hage and Dr. Richy Hauptmann extensively optimized this photosynthesis and synthesized a large scope of different derivatives hydroamination products. This extensive investigation left the question of the predominant reaction mechanism. Since alkene and amine activation are described in the literature, no unequivocal pre-assumption about the reaction trajectory could be made.

In the context of this work, the aim is to elucidate the reaction mechanism, leading to a plausible postulate. The starting materials will be studied electrochemically and compared to the excited redox states of the photocatalyst. The photo-mediated hydroamination will be examined regarding competent radical reaction intermediate by electron spin resonance experiments. The resulting radical intermediates will be characterized as far as the persistence allows. Fluorescence quenching experiments can give an insight into the initial reaction step. Density functional theory calculations shall aid to understand and undermine the resulting postulate (Figure 2.4).

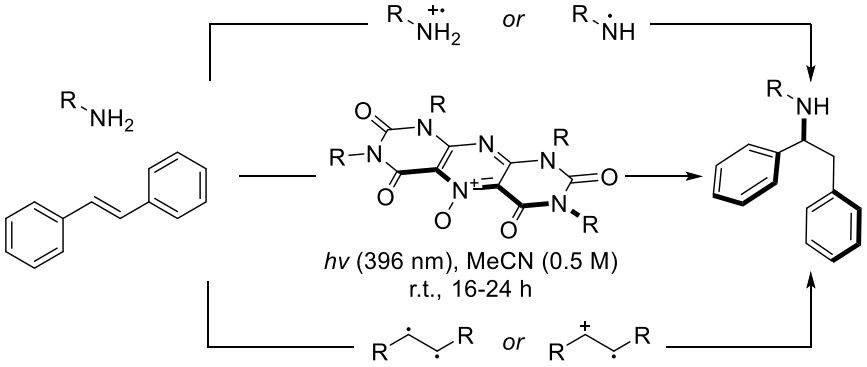

Figure 2.4: Photo mediated hydroamination of (*E*)-stilbene (2.5) utilizing PPTNO as pre-catalyst.

2.3 Results and discussion

Our group recently reported the optimized synthesis and characterization of pyrimidopteridine *N*-oxide (PPTNO) heterocycles.[15] Photo- and electrochemical analyses demonstrated that these compounds exhibit high excited state reduction potentials (E^*[PrPPTNO*/PrPPTNO$^{\bullet-}$] = +2.29 V vs SCE and +1.91 V vs Fc$^+$/Fc in MeCN). In Chapter 1 of this thesis, it was discussed and demonstrated that PPTNOs **1.1**-**1.4** serve as pre-catalyst to the unoxygenated PPTs **1.5**-**1.8**. With a similarly high excited state reduction potential ((E^*[PrPPT*/PrPPT$^{\bullet-}$] = +2.10 V vs SCE and +1.72 V vs Fc$^+$/Fc in MeCN), PrPPTs (**1.6**) provides a strong thermodynamic driving force for the oxidation of a wide range of organic substrates. In the following, the reaction trajectory of the pyrimidopteridine-catalyzed photo-mediated hydroamination of stilbenes with primary amines is discussed.

2.3.1 Electrochemical characterization of stilbenes and benzylamine

By comparing the excited state reduction potential of the catalyst with the oxidation potentials of the respective starting materials, it is possible to estimate whether a redox reaction can take place and which starting material is easier to oxidize. The electrochemical potentials were listed referenced to the Fc^+/Fc redox couple.[21] All measured voltammograms are depicted and discussed against the ferrocene reference system (Fc^+/Fc) and the final potentials are additionally listed against SCE by adding 0.38 V to the values referenced to Fc^+/Fc (Table 2.1). First, the ground-state oxidation potentials of the stilbene starting materials were determined by differential pulse voltammetry (Figure 2.5).

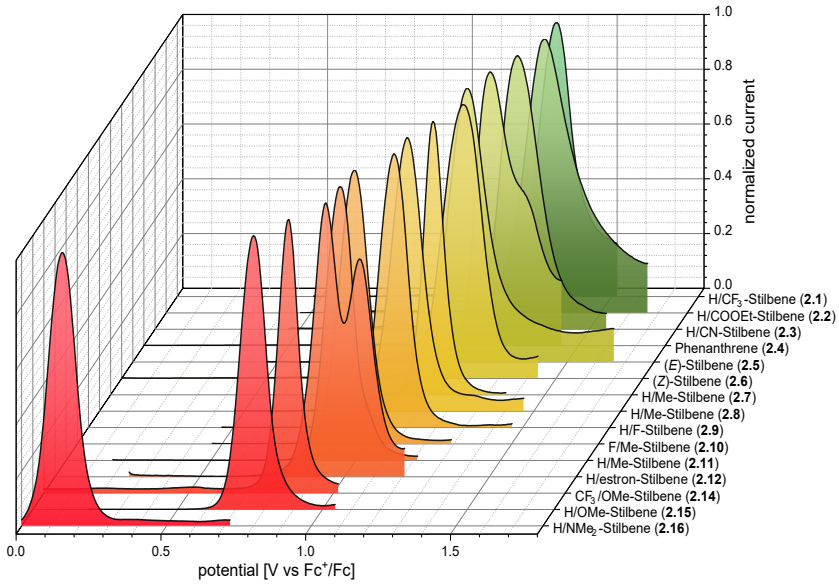

Figure 2.5: Overview of oxidation potential of various stilbenes 2.1-2.16 obtained by DPV measurements.

The DPV results of the different stilbene derivatives **2.1-2.16** are shown in Figure 2.5. It is evident that an estimation of the different oxidation potentials is clearly possible and that all single electron oxidation events are sufficiently separated to unambiguously assign the respective potentials. The different oxidation potentials of the investigated stilbenes are summarized in Table 2.1 below.

Table 2.1: Redox potentials of various stilbene derivatives and benzylamine (2.13).

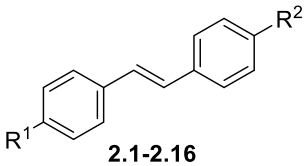

2.1-2.16

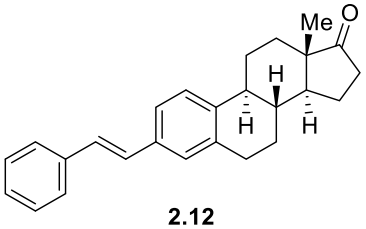

2.12

entry	R^1	R^2	note	$E_{1/2}^{red}$ [V vs Fc^+/Fc][a]	$E_{1/2}^{ox}$ [V vs Fc^+/Fc][a]	$E_{1/2}^{red}$ [V vs SCE][b]	$E_{1/2}^{ox}$ [V vs SCE][b]
1	CF_3	H	**(2.1)**	-2.95	+1.31	-2.57	+1.69
2	COOEt	H	**(2.2)**	-2.24	+1.27	-1.86	+1.65
3	CN	H	**(2.3)**	-2.21	+1.25	-1.83	+1.63
4			phenanthrene (**2.4**)	-2.92	+1.20	-2.54	+1.58
5	H	H	(*E*)-stilbene **(2.5)**	-2.68	+1.18	-2.30	+1.56
6	H	H	(*Z*)-stilbene **(2.6)**	-2.66	+1.15	-2.28	+1.53
7	Br	Br	**(2.7)**	-2.34	+1.11	-1.96	+1.49
8	OAc	H	**(2.8)**	-2.62	+1.06	-2.24	+1.44
9	F	H	**(2.9)**	-2.67	+1.06	-2.29	+1.44
10	Me	F	**(2.10)**	-2.34	+0.96	-2.35	+1.34
11	Me	H	**(2.11)**	-2.71	+0.95	-2.33	+1.33
12			**(2.12)**	-2.72	+0.94	-2.34	+1.32
13			benzylamine **(2.13)**	--	+0.91	--	+1.29
14	OMe	CF_3	**(2.14)**	-2.48	+0.85	-2.10	+1.23
15	OMe	H	**(2.15)**	-2.76	+0.76	-2.38	+1.14
16	NMe_2	H	**(2.16)**	-2.81	+0.14	-2.43	+0.52

Footnote: [a] Potentials were measured in MeCN with $TBAPF_6$ as electrolyte using cyclic voltammetry (CV) and differential pulse voltammetry (DPV) relative to Fc^+/Fc. [b] Referenced to SCE by adding 0.38 V to the value relative to Fc^+/Fc.

The voltammograms of the different stilbene starting materials showed that all stilbene derivatives can be oxidized by the excited state of pyrimidopteridine(-*N*-oxide) catalyst system. Unsubstituted *cis* and *trans* stilbenes as well as phenanthrenes show an oxidation potential of +1.15 V-+1.20 V in MeCN vs Fc^+/Fc (Table 2.1, entries 4-6). Electron-withdrawing substituents such as esters, cyano or trifluoromethyl groups increase the oxidation potential of the molecules **2.1**, **2.2** and **2.3** to +1.25 V-+1.31 V (Table 2.1, entries 1-3). Simple electron-donating substituents such as methyl, methoxy, acetoxy and fluoro groups lower the oxidation potential to +0.76 V-+1.06 V (Table 2.1, entries 8, 9, 11, 15). Stilbenes with substituents on both phenyl rings such as dibromostilbene, 4-fluoro-4'-methylstilbene and triflurmethyl-methoxystilbene (**2.7**, **2.10** and **2.14**) also show lower oxidation potentials of +0.85 V-+1.11 V (Table 2.1, entries 7, 10, 14). In the estrogen derivative **2.12**, an one oxidation potential was recorded at +0.94 V and a subsequent oxidation at +1.06 V was determined (Table 2.1, entry 12, Figure 2.5). It was noticeable that the derivative bearing a dimethylamine group **2.16** had a significantly lower oxidation potential of 0.14 V compared to all other the stilbenes (Table 2.1, entry 16).

Subsequently, the benzylamine (**2.13**) was investigated with respect to its electrochemical properties. The electrochemical measurement proved to be more challenging, which made it difficult to unambiguously assign the oxidation potential. The DP voltammogram of benzylamine (**2.13**) is depicted below (Figure 2.6).

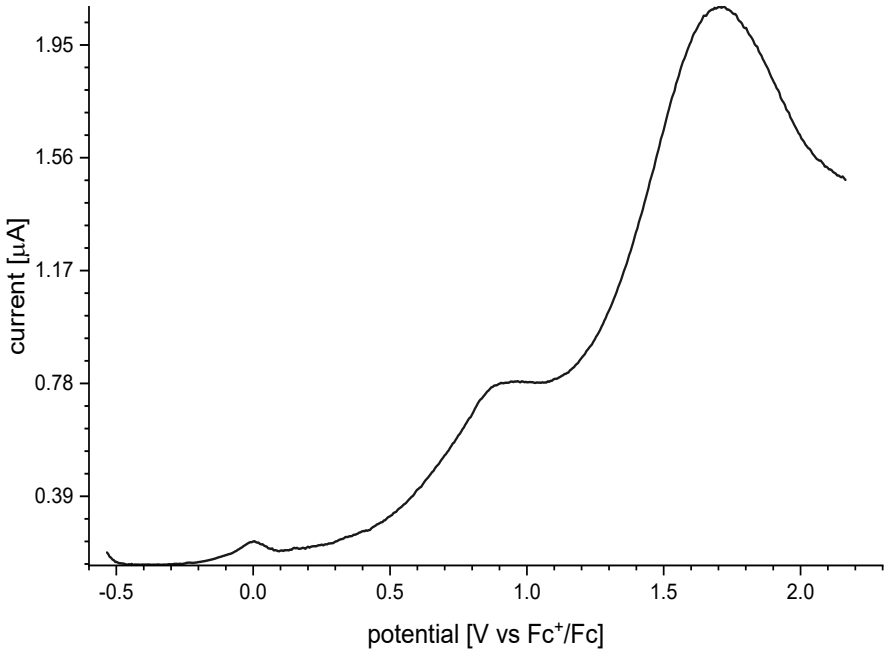

Figure 2.6: Differential pulse voltammetry of benzylamine (2.13).

The electrochemical analysis of benzylamine showed a voltammogram with broad peaks. The second oxidation potential at +1.70 V vs Fc^+/Fc can be clearly assigned. The first oxidation potential can only be estimated and was assigned at +0.91 V or less due to the overlay of the second potential. Furthermore, the first oxidation peak is broad with an onset point of +0.42 V. A similar response in the electrochemical measurement was also observed for other amines (See appendix: 5.3.2.1.2).

On the basis of the performed measurements, it can be concluded that both the oxidation of (*E*)-stilbene ((*E*)-**2.5**) ($E_{1/2}^{ox}$[(*E*)-**2.5**$^{\bullet+}$/(*E*)-**2.5**] = +1.53 V vs SCE in MeCN) and benzylamine (**2.13**) ($E_{1/2}^{ox}$[**2.13**$^{\bullet+}$/**2.13**] = +1.29 V vs SCE in MeCN) may induce a reductive quenching of the excited state photoredox catalyst **PrPPT*** (*E**[**PrPPT***/**PrPPT**$^{\bullet-}$] = +2.10 V vs SCE in MeCN). The oxidation of (*E*)-stilbene ((*E*)-**2.5**) is exergonic by −12.9 kcal·mol^{-1} and the oxidation of benzylamine (**2.13**) exergonic by −18.5 kcal·mol^{-1}.

2.3.2 Photoluminescence quenching experiments

The fluorescence spectrum of the optimal catalyst PrPPT (**1.5**) is necessary to estimate the energy in the excited state in many ways. Determining the reduction in fluorescence caused by the successive addition of a chemical compound indicates how much energy is transferred from the excited state of the catalyst to the substrate.[43] Fluorescence quenching constants of (*E*)- and (*Z*)-stilbene (**2.5** and **2.6**), (*E*)-4-methoxystilbene (**2.15**) and (*E*)-4-trifluoromethylstilbenes (**2.1**) were investigated in this respect. In addition, the fluorescence quenching properties of the primary benzylamine (**2.13**) and the secondary dibutylamine (**2.17**) were determined. All fluorescence spectra and tables with measured values are available in the appendix 5.3.2.4. The corresponding calculated quenching constants are summarized in Table 2.2.

Table 2.2: Stern-Volmer quenching constants of selected stilbene and amine derivatives.

entry	quencher	K_{SV} [M^{-1}]
1	(*E*)-CF_3-stilbene (**2.1**)	52.4
2	(*E*)-stilbene (**2.5**)	61.3
3	(*Z*)-stilbene (**2.6**)	64.5
4	(*E*)-MeO-stilbene (**2.15**)	100.8
5	benzylamine (**2.13**)	33.0
6	dibutylamine (**2.17**)	52.8

Footnote: A solution containing PrPPT (0.02 mM) and was successive titurated with 100 µL of solution containing the quencher (60 mM).

Based on the fluorescence quenching experiments, all investigated stilbenes were competent quenchers of the excited state of the PrPPT catalyst. Notably, electron-deficient substituents such as the trifluoromethyl group in **2.1** caused weaker quenching of the excited state of the catalyst (Table 2.2, entry 1). (*E*)- and (*Z*)-stilbenes (**2.5** and **2.6**) show similar quenching properties with a quenching constant of 61.3 M^{-1} and 64.5 M^{-1}, respectively (Table 2.2, entries 2-3). The more electron-rich (*E*)-4-methoxystilbene (**2.15**) exhibited the strongest fluorescence quenching performance with a quenching constant of 100.8 M^{-1} (Table 2.2, entry 4). Benzylamine (**2.13**) exhibited a significantly weaker quenching constant of 33.0 M^{-1} compared to all stilbenes (Table 2.2, entry 5). The more electron-rich dibutylamine (**2.17**), which did not provide isolable yields in the hydroamination reaction, showed comparatively higher quenching constant (Table 2.2, entry 5).

The Stern Volmer results reveal that both stilbenes and amines can quench the excited state of the PrPPT catalyst **1.6**. Based on the quenching constants of the investigated compounds, the stilbenes are twice as potent quenchers. To investigate this correlation in detail, competitive fluorescence quenching experiments were performed with benzylamine (**2.13**), (*E*)- and (*Z*)-

stilbene (**2.5** and **2.6**). The fluorescence quenching properties were investigated in the presence of the other quencher, as illustrated in Figure 2.7

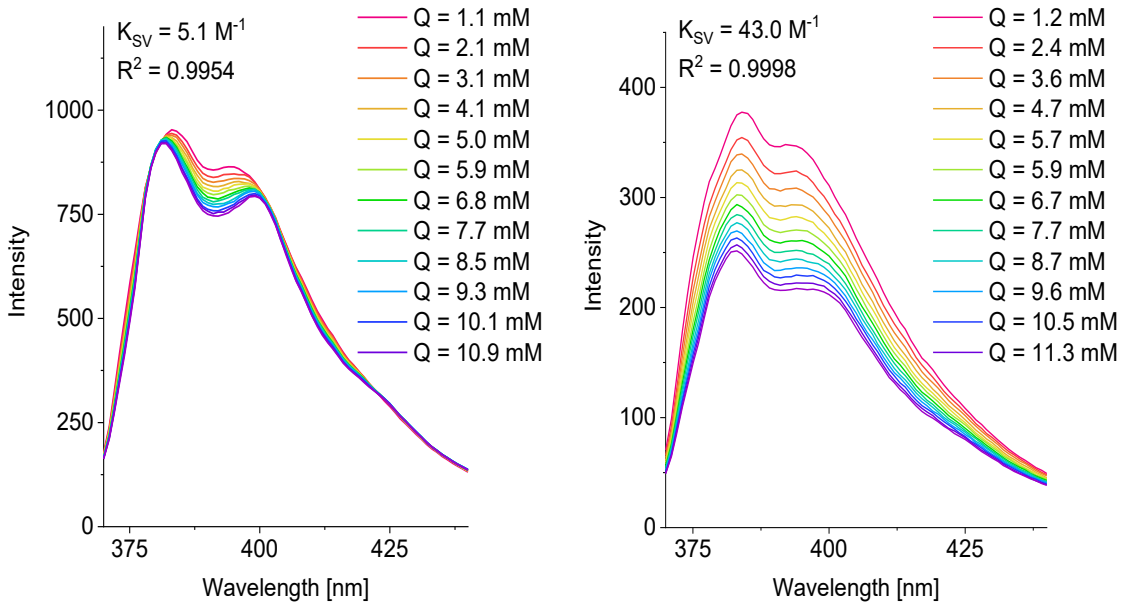

Figure 2.7: Competitive quenching of the luminescence of the excited state PrPPT*: Luminescence quenching by benzylamine (2.13) in the presence of stilbene ((*E*)-2.5) (left) and luminescence quenching by *E*-stilbene ((*E*)-2.5) in the presence of benzylamine (2.13) (right).

The competitive fluorescence quenching experiments of benzylamine and stilbenes differ clearly from the classical Stern-Volmer quenching experiment. The successive addition of benzylamine (**2.13**) to a solution containing a constant concentration of the photocatalyst PrPPT (**1.6**) and (*E*)-stilbene ((*E*)-**2.5**) only had a marginal effect on the luminescence quenching (Figure 2.7, top left). In contrast, adding stilbene to a solution of the photocatalyst PrPPT (**1.6**) and benzylamine (**2.13**) showed a distinct first-order dependence on the concentration of stilbene (Figure 2.7, top right). (*Z*)-Stilbene showed similar fluorescence quenching properties with a quenching constant of K_{SV} = 41.3 M^{-1} (Table 2.3, entry 2). The results from the competitive fluorescence quenching experiments are summarized in Table 2.3, below.

Table 2.3: Stern-Volmer quenching constants determined by competitive fluorescence quenching experiments.

entry	first quencher	K_{SV} [M^{-1}]	second quencher	K_{SV} [M^{-1}]
1	benzylamine (**2.13**)	33.0	(*E*)-stilbene (**2.5**)	43.0
2	benzylamine (**2.13**)	35.7	(*Z*)-stilbene (**2.6**)	41.3
3	(*E*)-stilbene (**2.5**)	64.5	benzylamine (**2.13**)	5.1

Footnote: A solution containing PrPPT (0.02 mM) was successively titrated to a concentration of 10 mM with a solution containing quencher Q_1 and subsequently titrated with 50 µL of a solution containing quencher Q_2 (60 mM).

A plot of the results of the fluorescence quenching experiments against the respective quencher concentration graphically illustrates the competitive Stern-Volmer quenching experiments (Figure 2.8).

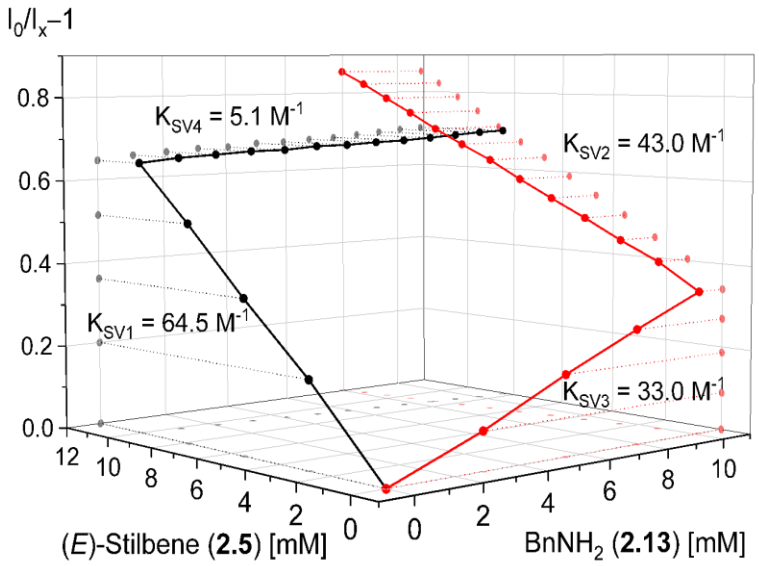

Figure 2.8: Graphic summary of classical and competitive Stern−Volmer experiments with stilbene (2.5) and benzylamine (2.13).

The results of the competitive fluorescence quenching experiment show that (*E*)-stilbene effectively quenched the excited state of the catalyst in the presence of benzylamine with a quenching constant of KSV = 43.0 M^{-1} (Table 2.3, entry 1). These experiments demonstrate that the electron transfer (ET) from stilbene to the excited state photocatalyst PrPPT* is kinetically favored over the ET from benzylamine.

2.3.3 Electron paramagnetic resonance spectroscopy

The results of the electrochemical analysis and photoluminescence quenching experiments revealed that the photochemical oxidation of both stilbenes and benzylamine (**2.13**) by the pyrimidopteridine photoredox catalyst **1.6** is thermodynamically and kinetically feasible. In the following section, both substrates are investigated concerning the formation of radical intermediates by one-electron oxidation under irradiation in the presence of the photoredox catalyst. The analysis is performed by means of electron paramagnetic resonance (EPR) spectroscopy.

The photo-mediated hydroamination can be achieved by using the pyrimidopteridine-*N*-oxide precursor as a pre-catalyst without diminishing the yield (See chapter 1.3.3). However, the following experiments were conducted exclusively with the plain pyrimidopteridine heterocycle **1.6** to avoid the number of possible radical species resulting from undesired side reactions. (*E*)-stilbene (**2.5**) was irradiated at 396 nm in the presence of PrPPT and results were examined.

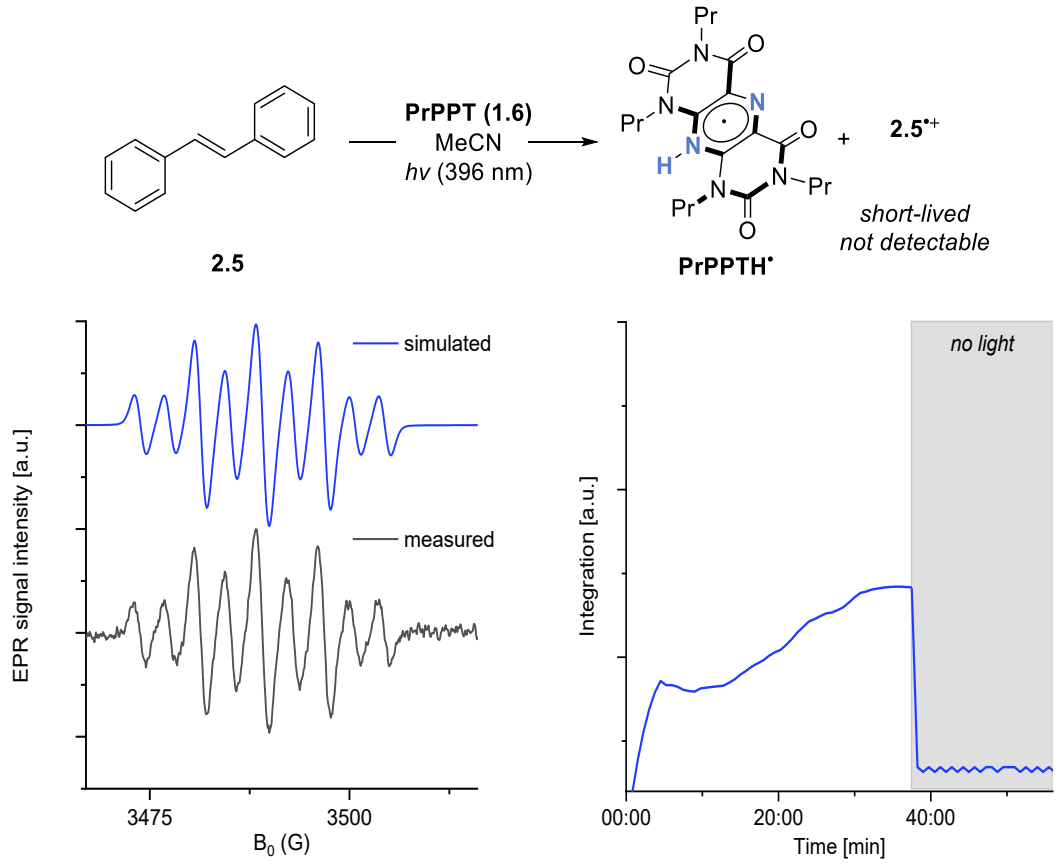

Figure 2.9: EPR spectrum of (*E*)-stilbene (2.5) and PrPPT (1.6) and a simulated spectrum considering a hyperfine splitting from two nonequivalent nitrogene nuclei and one hydrogen (blue line, A_{N1} = 7.84 G and A_{N2} = 3.72 G A_H = 7.45 G) (left) and radical accumulation through irradiation via operando EPR spectroscopy (right).

Electron paramagnetic resonance spectroscopy of a solution containing a 5:1 ratio of (*E*)-stilbene (**2.5**) and the photoactive heterocycle PrPPT (**1.6**) showed a nine-line signal at g = 2.005 upon irradiation (Figure 2.9, left, black). A simulation of the spectrum with a spin half-center (S = 1/2) interacting with two nonequivalent nitrogen nuclei (I = 1; A_{N1} = 7.84 G and A_{N2} = 3.72 G) and a hydrogen nucleus (I = 1/2; A_{N1} = 7.45 G) can assigned the radical to the PrPPT-catalyst (Figure 2.9, left, blue). An EPR experiment with d_2-deuterated (*E*)-stilbene revealed the same signal pattern as illustrated in Figure 2.9 (See Appendix). This excluded the incorporation of the alkene proton from the starting material in this hydrogen resonance. The aromatic protons of the (*E*)-stilbene or more likely the amine side chain of the catalyst and the solvent acetonitrile remains as possible hydrogen sources. The accumulation of the radical can be observed by integrating the EPR signal (Figure 2.9, right, blue). The signal of the protonated radical disappeared immediately in the absence of light.

Next, the amine starting materials were investigated. A solution containing the PrPPT catalyst and benzylamine (**2.13**) was irradiated at 396 nm and analyzed by means of EPR spectroscopy (Figure 2.10)

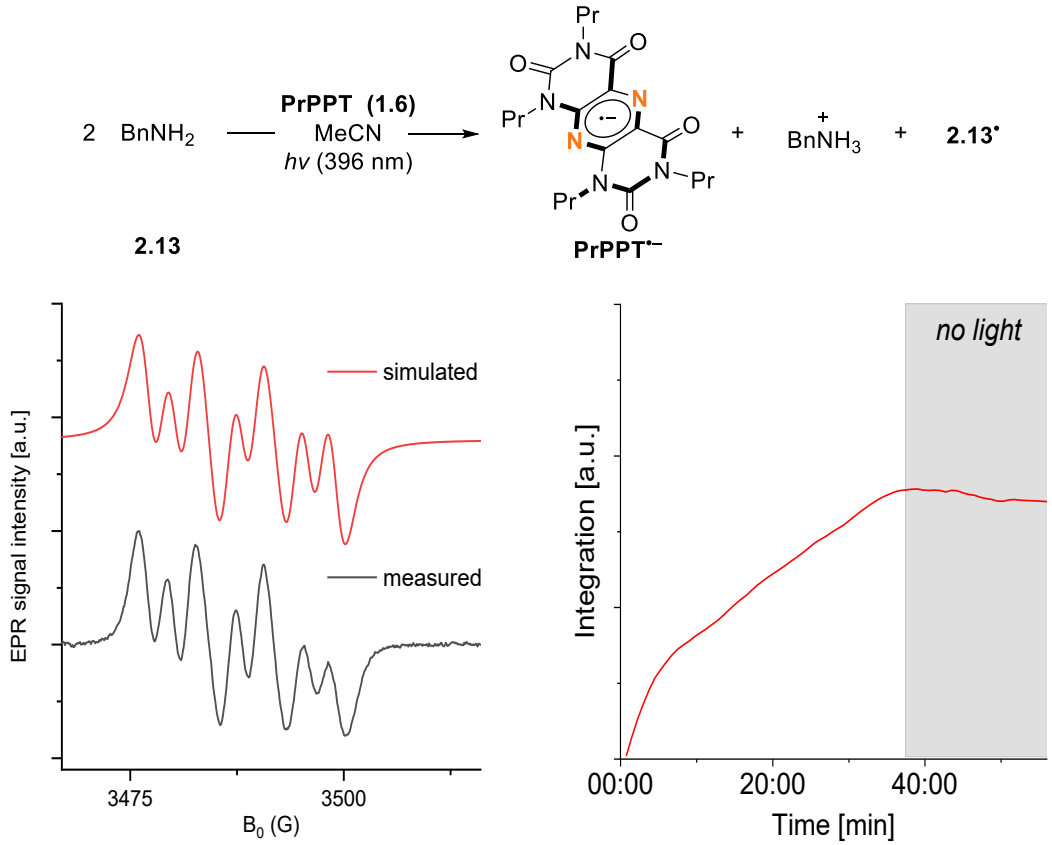

Figure 2.10: EPR spectrum of benzylamine (2.13) and PrPPT (black) and a simulated spectrum considering a hyperfine splitting from two nonequivalent N (red line, A_{N1} = 8.25 G and A_{N2} = 3.25 G) (left) and radical accumulation through irradiation via operando EPR spectroscopy (right).

The analysis of the sample containing benzylamine (**2.13**) and the heteroarene **1.6** in a 5:1 ratio showed a seven-line signal at g = 2.005 upon irradiation (Figure 2.10, left, black). The simulation of the spectrum reveals a spin half-center (S = 1/2) interacting with two inequivalent nitrogen nuclei (I = 1; A_{N1} = 7.84 G and A_{N2} = 3.72 G), which was assigned to the radical anion of the heterocycle PrPPT$^{\bullet-}$ (**1.6**$^{\bullet-}$) (Figure 2.10, left, red). Integration of the EPR spectra, revealed that the accumulated radical species possesses a long lifetime after irradiation, lasting several hours (Figure 2.10, right, red). In contrast to the measurement in an aprotic environment, no coupling with a hydrogen nucleus was observed. Based on the previous results, an initial electron transfer from benzylamine (**2.13**) to the excited state catalyst PrPPT* is undisputable. Moreover, it was shown that the radical anion of the catalyst PrPPT$^{\bullet-}$ may act as base. However, considering the amphoteric nature of amines, a proton transfer to excess amine is also conceivable. The thermodynamics of the proton-transfer from the protonated catalyst PPTH$^{\bullet}$ to benzylamine (**2.13**) was calculated applying DFT calculations. (Table 2.4).

Table 2.4: Calculated Gibbs free energies of selected compounds concerning the proton transfer from $PPTH^{\bullet-}$ to benzylamine.

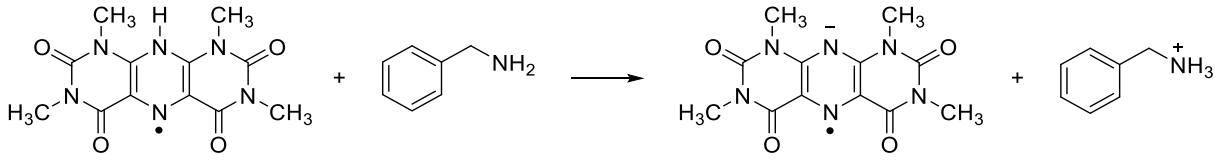

$PPTH^{\bullet}$ **$BnNH_2$ (2.13)** **$PPT^{\bullet-}$** **$BnNH_3^+$**

Entry	Compound	G [Hartree]	G [kcal·mol^{-1}]
1	**$PPTH^{\bullet}$**	1094.413940	686755.262513
2	**$BnNH_2$**	326.821509	205083.63701
3	**$PPT^{\bullet-}$**	1093.963957	686472.893857
4	**$BnNH_3^+$**	327.280673	205371.76683

Footnote: All calculations were carried out using Gaussian 16 program. [44] Geometry optimization was carried out in gas phase at the B3PW91[45] level with the all-electron TZVP[46] under the consideration of solvation effect of acetonitrile as solvent based on solute electron density (SMD[47]) and van der Waals dispersion (GD3BJ[48]).

The calculation confirmed that the deprotonation of the protonated catalyst $PPTH^{\bullet}$ by benzylamine (**2.13**) is exergonic by −5.76 kcal/mol. As a consequent, a competitive proton abstraction by excess amine is feasible. The separation of the radical and the accompanying charge impairs the back-electron-transfer (BET) which may serve as explanation for the longevity of the recorded radical.

Next, the EPR behavior of a solution containing both substrates was investigated. The solution contained equimolar amounts of (*E*)-stilbene (**2.5**), benzylamine (**2.13**) and the PrPPT photocatalyst and was irradiated at 396 nm.

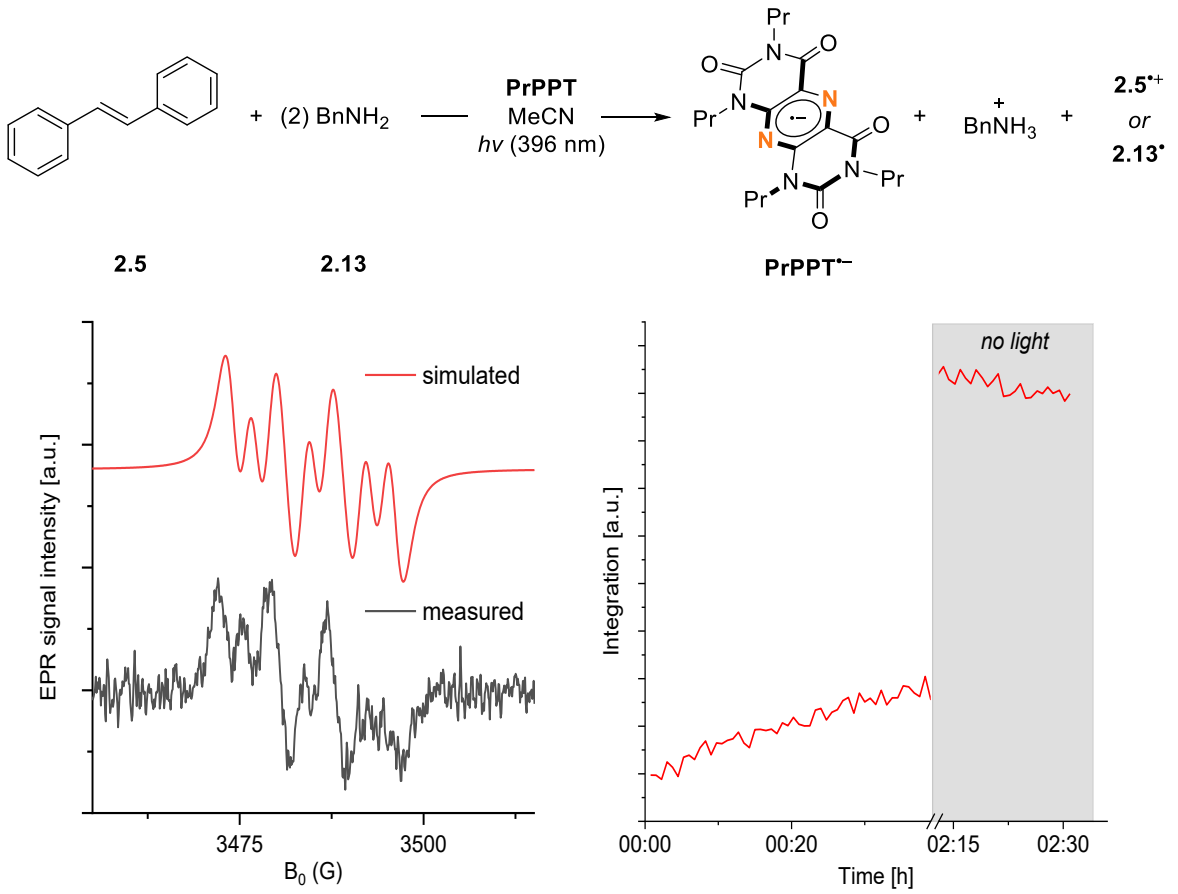

Figure 2.11: EPR spectrum of benzylamine (2.13), stilbene (2.5) and PrPPT (black) and a simulated spectrum considering a hyperfine splitting from two nonequivalent *N* (red line, A_{N1} = 8.25 G and A_{N2} = 3.25 G) (left) and radical accumulation through irradiation via operando EPR spectroscopy (right).

Due to the overall lower concentration of the starting materials, a weaker EPR signal was observed. Nevertheless, the accumulation of a nine-line signal at g = 2.005 was evident. The simulation of the spectrum revealed a spin half-center (S = 1/2) interacting with two unequal nitrogen nuclei (I = 1; A_{N1} = 7.84 G and A_{N2} = 3.72 G), which was assigned to the radical anion of the PrPPT catalyst (Figure 2.6, left, red). Based on the slower accumulation of the radical due to the low concentration, this experiment was irradiated for a longer time of 2 hours. The radical persists after irradiation and a slow degradation was observed.

2.3.4 Photo-mediated amine oxidation by pyrimidopteridines

The persistent radical intermediate formed upon irradiation of the organic photoredox catalyst **1.6** in the presence of an amine was further investigated by means of UV-vis spectroscopy. Differential UV-vis absorption spectra of a solution containing benzylamine (**2.13**) and PrPPT (**1.6**) in acetonitrile were recorded after irradiation at 396 nm in a cuvette. The absorption spectra were recorded in 5 minute intervals.

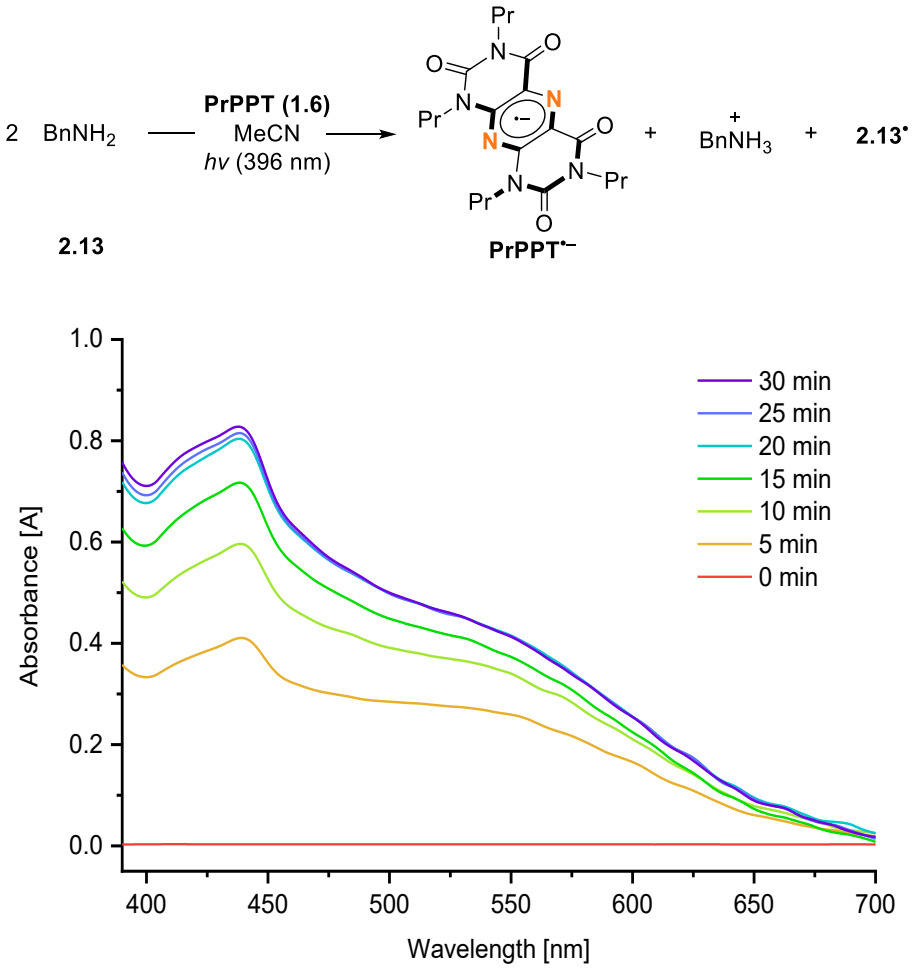

Figure 2.12: Differential UV-vis absorption spectra of a solution containing benzylamine (31 mM) and PrPPT (15 mM). Irradiated at 396 nm for the indicated time.

An alteration of the absorption spectra was quickly evident after irradiation at 396 nm. The accumulation reached saturation after approximately 20 min of irradiation, after which only minor changes in the absorption spectra were observed. A strong transient absorption at 439 nm and broad absorption in the 540 nm region was observed.

Next, the photochemically generated, stable radical resulting from the irradiation of a solution containing benzylamine (**2.13**) and the tetrapropylpyrimidopteridine photoredox catalyst **1.6** was investigated in an NMR experiment. In the following experiment, a solution containing PrPPT (**1.6**) and benzylamine (**2.13**) in a 1:2 ratio was irradiated at 396 nm. After the indicated

time, the irradiation was interrupted and a ^{1}H NMR spectrum was recorded. Subsequently, the irradiation was continued.

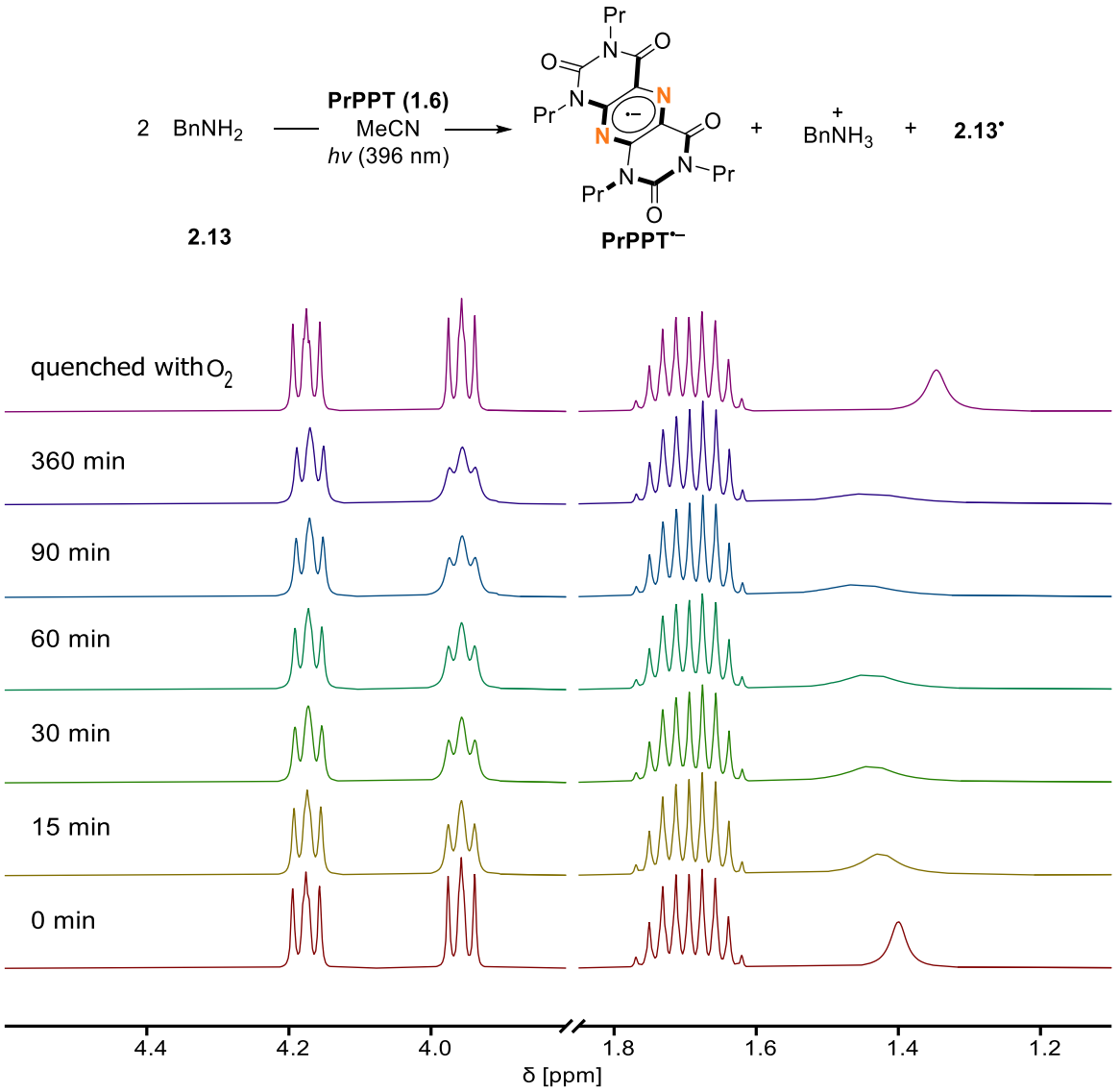

Figure 2.13: ^{1}H NMR spectra of PrPPT (1.6) and benzylamine (2.13) under irradiation at 396 nm. Irradiation time as indicated and after quenching with oxygen.

During the NMR experiment, the changes in the chemical shift and peak shapes of a 1:2 mixture of the activated catalyst PrPPT (**1.6**) and benzylamine (**2.13**) were tracked (Figure 2.13). It was evident that the protons of the amine underwent a shift from a sharp signal at 1.40 ppm to a broad signal at 1.46 ppm. Simultaneously, the peaks of the methylene groups adjacent to the nitrogen atoms in positions 3 and 7 of the heteroarene core broadened. After quenching with oxygen, the original peak shapes were reinstated. The protic protons of benzylamine experienced a slight shift up-field.

The spectroscopic analysis of the amine oxidation by the photo-excited pyrimidopteridine PrPPT (**1.6**) indicates the presence of an aminyl radical species. With an expected absorbance

in the region between 400 and 600 nm.[49] However, descriptions of aminyl radicals are relatively scarce in literature.[50]

Two experiments performed by Dr. Richy Hauptmann showed that under similar conditions the stereogenic center of α-chiral amines is completely preserved and no ring-opening reactions were detected with cyclopropylamine upon irradiation in the presence of PrPPT (**1.6**).[51] The difficulty in sustaining the stereo information of α-chiral amines is associated with the drastic acidification of the α-amino C−H bond (ΔpKa(α-C−H) ≈ −30) and a resulting decreased α-C−H bond dissociation energy (ΔBDFE(α-C−H) ≈ −45 kcal·mol^{-1}) upon single electron oxidation of an amine to the aminium radical leading to α-deprotonation and racemization of the stereogenic center.[30e, 33, 52] Furthermore, resonance delocalization of the unpaired spin of the *N*-centered radical cation would lead to C−C bond scission in cyclopropylamine.

In contrast, according to an account published by Zipse and co-workers, the stabilization of alkyl aminyl radicals occurs through hyperconjugantion between the unpaired spin and adjacent C–H or C–C bonds, respectively. This type of hyperconjugation leads to a stabilization of the *N*-centered radical of approximately −30 kJ·mol^{-1} for primary amines.[53] Interestingly, this stabilizing effect is most pronounced in *N*-centered cyclopropylamine and dicyclopropylamine radicals accounting for −44.4 kJ·mol^{-1} and −78.9 kJ·mol^{-1}, respectively.

2.3.5 Light on-light off experiment

On the basis of the conducted measurements of redox potentials, luminescence quenching studies and the investigation of transient radical species by EPR, NMR and UV-vis absorption spectroscopy, a simple light-on-off experiment aided to deduce a mechanistic postulate. In this experiment, carried out by Dr. Firas El-Hage, the product formation of the hydroamination of (*E*)-stilbene (**2.5**) with benzylamine (**2.13**) was followed by calibrated GC.[24] Over the course of 12 hours, the irradiation was interrupted at two-hour intervals. Samples were collected before and after each cycle and the conversion to the desired hydroamination product **2.18** was determined.

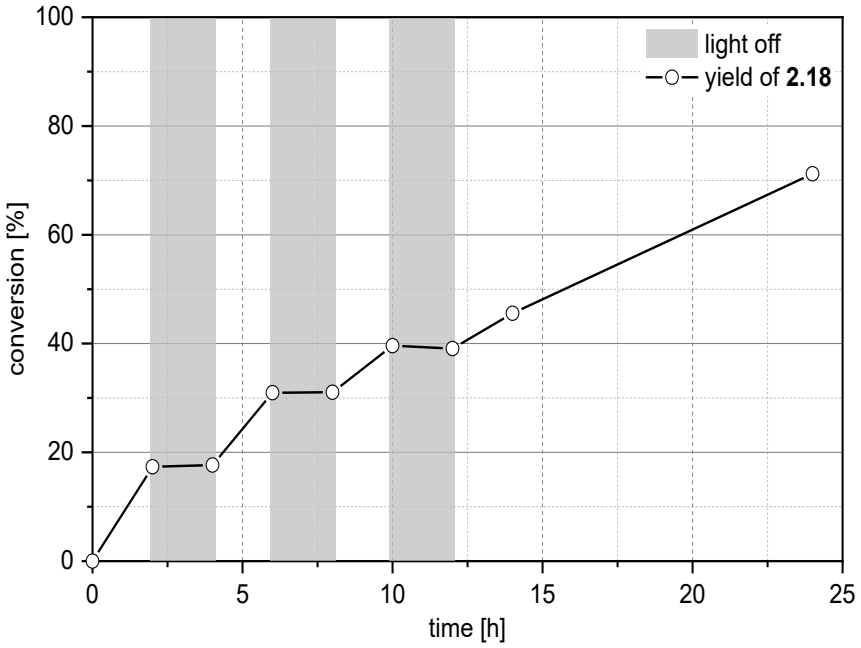

Figure 2.14: Reaction monitoring by calibrated GC using biphenyl as internal standard (experiment performed by Dr. Firas El-Hage).

The results reveal that the product was formed only during irradiation. No product formation was detected in the dark. Thus, a radical propagation mechanism could be excluded. Furthermore, the involvement of the accumulated persistent catalyst radical, which was observed in the EPR experiments by irradiating benzylamine (**2.13**) with the photocatalyst **1.6**, is unlikely to serve as catalytically active intermediate. Regarding the longevity of the radical species formed from benzylamine and the photoredox catalyst, product formation in the absence of light would be conceivable.

2.3.6 Density functional theory calculations

Density functional theory (DFT) calculations at a B3PW91 level of theory were employed to evaluate the assumption of stilbene activation. Due to the analogous properties of the different alkyl substituents of the pyrimidopteridines, the methyl-substituted MePPT was used as model

catalyst. The results of the calculations of the different intermediates are summarized in Figure 2.15.

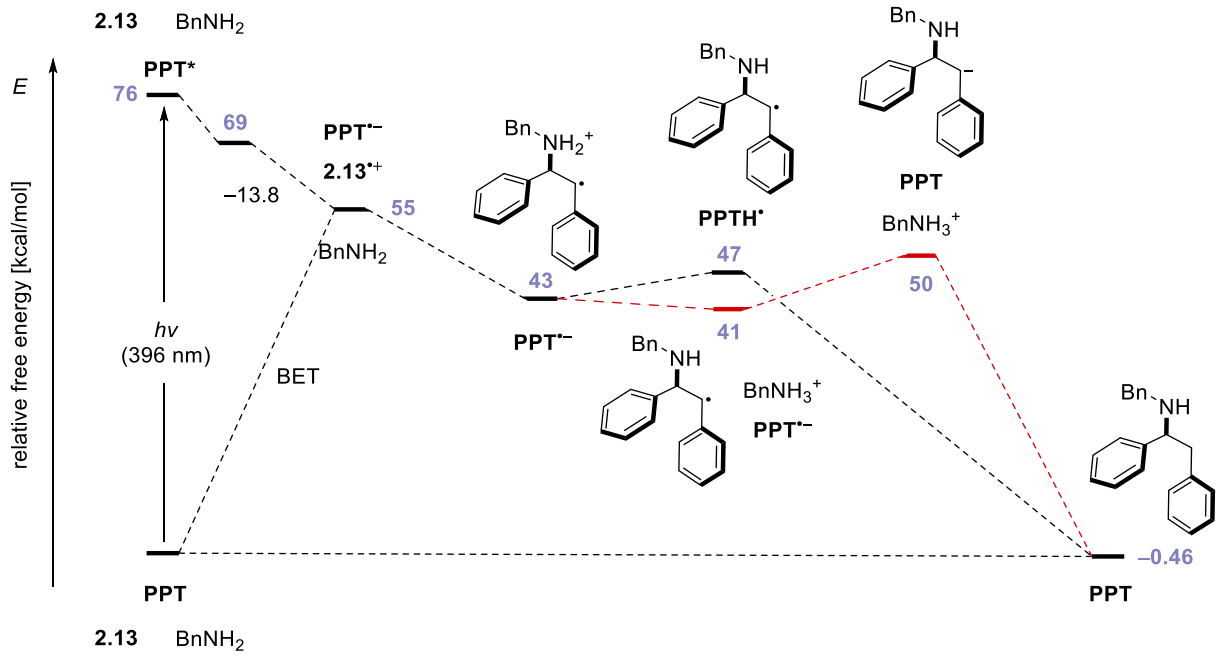

Figure 2.15: Calculation of free energy values in the proposed energy profile.

The overall reaction was calculated to be slightly endergonic by −0.46 kcal/mol (Figure 2.15).. However, a high activation barrier and orbital miss-match prohibits the direct addition of an amine to alkenes. The mechanism indisputably commences with the excitation of the photocatalyst. The potential energy of the excited state has been estimated to be 3.30 eV (76 kcal/mol) (see Chapter 1.3.2). The intermolecular back electron transfer (BET) between (*E*)-stilbene and the MePPT catalyst was calculated to account for 55 kcal/mol. Utilizing the excited state reduction potential of MePPT (*E**[**MePPT*/MePPT**$^{\bullet-}$] = +1.75 V vs Fc^+/Fc in MeCN) and the oxidation potential of (*E*)-stilbene ($E_{1/2}^{ox}$ = +1.15 V vs Fc^+/Fc in MeCN)., an energy difference of −13.8 kcal/mol was determined (equation 2.1).

$$\Delta G = (1.15 - 1.75) * 23.06 \frac{kcal}{mol} = -13.8\ kcal/mol \qquad \text{(equation 2.1)}$$

Accordingly, the required 69 kcal/mol serves as the estimated energy of MePPT in the excited state. The nucleophilic attack of benzylamine on the radical cation of stilbene was calculated to have an energy difference of −11.6 kcal/mol. The subsequent deprotonation of the adduct by the catalyst was calculated to be endothermic by 3.52 kcal/mol. The hydrogen atom transfer (HAT) reaction from the protonated radical catalyst PPTH$^{\bullet}$ was calculated from the Gibbs free energies of the products and substrates accounting for an energy gain of −47.4 kcal/mol.

Alternatively, benzylamine may act as a base and deprotonate the initial amine-stilbene radical cation adduct. However, this reaction trajectory would necessitate a subsequent direct

reduction of the C-centered radical which is thermodynamically unfavorable ($E_{1/2}^{red}$= −1.60 V vs SCE in MeCN for ethylenebenzene).[35]

2.3.7 Proposed reaction mechanism

The results from the EPR, Stern-Volmer, and the light-on light-off experiments suggested that the mechanism proceeds via activation of the alkene function. A postulated mechanism for the photo-mediated pyrimido-pteridine (PPT)-catalyzed hydroamination of stilbenes is shown in Figure 2.16.

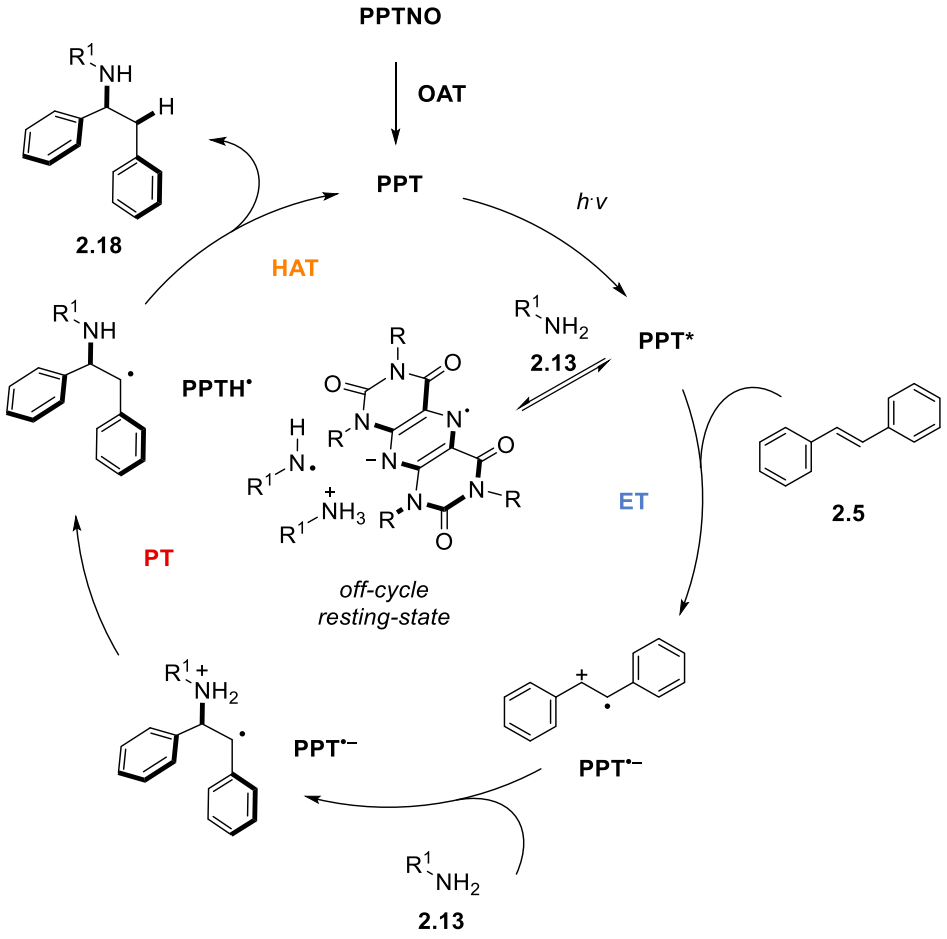

Figure 2.16: Plausible catalytic cycle of the photo-mediated hydroamination via stilbene oxidation.

The reaction sequence commences with the activation of the catalyst precursor **PrPPTNO** (ε_{396} = 1066 $M^{-1}{\cdot}cm^{-1}$) through oxygen atom transfer to stilbene to form stilbene oxide and the photoredox active hydroamination catalyst **PrPPT** (also see Chapter 1.3.1). The catalytic cycle starts with the excitation of the **PrPPT** (ε_{396} = 40 $M^{-1}{\cdot}cm^{-1}$) to **PrPPT*** bearing a high excited state reduction potential of *E**[PrPPT*/PrPPT$^{\bullet-}$] = +2.13 V. Predominantly, stilbene ($E_{1/2}^{ox}$[**2.5**$^{\bullet+}$/**2.5**] = +1.53 V vs SCE in MeCN) reacts with the excited state of PrPPT via a single electron transfer. However, benzylamine ($E_{1/2}^{ox}$[**2.13**$^{\bullet+}$/**2.13**] = +1.29 V vs SCE in MeCN) also

reacts with the catalyst to form a resting state. The oxidized cationic stilbene reacts with the primary amine to form the *C*-centered radical intermediate. Based on the computer simulation and the EPR results, a proton transfer onto the catalyst is suggested. Subsequently, hydrogen atom transfer from the protonated catalyst PrPPTH^{-} to the benzyl radical form the desired product. This assumption is further supported by the absence of an HAT cocatalyst. To substantiate the theory of the HAT reaction, the mechanism was investigated using density functional theory calculations.

2.3.8 Proof of concept

Optimization of the ratios between (*E*)-stilbene and benzylamine exhibited the highest yield at a ratio of 1:5 (yield: 73%), followed by the inverse 2:1 ratio (65%) (see dissertation: Richy Hauptmann).[51] The preceding mechanistic investigation suggests that an excess of amines favors the formation of an off-cycle intermediate. The imbalance should be especially pronounced for examples of electron-deficient stilbenes that possess higher oxidation potentials. Therefore, it should be investigated whether an increase in the overall yield can be observed with excess stilbenes. Electron-deficient stilbenes are converted with benzylamine in a 2:1 ratio. The pre-catalyst PrPPTNO was used to ensure comparability with the previously obtained scope (Table 2.5).

Table 2.5: Selected examples of the hydroamination of electron-deficient stilbenes with varying substrate ratios.

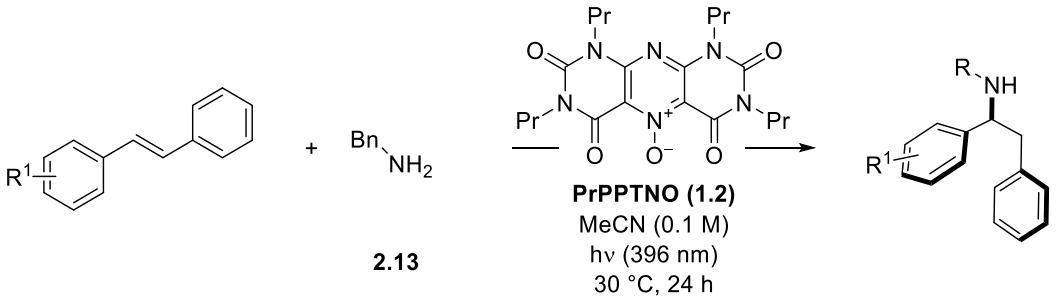

entry	substrate		product		isol. yield [1:5-Ratio]	isol. yield [2:1-Ratio]
1	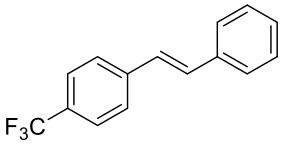	**2.1**	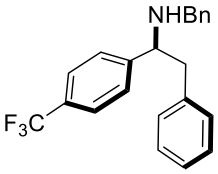	**2.19**	32%	42%
2	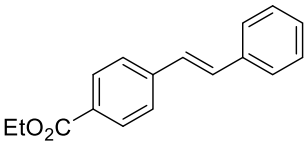	**2.2**	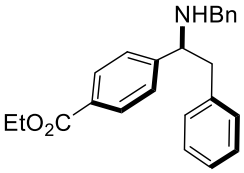	**2.20**	40%	49%
3	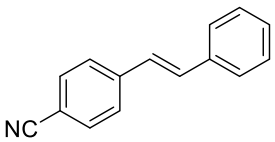	**2.3**	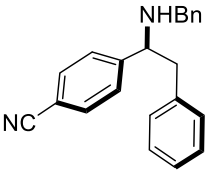	**2.21**	37%	45%

Footnote: The reaction was carried out with 0.5 mmol benzylamine (0.1 M), 2 equiv. stilbene and a catalyst loading of 5 mol% PrPPTNO. Isolated yields correspond to the average of two reactions.

Indeed, an inversion of the substrate ratios had a positive effect on the yield of the hydroamination product from electron-deficient stilbene derivatives. The trifluoromethyl derivative **2.1** was successfully converted and the corresponding product **2.19** was obtained in an isolated yield of 42% (Table 2.5, entry 1). Similarly, the ethyl ester-bearing stilbene **2.2** yielded an isolated yield of 49% (Table 2.5, entry 1). Similarly, the cyano-derivative (**2.21**) was isolated in 45% yield (Table 2.5, entry 2).

2.4 Conclusion

In conclusion, comprehensive mechanistic experiments concerning the reaction trajectory of the photochemical pyrimidopteridine-catalyzed hydroamination of (*E*)-stilbenes and primary amines allowed to provide a detailed proposal on the reaction mechanism.

The oxidation potentials of various (*E*)-stilbene derivatives and amines were successfully determined by cyclo-voltametric and differential-pulse-voltametric measurements. In electron paramagnetic resonance experiments, different radical species were observed with both reactants. The protonation of the radical anionic intermediated of the photoredox catalyst in an aprotic reaction environment was evident. In a protic environment, a long-lived radical species was formed presumably associated with a charge-separated radical pair. The persistent catalyst radical formed by irradiation of the catalyst in the presence of benzylamine was additionally analyzed by NMR and UV-vis spectroscopy. Involvement of this persistent radical in the reaction was ruled out based on the results of an on-off experiment. Moreover, a radical propagation mechanism was excluded. In classical and competitive fluorescence quenching experiments, it was shown that the stilbenes quench the excited state of the catalyst more efficiently than the benzylamine. Finally, a conceivable mechanism was postulated, which was further supported by quantum chemical calculations. Based on the findings of the reaction mechanism, the reaction conditions were adjusted, leading to an increase in yield.

3 Oxyfunctionalization through photoinduced oxygen atom transfer of pyridine *N*-oxide

3.1 Introduction

The hydroxyl functionality is of paramount importance in natural products, agrochemicals, and pharmaceuticals.[54] In nature, the implementation of C−OH bonds is routinely achieved by the direct oxygenation of C−H bonds by monooxygenase enzymes. This strategy converts hydrophobic into hydrophilic compounds which facilitates renal excretion or installs a reactive handle for further transformations in living organisms.[55]

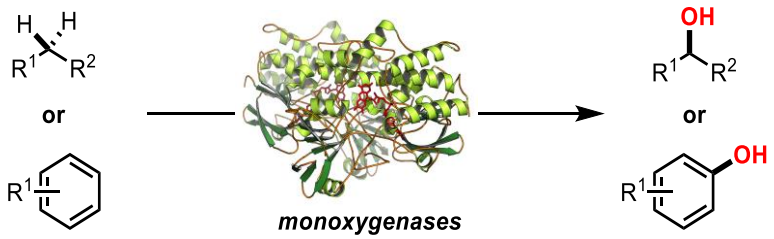

Figure 3.1: Hydroxylation of aliphatic as well as aromatic C–H bonds by monooxygenase enzymes.[56]

In nature, the oxidation of C–H bonds is routinely performed by highly selective enzymes and their tailored reaction sites.[57] These enzymatic methods provide a powerful means for the oxidation of small molecules under mild reaction conditions. Nevertheless, universal application of these methods in synthetic organic laboratories is hindered by the need for highly specialized equipment and generally low space-time yields.[58] Therefore, the development of a chemical equivalent of mammalian monooxygenase enzymes is of particular relevance to address the challenging highly selective late-stage functionalization of advanced intermediates for the synthesis of pharmaceutical and xenobiotic metabolites.

Currently, most catalytic methods for the oxidation of C−H bonds rely on transition metal catalysts.[59] Alternatively, recent research indicates that the design and use of non-metallic variants is a valuable extension to the existing methodological repertoire. This involves the application of oxidants such as peracids[60], dioxiranes[61] and perfluorinated oxaziridines.[62] However, the high reactivity and selectivity of these oxygen atom transfer (OAT) reagents is also associated with elaborate syntheses and increased hazardous potential.[62c]

Upon ultraviolet irradiation of pyridinium ylides and *N*-oxides, fragmentation of exocyclic polar bonds occurs, releasing highly reactive intermediates (Figure 3.2).[63] Whereas it is generally assumed that reactions of pyridinium methylides and iminopyridinium ylides proceed

via carbene and nitrene intermediates, respectively,[64] the mechanism of photomediated oxygen atom transfer is still ambiguous. Mechanistic proposals for the oxygen atom transfer mechanism range from the involvement of atomic oxygen (oxene), oxygen as a radical anion; and transfer via oxazaridine intermediates to a nitroxyl radical species.[65]

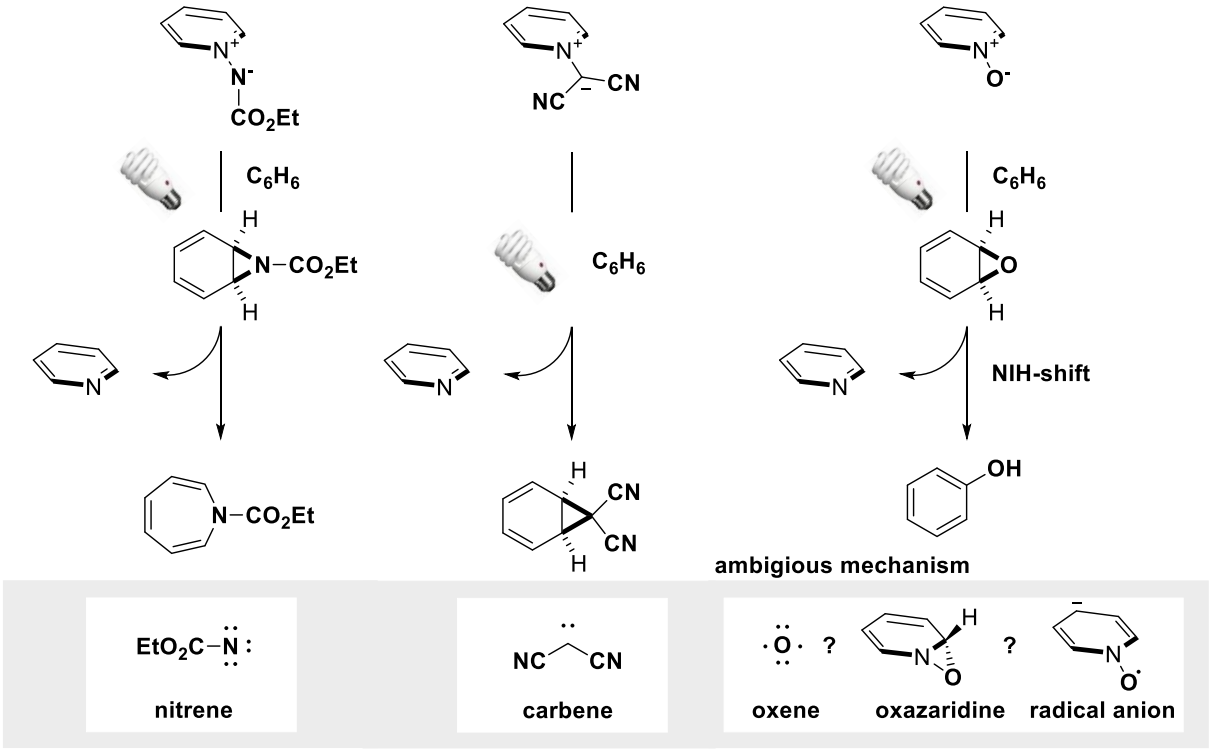

Figure 3.2: Photoinduced generation of reactive intermediates from *N*-substituted pyridines.[66]

Photo-mediated oxygen atom transfer (POAT) has been achieved by pyrimidopteridine-*N*-oxides (PPT) as mentioned in Chapter 1. Moreover, intramolecular POAT to electron-rich arenes tethered to 1-benzylisoquinoline 2-oxides was reported by Perez-Inestrosa.[67] The regioselectivity of the phenol synthesis is mostly governed by the rules of electrophilic aromatic substitution and is suggested to proceed via a Wieland intermediate.[68]

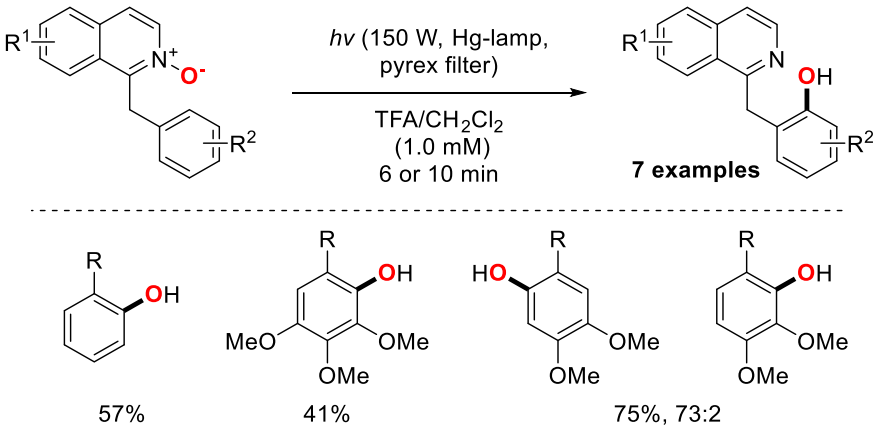

Figure 3.3: Photochemical transfer-hydroxylation in electron donor–acceptor systems.[14]

Another interesting class of compounds, which is becoming increasingly prominent, is the class of pyridinium salts.[69] Recently, the *N*-functionalized pyridinium core emerged as a promising new scaffold for redox-active reagents, allowing the generation of a wide range of synthetically important radicals (Figure 3.4).

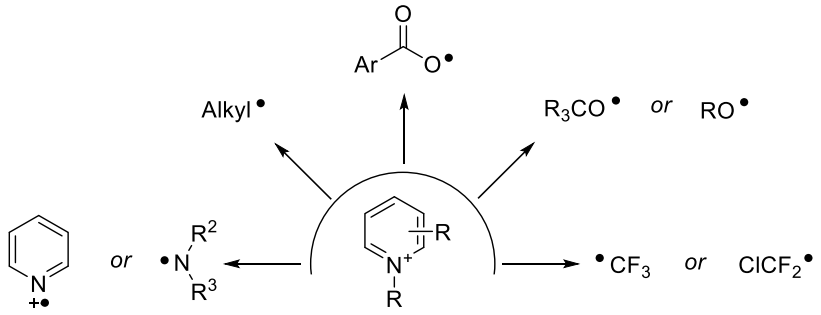

Figure 3.4: *N*-Functionalized pyridinium derivatives as radical precursors.[69]

The radical is generated by single electron reduction of the pyridinium cation. The electron occupies the energetically low-lying π^* LUMO. In order to enable the N–X bond cleavage, the electron must enter the orthogonal σ^*-orbital.[70] The mixing of the π^*- and σ^*-states in the planar radical is symmetrically forbidden and occurs when the N–X bond is bent out of the ring plane. The resulting three electron bond situation N∴X leads to N–X bond cleavage resulting in the corresponding X- or N-centered radical (Figure 3.5).

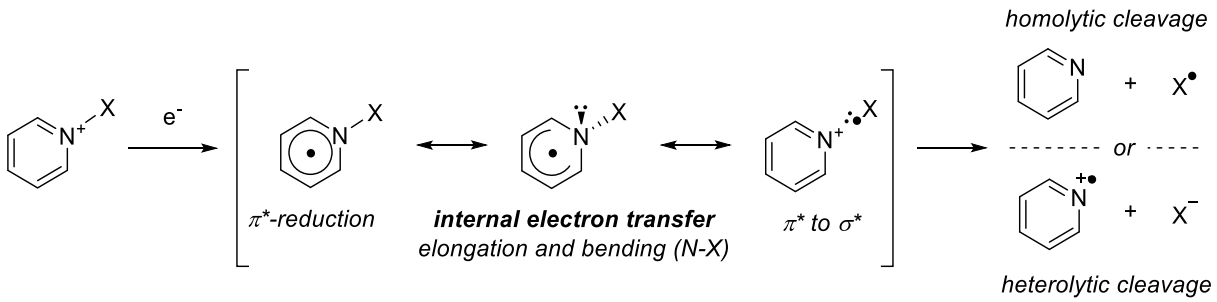

Figure 3.5: Simplified mechanistic approximation for the reductive cleavage of *N*-functionalized pyridinium compounds.[63, 70]

Depending on the electronic property of the N–X bond, various radical intermediates can be formed.[63] Strong electron-withdrawing substituents favor heterolytic fragmentation and generate pyridyl radical cations. In contrast, a variety of substituents preferentially lead to the formation of X-centered radicals. Remarkably, the single-electron reduction of alkyl and aryl pyridinium leads to stable intermediates and does not result in fragmentation (Figure 3.6).

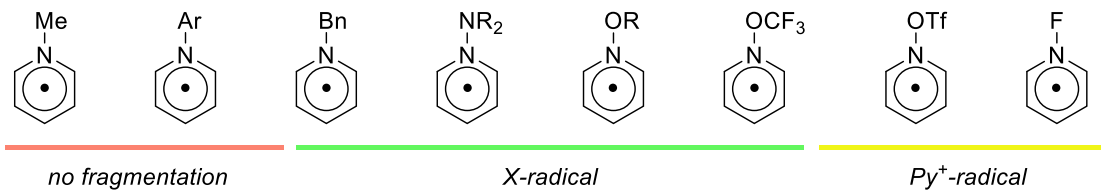

Figure 3.6: Fragmentation of representative *N*-substituted pyridinium compounds.[63]

The pyridinium moiety offers multifaceted possibilities of electronic and steric modifications, allowing fine-tuning of the reactivity for specific applications.[63] Electron donating and withdrawing substituents can change the reduction potential of the pyridinium structure which affects the initial single electron transfer. The of stabilizing the respective radical intermediate affects the N−X bond cleavage. Furthermore, substitution of the electrophilic position prevents undesired side reactions (Figure 3.7).

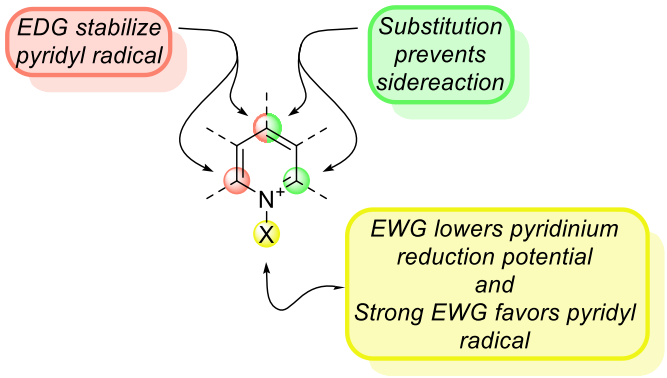

Figure 3.7: Substituent-effects of *N*-functionalized pyridinium salts.

In 2019, Tongi and Carreira published the photo mediated generation of the a cationic pyridyl radical.[71] The reaction occurs through the single-electron reduction of (trifluoromethyl-sulfonyloxy)pyridinium trifluoromethanesulfonate with the transition metal catalyst tris(2,2′-bipyridine) ruthenium hexafluorophosphate. The electrophilic pyridyl intermediates was successfully used for aromatic amination (Scheme 3.1)

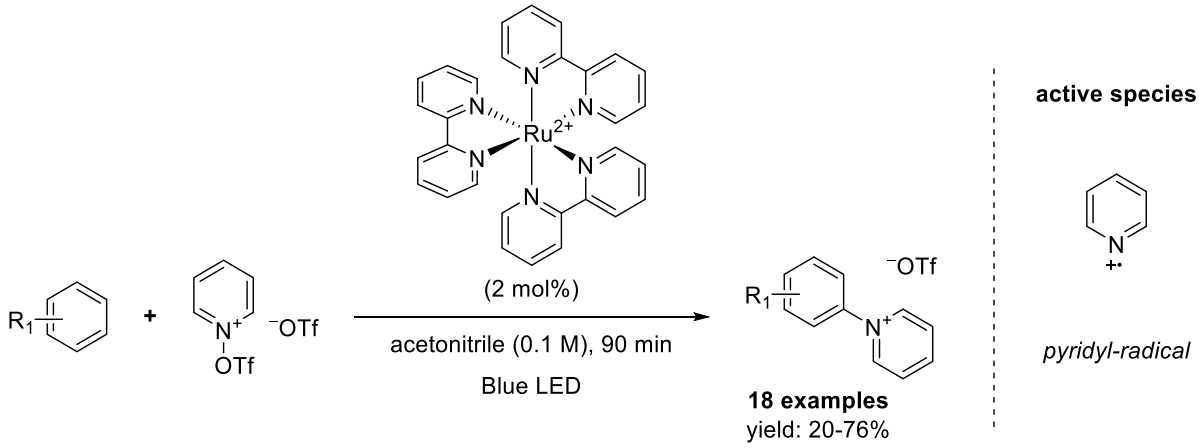

Scheme 3.1: Photo mediated C–H amination through a pyridyl radical cation.[71]

The group of Stephenson described the utilization of pyridine *N*-oxide derivatives in association with trifluoroacetic anhydride results in the in-situ formation of a pyridinium salt.[72] Single electron reduction of the transition metal catalyst leads to the formation of the trifluoroacetate radical, which rapidly undergoes decarboxylation. The resulting trifluoromethyl radical was used in electrophilic aromatic substitution (Scheme 3.2).

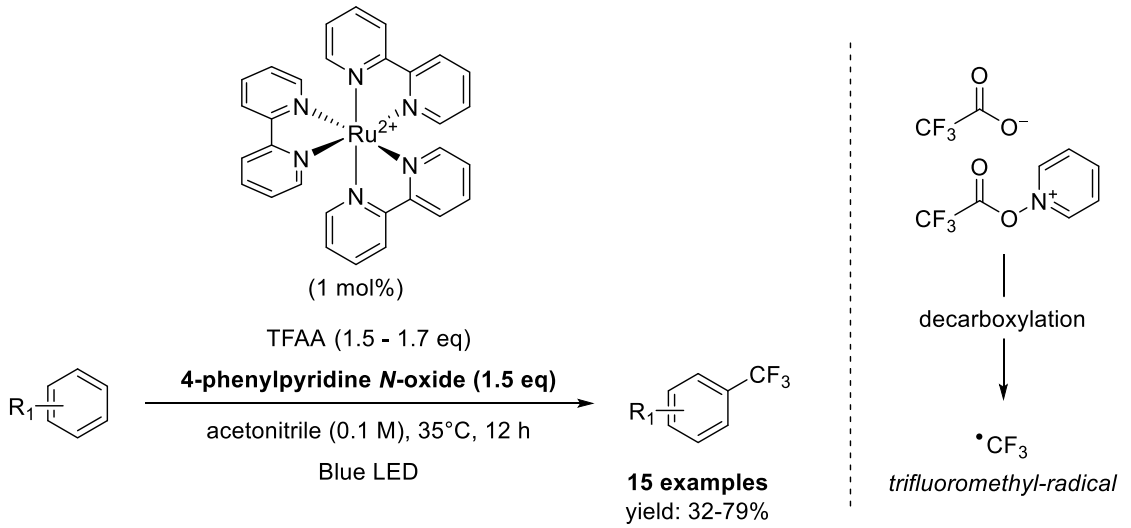

Scheme 3.2: Photochemical trifluoromethylation with pyridine *N*-oxide.[72]

Notable research on photochemical oxidation has been described by the group of Ritter. Bis(methanesulfonyl) peroxides was used as oxidant.[73] The irradiation in the presence of the transition metal catalyst converts the arene into the corresponding aryl sulfonate. The formation of the desired products by the photochemical reaction suggests the formation of an O-centered mesyloxyl radical.

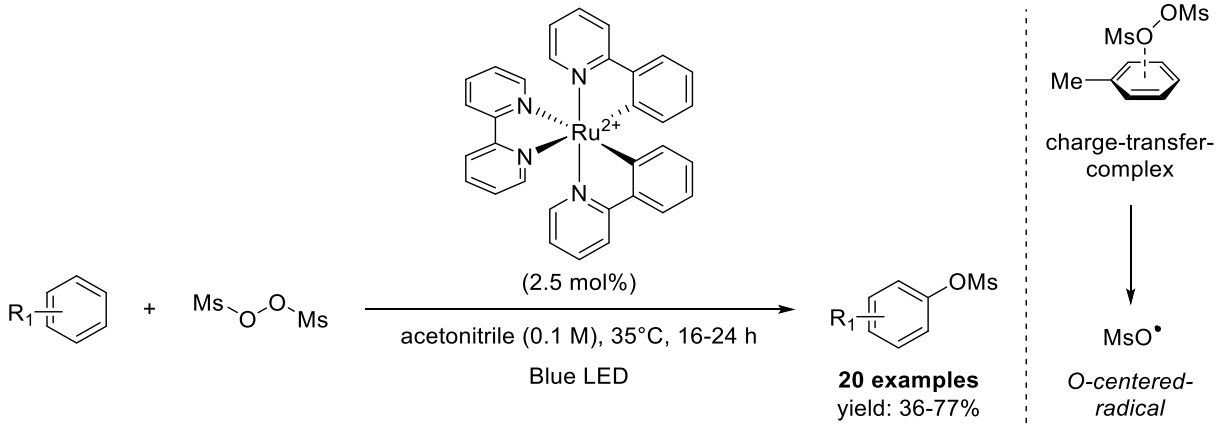

Scheme 3.3: Photo-mediated aromatic C–H-oxygenation using bis(methanesulfonyl) peroxide.[73]

The formation of O-centered-mesyloxyl radicals has already been described in non-photo-mediated reactions.[74] Triggered by the radical initiator copper(I) acetate, bis(methanesulfonyl) peroxide was converted into the corresponding mesyloxyl radical intermediate and engaged in benzylic oxidation. The reaction proceeds via chain propagation.

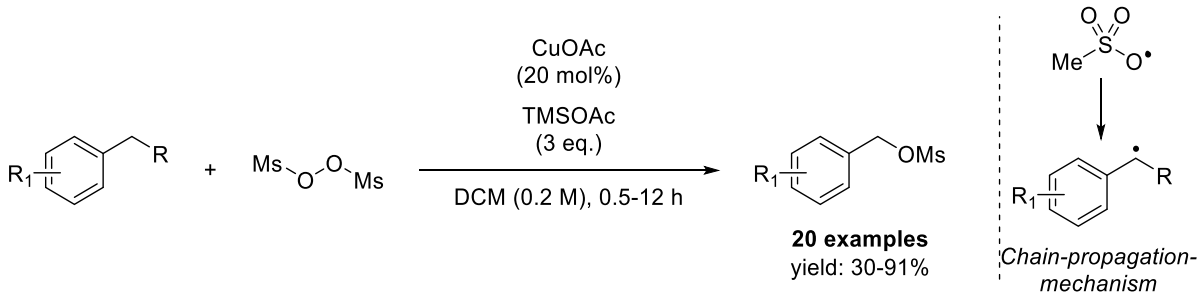

Scheme 3.4: Benzylic monooxygenation using bis(methanesulfonyl) peroxide.[74]

3.2 Objectives

The following chapter delineates to the development of a strategy of a photo-mediated anaerobic oxygenation using arene-*N*-oxides as a chemical mimicry of oxygenase enzymes. Detailed knowledge of the photochemical properties of representative subset of aromatic *N*-oxides are a prerequisite for a successful photo-mediated oxygen atom transfer.

The initial goal is the evaluation of a unified approach for the synthesis of a training set of 25 heteroarene-*N*-oxides, encompassing pyridines, bipyridines, pyrazines, pyrimidines, pyridazines, acridines, phenanzines and phthalazines.

Each compound will be characterized by UV-vis spectroscopy, cyclic voltammetry, and chemiluminescence measurements.

The electrochemical and photophysical properties of the synthesized heteroarene-*N*-oxides will be compared with the previously described pyrimidopteridine-*N*-oxides (also see chapter 1.3). Suitable representatives will be selected and their performance in photo-mediated oxygen atom transfer reaction will be evaluated.

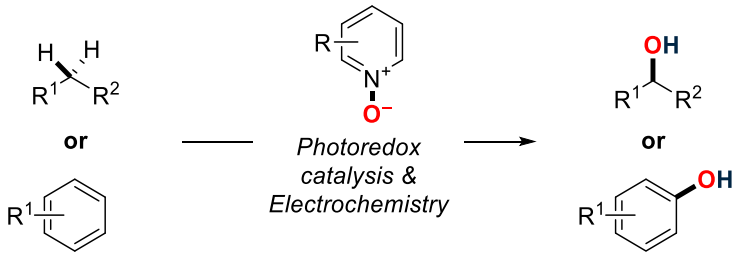

Figure 3.8: Oxygen atom transfer through pyridine *N*-oxides

3.3 Results and discussion

3.3.1 Scope of heterocyclic aromatic *N*-oxides

In order to study the photochemical oxygen atom transfer from heteroarene-*N*-oxides, a number of different candidates have to be synthesized and evaluated. This class of compounds is accessed by *N*-oxidation of the heteroarene with oxidants such as peroxides.[75] The utilization of *meta*-chloroperbenzoic acid (*m*-CPBA) has gained prominence due to its favorable price, stability, and reliable results. The disadvantage of this methodology is the superstoichiometric use of *meta*-chloroperbenzoic acid and the resulting *meta*-chlorobenzoic acid as side-product. The catalytic *N*-oxygenation can be accomplished using methyltrioxorhenium as a catalyst. [76] The low cost, high yields and very low catalyst loadings render methyltrioxorhenium an ideal practical oxidation catalyst. The application of these *N*-oxygenation methodology resulted in the synthesis of a set of 19 different *N*-oxides in collaboration with M.Sc. Jack Felix Christen (Table 3.1).[77]

Table 3.1-1/2: Synthesis of various heteroarene-*N*-oxides.

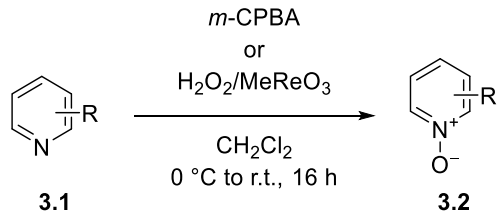

3.1 **3.2**

entry	substrate		product		isol. yield
1	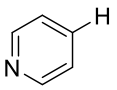	**3.1a**	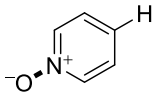	**3.2a**	99%[a]
2	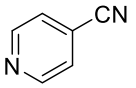	**3.1b**	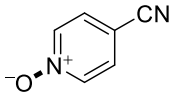	**3.2b**	78%[a]
3	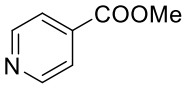	**3.1c**	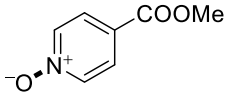	**3.2c**	92%[b]
4	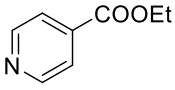	**3.1d**	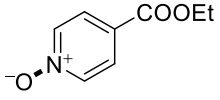	**3.2d**	98%[b]
5	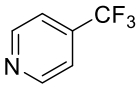	**3.1e**	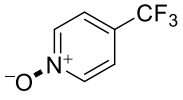	**3.2e**	92%[b]
6	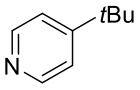	**3.1f**	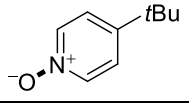	**3.2f**	95%[b]

Table 3.1-2/2: Synthesis of various pyridine *N*-oxides.

entry	substrate		product		isol. yield
7	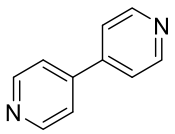	**3.1g**	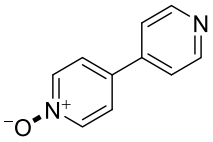	**3.2g**	34%[b]
			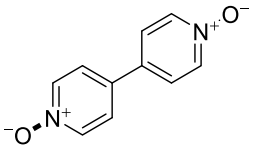	**3.2h**	53%[b]
8	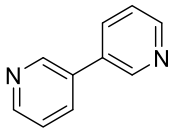	**3.1i**	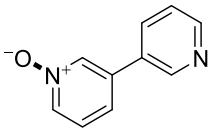	**3.2i**	51%[b]
			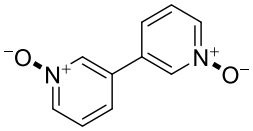	**3.2j**	42%[b]
9	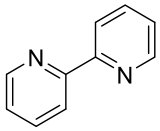	**3.1k**	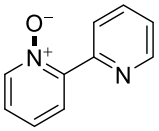	**3.2k**	72%[a]
10	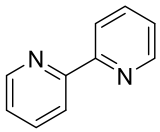	**3.1k**	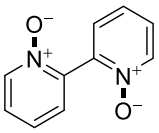	**3.2l**	25%[b]
11		**3.1m**	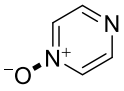	**3.2m**	70%[b]
12		**3.1n**	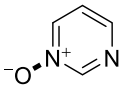	**3.2n**	90%[b]
13		**3.1o**	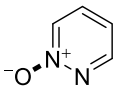	**3.2o**	92%[b]
14	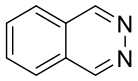	**3.1p**	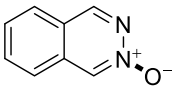	**3.2p**	92%[b]
15	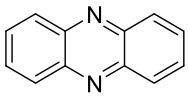	**3.1q**	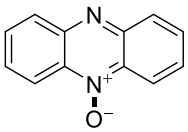	**3.2q**	64%[b]
			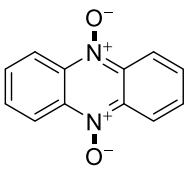	**3.2r**	32%[b]

Footnote: [a] *m*-CPBA (2.0 eq.) was used as oxidant. [b] Using methyltrioxorhenium (0.5 mol%) and hydrogen peroxide as oxidant.

The *N*-oxygenation using *m*-CPBA was the method of choice for two examples. Pyridine-*N*-oxide (**3.2a**) was furnished in an excellent isolated yield of 99% (Table 3.1, entry 1). The more electron-deficient 4-cyanopyridine-*N*-oxide (**3.2b**) was obtained in a good isolated yield of 78% (Table 3.1, entry 2). The catalytic *N*-oxygenation catalyzed by methyltrioxorhenium represented the most general approach for the *N*-oxide synthesis. More electron-deficient pyridines bearing ester or trifluoromethyl substituents were obtained in 92-98% isolated yield (Table 3.1, entries 3-5). The electron-rich 4-*tert*-butylpyridine-*N*-oxide (**3.2f**) was obtained in 95% isolated yield (Table 3.1, entry 6). To extend the structural scaffold of the heteroarene-*N*-oxide scope, different bipyridines were converted to the corresponding *N*-oxides. The conversion of 4,4'-bipyridine (**3.1g**) with the methyltrioxorhenium provided a mixture of mono- and di-*N*-oxygenated compounds in 34% and 53% isolated yield, respectively (Table 3.1, entry 7). Similarly, 3,3'-bipyridine (**3.1i**) afforded the corresponding mono- and di-*N*-oxygenated products in a 51% and 42% isolated yield, respectively (Table 3.1, entry 8). Oxidation of 2,2'-bipyridine (**3.1k**) with *m*-CPBA furnished the mono-*N*-oxygenated heteroarene (Table 3.1, entry 9). In contrast, the employment of the transition metal catalyst resulted in the di-*N*-oxygenated 2,2'-bipyridine-*N*-oxide (**3.2l**) in a modest yield of 25% (Table 3.1, entry 10). Presumably, complexation of the rhenium catalyst by 2,2'-bipyridine results in a deactivation of the catalyst. Next, heterocycles containing more than one nitrogen atom in the aromatic ring were investigated with respect to *N*-oxidation. Pyrazine (**3.1m**) was converted to the mono-*N*-oxygenated species in a synthetically useful yield of 70% (Table 3.1, entry 11). Pyridazin (**3.1n**) and pyrimidine (**3.1o**) achieved the mono-*N*-oxygenated products in 90% and 92% isolated yield, respectively (Table 3.1, entries 12-13). Similarly, mono- *N*-oxygenated phthalazine-*N*-oxide was obtained in a good yield of 92% (Table 3.1, entry 14). The reaction of phenazine (**3.1q**) provided a mixture of mono- and di-*N*-oxygenated compounds, that were isolated in 64% and 32% yields, respectively (Table 3.1, entry 15).

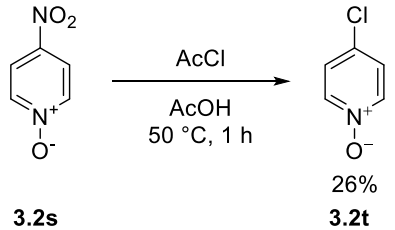

Scheme 3.5: Synthesis of 4-chloropyridine-*N*-oxide (3.2t).

4-Chloropyridine-*N*-oxide (**3.2t**) was synthesized from the commercially available 4-nitropyridine-*N*-oxide (**3.2s**) via nucleophilic aromatic substitution using acetyl chloride as chlorination reagent (Scheme 3.5).[78]

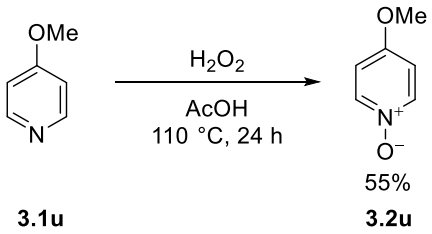

Scheme 3.6: Synthesis of 4-methoxypyridine-*N*-oxide (3.2u).

Pyridine-*N*-oxide **3.2u** bearing a methoxy-substituent at the para-position was synthesized in a thermal reaction utilizing hydrogenperoxide.[79]

3.3.2 Electrochemical and photophysical characterization of heterocyclic aromatic *N*-oxides

Cyclic voltammetry and differential pulse voltammetry

To determine the electrochemical properties of the prepared *N*-oxides, cyclic voltametric measurements were conducted. In addition, commercially available 4-nitropyridine-*N*-oxide (**3.2s**) and 4-phenylpyridine-*N*-oxide (**3.2v**) were investigated. 9-Chloroacridine-*N*-oxide (**3.2w**), synthesized in our group by M.Sc. Mario Frahm, completed the set of heterocyclic aromatic *N*-oxides.[80] Cyclovoltammetric measurements were performed in acetonitrile with tetrabutylammonium hexafluorophosphate ($TBAPF_6$) as electrolyte (c = 0.1 M) against the silver-silver chloride reference electrode. All signals were individually referenced to the Fc^+/Fc redox couple.[21] The trend of the electrochemical behavior is exemplified by the CV-measurements of methoxy-, phenyl-, cyanide-, and nitro-substituted *N*-oxides (**3.2u**, **3.2v**, **3.2b** and **3.2s**) (Figure 3.9).

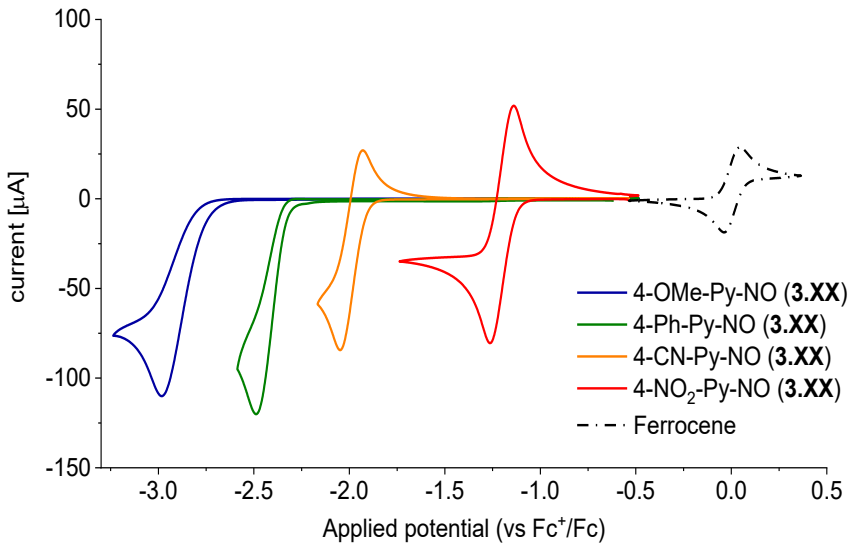

Figure 3.9: Cyclic voltammograms of selected pyridine *N*-oxide derivatives in MeCN.

The reduction potentials of the pyridine *N*-oxides ranged from –2.9 V to –1.2 V vs Fc^+/Fc. Electron-withdrawing substituents such as nitro- or cyano- radicals exhibit a relatively low reduction potential of the pyridine *N*-oxides (Figure 3.9, orange & red). The symmetrical signals show a reversible process, permitting determination of the reduction potentials at –1.2 V for **3.2s** and –1.9 V for **3.2b** vs Fc^+/Fc, respectively. Neutral and electron-donating substituents showed relatively high, irreversible reduction peaks below –2.0 V. The irreversible response prevented the accurate determination of these reduction potentials (Figure 3.9, **3.2u** & **3.2v**).

Consequently, differential pulse voltammetric experiments were conducted.[22] This method allows the determination of the redox potentials of irreversible processes. The heteroarene-*N*-oxides were dissolved in MeCN (0.01 M) and the voltammograms were recorded against the silver-silver chloride reference electrode and referenced to the Fc^+/Fc couple (Figure 3.10).[21]

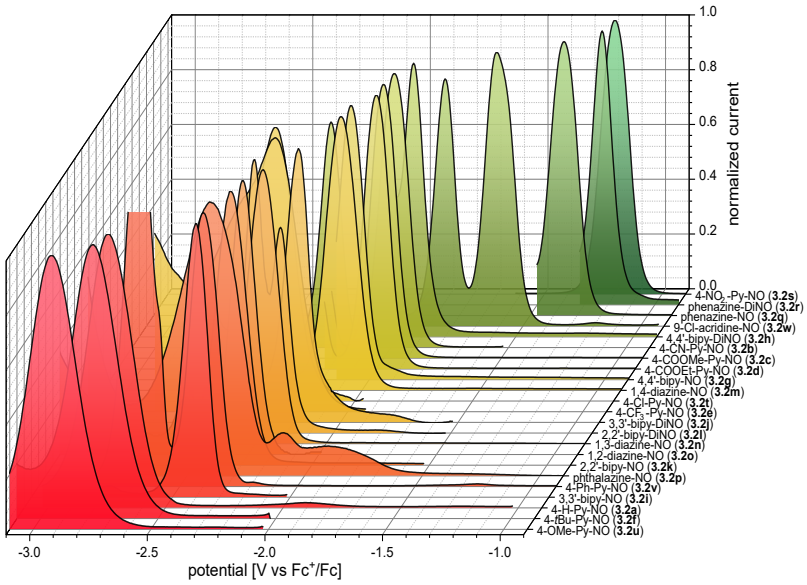

Figure 3.10: Differential pulsevoltammograms of various heteroarene *N*-oxide derivatives.

A comprehensive analysis of the heteroarene-*N*-oxides confirms the range of reduction potentials between –1.2 V and –2.9 V. Electron-deficient *N*-oxides such as 4-nitropyridine-*N*-oxide (**3.2s**), mono- and di-*N*-oxidized phenazine (**3.2q** and **3.2r**) and 9-chloroacridine *N*-oxide (**3.2w**) were reducible at low potentials between –1.2 V and –1.6 V (Figure 3.10, green area). The majority of the *N*-oxides showed reduction potentials between –1.9 V and –2.4 V (Figure 3.10, orange to yellow area). This range includes all the bipyridines (**3.2g**-**3.2l**), pyrazines (**3.2m**), pyridazines (**3.2n**) and pyrimidines (**3.2o**) studied, as well as pyridine *N*-oxides bearing CN-, Cl-, CF_3- or a phenyl-substituent in 4-position (**3.2b**, **3.2t**, **3.2e**, **3.2v**).

Neutral and electron-rich pyridine *N*-oxides were reduced by applying high cathodic potentials. Pyridine-*N*-oxide has a reduction potential of –2.76 V. *tert*-Butyl- and

methoxypyridine-*N*-oxide (**3.2f** and **3.2u**) possessed reduction potentials of −2.80 V and −2.94 V, respectively (Figure 3.10, red area). A tabular overview is shown below (Table 3.2).

UV-vis-absorption measurements

The synthesized *N*-oxides were analyzed for their light absorption properties. The compounds were dissolved in acetonitrile (c ~ 50 µM) and measured in a cuvette (d = 1 cm) using an UV-vis absorption spectrometer. The obtained absorption spectra were depicted in ascending order with respect to their absorption offsets (Figure 3.11). The absorption maxima are discussed.

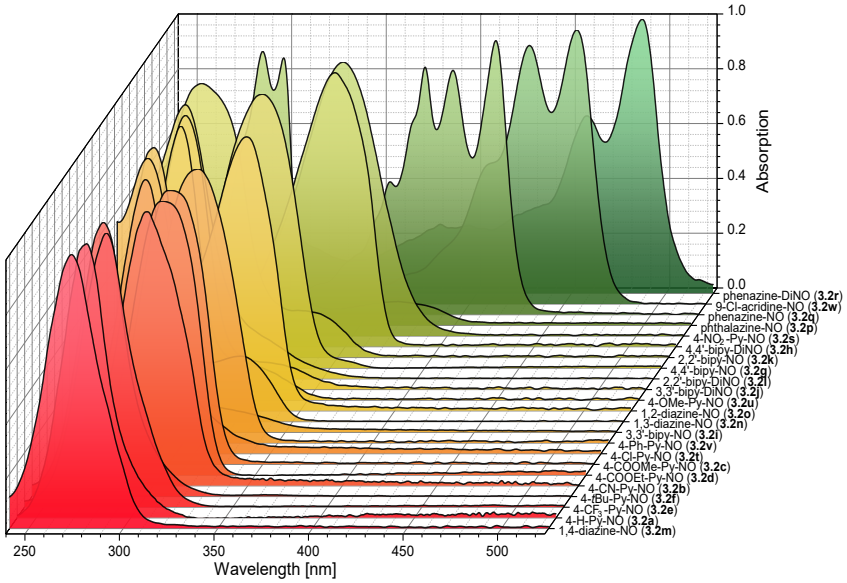

Figure 3.11: UV-vis absorption spectra of various heterocyclic aromatic *N*-oxides.

The comparison of the absorption spectra show that few *N*-oxides interact with visible light. The absorption maximum of the unsubstituted pyridine-*N*-oxide (**3.2a**) was determined in the UVC region at 277 nm (Figure 3.11, red area). Any kind of substitution at the 4-position causes a bathochromic shift of the absorption maximum. Aliphatic substituents without π-extending character, such as *tert*-butyl- and trifluoromethyl-groups (**3.2f** & **3.2e**) cause a maximum absorbance at 278 nm and 283 nm, respectively (Figure 3.11, red area). The extension of the aromatic π−orbital system causes a stronger red shift. Esters, cyanide, and phenyl-substituted pyridine *N*-oxides (**3.2b**-**3.2d** and **3.2v**) showed an absorption maximum in the higher-energy UVB region at 297-308 nm (Figure 3.11, orange area). The strongest bathochromic shift was caused by the nitro-substituent (**3.2s**) with an absorption maximum of 345 nm (Figure 3.11, red area). The absorption maximum of 1,4-diazine-*N*-oxide (**3.2m**) was determined at 278 nm (Figure 3.11, red area). In contrast, the absorption maxima of 1,3- and 1,2-diazine-*N*-oxide (**3.2n** and **3.2o**) were observed around 320 nm (Figure 3.11, orange area). The spectra of bipyridine-*N*-oxides collectively (**3.2g**, **3.2h**, **3.2k**, **3.2l**) show absorption maxima of above

300 nm. Noteworthy, the offset of the bipyridine *N*-oxide absorption spectra from about 350-370 nm demonstrates that lower-energy radiation can also utilized (Figure 3.11, yellow area). An exception is 3,3'-bipyridine-*N*-oxide (**3.2i**, **3.2j**). Mono- and di-*N*-oxidized phenazines as well as 9-chloro-acridine-*N*-oxides (**3.2q, 3.2r** and **3.2w**) show an interaction with lower energy light from the visible light region with maxima at 418 nm, 487 nm and 457 nm (Figure 3.11, green area). A tabular overview is shown below (Table 3.2).

Photoluminescence of heterocyclic aromatic *N*-oxides

With the light absorption results in hand, the fluorescence properties of the *N*-oxides were then determined to obtain inferences about the potential energy of the excited state $E_{0,0}$. The compounds were dissolved in acetonitrile (c = 20 µM) and measured in a cuvette (d = 1 cm) using a fluorescence spectrometer. The wavelength used for excitation corresponds to a wavelength from the absorption spectrum that yields a suitable emission response (Figure 3.11). The resulting fluorescence spectra were displayed in Figure 3.12 in ascending order with respect to their fluorescence maxima.

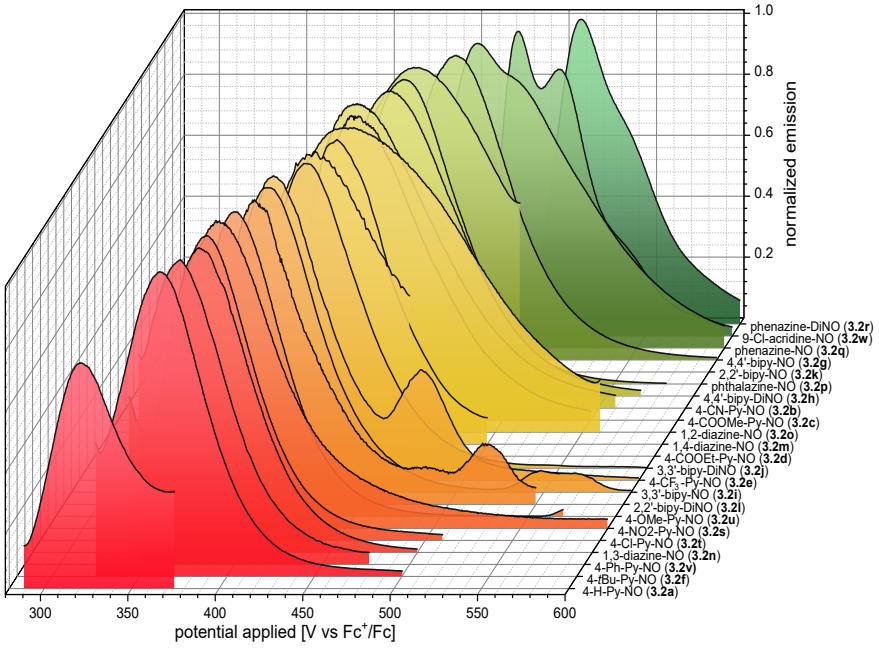

Figure 3.12: Emission spectra of various heterocyclic aromatic *N*-oxides.

The unsubstituted pyridine *N*-oxide (**3.2a**) shows an emission maximum at 321 nm (Figure 3.12, red area). Any kind of substitution results in a red-shift of the emission band. The majority of the analyzed pyridine *N*-oxides exhibited a fluorescence maximum between 361 nm and 413 nm. The *tert*-butyl-group in 4-position caused the least bathochromic effect (Figure 3.12, **3.2f**). Ester- and nitrile-substituents in 4-position caused a more pronounces red shift up to 412 nm (Figure 3.12, **3.2b**-**3.2d**). The fluorescence maxima of the 2,2'-bipyridine- and 4,4'-bipyridine-*N*-oxide (**3.2l** and **3.2g**) were determined at a higher wavelength of 431 nm and

451 nm, respectively (Figure 3.12, green area). The corresponding *N*,*N'*-dioxides **3.2l** and **3.2h** at 389 nm and 427 nm respectively. In contrast, a lower emission maximum for 3,3'-bipyridine was observed for the *N*-oxide **3.2i** at 392 nm than for the corresponding *N*,*N'*-dioxides **3.2j** at 404 nm (Figure 3.12, orange area). The emission maximum of 1,3-diazine-*N*-oxide (**3.2n**) was determined at 375 nm (Figure 3.12, orange area). The absorption maxima of 1,2- and 1,4-diazine-*N*-oxide (**3.2o** and **3.2m**) were observed at 412 and 419 nm, respectively (Figure 3.12, orange area). Mono- and di-*N*-oxidized phenazines as well as 9-chloro-acridine-*N*-oxides (**3.2q**, **3.2r** and **3.2w**) show an maximum emission at 459 nm, 510 nm and 478 nm, respectively (Figure 3.11, green area). A tabular overview is shown below (Table 3.2).

Excited state properties of heterocyclic aromatic *N*-oxides

Next, the excited state potential energy of the heterocyclic aromatic *N*-oxides needs to be determined. To estimate this energy, an energy between onset, an overestimate of the energy, and the emission maximum, corresponding to an underestimate of the energy, is usually used. For this purpose, the intersection point of the normalized absorption and emission spectra is used when possible. This method could be applied to the example of 4-nitropyridine-*N*-oxides (**3.2s**, Figure 3.13, bottom, red). However, compounds, such as 4-cyano-pyridine-*N*-oxides (**3.2b**), exhibited a large Stoke shift, therefore no intersection point could be obtained. The usage of half the stoke-shift as an energy estimate is also not suitable, since the resulting energy is above the overestimated energy (onset point emission) (Figure 3.13, middle, orange). Furthermore, in several emission spectra, as in the case of 4-phenyl-pyridine-*N*-oxide (**3.2v**), no onset point could be obtained (Figure 3.13, top, green). To ensure comparability among the heteroarene *N*-oxides, the maximum of the emission spectrum was chosen for estimating the excited state energy, in the awareness that this represents an underestimation. A tabular overview is shown below (Table 3.2).

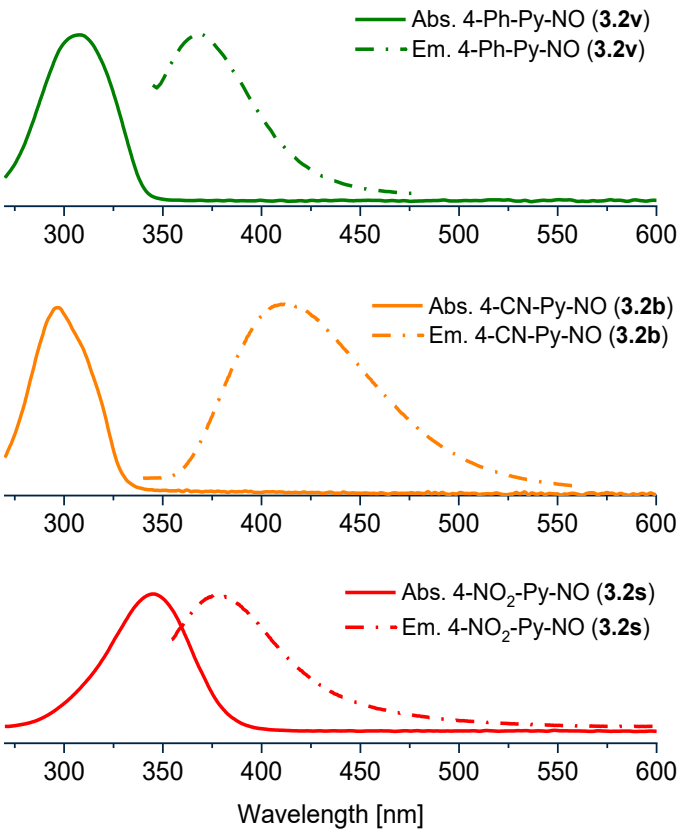

Figure 3.13: Normalized absorption- and emission spectra of 4-nitro (3.2v), 4-cyano und 4-phenyl-pyridine-*N*-oxide (3.2b and 3.2s).

Subsequently, the excited state reduction potential was calculated from the excited state energy. The combination of the voltametric determined potentials and the potential energy of the excited state enables the approximation of the excited state redox potentials using equation 3.1 and 3.2.[5] A tabular overview is shown below (Table 3.2).

$$E^*_{red} = E_{0,0} + E^{red}_{1/2} \qquad \text{equation 3.1}$$

$$E^*_{ox} = E^{ox}_{1/2} - E_{0,0} \qquad \text{equation 3.2}$$

Table 3.2: Photophysical and electrochemical properties of heterocyclic aromatic *N*-oxides.

entry	compound	λ_{max}^{abs} [nm]	λ_{max}^{em} [nm]	$E_{0,0}^{S1}$ [eV][c]	$E_{1/2}^{red}$ [V vs Fc^+/Fc][a]	$E_{1/2}^{red}$ [V vs SCE][b]	E_{red}^{*} [V vs Fc^+/Fc][d]	E_{red}^{*} [V vs SCE][d]
1	4-NO_2-Py-NO (**3.2s**)	345	378	+3.28	–1.20	–0.82	+2.08	+2.46
2	4-CN-Py-NO (**3.2b**)	297	412	+3.01	–1.99	–1.61	+1.02	+1.40
3	4-CF_3-Py-NO (**3.2e**)	283	391	+3.17	–2.32	–1.94	+0.85	+1.23
4	4-COOMe-Py-NO (**3.2c**)	301	413	+3.00	–2.02	–1.64	+0.98	+1.36
5	4-COOEt-Py-NO (**3.2d**)	301	406	+3.05	–2.05	–1.67	+1.01	+1.39
6	4-Cl-Py-NO (**3.2t**)	282	375	+3.31	–2.37	–1.99	+0.94	+1.32
7	4-H-Py-NO (**3.2a**)	276	321	+3.87	–2.76	–2.38	+1.10	+1.48
8	4-Ph-Py-NO (**3.2v**)	308	369	+3.36	–2.42	–2.04	+0.94	+1.32
9	4-*t*Bu-Py-NO (**3.2f**)	278	361	+3.43	–2.80	–2.42	+0.63	+1.01
10	4-OMe-Py-NO (**3.2u**)	283	383	+3.24	–2.94	–2.56	+0.30	+0.68
11	4,4'-bipy-NO (**3.2g**)	314	451	+2.75	–2.10	–1.72	+0.65	+1.03
12	4,4'-bipy-DiNO (**3.2h**)	345	427	+2.90	–1.95	–1.57	+0.95	+1.33
13	3,3'-bipy-NO (**3.2i**)	278	392	+3.16	–2.42	–2.04	+0.75	+1.13
14	3,3'-bipy-DiNO (**3.2j**)	327	404	+3.07	–2.20	–1.82	+0.87	+1.25
15	2,2'-bipy-NO (**3.2k**)	329	431	+2.88	–2.36	–1.98	+0.51	+0.89
16	2,2'-bipy-DiNO (**3.2l**)	278	389	+3.19	–2.24	–1.86	+0.94	+1.32
17	1,4-diazine-NO (**3.2m**)	273	412	+3.01	–2.10	–1.72	+0.91	+1.29
18	1,3-diazine-NO (**3.2n**)	323	375	+3.31	–2.28	–1.90	+1.03	+1.41
19	1,2-diazine-NO (**3.2o**)	322	419	+2.96	–2.35	–1.97	+0.60	+0.98
20	phthalazine-NO (**3.2p**)	372	430	+2.89	–2.42	–2.04	+0.47	+0.85
21	phenazine-NO (**3.2q**)	418	459	+2.70	–1.36	–0.98	+1.34	+1.72
22	phenazine-DiNO (**3.2r**)	487	510	+2.43	–1.23	–0.85	+1.21	+1.59
23	9-Cl-acridine-NO (**3.2w**)	457	478	+2.59	–1.63	–1.25	+0.97	+1.35

Footnote: [a] Potentials were measured using cyclic voltammetry (CV) and differential pulse voltammetry (DPV) relative to Fc^+/Fc. [b] Referenced to SCE by adding 0.38 V to the value relative to Fc^+/Fc. [c] $E_{0,0}$ values corresponding to the energy at the emission maximum. [d] Calculated by $E_{red}^{*} = E_{0,0} + E_{DPV}^{red}$ and $E_{ox}^{*} = E_{DPV}^{ox} - E_{0,0}$.

The calculation of the excited state reduction potentials of the pyridine *N*-oxides revealed a range from 0.68 to 2.46 V vs SCE (Table 3.2, entries 1-10). 4-Nitro-pyridine *N*-oxides (**3.2s**) exhibited the significantly highest excited state reduction potential of 2.46 V (Table 3.2, entry 1). Pyridine-*N*-oxides with cyanide, chloride, trifluoromethyl and ester groups (**3.2b**, **3.2t**, **3.2e**, **3.2c** and **3.2d**) resulted in an excited state reduction potential of 1.23 V to 1.48 V (Table

3.2, entries 2-6). For the unsubstituted and phenyl-bearing pyridine *N*-oxide (**3.2a** and **3.2v**), an excited state reduction potential of 1.48 V and 1.32 V was determined (Table 3.2, entries 7-8). Electron-rich pyridine-*N*-oxides with methoxy and *tert*-butyl groups (**3.2u** and **3.2f**) exhibited a reduced excited state reduction potential of 0.68 V and 1.01 V, respectively (Table 3.2, entries 9-10).

For bipyridine systems, a range of excited state reduction potentials from 0.89 V to 1.33 V was determined (Table 3.2, entries 11-16). The mono-*N*-oxidized bipyridines (**3.2g**, **3.2i** and **3.2k**) exhibited decreased excited state reduction potentials of 0.89 V to 1.13 V (Table 3.2, entries 11; 13; 15). Bipyridines bearing two *N*-oxide-functionality (**3.2h**, **3.2j** and **3.2l**) revealed higher excited state reduction potentials of 1.25 V to 1.33 V (Table 3.2, entries 12; 14; 16). The excited state reduction potentials of pyrazines and pyrimidine *N*-oxide (**3.2m** and **3.2n**) were calculated to be 1.29 V and 1.41 V (Table 3.2, entries 17-18), respectively. In contrast, the calculation for pyridazine and phthalazine *N*-oxide (**3.2o** and **3.2p**) resulted in a reduced potential of 0.85 V to 0.98 V (Table 3.2, entries 19-20). Mono- and di-*N*-oxidized phenazine as well as 9-chloroacridine *N*-oxide (**3.2q**, **3.2r** and **3.2w**) showed improved excited state reduction potentials from 1.35 V to 1.72 V (Table 3.2, entries 21-23).

3.3.3 Application of heterocyclic aromatic *N*-oxides as oxygen atom transfer reagent

The results from the previous section were analyzed to identify suitable heteroarene *N*-oxides with respect to their application as oxygen atom transfer agents. In particular, the utilization of the lowest possible energy light ($h\nu$ = 396 nm) in order to achieve an excitation of the substrates was desirable. Consequently, 4-nitro-pyridine-*N*-oxide (**3.2s**) and mono- and di-*N*-oxidized (**3.2q** and **3.2r**) phenazine were identified as suitable candidates (Figure 3.14).

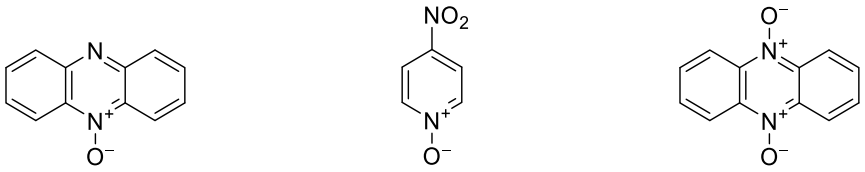

3.2q
λ_{max}^{abs} = 418 nm
E_{red}^{*} = +1.72 V
[vs SCE]

3.2s
λ_{max}^{abs} = 345 nm
E_{red}^{*} = +2.46 V
[vs SCE]

3.2r
λ_{max}^{abs} = 487 nm
E_{red}^{*} = +1.59 V
[vs SCE]

Figure 3.14: Potential POAT reagents.

The absorption maxima of 418 nm and 487 nm of phenazine mono- and di-*N*-oxide (**3.2q** and **3.2r**) show that blue to green light would be sufficient for excitation to the excited state. The absorption spectrum of 4-nitropyridine *N*-oxide (**3.2s**) shows a maximum at 345 nm, which

is clearly in the UVA range. Nevertheless, this compound can be excited by a blue LED (hν = 396 nm). The calculation of the excited state reduction potentials of 4-nitropyridine-*N*-oxide showed impressive values of 2.46 V vs SCE. Mono and di-*N*-oxidized phenanzine (**3.2q** and **3.2r**) also show good excited state reduction potentials of 1.72 V and 1.59 V, respectively. The derivatives were studied in terms of photochemical oxygen atom transfer (Figure 3.15).

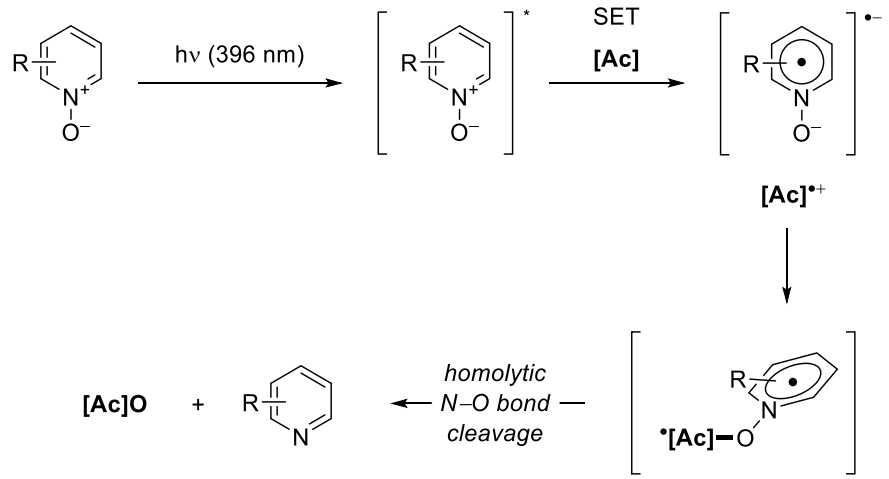

Figure 3.15: Schematic sequence of the photo-mediated oxygen atom transfer reaction.

The reaction proceeds via the excited state, which is accessed upon irradiation. The oxygen acceptor molecule is oxidized and the *N*-oxide species is reduced via a single electron transfer mechanism. Nucleophilic attack result in the formation of an adduct. Homolytic N–O bond cleavage yields the oxidation product and the heteroaromatic compound.

The photo-mediated anaerobic oxidation of xanthene (**3.3**) was chosen as test substrate to evaluate the *N*-oxides in the photochemical oxygen atom transfer. The oxidation potential of xanthene is +1.51 V vs SCE in MeCN.[81] Thus oxidation of xanthene should be feasible by means of the selected reagents (E^*_{red} > +1.59 V vs SCE in MeCN). Since 4-nitropyridine-*N*-oxide (**3.2s**) possesses the highest excited state reduction potential, the POAT has been investigated. The reaction mixture was irradiated at 396 nm for 16 h.

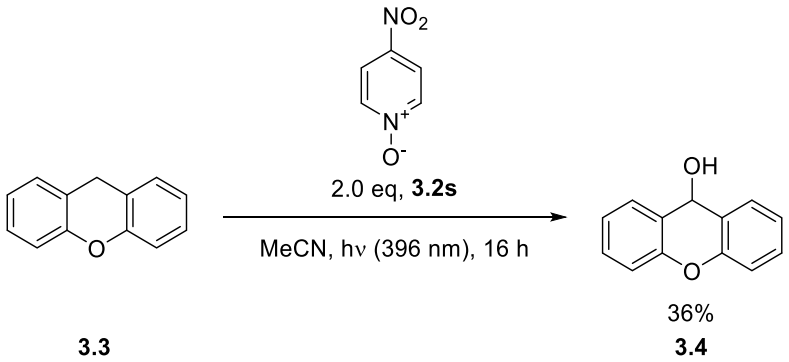

Scheme 3.7: Photo-mediated oxygen atom transfer utilizing 4-nitropyridin-*N*-oxide (3.2s).

The photo-mediated oxygen atom transfer reaction of 4-nitropyridine-*N*-oxide (**3.2s**) was successfully achieved. The corresponding oxygenation product xanthenol (**3.4**) was obtained in an isolated yield of 36% under unoptimized reaction conditions. Analysis of the crude reaction mixture showed that the substrate was completely consumed.

In the following, the scope of application of 4-nitro-pyridine-*N*-oxide (**3.2s**) as POAT reagent should be defined in a short study. The C−N bond cleavage, oxidation of thioethers, decarboxylative oxygenation and epoxidation of alkenes was attempted. In contrast to pyrimidopteridine-*N*-oxides, no stilbene oxide was observed under similar reaction conditions. Similarly, no successful oxygen atom transfer was observed with thioanisole (**3.7**), dimethylaniline (**3.5**), adamatanecarboxylic acid (**3.10**) or stilbene (**3.12**) as starting materials (Scheme 3.8).

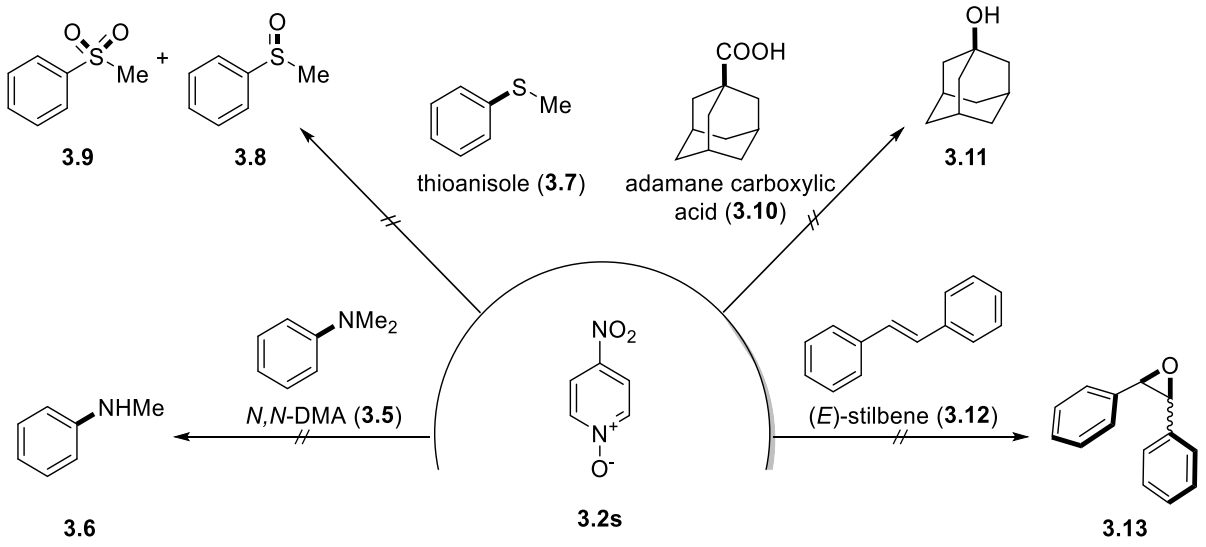

Scheme 3.8: Different approaches for the photo-mediated oxygen atom transfer from 4-nitropyridin-*N*-oxide (3.2s).

Since the formation of O-centered radicals by sulfonyloxy pyridinium sulfonates and the benzylic C−O bond formation by electrochemically generated bis(methanesulfonyl) peroxides was demonstrated in several instances a joint venture of these methodologies was envisioned.[73-74]

Synthesis of (methylsulfonyloxy)pyridinium methanesulfonate

The application of pyridinium salts as reagents in photochemical redox processes has already been realized in several examples.[63, 82] The reaction mechanism corresponds to an oxidative quenching cycle of the photocatalyst, which reduces the pyridinium cation. The subsequent N–X bond cleavage results in an N- or X-centered radical species, depending on which of the two decomposition products has the stronger electron-withdrawing properties.[63] Three different types of N−oxygen pyridinium species have been applied in photo-mediated reactions, namely *N*-alkoxy, *N*-trifluoromethoxy and trifluorosulfonoxy pyridinium salts (Figure 3.16).[63] The synthesis of bis(methanesulfonyl) peroxides was performed by electrochemical means from methanesulfonic acid.[73]

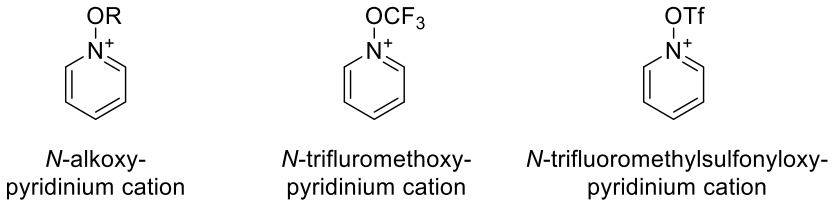

Figure 3.16: Utilized *N*−oxygen pyridinium species in photo-mediated reactions.

In a procedure adapted from the synthesis of 1-(((trifluoromethyl)sulfonyl)oxy)pyridin-1-ium trifluoromethanesulfonate,[71] sulfonation of pyridine-*N*-oxide (**3.2a**) with methanesulfonic anhydride results in the conversion to the corresponding (methylsulfonyloxy)pyridinium methanesulfonate.

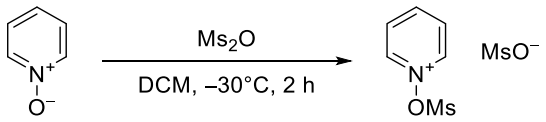

Scheme 3.9: Synthesis of (methylsulfonyloxy)pyridinium methanesulfonate (3.14).

The reaction was carried out by dropwise addition of a methanesulfonic anhydride in dichloromethane to a stirring solution of pyridine-*N*-oxide (**3.2a**) at –30°C. The desired product precipitated from the reaction mixture and was collected by filtration. The structure of the (methylsulfonyloxy)pyridinium methanesulfonate (**3.14**) was confirmed by X-ray crystallography (Figure 3.17).

Figure 3.17: X-ray crystal structure of (methylsulfonyloxy)pyridinium methanesulfonate (3.14). Displacement ellipsoids correspond to 30% probability.

Photo-mediated dehydrogenation of alkylarenes

With the (methylsulfonyloxy)pyridinium methanesulfonate in hand, a oxysulfonation of benzylic C−H was attempted. The transition metal photocatalyst tris(2,2′-bipyridine)ruthenium hexafluorophosphate (E^*[Ru*/Ru$^{\bullet+}$] = -0.81 V vs SCE)[83] was employed in order to photochemically reduce the pyridinium compound ($E_{1/2}^{red}$[Py(OTf)$_2$/ Py(OTf)$_2^{\bullet-}$] = +0.08 V vs SCE)[71]. 1-Bromo-4-ethylbenzene (**3.15**) was chosen as the model substrate. In seminal reactions, the reaction medium was optimized (Table 3.3).

Table 3.3: Solvent screening of the photo-mediated benzylic oxidation.

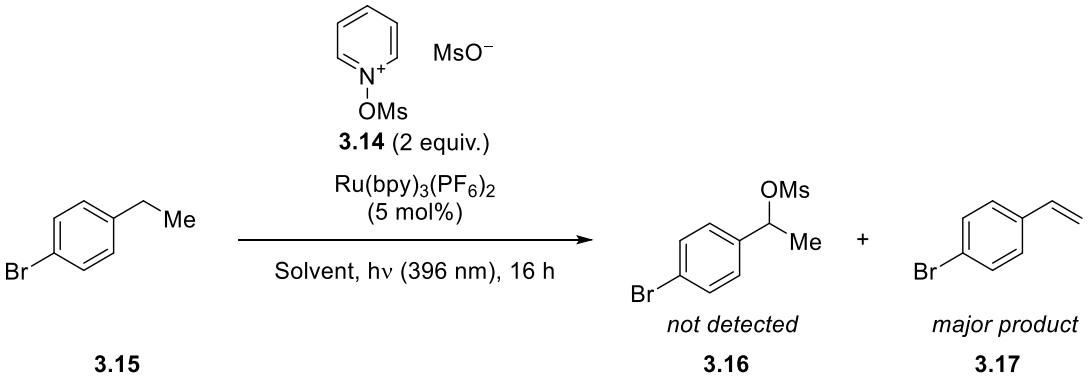

entry	solvent	GC-yield **3.17** [%][a]
1	DCM	44
2	acetone	34
3	MeCN	31
4	DCE	30
5	nitromethane	27
6	$CHCl_3$	18
7	DMF	0
8	ethylacetate	0
9	diethylether	0
10	THF	0
11	pyridine	0
12	PhMe	0

Footnote: The reaction was carried out on a 0.5 mmol scale (0.1 M in the respective solvent) with 2 equiv. (methylsulfonyloxy)pyridinium methanesulfonate and 5 mol % $Ru(bpy)_3(PF_6)_2$. [a] biphenyl was used as internal standard.

The desired C–O bond formation was not achieved at an isolatable scale, but synthetically useful dehydrogenation was obtained in a variety of different aprotic solvent systems. The utilization of dichloromethane afforded the product in the highest yield of 44% (Table 3.3, entry 1). Acetone, acetonitrile and 1.2-dichloroethane provided product yields of 30-34% (Table 3.3, entries 2-4). In nitromethane and chloroform, formation of the product was observed in yields of 27% and 18%, respectively (Table 3.3, entries 5-6). In contrast, no formation of the desired product was observed in DMF (Table 3.3, entry 7). Esters and ether-based solvents such as ethyl acetate, THF and diethyl ether were also not suitable for photochemical oxidation (Table 3.3, entries 8-10). Aromatic solvents such as pyridines or toluene also resulted in no observable product (Table 3.3, entries 11-12).

After dichloromethane was determined as the solvent providing the highest yield, the influence of the photocatalyst was investigated. Both transition metal and organic photocatalysts were used in the reaction (Table 3.4).

Table 3.4: Catalyst screening of the photo-mediated benzylic oxidation.

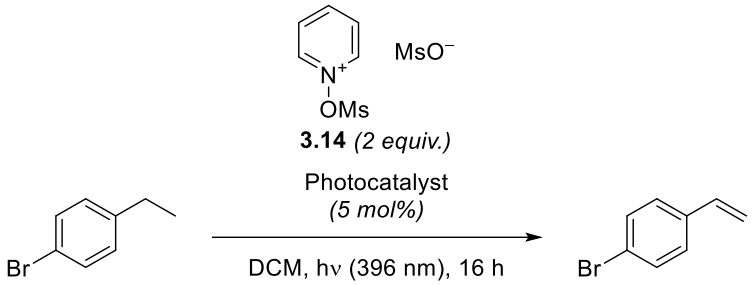

3.15 **3.17**

entry	catalyst	GC-yield [%][a]
1	$Ru(bpy)_3(PF_6)_2$	44
2	$[Ir\{dFCF_3ppy\}_2(bpy)]PF_6$	12
3	$Ru(bpz)_3(PF_6)_2$	<5
4	Rhodamine 6G	<5
5	Eosin Y	<5
6	Rose Bengal	<5
7	BuPPT	<5
8	-	<5

Footnote: The reaction was carried out on a 0.5 mmol scale (0.1 M in DCM) with 2 equiv. (methylsulfonyloxy)pyridinium methanesulfonate and 5 mol % catalyst loading. [a] biphenyl was used as internal standard.

The investigation of the catalyst system revealed that only the transition metal catalysts provided the desired product. Utilizing tris(2,2′-bipyridine)ruthenium hexafluorophosphate yielded the product in a 44% (Table 3.4, entry 1). The iridium photocatalyst exhibited a 12% yield of the product (Table 3.4, entry 2). By varying the ligands of the ruthenium photocatalyst, no product formation was observed (Table 3.4, entry 3). Similarly, no product was detected by using organic photocatalysts (Table 3.4, entries 4-7). In the blank experiment without photocatalyst, no conversion to the desired product was observed (Table 3.4, entry 8).

Subsequently, the benzylic oxidation was examined in terms of the ratios of the reactants. Furthermore, the reaction in lower molarities was investigated. The mixture was irradiated in the presence of tris(2,2′-bipyridine)ruthenium hexafluorophosphate for 16 h in DCM (Table 3.5).

Table 3.5: Substrate ratios and molarity screening.

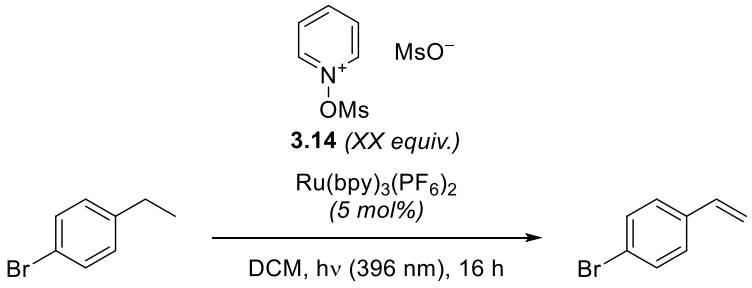

3.15 **3.17**

entry	ratio reactant	molarity	GC-yield [%][a]
1	1 : 4	0.10 M	39
2	1 : 2	0.10 M	44
3	1 : 1	0.10 M	28
4	2 : 1	0.10 M	43
5	5 : 1	0.10 M	50
6	1 : 2	0.05 M	40
7	1 : 2	0.03 M	40

Footnote: The reaction was carried out on a 0.5 mmol scale (0.1 M in DCM) with 2 equiv. (methylsulfonyloxy)pyridinium methanesulfonate and 5 mol % catalyst loading. [a] biphenyl was used as internal standard.

The experiments revealed that an excess of (methylsulfonyloxy)pyridinium methanesulfonate (**3.14**) with 4.0 equivalents furnished the product in 39% yield (Table 3.5, entry 1). Reduced amounts of 2.0 equivalents of pyridinium sulfonate produced a slightly better yield of 44% (Table 3.5, entry 2). An equal distribution of the reactants yielded the product in 28% (Table 3.5, entry 3). An excess of ethylbenzene **3.15** of 2.0 equivalents led to an improved yield of 43% (Table 3.5, entry 4). Further increase of the ethylbenzene amount led to an improvement of the product yield of up to 50% (Table 3.5, entry 5). However, large excess of either substrates ought to be avoided to provide an economic methodology. Thus, the conditions from entry 2 with a slight excess of (methylsulfonyloxy)pyridinium methanesulfonate (**3.14**) of 2.0 eq. was chosen as the optimum ratio for further experiments. Decreasing the molarity to 0.5 M and 0.3 M showed no improvement in yield (Table 3.5, entries 6-7).

To ensure optimal use of resources, the reaction was investigated with respect to catalyst loading. The reaction was irradiated with 2 equivalent (methylsulfonyloxy)pyridinium methanesulfonate (**3.14**) for 16 h in DCM. Tris(2,2′-bipyridine)ruthenium hexafluorophosphate was employed as the catalyst (Table 3.6).

Table 3.6: Screening of the catalyst-loading.

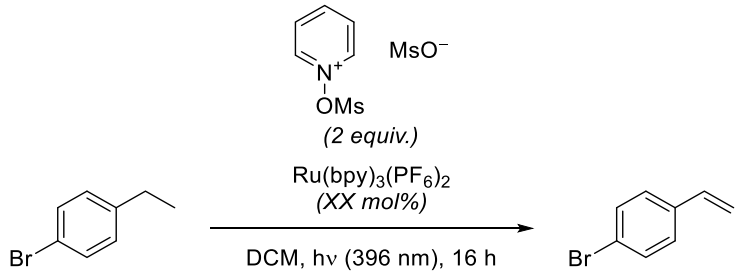

3.15 **3.17**

entry	catalyst-loading	GC-yield [%][a]
1	5.0 mol%	44
2	2.5 mol%	42
3	1.0 mol%	42

Footnote: The reaction was carried out on a 0.5 mmol mass scale (0.1 M) with 2 equiv. (methylsulfonyloxy)pyridinium methanesulfonate and 5 mol % catalyst loading. [a] biphenyl was used as internal standard.

The experiments demonstrated that the loading of the tris(2,2′-bipyridine)-rutheniumhexafluorophosphate catalyst can be reduced without a major decline in yield. The employment of the transition metal catalyst with 5.0 mol% loading furnished the product in 44% yield (Table 3.6, entry 1). Reducing the catalyst loading to 2.5 mol% provided the product in 42% yield (Table 3.6, entry 2). Similarly, a loading of 1.0 mol% afforded the desired product in 42% yield (Table 3.6, entry 3).

Next, the turnover after varying reaction times was examined.

Table 3.7: Variation of the reaction time.

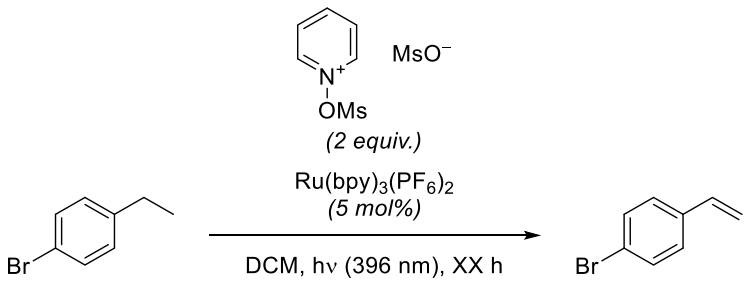

3.15 **3.17**

entry	reaction time	GC-yield [%][a]
1	30 min	<5
2	1 h	6
3	16 h	42
4	24 h	38
5	48 h	46

Footnote: The reaction was carried out on a 0.5 mmol mass scale (0.1 M) with 2 equiv. (methylsulfonyloxy)pyridinium methanesulfonate and 5 mol % catalyst loading. [a] biphenyl was used as internal standard.

The results show that a short reaction time of 30 min does not lead to observable product formation (Table 3.7, entry 1). Even after one hour a yield of 6% was observed (Table 3.7, entry 2). After 16 h, a yield of 42% was identified (Table 3.7, entry 3). The extension of the reaction time to 24 h showed a similarly high yield of 38% (Table 3.7, entry 4). Furthermore, a prolonged reaction time of 48 h did not lead to increased product formation (Table 3.7, entry 5).

3.3.4 Proposed Mechanism

The proposed reaction mechanism for the photo-mediated dehydrogenation of ethyl benzenes utilizing (methylsulfonyloxy)pyridinium methanesulfonate is depicted in Scheme 3.10 below.

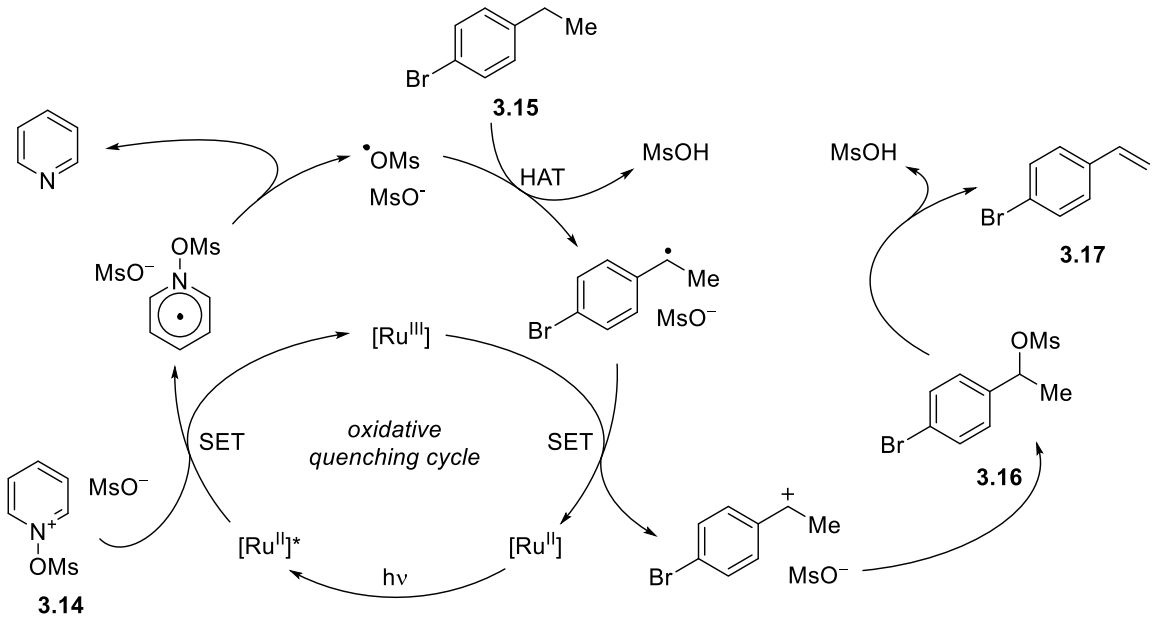

Scheme 3.10: Proposed mechanism for the photo-catalytic benzylic oxidation utilizing (methylsulfonyloxy)pyridinium methanesulfonate (3.14).

In a mechanistic proposal, the mechanism proceeds through the light-induced excitation of the transition metal photocatalyst (λ_{max}^{abs} = 450 nm)[84]. The excited state of the photocatalyst (E^*[Ru^{III}/Ru^{II*}] = −0.81 V vs SCE)[83] reacts with the (methylsulfonyloxy)pyridinium cation **3.14** ($E_{1/2}^{red}$[$Py(OMs)_2/Py(OMs)_2^{\bullet-}$] ~ −0.1 V vs SCE)[71] to deliver the neutral (methylsulfonyloxy)pyridinium radical. Subsequent N−O bond cleavage leads to the formation of pyridine and the mesyl radical. Hydrogen atom transfer from the benzylic position to the mesyl radical yields a benzylic radical and methanesulfonic acid. The low oxidation potential of the benzylic radical ($E_{1/2}^{ox}$[$PhC^+HCH_3/PhC^\bullet HCH_3$] = +0.37 V vs SCE)[35] is suitable to reduce the Ru^{III} complex ($E_{1/2}^{ox}$[Ru^{III}/Ru^{II}] = +1.29 V vs SCE)[10] which regenerates the photoredox catalyst. Subsequently, the electrophilic benzylic cation reacts with a methanesulfonate anion,

forming the intermediate benzylsulfonate species **3.16**. Finally, the desired product **3.17** is formed by elimination of methanesulfonic acid molecule.

3.4 Conclusion

In summary, the synthesis of heteroarene-*N*-oxide derivatives from the corresponding *N*-heterocycles was reported. *N*-oxygenation was conveniently achieved using meta-chloroperbenzoic acid or hydrogen peroxide with methyltrioxorhenium as catalyst. All heteroaromatic *N*-oxides were structurally fully elucidated. UV-vis absorption measurements have been conducted to determine the wavelength required for excitation. It was shown that most of the pyridine *N*-oxide derivatives require excitation with higher energy light in the UVB to UVC region. In addition, the energies of the excited states were estimated by means of absorption and fluorescence measurements. By applying cyclo-voltametric and differential pulse voltametric measurements, the ground state reduction potentials of the heteroarene-*N*-oxides were determined. The respective excited state reduction potentials were calculated. Considering the utilization of a low-energy excitation wavelength, 4-nitro-pyridine-*N*-oxide (**3.2s**) and mono- and di-*N*-oxidized (**3.2q** and **3.2r**) phenazine were identified as suitable candidates for direct photochemical oxygen atom transfer. The potential as oxygen atom transfer reagent was exemplified by the photochemical oxidation of xanthene using 4-nitropyridine-*N*-oxides (**3.2s**). Further optimization of this oxygen atom transfer reaction is the topic of continuing research work, which due to time constraints is not part of this thesis.

In addition, the synthesis of (methylsulfonyloxy)pyridinium methanesulfonate (**3.14**) from pyridines was described. The structure of the pyridinium salt was successfully determined by X-ray crystallalography. The salt was successfully used in photochemical benzylic oxidation, yielding styrenes from alkylbenzenes. Extensive optimization of the reaction conditions identified the transition metal catalyst tris(2,2′-bipyridine)ruthenium hexafluorophosphate in dichloromethane. The generality of the reaction conditions will be investigated in due course.

4 Palladium-catalyzed synthesis of *N,N*-dimethylanilines via Buchwald-Hartwig amination of (hetero)aryl triflates

4.1 Introduction

The synthesis and structural elucidation of *N*,*N*-dimethylaniline was first reported in 1850.[85] Despite the fact that the compound class has been reported for a long time, its application was mainly limited to specific areas, such as the use as an promotor in the curing of polymers[86] or the synthesis of triarylmethane dyes.[87] The strong electron-donating inductive and mesomeric effect (+*I* and +*M*), renders the dimethylamine functionality an ideal substituent of push-pull systems (Figure 4.1).

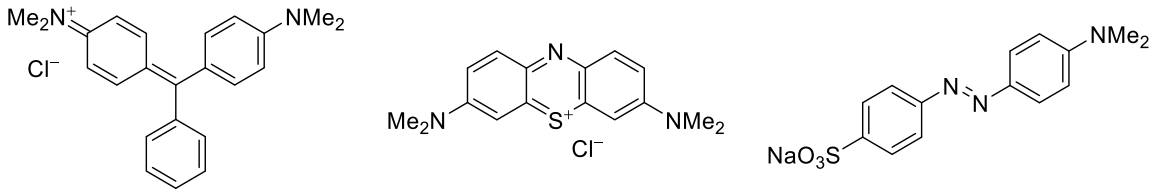

malachite green *methylene blue* *methyl orange*

Figure 4.1: Selected dimethylaniline-based dyes.

In recent decades, modification and utilization of *N*,*N*-dimethylaniline derivatives has been reported in increasing frequency, unraveling an extended synthetic value of these compounds. The activating property of the *N*,*N*-dimethylamine group facilitates a number of diverse functionalization reactions on the arene moiety.[88] In 2014, an elegant method for the *ortho*-functionalization of dimethylanilines-*N*-oxide was described.[88d] By an *aza*-Claisen-type rearrangement of the trifluoroacetic anhydride adduct of the *N*-oxide intermediate, an oxygenation in 2-position can be achieved(Scheme 4.1).

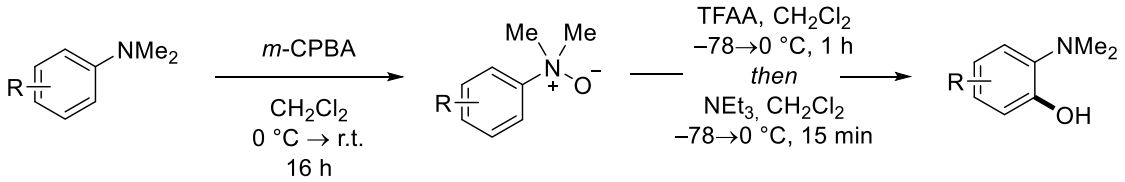

Scheme 4.1: *Ortho*-functionalization through an *aza*-Claisen-type rearrangement via an *N*-oxide intermediate.

The special redox activity of *N*,*N*-dimethylaniline can be utilized for *C*(sp^3)–*C* and *C*(sp^3)–heteroatom bond formation reaction.[89] In this context, an efficient [4+2] cyclization of *N*,*N*-dimethylaniline with maleimides to tetrahydroquinolines could be carried out, using *N*-hydroxyphthalimide as a metal-free organic photoredox catalyst (Scheme 4.2).[89b]

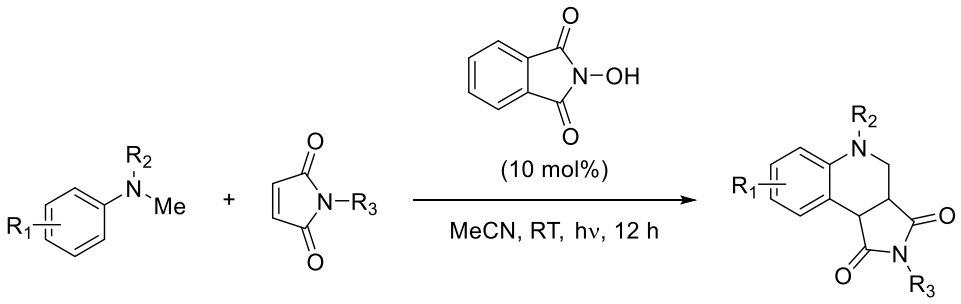

Scheme 4.2: [4+2] Cyclization of *N*-methylanilines with maleimides to tetrahydroquinolines using an organophotoredox catalyst.

Reports on the employment of *N,N*-dimethylanilines as electrophiles in cross-coupling reactions expand the repertoire of applications. As an application, a $C(sp^2)$–$C(sp^2)$ bond formation reaction of dimethylaniline derivatives with phenylboronic acid esters can be achieved by an *in-situ* reduced nickel-carbene catalyst complex (Scheme 4.3).[90]

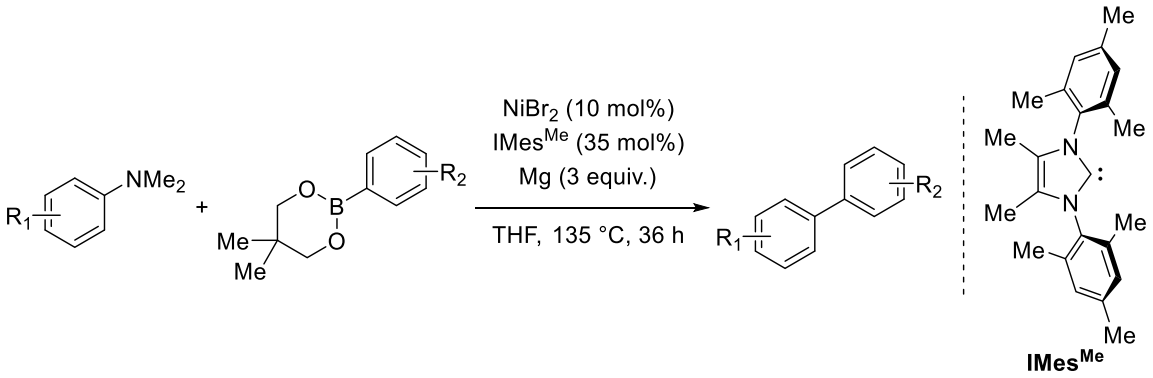

Scheme 4.3: Nickel-catalyzed cross-coupling of *N,N*-dimethylanilines with phenylboronic acid esters.

The possibility for the global derivatization around the core-structure turns *N*,*N*-dimethylaniline into versatile building blocks in organic synthesis. However, considering the high number of applications of *N*,*N*-dimethylaniline, synthetic access of these compounds has made little progress.

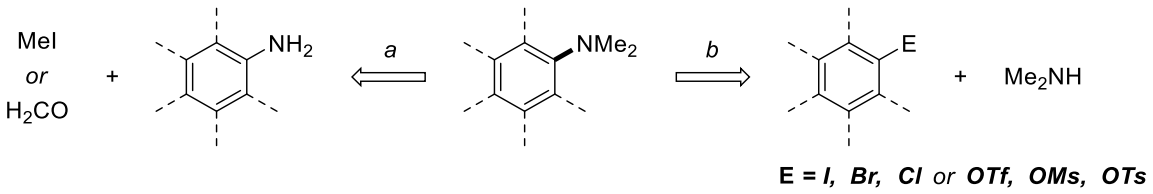

Figure 4.2: Different pathways to access *N,N*-dimethylanilines.

The main access to *N*,*N*-dimethylanilines is via *N*-alkylation[90-91] or reductive elimination with formaldehyde.[88c, 92] Both synthetic routes require aniline derivatives as starting materials, which are of limited availability and sometimes difficult to access (Figure 4.2a). The formation of a C–N bond plays a crucial role in organic chemistry and many research groups are working

on the development and optimization of this reaction (Figure 4.2b).[93] The Buchwald-Hartwig amination, developed in 1983, is one of the most important transition metal-catalyzed reactions and offers the possibility of *C(sp²)−N* bond formation via the palladium-catalyzed coupling of amines with (hetero)aryl halides.[93-94] The reaction mechanism proceeds through steps similar to those known for palladium-catalyzed *C–C* cross-coupling reactions (Figure 4.3).[94b] The identified active catalyst species is the mono-ligand complex L_1[Pd] which is formed from an equilibrium reaction of the diphosphine complex. Subsequently, oxidative addition of the palladium center into the (pseudo)halogen-aryl bond occurs. The aryl-palladium complex is coordinated by the amine in a ligand exchange reaction, resulting in a formal extrusion of an acid compound HX. The catalytic cycle is completed by reductive elimination, leading to the re-formation of the active palladium(0) species L_1[Pd] and the formation of the product.

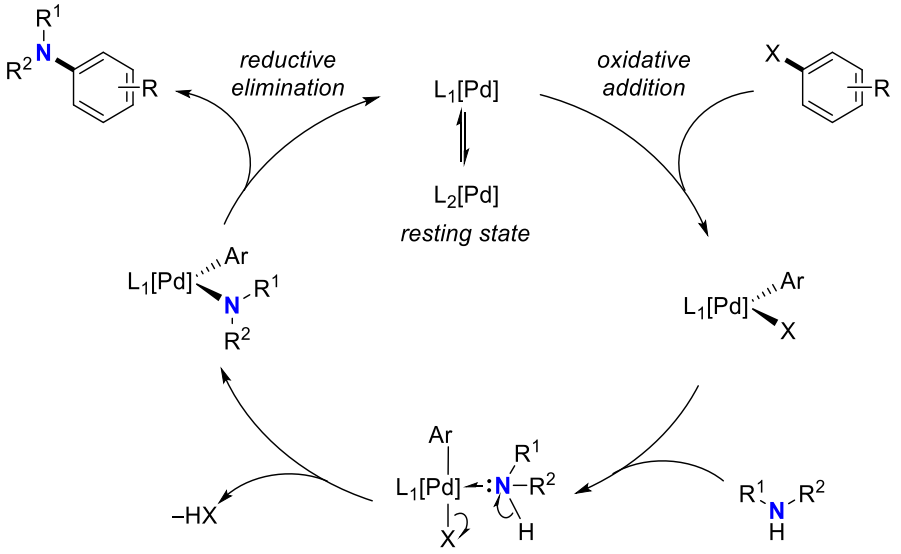

Figure 4.3: Mechanism of the Buchwald Hartwig amination.

Notably, this reaction is most reliable for the arylation of cyclic amines.[95] In contrast, free rotation of the *C–N* bond in acylic amines can initiate *β*-hydride elimination, leading to a palladium-hydride species that causes an undesired proto-(pseudo)dehalogenation of the electrophile (Figure 4.4).

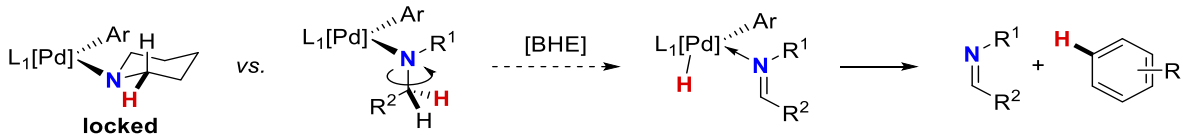

Figure 4.4: Comparison of cyclic and acyclic amines with in respect to *β*-hydride elimination and subsequent proto-(pseudo)dehalogenation.

The synthetic success and widespread use of the Buchwald-Hartwig and palladium-cross coupling reactions in general since the first appearance in 1994 was not insignificantly advanced by the concomitant development of biphenylphosphine ligands.[96] The use of the

biphenyl backbone introduced new possibilities for electronic and steric fine-tuning of phosphine ligands. The group of Buchwald optimized the synthesis and derivatization of these types of ligands and determined the influence of the different substituents on the elementary steps of the catalytic cycle (Figure 4.5).[97]

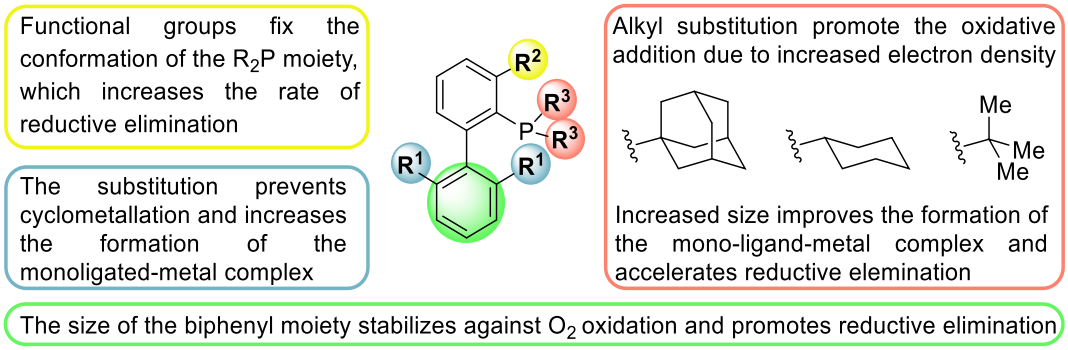

Figure 4.5: The individual influence of substituents on biphenyl phosphine ligands.

The bulky and electron-donating character of biphenylphosphine ligands is important for the stabilization of the mono ligated palladium species L_1[Pd], which are considered as a key intermediate in the catalytic cycle.[98] The oxidative addition of aryl halides with monophosphine palladium complexes has been shown to proceed much faster compared to more highly coordinated complexes.[99] Studies have shown that the introduction of *ortho*-substituents to the phenyl ring of the biarylphosphine (e.g., SPhos and XPhos) leads to a significant increase in activity and stability by preventing the formation of palladacycles.[100] Moreover, this *ortho*-, *ortho'*-substitution increases the size of the ligand as compared to those without *ortho*-substituents, and thus enhances the concentration of the mono-ligated L_1[Pd] species.

The application of *N*,*N*-dimethylamine (boiling point, 7 °C; 10 atm at 80 °C) and other gaseous amines is not desirable under harsh conditions and could be problematic without proper equipment.[101] Also the tendency of aliphatic amines to cause undesired protodehalogenation reactions in Buchwald-Hartwig aminations resulted in the development of only few such examples.

The group of Buchwald published a method for the *N*,*N*-dimethylation of aryl chlorides back in 2009.[102] In this protocol, a pre-synthesized activated palladium catalyst and LiHMDS at room temperature or tribasic potassium phosphate at 110 °C was used. Aryl chlorides, if commercially available, serve as inexpensive electrophiles. However, more advanced substrates difficult to synthetically access under mild-conditions which renders this reaction less suitable for late-stage functionalization (Scheme 4.4).

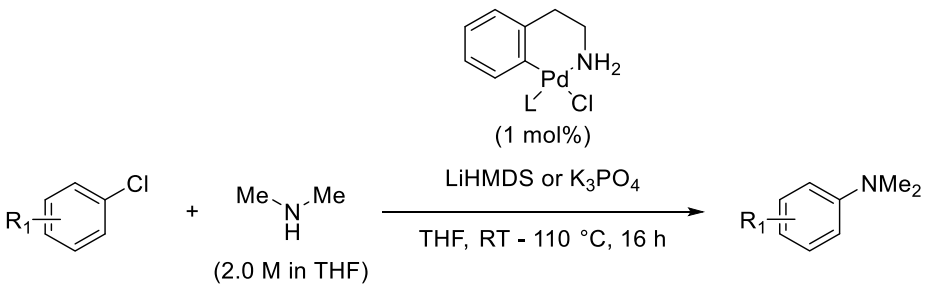

Scheme 4.4: *N,N*-Dimethyl-amination of aryl chlorides with an activated palladium catalyst.

Other related examples for the dimethylamination were conducted under even harsher conditions at 160 °C or more specialized catalytic systems.[103] In addition, the focus was again placed on the activation of aryl chlorides (Scheme 4.5).

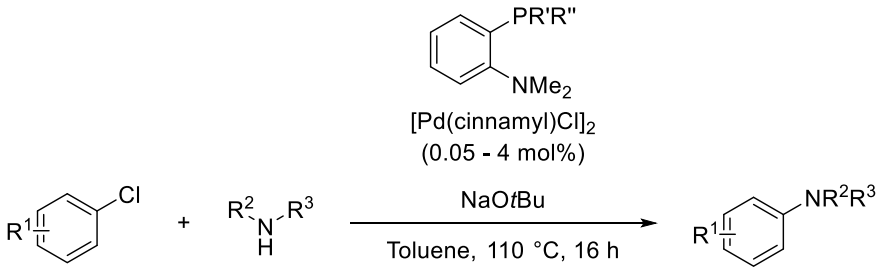

Scheme 4.5: Buchwald-Hartwig amination with arylchlorides.

Arylhalides in general qualify as electrophiles in palladium-catalyzed reactions. Besides chlorine, bromine and iodine compounds are also suitable for the oxidative addition of the palladium complex.[104] During the development of metal-catalyzed reactions, pseudehalogen compounds such as arylsulfonates also turned out to be suitable reaction partners.[105] In particular, the strongly electron-withdrawing trifluoromethylsulfon substituent readily undergo oxidative addition to a metal center.[106] Moreover, all sulfonates are easily accessible from abundant and structurally divers phenols.[107]

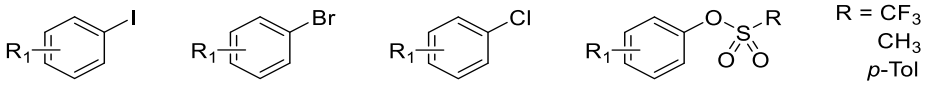

Figure 4.6: Different electrophiles in transition metal cross coupling reactions.

4.2 Objectives

For an ongoing project, our group required a selection of facetiously substituted dimethylanilines for the study of biomimetic C-N bond cleavage. Due to the lack of suitable examples in literature, requiring harsh reaction conditions and demonstrating limited functional group tolerance, we strived to find a more general approach for the synthesis of these compounds.

Basic requirements for this endeavor were (i) facile and safe reaction set-up, (ii) a wide functional group tolerance and (iii) the implementation of easily accessible starting materials. Considering that dimethylamine poses a challenge due to its gaseous aggregate state and toxicity, an application of the commercially available 2 M THF solution will be investigated. Inspired by the possibility of the utilization of pseudohalides as versatile electrophiles in C–C and C–X cross-coupling reaction drew our attention to trifluoromethylsulfonates that are easily accessible from abundant phenols. In addition, the potential side reactions such as *β*-hydride elimination should be circumvented under the developed reaction conditions.

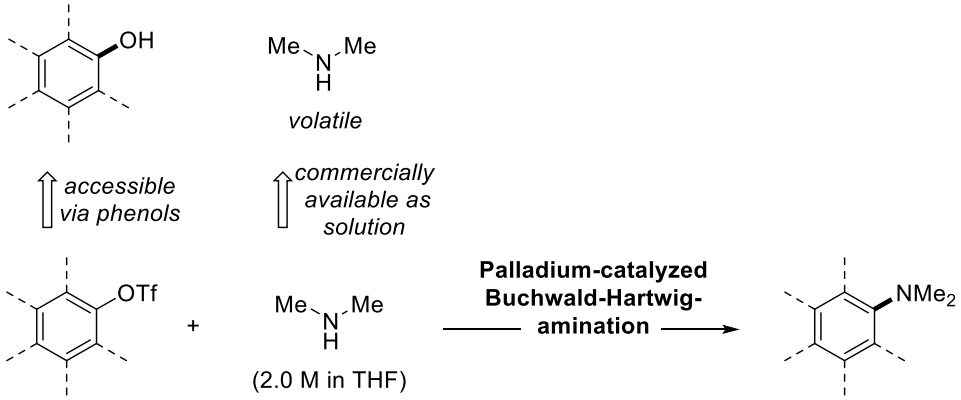

Figure 4.7: Palladium-catalyzed Buchwald-Hartwig amination of triflates using dimethylamine.

4.3 Results and Discussion

4.3.1 Optimization of the reaction conditions

The optimization commenced with the screening of various solvents. In this optimization, *tert*-butylbenzene triflate (**4.1a**) and commercially available 2.0 M solution of dimethylamine in THF (**4.2a**) was utilized as a model system. Furthermore, the catalyst system $Pd_2(bda)_3$ (10 mol%) with XPhos (1.5 equiv. per palladium core) was chosen in combination with cesium carbonate as a base (Table 4.1).

Table 4.1: Solvent screening.

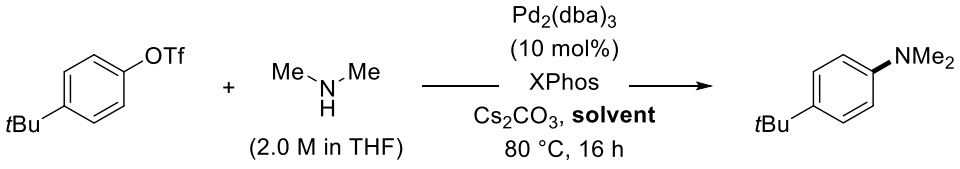

4.1a **4.2a** **4.3a**

entry	solvent	GC-yield [%][a]	isol. yield [%]
1	*n*-hexanes	>99	99
2	PhMe	91	90
3	THF	>99	97
4	1,4-dioxane	97	97
5	DMA	92	92
6	MeCN	96	92
7	DMF	86	68
8	DMSO	28	n.d.
9	EtOH	4	n.d.
10	*i*-PrOH	5	n.d.
11	acetone	11	n.d.
12	ethylene carbonate	4	n.d.
13	$CHCl_3$	3	n.d.

Footnote: The reaction was carried out on a 0.5 mmol mass scale (0.25 M) with 1.2 equiv. cesium carbonate, 4 equiv. *N,N*-dimethylamine and a catalyst loading of 10 mol% Pd_2dba_3 and 30 mol% XPhos. [a] biphenyl was used as internal standard.

To our delight, the desired product **4.3a** was obtained in excellent yields in a variety of different aprotic solvent systems. THF and 1,4-dioxane, as well as nonpolar aliphatic and aromatic solvents such as *n*-hexane and toluene, are suitable for the synthesis of the desired compound (Table 4.1, entries 1-4). Furthermore, the nitrogen-containing polar aprotic solvents DMA, MeCN and DMF also led to product formation in good to very good yields of up to 92% (Table 4.1, entries 5-7). The isolation of the product from the reaction in DMF was more difficult

due to the formation of by-products (Table 4.1, entry 7). In contrast, no satisfactory yield was obtained in the polar aprotic solvent DMSO (Table 4.1, entry 8). The protic solvents EtOH and *i*-PrOH as well as solvents with carbonyl functionalities or chlorinated solvents also proved to be unsuitable (Table 4.1, entries 9-13). Due to the toxicity of *n*-hexane and the enhanced solubility of polar starting materials in THF, THF was selected for further investigation.

Following the optimization of the solvent, the reaction conditions were evaluated with respect to the base.

Table 4.2: Screening of different bases.

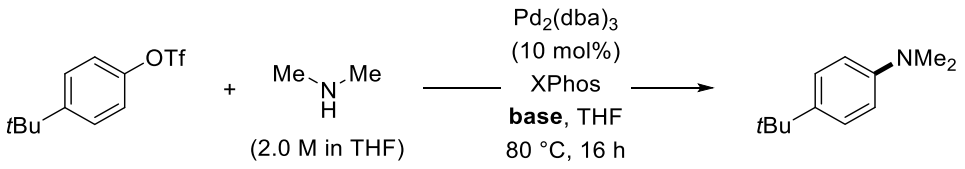

4.1a **4.2a** **4.3a**

entry	base	GC-yield [%][a]	isol. yield [%]
1	none	0	n.d.
2	Cs_2CO_3	>99	97
3	K_2CO_3	68	66
4	K_3PO_4	>99	99
5	K_2HPO_4	1	n.d.
6	MeOK	0	n.d.
7	NEt_3	3	n.d.
8	pyridine	5	n.d.
9	*N*-methylmorpholine	3	n.d.
10	Hünig's base	0	n.d.
11	Na_2CO_3	4	n.d.
12	$NaHCO_3$	3	n.d.
13	$KHCO_3$	3	n.d.
14	NaOH	18	n.d.
15	KOH	29	n.d.
16	NaO*t*-Bu	10	n.d.
17	NaOAc	4	n.d.
18	KOAc	3	n.d.
19	NaOTFA	4	n.d.

Footnote: The reaction was carried out on a 0.5 mmol mass scale (0.25 M) with 1.2 equiv. base, 4 equiv. *N,N*-dimethylamine and a catalyst loading of 10 mol% Pd_2dba_3 and 30 mol% XPhos. [a] biphenyl was used as internal standard.

A comprehensive screening of different bases revealed that only a limited number of bases are suitable in the palladium-catalyzed amination reaction (Table 4.2). In the absence of base, no conversion of the starting materials was observed (Table 4.2, entry 1). Caesium carbonate resulted in a complete conversion to the desired product which was isolated in 97% yield (Table

4.2, entry 2). The variation of the cation from cesium to potassium led to a moderate yield of 66% (Table 4.2, entry 3). Furthermore, the use of sodium carbonate leads to almost no conversion of the starting material (Table 4.2, entry 11). To our delight, tribasic potassium phosphate yielded the product in 99% isolated yield (Table 4.2, entry 4). Hydrogen carbonates and hydrogen phosphates proved unsuitable for the reaction (Table 4.2, entries 5, 12 & 13). Sodium and potassium hydroxide yielded the desired product in 18% and 29% GC yields, respectively. (Table 4.2, entries 14, 15). Organic bases such as triethylamine, Hünig's base, pyridine, *N*-methyl morpholine or acetate bases were unsuitable (Table 4.2, entries 7-10, entries 17-19). Most surprisingly, the alcoholate bases, frequently used in the literature furnished the product also in very low yields (Table 4.2, entries 6, 16). Tribasic potassium phosphate was chosen as the optimal base due to its higher abundance and low cost.

The next crucial step in the optimization concerned the variation of the ligand in the catalytic system. The reactions were carried out in dry THF, which is also the solvent of the *N,N*-dimethylamine solution. Due to the continuous development of biphenylphosphine ligand systems, the number of possible metal-ligand combinations is increasing. The focus of this ligand screening was limited to bidentate ligands and established commercially available ligands, aiming to provide reaction conditions that are readily reproducible in other laboratories (Table 4.3). As before, Pd_2dba_3 with a catalyst loading of 10 mol% was used as the palladium source. The ligands were used in slight access of 30 mol% equaling of metal to ligand ratio to 1:1.5.

Table 4.3: Screening of different ligands.

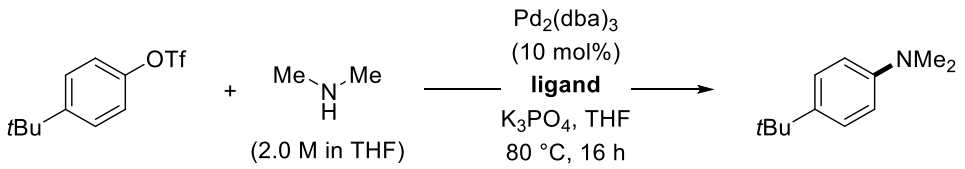

4.1a **4.2a** **4.3a**

entry	ligand	GC-yield [%][a]	isol. yield [%]
1	MePhos	90	75
2	BrettPhos	37	n.d.
3	**XPhos**	**99**	**99**
4	*t*BuXPhos	89	83
5	IndPhAd$_2$	94	89
6	SPhos	99	94
7	JohnPhos	85	80
8	RuPhos	99	94
9	CataxiumA	16	n.d.
10	Xanthphos	10	n.d.
11	dppe	3	n.d.
12	dppp	3	n.d.
13	dppb	3	n.d.
14	dppf	12	n.d.
15	dppox	7	n.d.

Footnote: The reaction was carried out on a 0.5 mmol scale (0.25 M) with 1.2 equiv. K_3PO_4, 4 equiv. *N,N*-dimethylamine and a catalyst loading of 10 mol% Pd_2dba_3 and 30 mol% ligand. [a] biphenyl was used as internal standard.

First, a number of biphenyl phosphine ligands developed by the group of Buchwald were tested in the palladium-catalyzed *N,N*-dimethylamination.[108] The strong influence of the ligand design on the productivity of the catalytic system was evident. The ligand MePhos proved to be suitable for obtaining the desired product in a good yield (Table 4.3, entry 1). The methoxy substituents at position 3 and 6 of the aryl backbone present in BrettPhos show a diminished GC-yield of 37% (Table 4.3, entry 2). In contrast, an increased steric demand at position 2' and 6' resulted in enhanced product formation (Table 4.3, entry 3). The product **4.3a** was obtained in excellent yield of 99% isolated yield using XPhos as ligand. Employing the more basic variant *t*BuXPhos bearing di-*tert*-butyl phosphine groups, thus result in a shorter ligand-metal distance which facilitates oxidative addition, did not benefit the product formation (Table 4.3, entry 4). The biphenyl phosphine ligand SPhos and RuPhos also furnished the product in excellent yields (Table 4.3 entries 6, 8). JohnPhos, with a biphenyl backbone without substituents, yielded the product in 80% isolated yield (Table 4.3, entry 7). The none-biphenyl ligand CataxiumA delivered the product in only 16% (Table 4.3, entry 7). Utilization of bidentate

ligands did not increase the yield of the desired product. The best of 10-12% was obtained with dppf and Xantphos as ligand according to calibrated GC (Table 4.3, entries 10, 14). Based on this assay, XPhos was and remained the ligand of choice of further investigations.

Next, the catalyst loading was examined to ensure that the developed process is as gentle on resources as possible. THF and tribasic potassium phosphate were used in this optimization. Table 4.4 below shows the screening of catalyst loading of 10 mol% to 0.5 mol%.

Table 4.4: Screening of different catalyst loading.

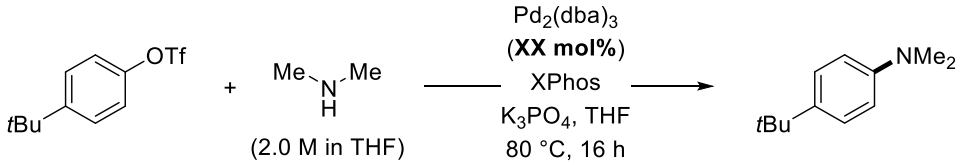

4.1a **4.2a** **4.3a**

entry	catalyst loading (XX mol%)[a]	GC-yield [%][b]	isol. yield [%]
1	10	100	99
2	7.5	100	99
3	5.0	100	99
4	2.5	99	97
5	1.0	94	92
6	0.75	49	n.d.
7	0.5	6	n.d.

Footnote: [a] The reaction was carried out on a 0.5 mmol scale (0.25 M) with 1.2 equiv. K_3PO_4, 4 equiv. *N,N*-dimethylamine, Pd_2dba_3 and XPhos (ligand to metal ratio L/M = 1.5). [b] biphenyl was used as internal standard.

A catalyst loading of 5.0 mol% - 10 mol% shows that the desired product is formed without any losses in yield (Table 4.4, entries 1-3). Only a slightly diminished yield was observed with a catalyst loading of 2.5 mol% and 1.0 mol% (Table 4.4, entries 4, 5). Lower catalyst loadings to 0.75 mol% and 0.5 mol%, resulted in a significant decline in yield as handling issues increase (Table 4.4, entries 6, 7). To ensure a reliable methodology, a catalyst loading of 2.5 mol% was chosen for further transformations.

4.3.2 Scope of the Buchwald-Hartwig amination

With the optimal reaction conditions in hand, the limits of the scope were investigated. The corresponding triflates were synthesized following literature procedures.[109] A vast variety of dimethylanilines **4.3** were prepared, demonstrating a broad functional group tolerance (Table 4.5)

Table 4.5-1/2: Palladium-catalyzed *N,N*-dimethylamination of various aryl triflates.

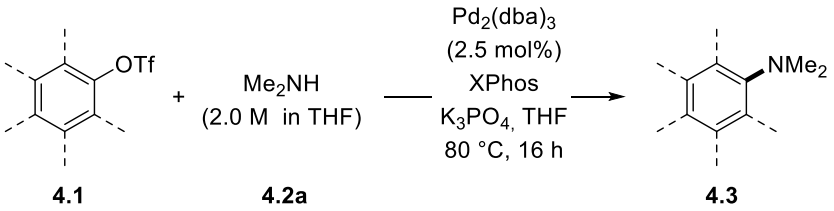

4.1 **4.2a** **4.3**

entry	substrate		product		isol. yield
1	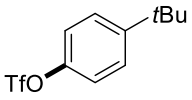	**4.1a**	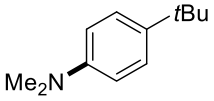	**4.3a**	99%[a]
2	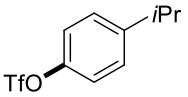	**4.1b**	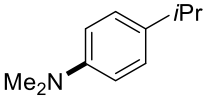	**4.3b**	90%
3	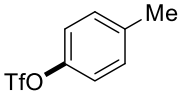	**4.1c**	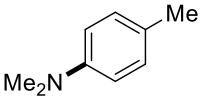	**4.3c**	90%
4	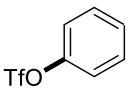	**4.1d**	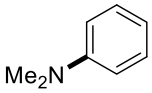	**4.3d**	99%
5	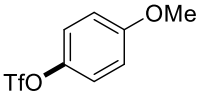	**4.1e**	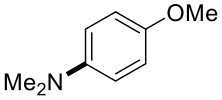	**4.3e**	92%
6	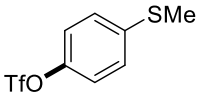	**4.1f**	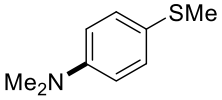	**4.3f**	99%
7	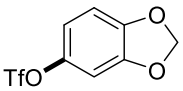	**4.1g**	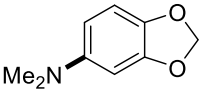	**4.3g**	95%
8	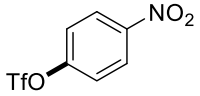	**4.1h**	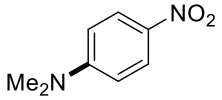	**4.3h**	71%
9	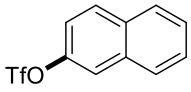	**4.1i**	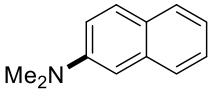	**4.3i**	95%

Table 4.5-2/2: Palladium-catalyzed *N,N*-dimethylamination of various aryl triflates.

entry	substrate		product		isol. yield
10	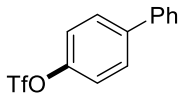	**4.1j**	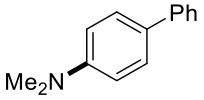	**4.3j**	99%
11	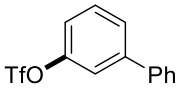	**4.1k**	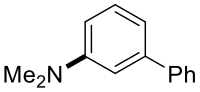	**4.3k**	77%
12	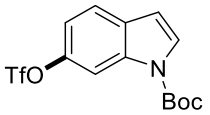	**4.1l**	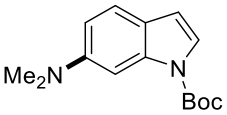	**4.3l**	67%
13	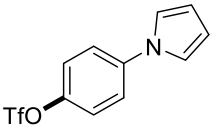	**4.1m**	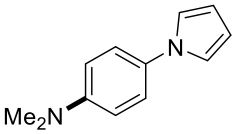	**4.3m**	99%
14	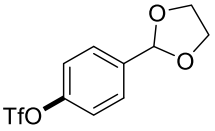	**4.1n**	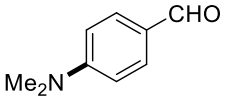	**4.3n**	99%[b]
15	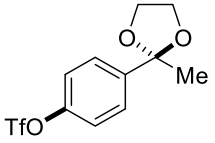	**4.1o**	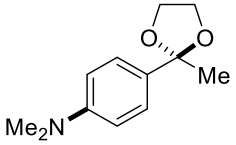	**4.3o**	99%
16	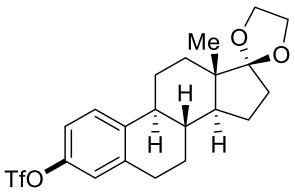	**4.1p**	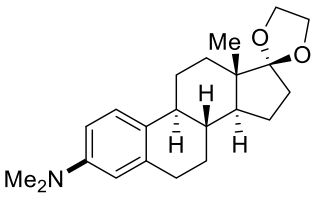	**4.3p**	88%
17	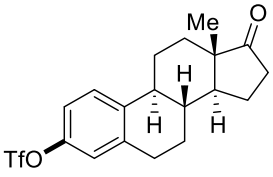	**4.1q**	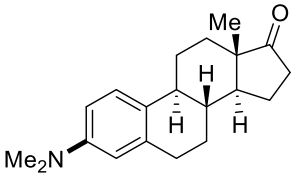	**4.3q**	87%
18	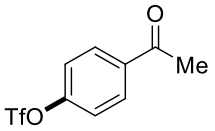	**4.1r**	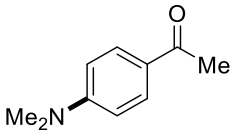	**4.3r**	18%

Footnote: The reaction was carried out on a 0.5 mmol scale (0.25 M) with 1.2 equiv. K_3PO_4, 4 equiv. *N,N*-dimethylamine and a catalyst loading of 2.5 mol% Pd_2dba_3 and 7.5 mol% Ligand. [b] Acetal cleavage during aqueous workup

To our delight, a wide range of this aryltriflates **4.1** were suitable substrates in the palladium-catalyzed *N*,*N*-dimethylamination reaction. In addition to the *tert*-butyl group bearing compound **4.1a**, other branched and linear alkyl substituents proved also suitable for this reaction and the corresponding products **4.3b** and **4.3c** were obtained excellent yields (Table 4.5, entries 1-3). Likewise, plain phenyltriflate (**4.3d**) was isolated in 99% yield (Table 4.5, entry 4). Compounds bearing electron donating ether and thioether functions **4.1e** and **4.1f**

were converted into the desired products **4.3e** and **4.3f** in excellent yields of 92% and 99%, respectively (Table 4.5, entries 5, 6). Also, the protected catechol derivative **4.1g** bearing a methylendioxo moiety was successfully converted (Table 4.5, entry 7). Transformation of compound bearing an electron-withdrawing nitro substituent (**4.1h**) was successfully converted, resulting in a moderate yield of 71% (Table 4.5, entry 8). Naphthyl and biphenyl substrates **4.1i** and **4.1j** were also converted to the desired products (Table 4.5, entries 9-10). Notably, [1,1'-biphenyl]-3-yl triflate (**4.1k**) resulted in a slightly decreased yield of 77% (Table 4.5, entry 11). Heterocyclic compounds such as indole and pyrrole derivatives **4.1l** and **4.1m** were readily converted into the corresponding products (Table 4.5, entries 12, 13). The carbonyl functionalities in substrates derived from acetophenone **4.1n** and benzaldehyde **4.1o** had to be acetal-protected to avoid undesired side reactions (Table 4.5, entries 14, 15). To our delight, in addition to the acetal-protected estrogen derivative **4.1p**, the unprotected estrogen derivative **4.1q** was also converted in similar isolated yield (Table 4.5, entries 16, 17). The structure of the estrogen derivative (**4.3q**) was confirmed by X-ray crystallography (Figure 4.8).

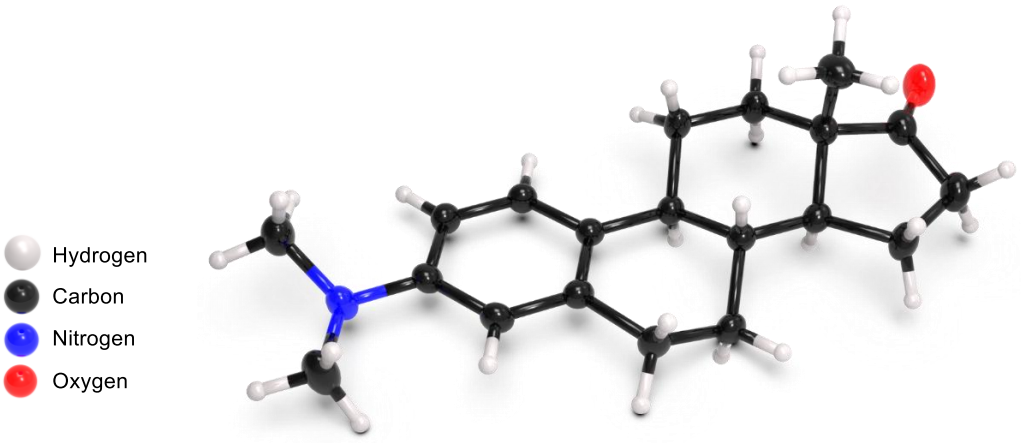

Figure 4.8: X-ray crystal structure of estrogen derivative 4.3q. Displacement ellipsoids correspond to 30% probability.

After investigating the scope of different *para*- and *meta*-substituted aryl triflates, *ortho*-substituted aryl triflates were further examined. Table 3.6 presents the results of the reaction under optimized reaction condition with compounds bearing *ortho*-substituents.

Table 4.6: Palladium-catalyzed *N,N*-dimethylamination of challenging aryl triflates.

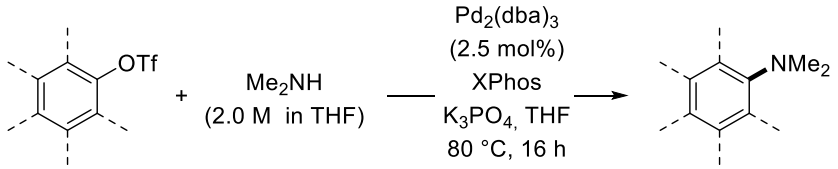

4.1 **4.2a** **4.3**

entry	substrate		product		isol. yield
1	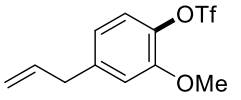	**4.1s**	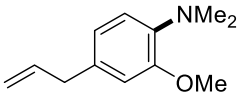	**4.3s**	29%
2	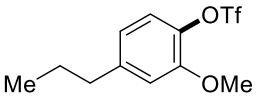	**4.1t**	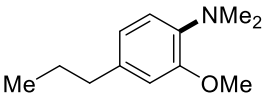	**4.3t**	34%
3	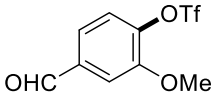	**4.1u**	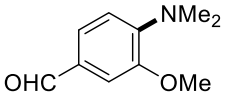	**4.3u**	15%
4	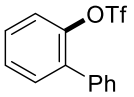	**4.1v**	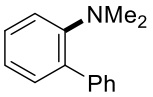	**4.3v**	0%
5	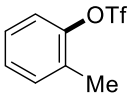	**4.1w**	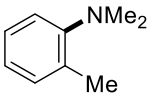	**4.3w**	77%
6	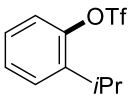	**4.1x**	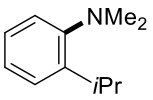	**4.3x**	24%

Footnote: The reaction was carried out on a 0.5 mmol scale (0.25 M) with 1.2 equiv. K_3PO_4, 4 equiv. *N,N*-dimethylamine and a catalyst loading of 2.5 mol% Pd_2dba_3 and 7.5 mol% XPhos.

The palladium-catalyzed amination of aryl triflates bearing an *ortho*-substituent proved to be more challenging. For eugenol or vanillin derived triflates **4.1s**, **4.1t** and **4.1u** bearing a coordinating *ortho*-methoxy group, the reaction proceeded only in poor yields of 15%-34% (Table 4.6, entries 1-3). Similarly, no product formation was observed in the presence of a phenyl substituent in the *ortho*-position (Table 4.6, entry 4). In contrast, the reaction of aryl triflates with a methyl group **4.1w** proceeded in moderate yield of 77% (Table 4.6, entry 5). Substrate bearing a more sterically demanding *ortho*-isopropyl substituent **4.1x** significantly reduces the yield to 24% (Table 4.6, entry 6). These results suggest that a coordinative character of the substrate may inhibit the reaction by complexation by palladium or unfavorable steric repulsion. A potential mode for the deactivation by ortho-coordinating groups is shown in Scheme 4.6 below.

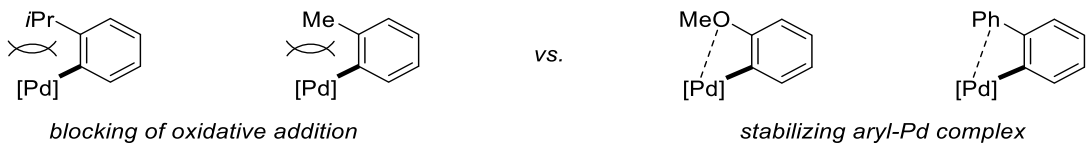

Scheme 4.6: Plausible deactivation pathways.

Next, the scope of the amine component was investigated by selecting various symmetrical and unsymmetrical amines. The focus of this investigation lies on open-chain, aliphatic amines **4.2a**-**4.2n** (Table 4.7).

Table 4.7-1/2: Palladium-catalyzed arylation of acyclic, alkyl amines.

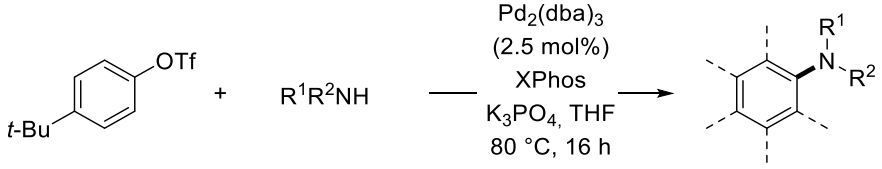

4.1a **4.2** **4.4**

entry	substrate		product		isol. yield
1	Me_2NH	**4.2a**	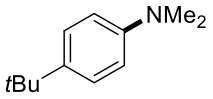	**4.4a**	99%
2	Et_2NH	**4.2b**	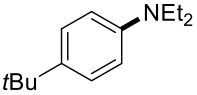	**4.4b**	95%
3	nPr_2NH	**4.2c**	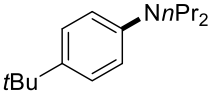	**4.4c**	95%
4	nBu_2NH	**4.2d**	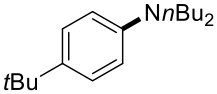	**4.4d**	97%
5	iPr_2NH	**4.2e**	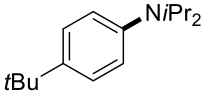	**4.4e**	0%
6	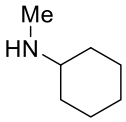	**4.2f**	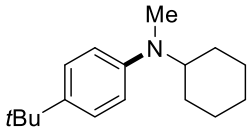	**4.4f**	96%
7	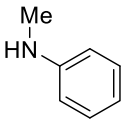	**4.2g**	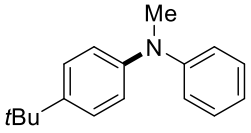	**4.4g**	93%

Table 4.7-2/2: Palladium-catalyzed arylation of acyclic alkyl amines.

entry	substrate		product		isol. yield
8	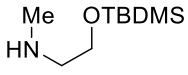	**4.2h**	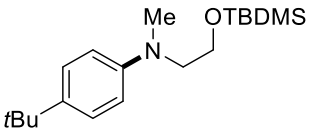	**4.4h**	94%
9	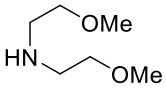	**4.2i**	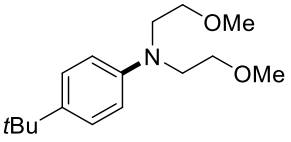	**4.4i**	66%
10	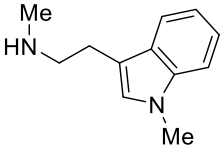	**4.2j**	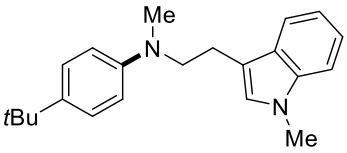	**4.4j**	85%
11	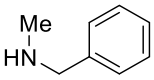	**4.2k**	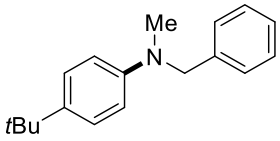	**4.4k**	99%
12	$BnNH_2$	**4.2l**	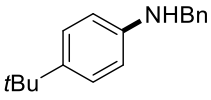	**4.4l**	87%
13	nBuNH$_2$	**4.2m**	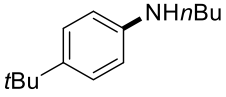	**4.4m**	-
14	tBuNH$_2$	**4.2n**	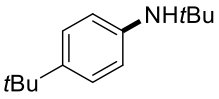	**4.4n**	-

Footnote: The reaction was carried out with 0.5 mmol *tert*-butylbenzene triflate (0.25 M) 1.2 equiv. K_3PO_4, 4 equiv. amine and a catalyst loading of 2.5 mol% Pd_2dba_3 and 7.5 mol% XPhos.

To our delight, the electron-rich, linear secondary alkylamines formed the corresponding products in excellent isolated yields of up to 99% (Table 4.7, entries 1-4). Branched diisopropyl amine (**4.2e**), which exhibit an increased propensity for *β*-hydride elimination, showed no formation of product **4.4e** under the applied conditions (Table 4.7, entry 5). In contrast, a similar branched substituent bearing a cyclohexane ring **4.2f** reacted readily to obtain the product **4.4f** in 96% yield (Table 4.7, entry 6). In addition, *N*-methyl aniline (**4.2g**) was successfully converted with a yield of 93% (Table 4.7, entry 7). In addition, amines with methyl and silyl ether moieties (**4.2h** and **4.2i**) were also tolerated under the reaction conditions (Table 4.7, entries 8-9). Likewise, the tryptamine-based substrate **4.2j** provided the desired product **4.4j** in a good yield of 85% (Table 4.7, entry 10). Primary and secondary benzylamine **4.2k** and **4.2l** proved to be a suitable substrate with good to excellent yields of 87% and 99% (Table 4.7,

entries 11-12). The primary linear and branched butylamines **4.2m** and **4.2n** were unsuitable in this reaction.

To assess the possible extension of the reaction spectrum to other electrophiles, various aryl (pseudo)halides were tested under the optimized conditions (Table 4.8).

Table 4.8: Comparison of different electrophiles in the Palladium-catalyzed *N,N*-dimethylamination.

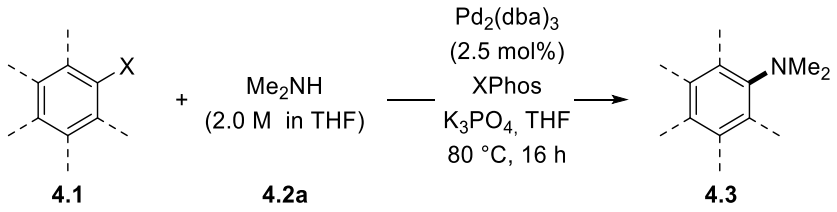

4.1 **4.2a** **4.3**

entry	substrate		product		isol. yield
1	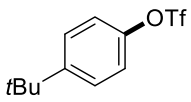	**4.1a**	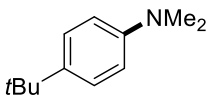	**4.3a**	99%
2	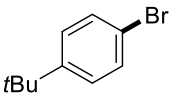	**4.1aa**	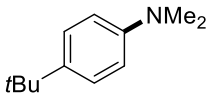	**4.3a**	99%
3	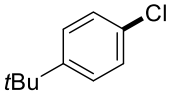	**4.1ab**	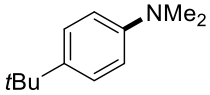	**4.3a**	57%
4	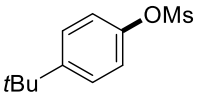	**4.1ac**	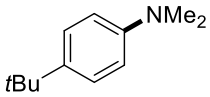	**4.3a**	-
5	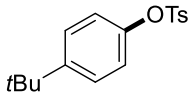	**4.1ad**	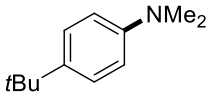	**4.3a**	-

Footnote: The reaction was carried out with 0.5 mmol *tert*-butylbenzene triflate (0.25 M) 1.2 equiv. K_3PO_4, 4 equiv. amine and a catalyst loading of 2.5 mol% Pd_2dba_3 and 7.5 mol% XPhos.

Aryl triflate and aryl bromide (**4.1a** and **4.1aa**) proved to be suitable substrates with excellent yields of 99%. (Table 4.8, entries 1-2). Aryl chloride (**4.1ab**) provided the desired product in moderate yields of 57% (Table 4.8, entry 3). In contrast, methyl and tosyl sulfonate (**4.1ac** and **4.1ad**) were not converted under these reaction condition (Table 4.8, entries 4-5).

The system was thereafter examined concerning the reactivity of the respective electrophiles. In an intramolecular competition reaction, *para*-bromo aryl triflate (**4.1y**) was subjected to the optimized reaction conditions (Scheme 4.7).

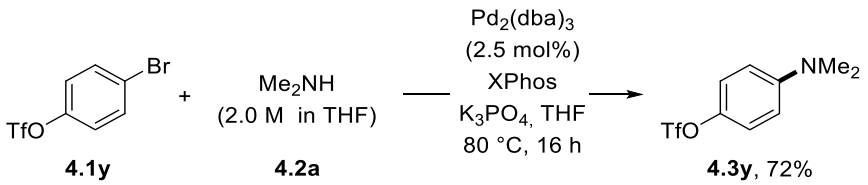

Scheme 4.7: Intramolecular competition experiments of two different electrophiles.

In this intramolecular competition reaction, the aryl bromine bond was shown to be more activated towards oxidative addition as compared to the sulfonate bond. The isolated yield of 72% of the corresponding product **4.3y** was comparable to the yield obtained for the electron-deficient nitro derivative **4.3h**. Remarkably, the triflate functionality remained intact and can be transformed in a subsequent coupling reaction.

4.3.3 Derivatization of *N,N*-dimethylanilines

Subsequently, the synthetic utility of *N,N*-dimethylanilines **4.3** class was investigated. Various synthetic modifications were carried out around the core structure of the aniline products. In 2014, the group of Chain reported a useful protocol for the facile *ortho*-functionalization of *N,N*-dialkyl anilines.[88d] Following the protocol of Chain and co-workers, an *ortho*-hydroxylation of 4-*tert*-butyl-*N,N*-dimethylaniline (**4.3a**) was achieved in two steps via the *N*-oxide intermediate **4.5**.

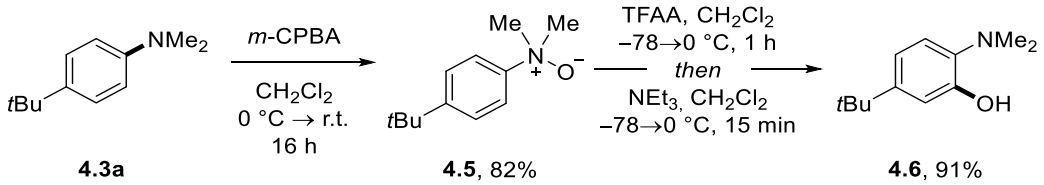

Scheme 4.8: *Ortho*-functionalization via aniline-*N*-oxide intermediate using trifluoroacetic acid anhydride.

4-*tert*-butyl-*N,N*-dimethylaniline (**4.3a**) was readily oxidized with *m*-CPBA to give the corresponding *N*-oxide (**4.5**) in good yield of 82% (Scheme 4.8). This intermediate can be converted to the *ortho*-substituted phenol **4.6** in 91% yield using trifluoroacetic acid anhydride. The structure of the aniline-*N*-oxide was confirmed by X-ray crystallography.

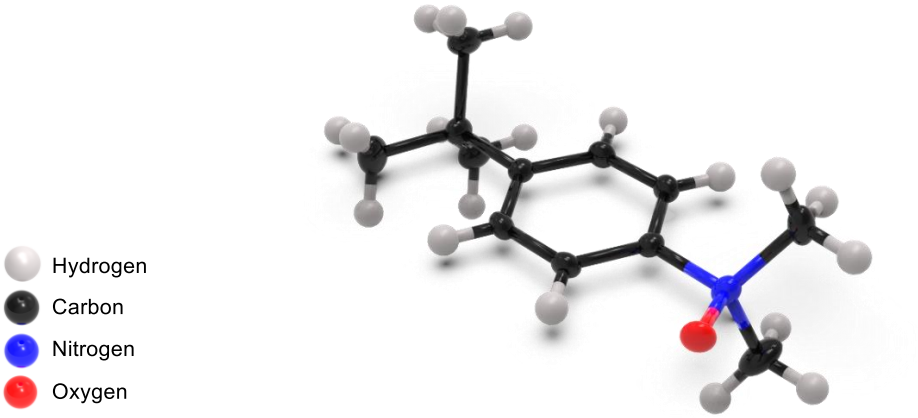

Figure 4.9: X-ray crystal structure of derivative 4.6. Displacement ellipsoids correspond to 30% probability.

N,N-dimethylanilines **4.3** are electron-rich compounds, activated for electrophilic aromatic substitution. Therefore, *para*-iodination represents a preparative useful functionalization to convert the aniline derivative into an electrophile.[88e]

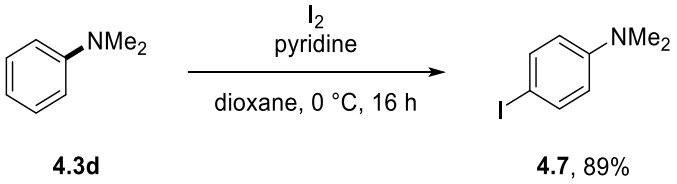

4.3d **4.7**, 89%

Scheme 4.9: Electrophilic aromatic *para*-iodination of *N,N*-dimethylanilines.

Utilizing *N,N*-dimethylaniline (**4.3d**), the *para*-iodination was accomplished in the presents of iodine and pyridine at 0 °C. 4-Iodo-*N,N*-dimethylaniline (**4.7**) was isolated in 89% yield.

The special redox activity of the amine functionality enables the possibility of a substitution at the *N*-methyl group. The group of Li described a *C(sp^3)–C(sp)* bond formation by a copper-catalyzed oxidation of *N,N*-dimethylaniline and subsequent coupling with a terminal alkyne.[89a]

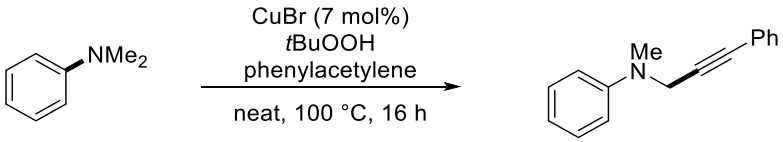

4.3d **4.8**, 56%

Scheme 4.10: Copper-catalyzed oxidation to form a *C(sp^3)–C(sp)* bond.

The methyl functionalization was conducted starting from *N,N*-dimethylaniline (**4.3d**) in the presents of phenylacetylene, *tert*-butyl hydroperoxide and catalytic amounts of copper bromide at 100 °C. The desired product (**4.8**) was isolated in 56% yield.

4.4 Conclusion

In summary, the convenient synthesis of *N,N*-dimethylaniline derivatives from dimethylamine (**4.2a**) and aryl triflates (**4.1**) was reported. In a comprehensive optimization of the reaction conditions with respect to the solvent, the base and phosphine ligands, a suitable protocol for the conversion of aryl triflates could be elaborated. The resulting protocol offers the convenient synthesis of *N,N*-dimethylaniline derivatives using an unsophisticated catalytic system, a mild base and triflates as electrophiles which are readily available from inexpensive phenols. The presented method shows a broad reaction spectrum with good yields for substrates bearing electron-rich as well as electron-poor substituents under mild reaction conditions on small and gram-scale. Other sulfonates were not converted by the catalyst system. However, the reaction conditions can be readily adapted to convert for bromo and chloroarenes to *N,N*-dimethylanilines. Noteworthy, a competition experiment showed that the oxidative addition proceeds preferentially into the C–Br in the presence of a trifluoromethylsulfonate group. Furthermore, the broad applicability of *N,N*-dimethylanilines as starting material was demonstrated by facile functionalization of the methyl groups, as well as *ortho*- and *para*-substitution of the aromatic ring.

5 Experimental section

5.1 General remarks

All reactions involving moisture- or air-sensitive reagents or products were performed under an atmosphere of dry argon using standard Schlenk techniques and pre-dried glassware. Syringes for handling of dry solvents or liquid reagents were flushed with dry argon prior to use. Analytical data of substances that are known in literature (marked by corresponding references) were compared with those described in the literature.

Solvents

All solvents for reactions containing moisture-sensitive reagents were dried, distilled and stored under inert atmosphere (argon or nitrogen) according to following standard procedures.

***N,N*-Dimethylacetamide** was dried over KH and distilled under ambient pressure.

***N,N*-Dimethylformamide** was dried over CaH_2 for 8 h, degassed and distilled under reduced pressure.

Methanol was dried over Mg and refluxed prior to distillation.

***N*-Methyl-2-pyrrolidone** was stirred at 150 °C for 4 h and subsequently distilled under reduced pressure.

Tetrahydrofuran using a SPS solvent purification system by MBRAUN.

Toluene was pre-dried over KH and distilled over sodium/benzophenone.

Water was degassed for 2 h and ultrasonicated.

1,2-Dichloroethane was pre-dried over molecular sieves 4Å, distilled and stored over molecular sieves.

Commercially available dry solvents were purchased from SIGMA-ALDRICH and ACROS ORGANICS.

Chromatography

Analytical thin layer chromatography (TLC) was performed on 0.25 mm silica gel 60F plates (MACHEREY-NAGEL) with 254 nm fluorescent indicator from MERCK. Plates were visualized under ultraviolet light (254 nm) and developed by treatment with the $KMnO_4$ solution or Chromatographic purification of products was accomplished by flash column chromatography on MERCK silica gel, grade 60 (0.063-0.200 mm, 70–230 mesh ASTM).

Vacuum

Following pressures were measured on the used vaccuum pump and are not corrected: membrane pump vacuum (MPV): 3.1 mbar, oil pump vacuum (OPV): 0.05 mbar.

Analytical Data

Analytical data of substances that are known in literature (marked by corresponding references) were compared with those described in the literature.

Infrared Spectroscopy

Infrared spectra were recorded using a BRUKER ALPHA-P spectrometer. Liquid probes were measured as film, solid probes were measured neat. Absorption is given in wave numbers (cm^{-1}). Spectra were recorded in the range of 4000–400 cm^{-1}. Following abbreviations were used for characterization: s (strong), m (medium), w (weak).

Nuclear Magnetic Resonance Spectroscopy

Nuclear magnetic resonance (NMR) spectra were recorded at 300 or 600 MHz (^{1}H-NMR) and 75 or 125 MHz (^{13}C-NMR, APT (Attached Proton Test) on BRUCKER AM 250, VARIAN Unity-300 and Inova 500 instruments. Chemical shifts are reported as δ-values in ppm relative to the residual proton peak of the deuterated solvent or its carbon atom, respectively.

	^{1}H-NMR	^{13}C-NMR
d_1-Chloroform	7.26 ppm,	77.0 ppm
d_6-DMSO	2.49 ppm 7	7.0 ppm

For characterization of the observed signal multiplicities the following abbreviations were applied: s (singlet), d (doublet), t (triplet), q (quartet), m (multiplet). Coupling constants *J* are reported in Hertz (Hz).

Mass spectroscopy

Mass spectra were measured on FINNIGAN MAT 95 (200 eV, EI-MS) or LCQ (70 eV, ESI-MS). The ratio of mass to charge are indicated, intensities relative to the base peak (I = 100) are written in parentheses. High resolution mass spectras (HRMS) were recorded on BRUKER APEX IV (7 T, Transform Ion Cyclotron Resonance (FTICR) mass spectrometer).

Melting Points

Melting points were measured using a BÜCHI melting point apparatus. Reported values are uncorrected.

Crystallographic data

Crystallographic data were collected on a BRUKER KAPPA APEX II DUO diffractometer. The structure was solved by direct methods and refined by full-matrix least-squares procedures on F^2 with the SHELXTL software package (Sheldrick, G. M. *Acta Crystallogr.* **2008**, *A64*, 112.). XP (BRUKER AXS) was used for graphical representation. Displacement ellipsoids are drawn at the 30% probability level.

High-pressure reactions

High-pressure reactions were carried out in WEATHON screw capped glass vials (5 mL) with silicone/PTFE septum, equipped with a magnetic stirring bar and a needle. The reaction mixtures were placed in a PARR 300 mL stainless steel autoclave and pressurized with carbon monoxide (LINDE).

5.2 General procedures

5.2.1 General procedures of chapter 1

5.2.1.1 General procedure 1.A: Deoxygenation of pyrimidopteridine *N*-oxides

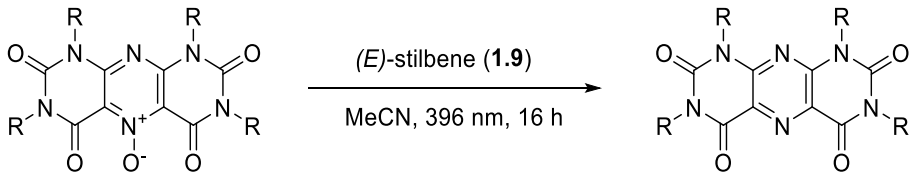

1.1-1.4 **1.5-1.8**

The following procedure was carried out under argon. The selected pyrimidopteridine *N*-oxide (0.25 mmol) and *(E)*-stilbene **1.9** (1.2 equiv.) was transferred into a pre-heated 8 mL tube and dissolved in acetonitrile (5.0 mL, 50 mM). The flask was sealed with a septum and irradiated for 16 h (398 nm). Afterwards, the reaction and quenched with water. The mixture was extracted 3 times with CH_2Cl_2 and dried over anhydrous Na_2SO_4. The crude product was then purified by column chromatography to furnish the desired deoxygenated pyrimidopteridine.

5.2.2 General procedures of chapter 2

5.2.2.1 General procedure 2.A: Photo-mediated hydroamination of stilbenes

Reactions were performed under Schlenk conditions using a 5 ml microwave vial equipped with a NS 14.5 rubber septum. The vial containing the corresponding stilbene (0.50 mmol, 1.0 equiv.) and photoredox catalyst (5.0 mol%) was evacuated for 5 min and purged with argon. Acetonitrile (2.5 mL) and the corresponding amine (1.50 mmol, 3.0 equiv.) was added to the stirring solution. The flask was rinsed with acetonitrile (2.5 mL). The reaction mixture was irradiated at 396 nm for 16-24 h. The reaction temperature was monitored in an adjacent microwave vial filled with oil and equipped with a thermal sensor. A constant temperature of 30 °C was measured due to heat emission of the LED. No extra heating or cooling was applied. After the indicated time, the reaction was quenched upon exposure to air and bubbling air through the solution using a pipette. The reaction was concentrated under reduced pressure and the crude product was purified by column chromatography.

5.2.1 General procedures of chapter 3

5.2.1.1 General procedure 3.A: Synthesis of heteroarene-*N*-oxides using *m*-CPBA

Following a modified literature procedure[110], *m*-CPBA (70%, 12.0 mmol, 1.2 eq.) was added portion-wise to a solution of *N*-heteroarene (10.0 mmol, 1.0 eq.) in CH_2Cl_2 (20 mL) at 0 °C whilst stirring. Following completion of the addition, the reaction mixture was stirred overnight for 16 h at 20 °C and conversion checked by TLC. Subsequently, the reaction was quenched with sodium thiosulfate (24.0 mmol, 2.4 eq.) and stirred for 10 min to eliminate any unreacted *m*-CPBA. Silica was added to the solution and the solvent was evaporated under reduced pressure. The mixture was then purified by column chromatography (dry loading) affording the *N*-oxide as a solid. When needed the crude product was then recrystallized to yield analytically pure product.

5.2.1.2 General procedure 3.B: Synthesis of heteroarene-*N*-oxides using $MeReO_3$

Following a modified literature procedure[76], a mixture of *N*-heteroarene (8.0 mmol, 1.0 eq.) and $MeReO_3$ (40.0 µmol, 0.5 mol%) in CH_2Cl_2 (20 mL) was treated with 30% aqueous H_2O_2 (16.0 mmol, 2.0 eq.) after which the solution turned light yellow/green. After complete addition, the reaction mixture was stirred overnight for 16 h at 20 °C and conversion was checked by TLC. Silica was added to the solution and the solvent was evaporated under reduced pressure. The mixture was then purified by column chromatography (dry loading) affording the *N*-oxide as a solid. When needed the crude product was then recrystallized to yield analytically pure product.

5.2.2 General procedures of chapter 4

5.2.2.1 General procedure 4.A: Synthesis of aryl sulfonates

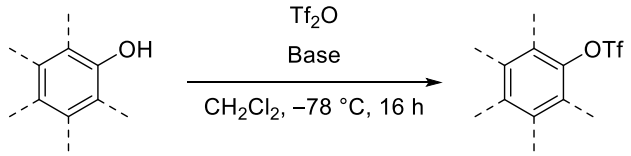

The following procedure was carried out under air. The selected phenol (1-5 mmol) and the base (2.0 eq) was transferred into a 25 ml flask and dissolved in CH_2Cl_2 (1.0 M). The flask was sealed with a septum and cooled to −78 °C. Afterwards, trifluoromethanesulfonic anhydride (1.2 eq) was added via syringe dropwise over a period of 5 min. Overnight (approximately 16 h), the reaction was allowed to warm to ambient temperature and quenched with water. The mixture was extracted 3 times with CH_2Cl_2 and dried over Na_2SO_4. The crude product was the purified with column chromatography to furnish the desired aryl sulfonate.

5.2.2.2 General procedure 4.B: Synthesis of *N,N*-dimethylanilines

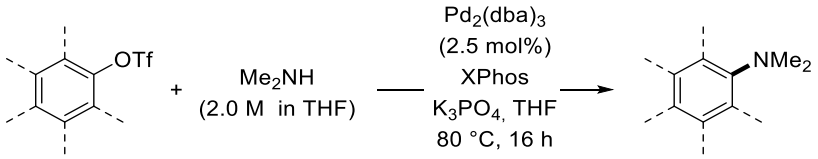

All reactions were carried out in septum sealed 4 ml Vials. Subsequently, $Pd_2(dba)_3$ (2.5 mol%), XPhos (1.5 eq of the metal), K_3PO_4 (1.2 eq) and appropriate trifluoromethanesulfonate (0.5 mmol) were added and the vial was sealed. The mixture was 3 times securated under vacuo and flushed with argon. Afterwards 1 ml THF was added and the suspension was stirred at 80 °C in a block of aluminum. After 5 min a dimethylamine solution (2 M THF, 1 ml) was added through the septum in one portion. After 16 h the reaction was quenched water and extracted 3 times with CH_2Cl_2. The organic layer was analyzed via GCMS. After a positive result the solvent was removed in vacuo (500 mbar) and the desired dimethylaniline was purified with column chromatography. In order to avoid a loss of yields due to volatility of the desired amines, the fraction was treated with an HCl solution (2.0 M in diethyl ether) to form the corresponding hydrochloride salts.

5.2.2.3 General procedure 4.C: Arylation of none-volatile alkyl amines.

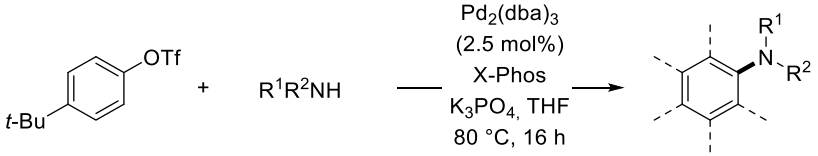

1d **2** **4**

All reactions were carried out in septum sealed 4 ml Vials. Subsequently, $Pd_2(dba)_3$ (2.5 mol%), XPhos (1.5 eq of the metal), K_3PO_4 (1.2 eq), 4-(tert-butyl)phenyl trifluoromethane-sulfonate (0.5 mmol) and the appropriate amine (2-4 eq) were added and the vial was sealed. The mixture was securated under vacuo and flushed with argon for 3 times. Afterwards 1 ml THF was added and the suspension was stirred at 80 °C. After 16 h, the reaction was quenched with water and extracted with CH_2Cl_2 3 times. The organic layer was analyzed via GCMS and TLC. After a positive result the solvent was removed in vacuo (500 mbar) and the desired dimethylaniline was purified with column chromatography. In order to avoid a loss of yields due to volatility of the desired amines, the fraction was treated with an HCl solution (2.0 M in diethyl ether) to form the corresponding hydrochloride salts.

5.3 Analytical data

5.3.1 Analytical data of chapter 1

5.3.1.1 Characterization of pyrimidopteridines

5.3.1.1.1 Synthesis of 1,3,7,9-tetramethyl-9,10a-dihydropyrimido[5,4-g]pteridine-2,4,6,8(1*H*,3*H*,4a*H*,7*H*)-tetraone (1.5):

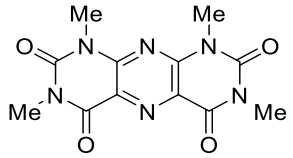

1.5

Following general procedure A, using 0.25 mmol of MePPTNO (**1.1**) afforded the title compound **1** (68.4 mg, 0.22 mmol, 90%) as a white solid after purification via column chromatography (*n*-pentane:EtOAc = 1:4).

R_f = 0.32 (EtOAc, UV).

m.p. = > 300 °C.

^{1}H NMR (300 MHz, DMSO-d_6): δ = 3.36 (s, 6H), 3.60 (s, 6H).

^{13}C NMR (101 MHz, DMSO-d6) δ 159.0, 150.9, 149.7, 123.8, 29.9, 28.9.

MS (EI): *m*/*z* (relative intensity): 304 (100) [M^+], 275 (20), 246 (12), 233 (16), 221 (27), 207 (15), 192 (53), 176 (11), 134 (18), 107 (56), 96 (31), 80 (43), 67 (71), 56 (47), 52 (44), 42 (32).

HRMS (ESI-TOF, *m*/*z*): calcd. for $C_{12}H_{12}N_6O_4$ 304.0915; found 304.0920.

IR (ATR, neat, cm^{-1}): 3373 (w), 2956 (w), 1665 (s), 1563 (s), 1255 (s), 1112 (m), 1053 (s), 811 (m), 745 (s), 486 (s), 414 (s).

UV-Vis (max. abs., [nm], MeCN): 232, 262, 269, 354, 361, 368.

Crystallographic data of MePPT (1.5):

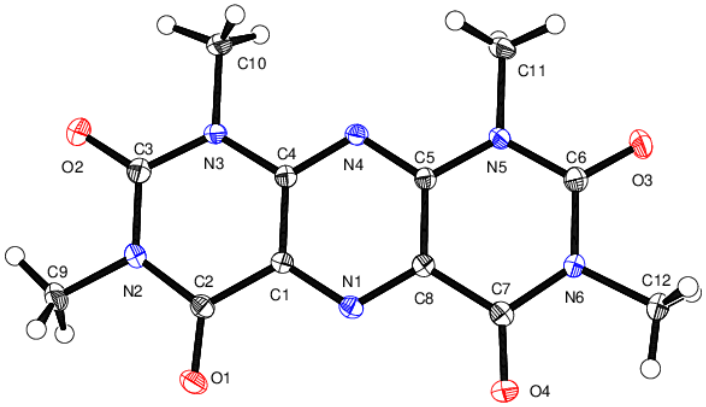

Figure 5.1: Crystallographic data of MePPT (1.5). Displacement ellipsoids correspond to 50% probability

Chemical formula	$C_{12}H_{12}N_6O_4$
M_r	304.28
Crystal system, space group	Monoclinic, $P2_1/c$
Temperature (K)	123
a, b, c (Å)	12.0708 (9), 13.1161 (8), 8.0652 (5)
β (°)	103.256 (2)
V (Å^3)	1242.87 (14)
Z	4
Radiation type	Mo $K\alpha$
μ (mm^{-1})	0.13
Crystal size (mm)	0.17 × 0.10 × 0.03
No. of measured, independent and observed [$I > 2\sigma(I)$] reflections	29045, 3000, 2042
R_{int}	0.063
(sin θ/λ)$_{max}$ (Å^{-1})	0.661
$R[F^2 > 2\sigma(F^2)]$, $wR(F^2)$, S	0.048, 0.141, 1.05
No. of parameters	203
H-atom treatment	H-atom parameters constrained
Δρ$_{max}$, Δρ$_{min}$ (e Å^{-3})	0.34, −0.31

5.3.1.1.2 Synthesis of 1,3,7,9-tetrapropyl-9,10a-dihydropyrimido[5,4-*g*]pteridine-2,4,6,8(1*H*,3*H*,4a*H*,7*H*)-tetraone (1.6):

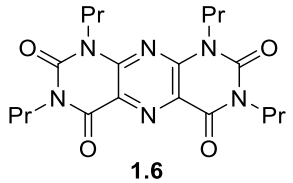

1.6

Following general procedure A, using 0.25 mmol of PrPPTNO (**1.2**) afforded the title compound **2** (106.9 mg, 0.25 mmol, *quant.*) as a white solid after purification via column chromatography (*n*-pentane:EtOAc = 1:2).

R_f = 0.16 (*n*-pentane:EtOAc – 1:2, UV)

m.p. = 106–108 °C

^{1}H NMR (300 MHz, Chloroform-*d*) δ 4.29 – 4.12 (m, 4H), 4.09 – 3.88 (m, 3H), 1.83 – 1.56 (m, 8H), 0.98 (t, *J* = 7.4 Hz, 6H), 0.91 (t, *J* = 7.4 Hz, 6H).

^{13}C NMR (75 MHz, Chloroform-*d*) δ 157.8, 149.9, 149.2, 123.6, 45.0, 43.9, 21.1, 20.9, 11.3, 11.2.

MS (EI): *m*/*z* (relative intensity) 416 (73) [M^+], 302 (23), 290 (11), 232 (11), 147 (15), 93 (12), 68 (12), 56 (21), 43 (100), 29 (24).

HRMS (EI): calcd. for $C_{20}H_{28}N_6O_4$ 416.2167; found 416.2169.

IR (ATR, neat, cm-1): 3506 (w), 2962 (w), 2935 (w), 2875 (w), 1713 (s), 1662 (s), 1555 (s), 1432 (s), 1410 (s), 1377 (s), 1341 (m), 1321 (m), 1280 (s), 1230 (m), 1205 (m), 1124 (m), 1093 (m), 1037 (w), 893 (w), 813 (m), 783 (w), 751 (m), 707 (w), 662 (w), 605 (m), 555 (m), 508 (s), 485 (s).

Crystallographic data of PrPPT (1.6):

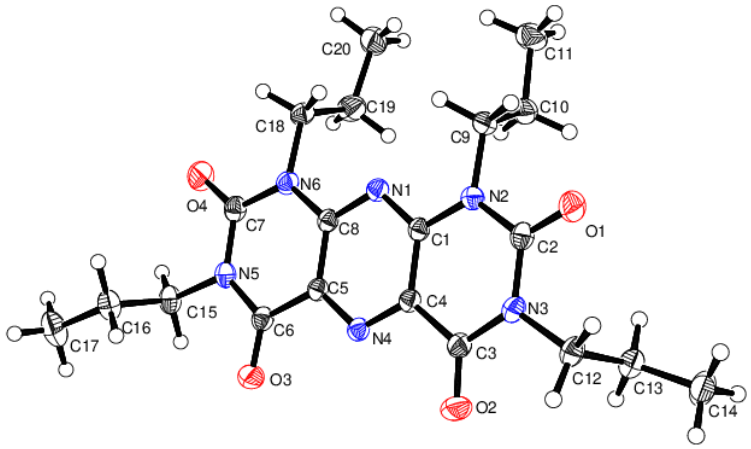

Figure 5.2: Crystallographic data of PrPPT (1.6). Displacement ellipsoids correspond to 50% probability

Chemical formula	$C_{20}H_{28}N_6O_4$
M_r	416.48
Crystal system, space group	Triclinic, *P*
Temperature (K)	150
a, *b*, *c* (Å)	8.5132 (6), 11.0743 (8), 11.4658 (8)
β (°)	99.3899 (19), 92.3345 (19), 98.1695 (19)
V (Å^3)	1053.40 (13)
Z	2
Radiation type	Mo *K*α
μ (mm^{-1})	0.09
Crystal size (mm)	0.38 × 0.14 × 0.10
No. of measured, independent and observed [*I* > 2σ(*I*)] reflections	50282, 5089, 4165
R_{int}	0.027
(sin θ/λ)$_{max}$ (Å^{-1})	0.661
$R[F^2 > 2\sigma(F^2)]$, $wR(F^2)$, *S*	0.039, 0.120, 1.04
No. of parameters	275
Δρ$_{max}$, Δρ$_{min}$ (e Å^{-3})	0.31, −0.23

5.3.1.1.3 Synthesis of 1,3,7,9-tetrabutyl-9,10a-dihydropyrimido[5,4-*g*]pteridine-2,4,6,8(1*H*,3*H*,4a*H*,7*H*)-tetraone (1.7):

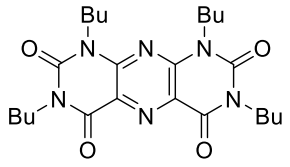

1.7

Following general procedure A, using 0.25 mmol of BuPPTNO (**1.3**) afforded the title compound **3** (118.4 mg, 0.25 mmol, 99%) as a white solid after purification via column chromatography (*n*-pentane:EtOAc = 1:4).

R_f = 0.44 (*n*-pentane:EtOAc – 1:2, UV)

m.p. = 112–114 °C

^{1}H NMR (300 MHz, Chloroform-*d*) δ 4.30 – 4.13 (m, 4H), 4.11 – 3.93 (m, 4H), 1.76 – 1.51 (m, 8H), 1.36 (dh, *J* = 22.1, 7.3 Hz, 8H), 0.99 – 0.82 (m, 12H).

^{13}C NMR (75 MHz, Chloroform-*d*) δ 157.7, 149.9, 149.1, 123.6, 43.3, 42.2, 29.8, 29.7, 20.2, 20.1, 13.8, 13.7.

MS (EI): *m*/*z* (relative intensity): 472 (100) [M^+], 430 (24), 417 (21), 361 (10), 249 (9), 207 (6), 147 (4), 56 (7), 41 (14).

HRMS (ESI-TOF, *m*/*z*): calcd. for $C_{24}H_{36}N_6O_4$ 472.2793; found 472.2784.

IR (ATR, neat, cm^{-1}): 2957 (m), 2932 (m), 2872 (s), 1671 (w), 1550 (w), 1408 (w), 1372 (m), 1273 (w), 1114 (m), 812 (s), 755 (m), 505 (m).

UV-Vis (max. abs., [nm], MeCN): 236, 265, 272, 357, 363, 371.

Crystallographic data of BuPPT (1.7):

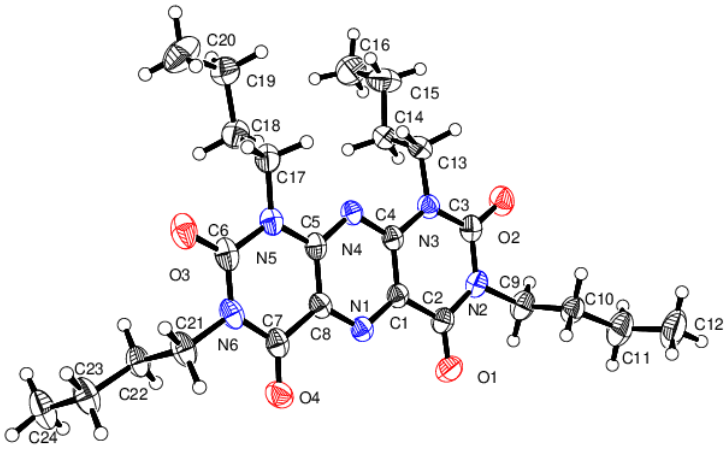

Figure 5.3: Crystallographic data of BuPPT (1.7). Displacement ellipsoids correspond to 50% probability.

Chemical formula	$C_{24}H_{36}N_6O_4$
M_r	472.59
Crystal system, space group	Orthorhombic, *Pbca*
Temperature (K)	150
a, *b*, *c* (Å)	20.4881 (8), 8.5836 (4), 29.5607 (12)
V (Å^3)	5198.6 (4)
Z	8
Radiation type	Cu *K*α
μ (mm^{-1})	0.68
Crystal size (mm)	0.42 × 0.23 × 0.22
No. of measured, independent and observed [$I > 2\sigma(I)$] reflections	39417, 4597, 4288
R_{int}	0.029
$(\sin \theta/\lambda)_{max}$ (Å^{-1})	0.596
$R[F^2 > 2\sigma(F^2)]$, $wR(F^2)$, S	0.054, 0.160, 1.04
No. of parameters	311
$\Delta\rho_{max}$, $\Delta\rho_{min}$ (e Å^{-3})	1.08, −0.28

5.3.1.1.4 Synthesis of 1,3,7,9-tetraphenyl-9,10a-dihydropyrimido[5,4-*g*]pteridine-2,4,6,8(1*H*,3*H*,4a*H*,7*H*)-tetraone (1.8):

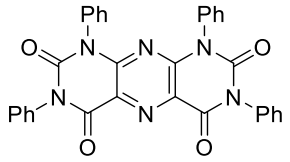

1.8

Following general procedure A, using 0.25 mmol of PhPPTNO (**1.4**) afforded the title compound **4** (140.0 mg, 0.25 mmol, *quant.*) as a white solid after purification via column chromatography (*n*-pentane:EtOAc = 1:4).

R_f = 0.45 (*n*-pentane/EtOAc/MeOH = 1:1:0.1, UV)

m.p. > 300 °C

^{1}H NMR (400 MHz, DMSO-d_6) δ 12.27–12.32 (m, 4H), 12.18–12.24 (m, 6H), 11.99–12.06 (m, 6H), 11.90–11.93 (m, 4H).

^{13}C NMR (100 MHz, DMSO-d_6) δ 158.7, 149.9, 149.8, 135.5, 134.6, 129.0, 128.7, 128.5, 128.4, 128.8, 124.2.

MS (EI): *m*/*z* (relative intensity) 552 (100) [M^+], 433 (81), 286 (26), 258 (14), 216 (9), 169 (42), 141 (12), 119 (7), 77 (29).

HRMS (EI): calcd. for $C_{32}H20N_6O_4$ 552.1541; found 552.1536.

IR (ATR, neat, cm^{-1}): 2920 (w), 1725 (m), 1681 (s), 1555 (s), 1492 (m), 1366 (s), 1265 (s), 1196 (m), 1024 (s), 810 (m), 745 (s), 529 (s).

Crystallographic data of PhPPT (1.8)

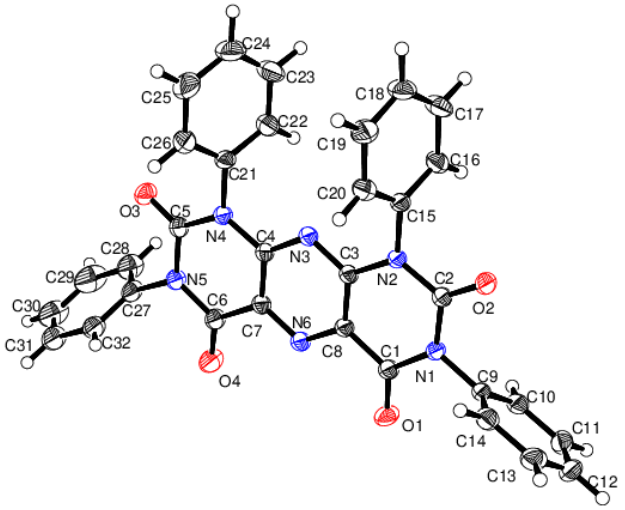

Figure 5.4: Crystallographic data of PhPPT (1.8). Displacement ellipsoids correspond to 50% probability

Chemical formula	$C_{36}H_{26}N_8O_4$
M_r	634.65
Crystal system, space group	Monoclinic, $P2_1/c$
Temperature (K)	150
a, b, c (Å)	11.1735 (3), 15.5859 (4), 18.3286 (5)
β (°)	99.5737 (9)
V (Å^3)	3147.45 (15)
Z	4
Radiation type	Mo $K\alpha$
μ (mm^{-1})	0.09
Crystal size (mm)	0.43 × 0.33 × 0.31
No. of measured, independent and observed [$I > 2\sigma(I)$] reflections	80900, 7597, 6367
R_{int}	0.028
$(\sin \theta/\lambda)_{max}$ (Å^{-1})	0.661
$R[F^2 > 2\sigma(F^2)]$, $wR(F^2)$, S	0.043, 0.120, 1.02
No. of parameters	452
$\Delta\rho_{max}$, $\Delta\rho_{min}$ (e Å^{-3})	0.49, −0.33

5.3.1.2 Characterization of oxidation products

5.3.1.2.1 Synthesis of *trans*-2,3-diphenyloxirane (1.11) and *cis*-2,3-diphenyloxirane (1.12):

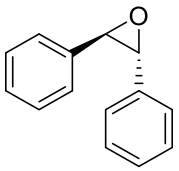

1.11

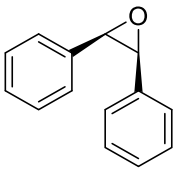

1.12

Following general procedure A, using 0.25 mmol of PrPPTNO (**2**) afforded the title compounds *cis*-**6** (10.3 mg, 0.10 mmol, 21%) and *trans*-**6** (20.3 mg, 0.05 mmol, 43%) as white solids after purification through column chromatography (*n*-pentane:EtOAc = 100:1 → 20:1).

1.11:

R_f = 0.53 (*n*-pentane:EtOAc = 50:1, UV)

^{1}H NMR (300 MHz, Chloroform-*d*) δ 7.49 – 7.30 (m, 10H), 3.90 (s, 2H).

^{13}C NMR (75 MHz, Chloroform-*d*) δ 137.3, 128.7, 128.5, 125.6, 63.0.

MS (EI): m/z (relative intensity) 196 (28), 195 (32), 178 (18), 168 (18), 167 (100), 166 (14), 165 (36), 152 (21), 105 (18), 90 (26), 89 (32), 77 (16).

IR (ATR, neat, cm-1): 3035 (w), 2988 (w), 1602 (w), 1492 (w), 1452 (m), 1412 (w), 1347 (w), 1310 (w), 1284 (w), 1244 (w), 1220 (w), 1176 (w), 1157 (w), 1094 (w), 1072 (w), 1025 (w), 847 (m), 835 (m), 795 (w), 745 (s), 689 (s), 610 (s), 507 (s), 421 (w).

The analytical data is in accordance with those reported in the literature.[111]

1.12:

R_f = 0.44 (*n*-pentane:EtOAc = 50:1, UV)

^{1}H NMR (300 MHz, Chloroform-*d*) δ 7.24 – 7.12 (m, 10H), 4.38 (s, 2H).

^{13}C NMR (75 MHz, Chloroform-*d*) δ 134.5, 127.9, 127.6, 127.0, 59.9.

MS (EI): m/z (relative intensity) 196 (28), 195 (33), 168 (18), 167 (100), 166 (15), 165 (39), 152 (21), 105 (27), 90 (25), 89 (33), 77 (18), 63 (10), 51 (10).

HRMS (ESY-TOF, *m*/*z*): calcd. for $C_{14}H_{12}O$ $[M+H]^+$ 197.0966, found 197.0968.

IR (ATR, neat, cm-1): 3032 (w), 2968 (w), 1604 (w), 1494 (w), 1452 (m), 1407 (w), 1372 (w), 1316 (w), 1257 (w), 1177 (w), 1157 (w), 1077 (w), 1053 (w), 1026 (w), 921 (w), 885 (m), 864 (m), 834 (w), 757 (w), 746 (s), 732 (s), 691 (s), 641 (m), 585 (s), 526 (s), 499 (m), 412 (w).

The analytical data is in accordance with those reported in the literature.[112]

5.3.1.3 Electrochemical properties

Cyclic voltammetry and differential pulse voltammetry

All electrochemical investigations were performed at room temperature in dried acetonitrile p.A. (VWR) under an Argon atmosphere with 0.1 M tetrabutylammonium hexafluorophosphate (Fluka) as conducting salt using an Autolab (PGSTAT 204, Metrohm). A glassy carbon disk electrode (d = 2 mm) was used as working electrode, a Pt-electrode as the counter electrode and an Ag/AgCl/LiClsat. in EtOH-system as the reference electrode (all electrodes: Metrohm). All potentials mentioned in this paper were measured with respect to this reference system and were checked by using the ferrocenium/ferrocene-internal reference system (potential of Fc^+/Fc: CV = 0.54 V & DPV = 0.53 V [vs. Ag/AgCl/LiClsat. In EtOH]. The CV scans were done three times at a scan rate of 40 mV s^{-1}. The measurements were performed with 1 mM compound dissolved in the electrolyte.

5.3.1.3.1 1,3,7,9-tetramethyl-9,10a-dihydropyrimido[5,4-g]pteridine-2,4,6,8(1H,3H,4aH,7H)-tetraone

-CV:

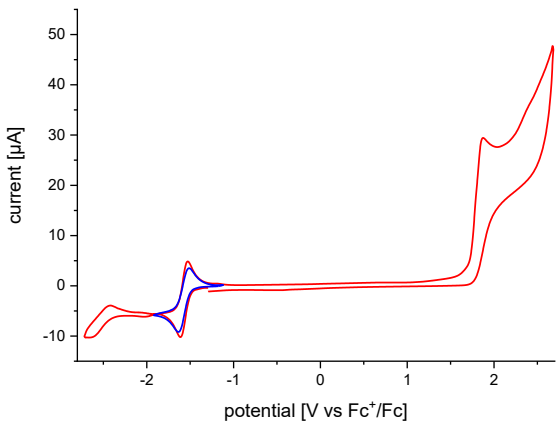

DPV:

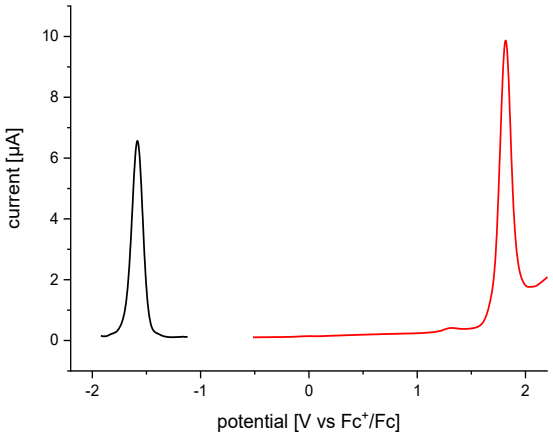

5.3.1.3.2 1,3,7,9-tetrapropyl-9,10a-dihydropyrimido[5,4-g]pteridine-2,4,6,8(1H,3H,4aH,7H)-tetraone

-CV:

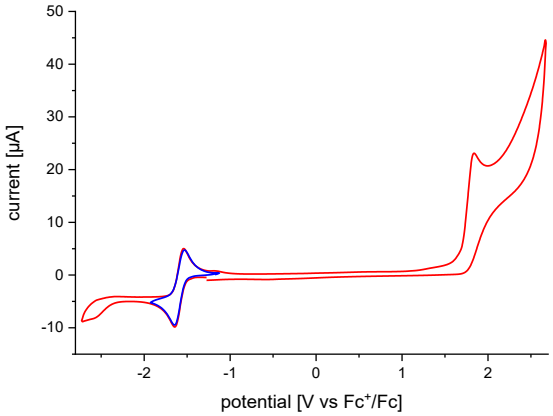

DPV:

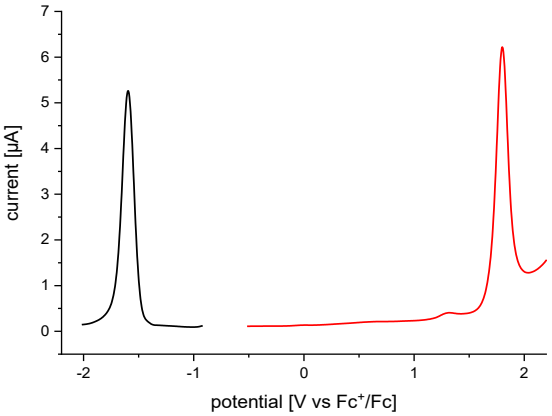

5.3.1.3.3 1,3,7,9-tetrabutyl-9,10a-dihydropyrimido[5,4-g]pteridine-2,4,6,8(1H,3H,4aH,7H)-tetraone

-CV:

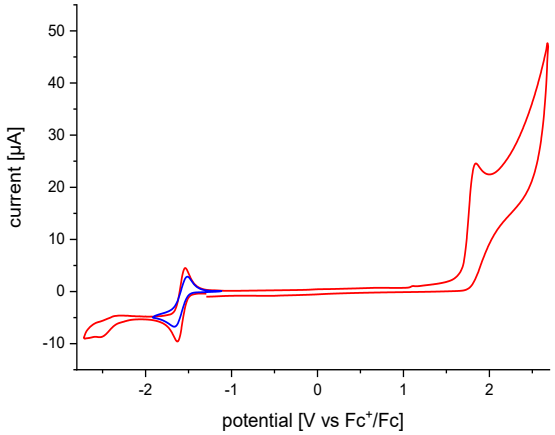

DPV:

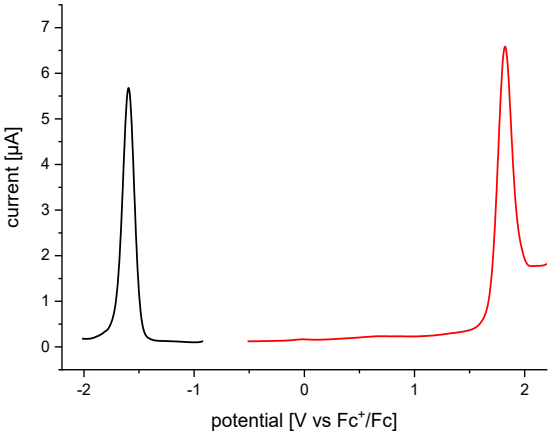

1,3,7,9-tetraphenyl-9,10a-dihydropyrimido[5,4-g]pteridine-2,4,6,8(1H,3H,4aH,7H)-tetraone

-CV: DPV:

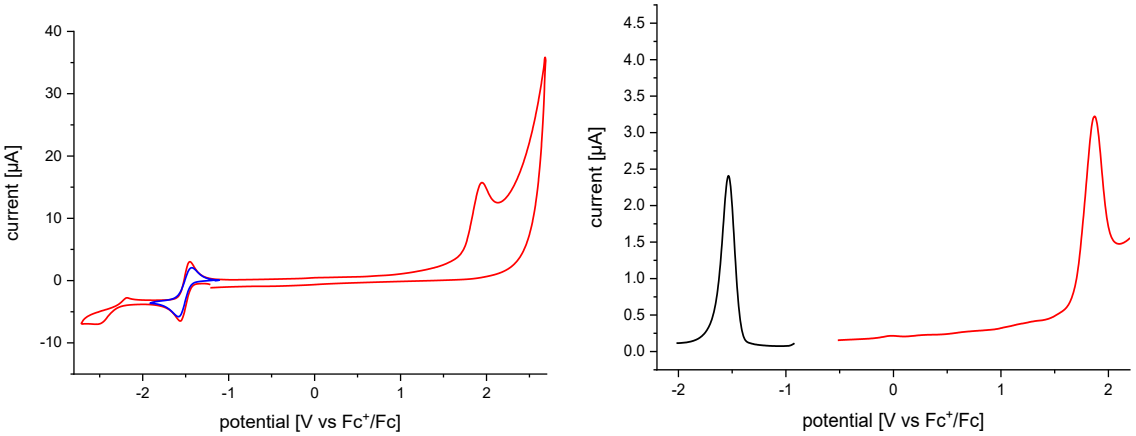

5.3.1.4 Photo-mediated oxidative cyclization

5.3.1.4.1 Synthesis of 6H-benzo[c]chromen-6-one (1.16):

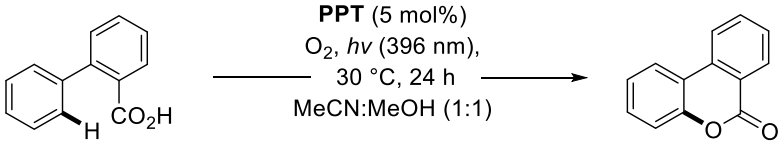

1.15 **1.16**

The following procedure was carried out under an oxygen atmosphere. 2-Phenylbenzoic acid (**1.15**) (0.5 mmol, 1.0 eq.) and the pyrimidopteridine photosensitizer (5.0 mol%) were dissolved in a 1:1 mixture of dry acetonitrile and dry methanol (5.0 mL) and stirred for the specified time under UV-light irradiation (396 nm) for 24 h. The reaction mixture was concentrated in vacuo and purified by flash chromatography (SiO_2, n-pentane:EtOAc = 20:1), yielding the title compound **1.16** as a colorless solid.

entry	catalyst	isolated yield [%]
1	MePPT (**1.5**)	80
2	PrPPT (**1.6**)	66
3	BuPPT (**1.7**)	66
4	PhPPT (**1.8**)	85

R_f = 0.40 (*n*-hexane/EtOAc = 10:1, UV)

^{1}H NMR (300 MHz, Chloroform-*d*) δ 8.40 (ddd, *J* = 7.9, 1.4, 0.5 Hz, 1H), 8.13 – 8.09 (m, 1H), 8.05 (dd, *J* = 7.9, 1.6 Hz, 1H), 7.82 (ddd, *J* = 8.1, 7.3, 1.4 Hz, 1H), 7.58 (ddd, *J* = 8.3, 7.3, 1.1 Hz, 1H), 7.48 (ddd, *J* = 8.5, 7.1, 1.6 Hz, 1H), 7.39 – 7.29 (m, 2H).

^{13}C NMR (75 MHz, Chloroform-*d*) δ 161.2, 151.3, 134.9, 134.8, 130.6, 130.5, 128.9, 124.6, 122.8, 121.7, 121.2, 118.0, 117.8.

MS (EI): *m*/*z* (relative intensity) 196 (100) [M^+], 168 (44), 139 (44), 113 (5), 70 (8).

The analytical data is in accordance with those reported in the literature.[15, 113]

5.3.1.5 Photo-mediated hydroamination of stilbene

5.3.1.5.1 Synthesis of N-benzyl-1,2-diphenylethan-1-amine (1.18):

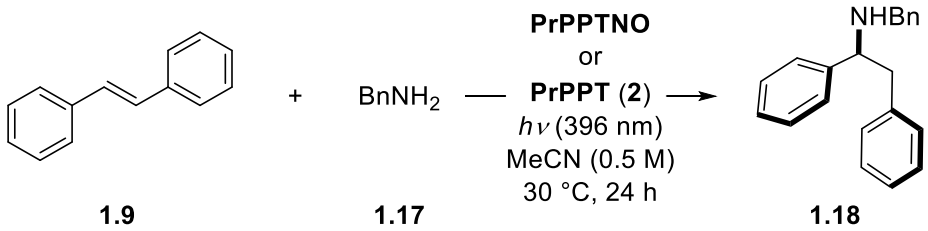

1.9 **1.17** **1.18**

The following procedure was carried out under argon. *(E)*-stilbene (**1.9**) (90.6 mg, 0.5 mmol) and the corresponding pyrimidopteridine(-*N*-oxide) photosensitizer (XX mol%) was transferred into a 10 mL Schlenk finger and evacuated 3 times. Anhydrous benzylamine (**1.17**) (267 mg, 2.5 mmol) and acetonitrile (5.0 mL, 0.1 M) was added. The flask was sealed with a septum and irradiated for 16 h (398 nm). Afterwards, the reaction and quenched with water. The mixture was extracted 3 times with CH_2Cl_2 and dried over anhydrous Na_2SO_4. The crude product was then purified by column chromatography (*n*-pentane:EtOAc = 100:1) to furnish the title compound **1.18**.

entry	catalyst	catalyst loading [mol%]	yield [%]^b
1	PrPPT (**1.6**)	5	72
2	PrPPTNO (**1.2**)	5	72
3	PrPPT (**1.6**)	10	77
4	PrPPTNO (**1.2**)	10	77
5	PrPPT (**1.6**)	25	86
6	PrPPTNO (**1.2**)	25	71

R_f = 0.3 (*n*-pentane:EtOAc = 9:1, $KMnO_4$).

m.p. = 52–54 °C.

^{1}H NMR (400 MHz, $CDCl_3$) δ 7.29 – 7.19 (m, 4H), 7.19 – 7.06 (m, 7H), 7.00 (dt, *J* = 7.9, 1.4 Hz, 4H), 3.79 (dd, *J* = 8.5, 5.5 Hz, 1H), 3.56 (d, *J* = 13.5 Hz, 1H), 3.36 (d, *J* = 13.5 Hz, 1H), 2.97 – 2.70 (m, 2H), 1.64 (s, 1H).

^{13}C NMR (101 MHz, $CDCl_3$) δ 143.8, 140.6, 138.9, 129.4, 128.5, 128.5, 128.4, 128.0, 127.5, 127.2, 126.8, 126.5, 63.7, 51.5, 45.4.

MS (EI): *m*/*z* (relative intensity) 286 (1), 197 (15), 196 (100), 91 (87).

HRMS (EI, *m*/*z*): calcd. for $C_{21}H_{21}N$ [M^+] 288.1752; found 288.1759.

IR (ATR, neat, cm^{-1}): 2704(w), 1952(w), 1871(w), 1813(w), 1601(w), 1582(w), 1491(m), 1452(m), 1398(w), 1357(w), 1315(w), 1288(w), 1269(w), 1227(w), 1195(w), 1179(w), 1162(w), 1153(w), 1120(m), 1068(m), 1028(m), 1000(w), 988(w), 946(w), 911(w), 832(w), 820(w), 793(w), 758(m), 741(m), 728(s), 695(s), 635(m), 619(w), 579(w), 547(s), 506(m), 460(m).

The analytical data is in accordance with those reported in the literature.[16b, 114]

5.3.2 Analytical data of chapter 2

5.3.2.1 Electrochemical Properties

Cyclic Voltammetry and Differential Pulse Voltammetry

All electrochemical investigations were performed at room temperature in dried acetonitrile p.A. (VWR) under an Argon atmosphere with 0.1 M tetrabutylammonium hexafluorophosphate (Fluka) as conducting salt using an Autolab (PGSTAT 204, Metrohm). A glassy carbon disk electrode (d = 2 mm) was used as working electrode, a glassy carbon electrode as the counter electrode and an Ag/AgCl/LiCl sat. in EtOH-system as the reference electrode (all electrodes: Metrohm). All potentials mentioned in this paper were measured with respect to this reference system and were checked by using the ferrocenium/ferrocene-internal reference system (potential of Fc^+/Fc: 0.54 V [vs. Ag/AgCl/LiCl sat. in EtOH]. The potentials reported relative to the Fc^+/Fc redox couple was converted to SCE by adding 0.38 V.[21] The CV scans were done three times at a scan rate of 40 mV s^{-1}. The measurements were performed with 5 μM compound dissolved in the electrolyte.

Differential pulse voltammetry was measured using a step potential of 5 mV, modulation amplitude of 25 mV, modulation time 0.05 s, interval time 0.05 s.

Redox potentials from DPV-peak:

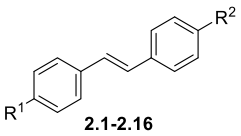

2.1-2.16

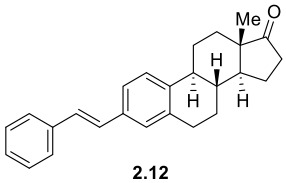

2.12

entry	R^1	R^2	note	$E_{1/2}^{red}$ [V vs Fc^+/Fc][a]	$E_{1/2}^{ox}$ [V vs Fc^+/Fc][a]	$E_{1/2}^{red}$ [V vs SCE][b]	$E_{1/2}^{ox}$ [V vs SCE][b]
1	CF_3	H	**(2.1)**	-2.95	+1.31	-2.57	+1.69
2	COOEt	H	**(2.2)**	-2.24	+1.27	-1.86	+1.65
3	CN	H	**(2.3)**	-2.21	+1.25	-1.83	+1.63
4			phenanthrene (**2.4**)	-2.92	+1.20	-2.54	+1.58
5	H	H	(*E*)-stilbene **(2.5)**	-2.68	+1.18	-2.30	+1.56
6	H	H	(*Z*)-stilbene **(2.6)**	-2.66	+1.15	-2.28	+1.53
7	Br	Br	**(2.7)**	-2.34	+1.11	-1.96	+1.49
8	OAc	H	**(2.8)**	-2.62	+1.06	-2.24	+1.44
9	F	H	**(2.9)**	-2.67	+1.06	-2.29	+1.44
10	Me	F	**(2.10)**	-2.34	+0.96	-2.35	+1.34
11	Me	H	**(2.11)**	-2.71	+0.95	-2.33	+1.33
12			**(2.12)**	-2.72	+0.94	-2.34	+1.32
13			benzylamine **(2.13)**	--	+0.91	--	+1.29
14	OMe	CF_3	**(2.14)**	-2.48	+0.85	-2.10	+1.23
15	OMe	H	**(2.15)**	-2.76	+0.76	-2.38	+1.14
16	NMe_2	H	**(2.16)**	-2.81	+0.14	-2.43	+0.52

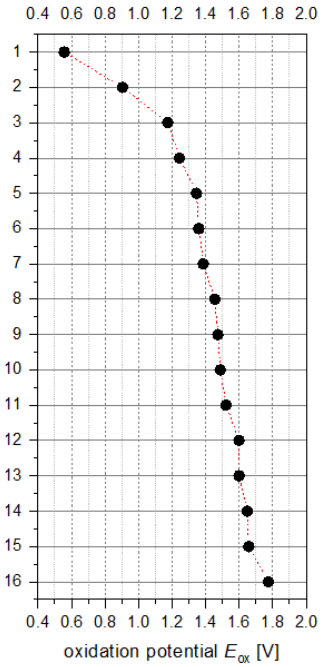

Redox potentials of stilbenes

5.3.2.1.1.1 (*E*)-*N,N*-Dimethyl-4-styrylaniline:

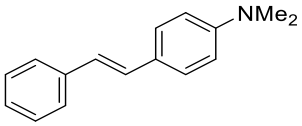

Cyclovoltammogram

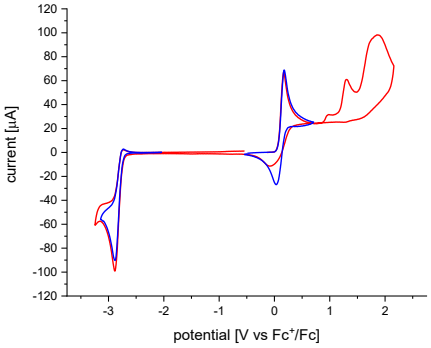

Differential pulse voltammetry

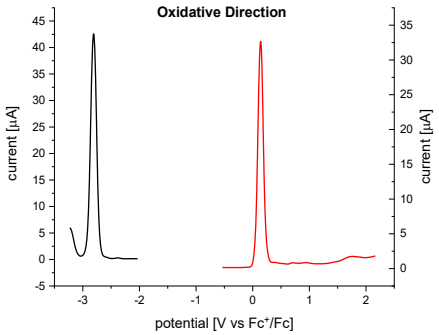

5.3.2.1.1.2 (*E*)-1-Methoxy-4-styrylbenzene:

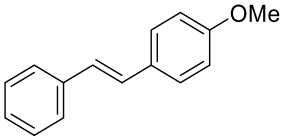

Cyclovoltammogram

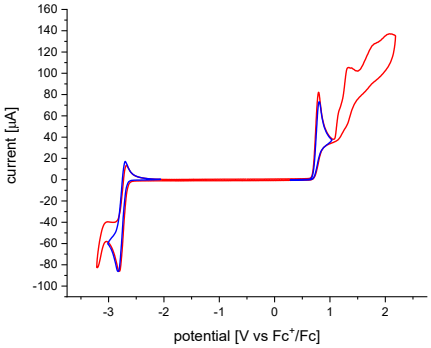

Differential pulse voltammetry

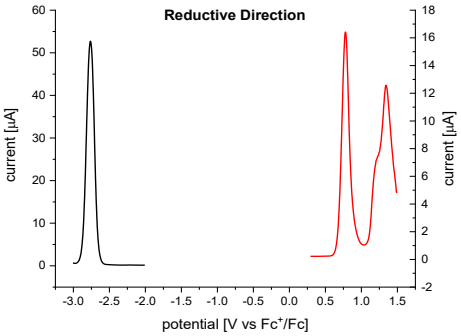

5.3.2.1.1.3 (*E*)-1-Methoxy-4-(4-(trifluoromethyl)styryl)benzene:

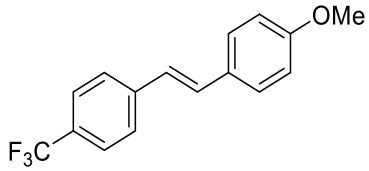

Cyclovoltammogram

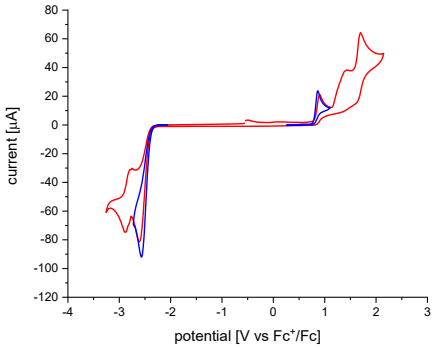

Differential pulse voltammetry

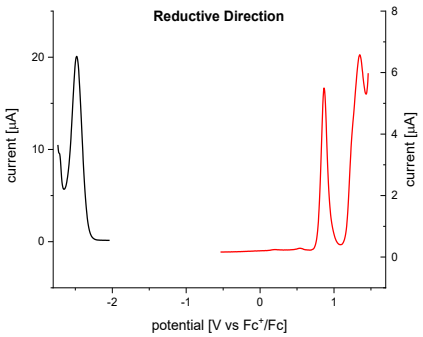

5.3.2.1.1.4 (8R,9S,13S,14S)-13-Methyl-3-((*E*)-styryl)-6,7,8,9,11,12,13,14,15,16-decahydro-17H-cyclopenta[a]phenanthren-17-one:

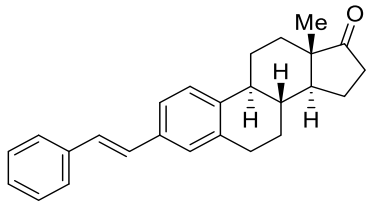

Cyclovoltammogram

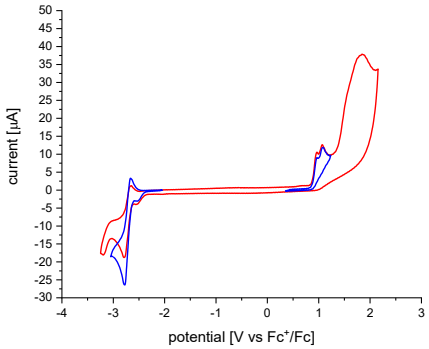

Differential pulse voltammetry

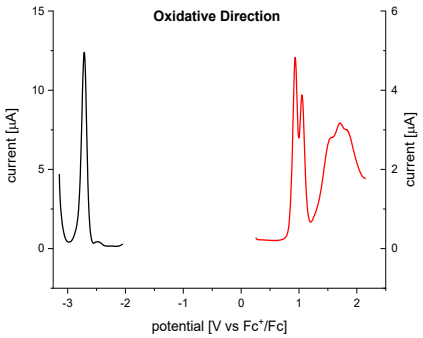

5.3.2.1.1.5 (*E*)-1-Methyl-4-styrylbenzene

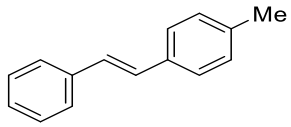

Cyclovoltammogram

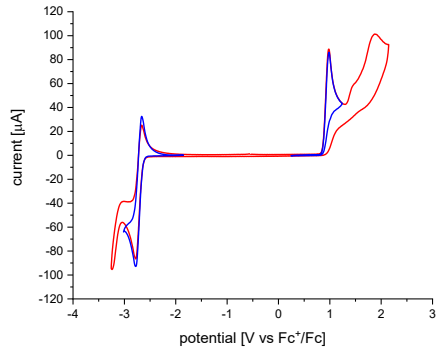

Differential pulse voltammetry

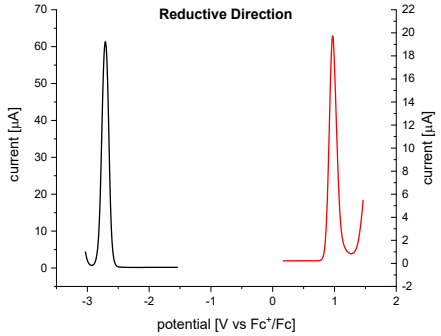

5.3.2.1.1.6 (*E*)-1-Fluoro-4-(4-methylstyryl)benzene

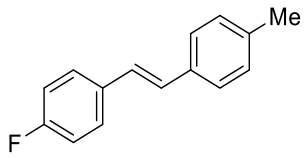

Cyclovoltammogram

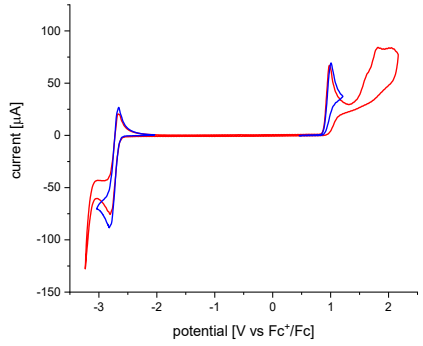

Differential pulse voltammetry

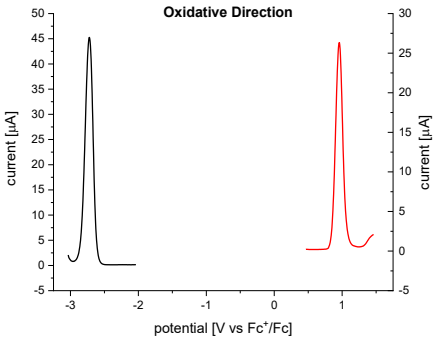

5.3.2.1.1.7 (*E*)-1-Fluoro-4-styrylbenzene

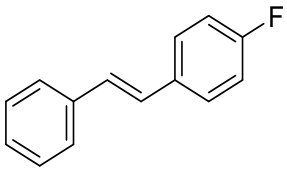

Cyclovoltammogram

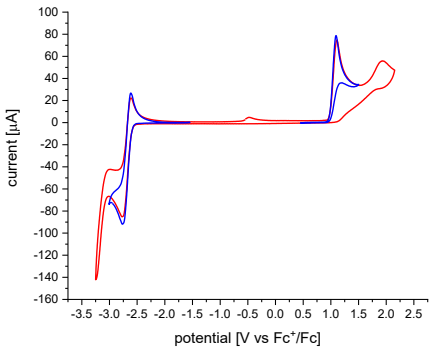

Differential pulse voltammetry

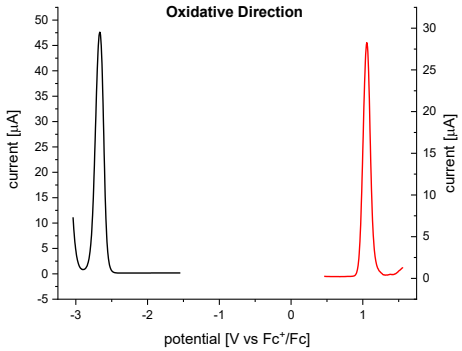

5.3.2.1.1.8 (*E*)-4-Styrylphenyl acetate

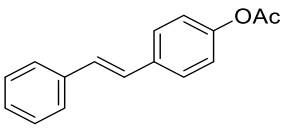

Cyclovoltammogram

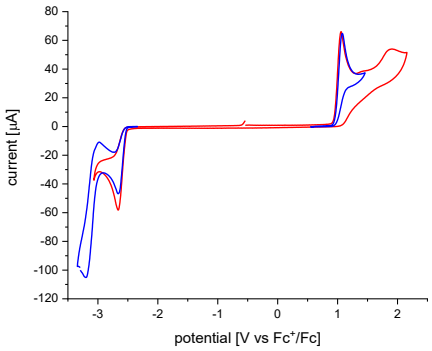

Differential pulse voltammetry

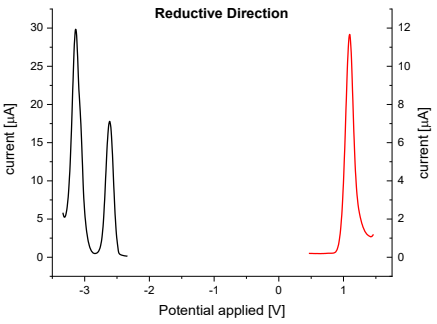

5.3.2.1.1.9 (*E*)-1,2-Bis(4-bromophenyl)ethene:

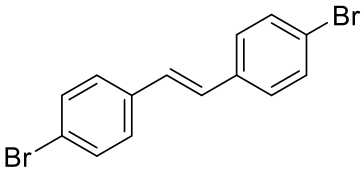

Cyclovoltammogram

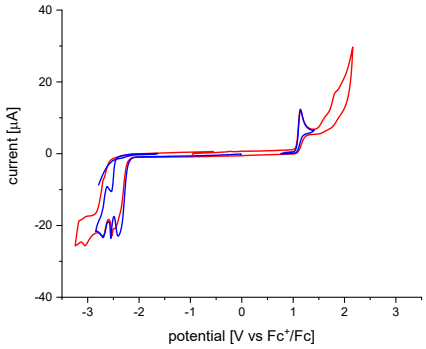

Differential pulse voltammetry

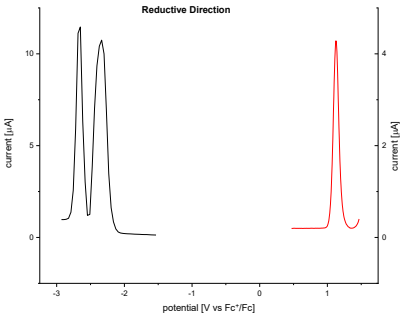

(*E*)-1,2-Diphenylethene ((E)-2b):

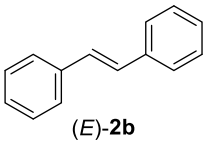

(*E*)-**2b**

Cyclovoltammogram

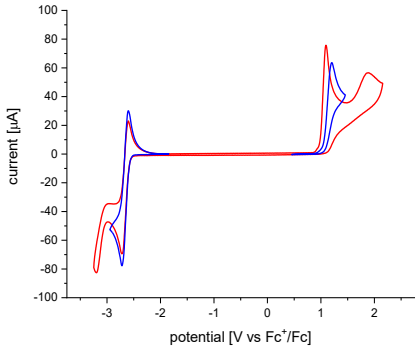

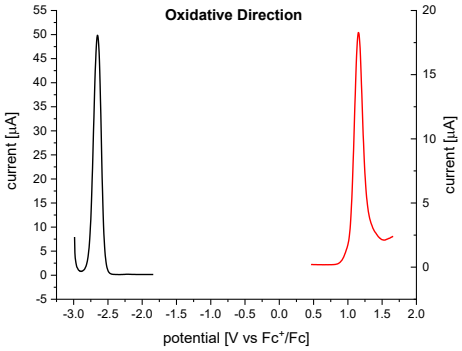

5.3.2.1.1.11 (*Z*)-1,2-Diphenylethene ((Z)-2b):

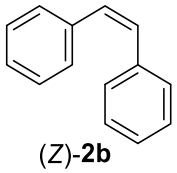

(*Z*)-**2b**

Cyclovoltammogram

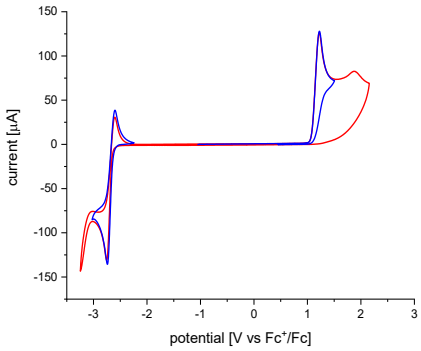

Differential pulse voltammetry

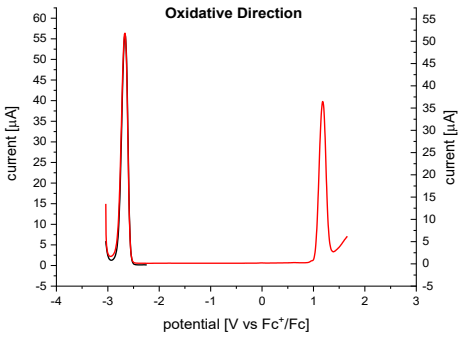

5.3.2.1.1.12 **P**henanthrene:

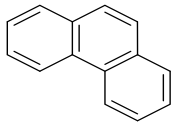

Cyclovoltammogram

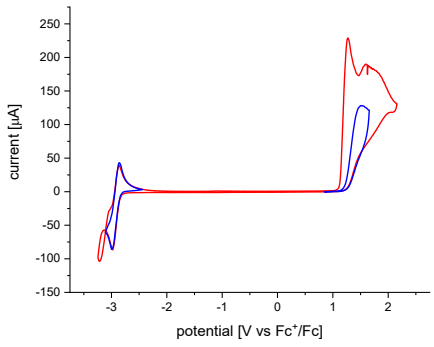

Differential pulse voltammetry

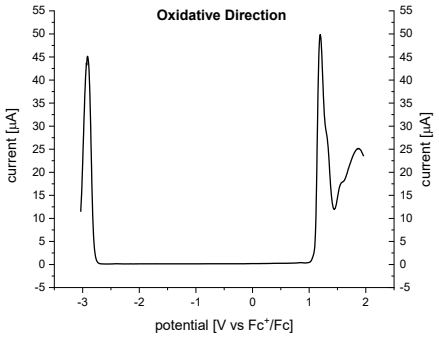

5.3.2.1.1.13 (*E*)-4-Styrylbenzonitrile

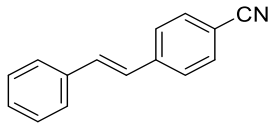

Cyclovoltammogram

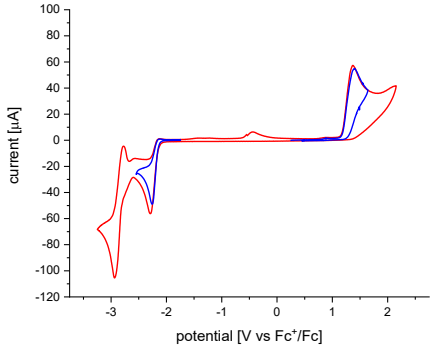

Differential pulse voltammetry

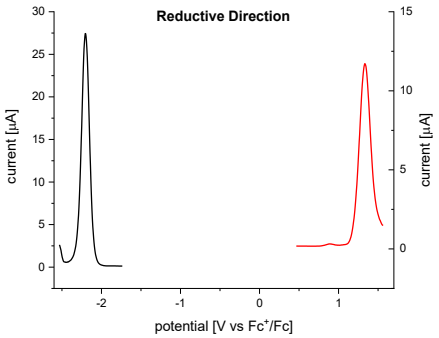

5.3.2.1.1.14 Ethyl (*E*)-4-styrylbenzoate

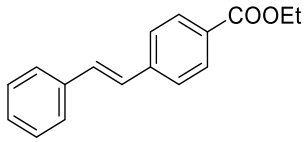

Cyclovoltammogram

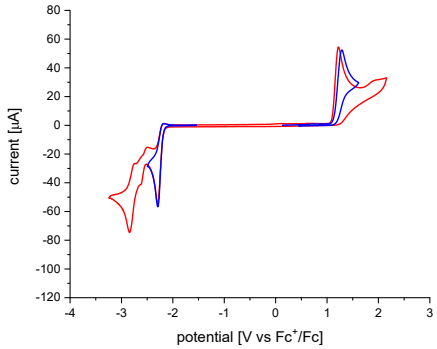

Differential pulse voltammetry

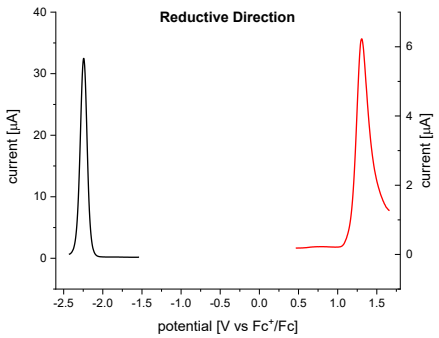

(*E*)-1-Styryl-4-(trifluoromethyl)benzene

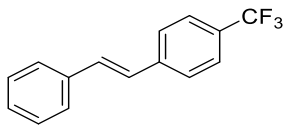

Cyclovoltammogram

Differential pulse voltammetry

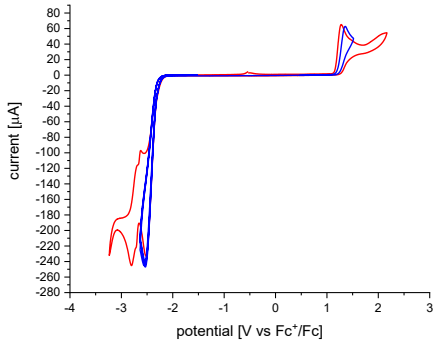

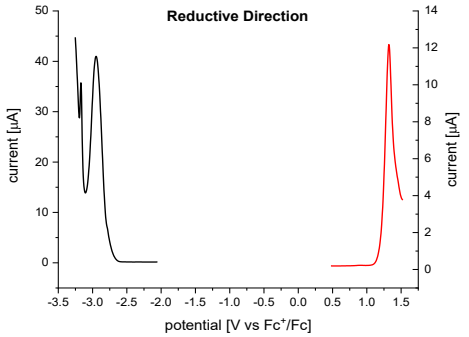

5.3.2.1.2 Oxidation potentials of amines

Phenylmethanamine **1a**:

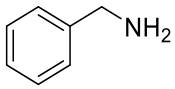

1a

Cyclovoltammogram

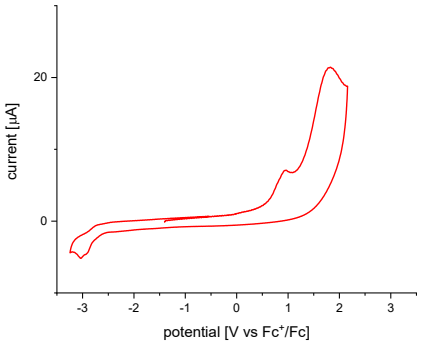

Differential pulse voltammetry

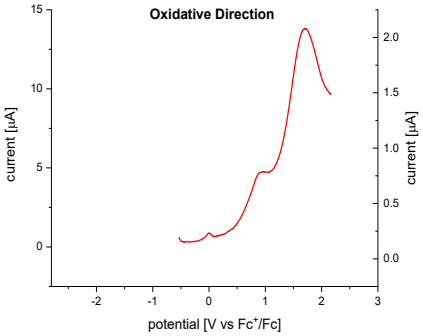

5.3.2.1.2.1 *N*-(1,2-diphenylethyl)adamantan-1-amine:

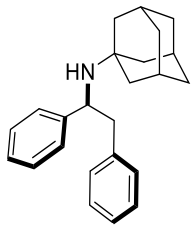

8

Cyclovoltammogram

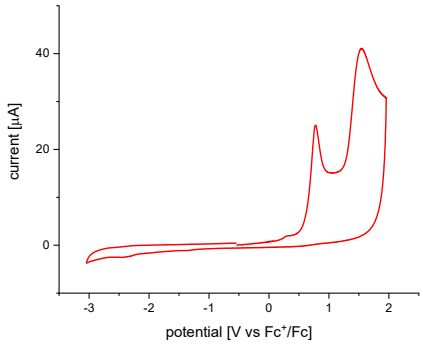

Differential pulse voltammetry

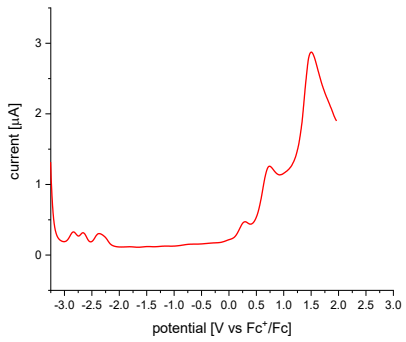

5.3.2.2 EPR-results

EPR spectra were recorded on an X-band Bruker EMX CW-micro EPR spectrometer equipped with an ER4119HS high-sensitivity resonator using a microwave power of Ca 6.9 mW, modulation frequency of 100 kHz and modulation amplitude up to 5 G. For low temperature measurements, the EPR spectrometer was equipped with a temperature controller and liquid N_2 cryostat. The hv =gβB_0 equation was used to calculate g values with B_0v and B_0v being the frequency and resonance field, respectively. 2,2-Diphenyl-1-picrylhydrazyl g values calibration was performed using 2,2-Diphenyl-1-picrylhydrazyl as a standard (g = 2.0036 ± 0.0004). EPR spectrum simulation was done by Bruker SimFonia software.

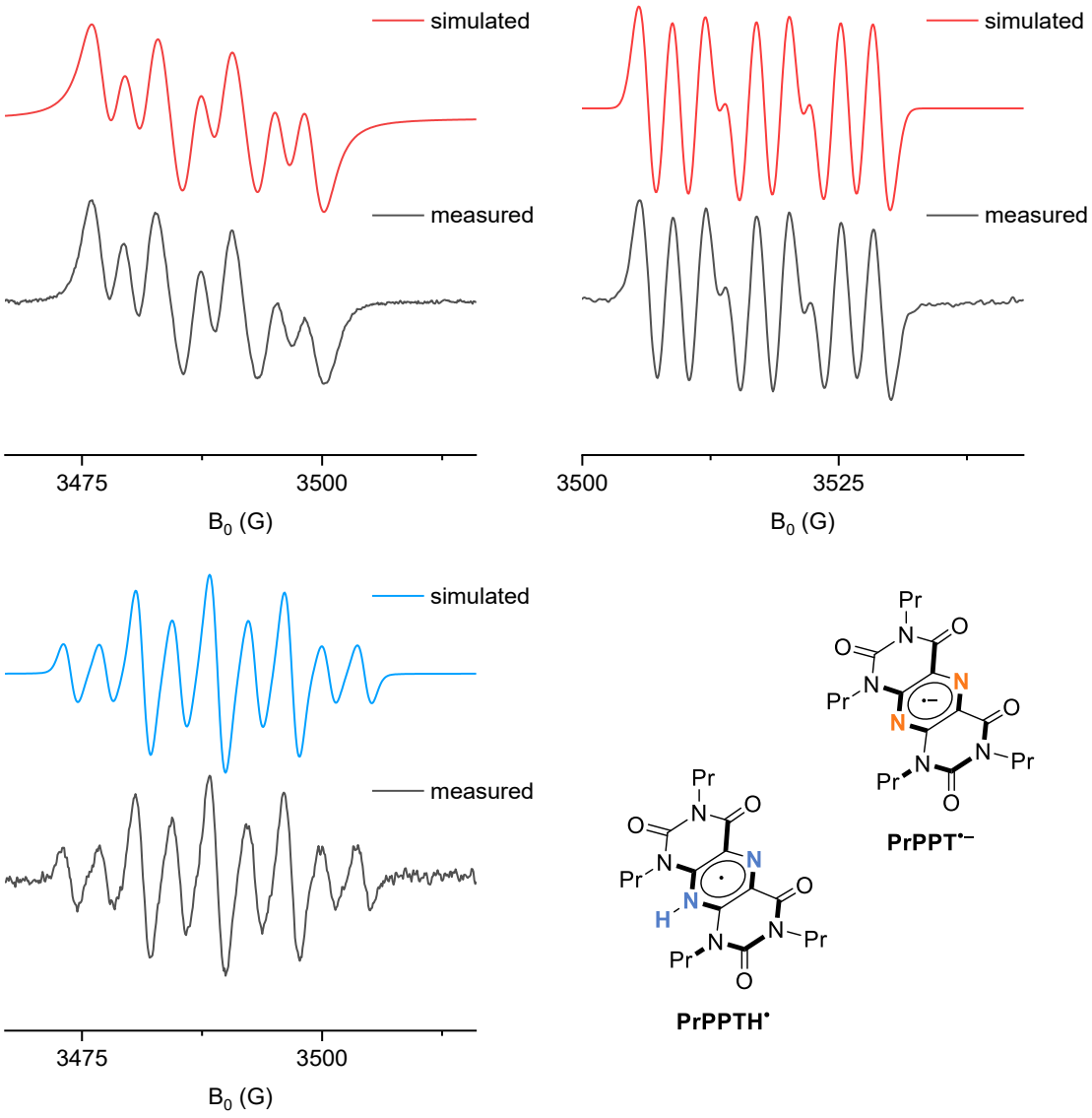

Figure 5.5: EPR spectrum of benzylamine and PrPPT (upper black line; Left: operando spectroscopy in a EPR-Flatcell; Right: accumulated radical in an EPR-tube) and stilbene 2.5 and PrPPT (bottom black line; operando spectroscopy in a EPR-Flatcell); blue and red lines are simulated spectra considering a hyperfine splitting from two nonequivalent *N* (red line,

A_{N1} = 8.25 G and A_{N2} = 3.25 G) and two nonequivalent N and one hydrogen (blue line, A_{N1} = 7.84 G and A_{N2} = 3.72 G A_H = 7.45 G).

5.3.2.2.1 EPR-experiment Nr.1: 2.5 & PrPPT

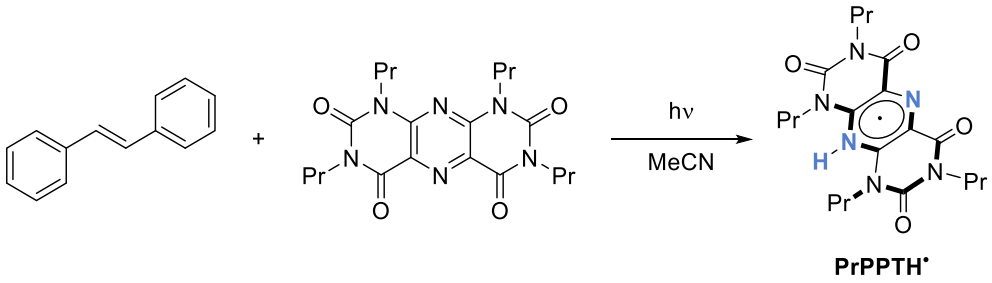

The reaction was performed under Schlenk conditions using a septum sealed EPR-flatcell. The photocatalyst PrPPT (**1.6**, 50 mg, 0.120 mmol) and stilbene (**2.5**, 76 mg, 0.42 mmol, 3.5 equiv.) were solved in dry acetonitrile (1.0 ml). The mixture was irradiated at 396 nm (1x30 W, ONFURO LED) without stirring while operando EPR-spectroscopy.

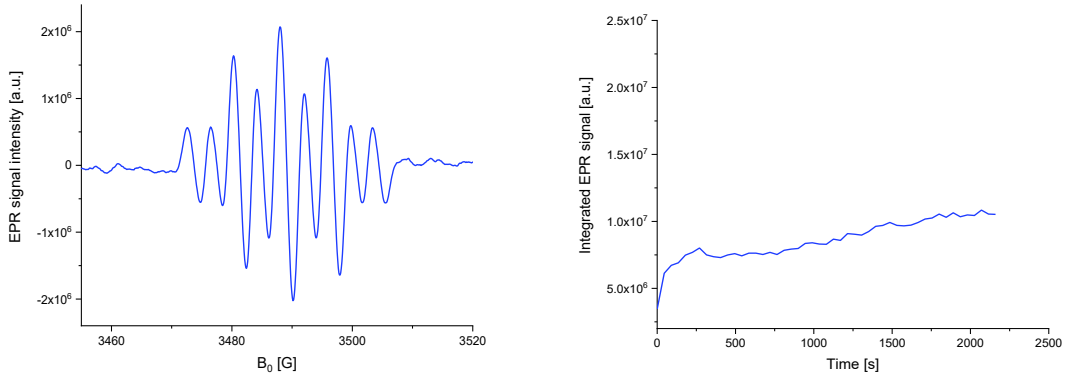

Figure 5.6: EPR spectrum of stilbene (2.5) and PrPPT (left) and radical accumulation (right).

5.3.2.2.2 EPR-experiment Nr.2: 2.13 & PrPPT

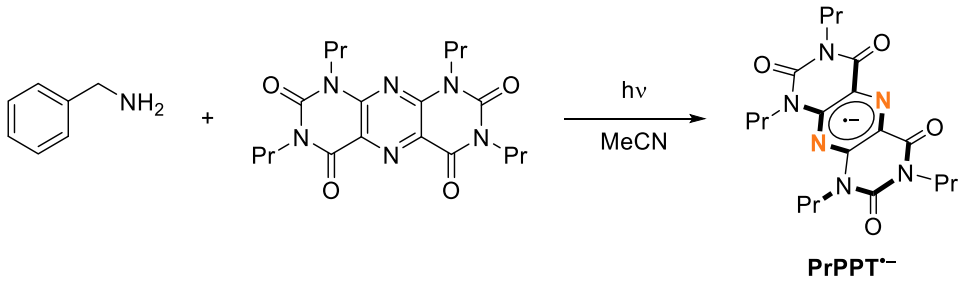

The reaction was performed under Schlenk conditions using a septum sealed EPR-flatcell. The photocatalyst PrPPT (50 mg, 0.120 mmol) and benzylamine (**2.13**, 68 mg, 0.634 mmol, 5.3 equiv.) were solved in dry acetonitrile (1.0 ml). The mixture was irradiated at 396 nm (1x30 W, ONFURO LED) without stirring while operando EPR-spectroscopy.

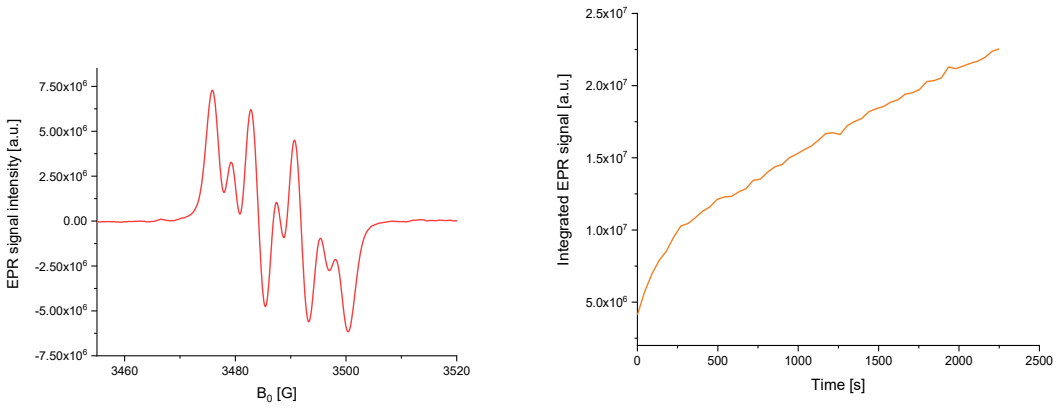

Figure 5.7: EPR spectrum of benzylamine (2.13) and PrPPT (left) and radical accumulation (right).

5.3.2.2.3 EPR-experiment Nr.3: d_2-2.13 & PrPPT

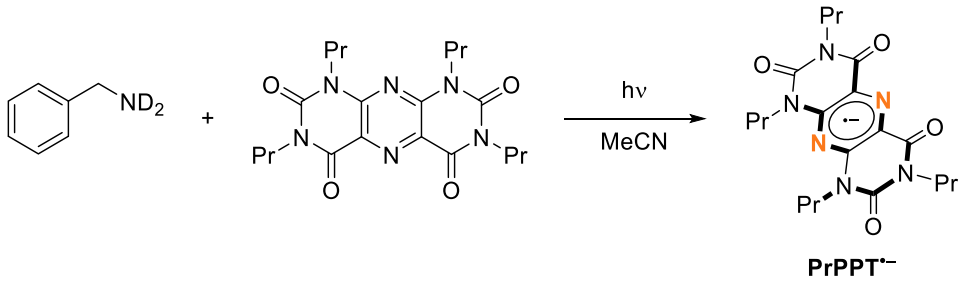

The reaction was performed under Schlenk conditions using a septum sealed EPR-flatcell. The photocatalyst PrPPT (50 mg, 0.120 mmol) and benzylamine (**d_2-2.13**, 68 mg, 0.634 mmol, 5.3 equiv.) were solved in dry acetonitrile (1.0 ml). The mixture was irradiated at 396 nm (1x30 W, ONFURO LED) without stirring while operando EPR-spectroscopy.

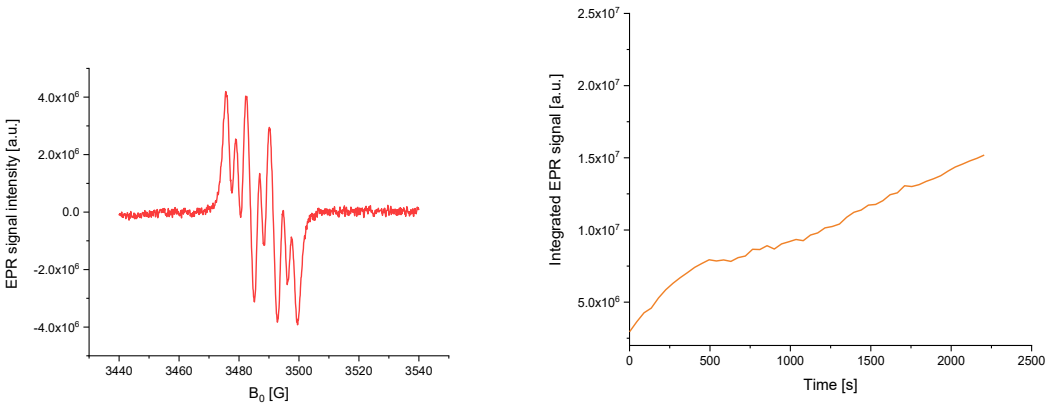

Figure 5.8: EPR spectrum of d_2-benzylamine (d_2-2.13) and PrPPT (left) and radical accumulation (right).

5.3.2.2.4 EPR-experiment Nr.4: 2.5, 2.13 & PrPPT (1:5:1)

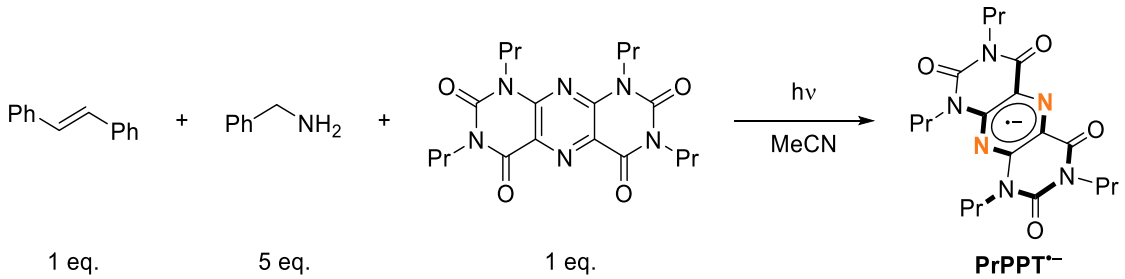

The reaction was performed under Schlenk conditions using a septum sealed EPR-flatcell. The photocatalyst PrPPT (52 mg, 0.124 mmol), benzylamine (**2.13**, 75 mg, 0.700 mmol, 5.6 equiv.) and stilbene (**2.5**, 27 mg, 0.150 mmol, 1.2 equiv.) were solved in dry acetonitrile (1.0 ml). The mixture was irradiated at 396 nm (1x30 W, ONFURO LED) without stirring while operando EPR-spectroscopy.

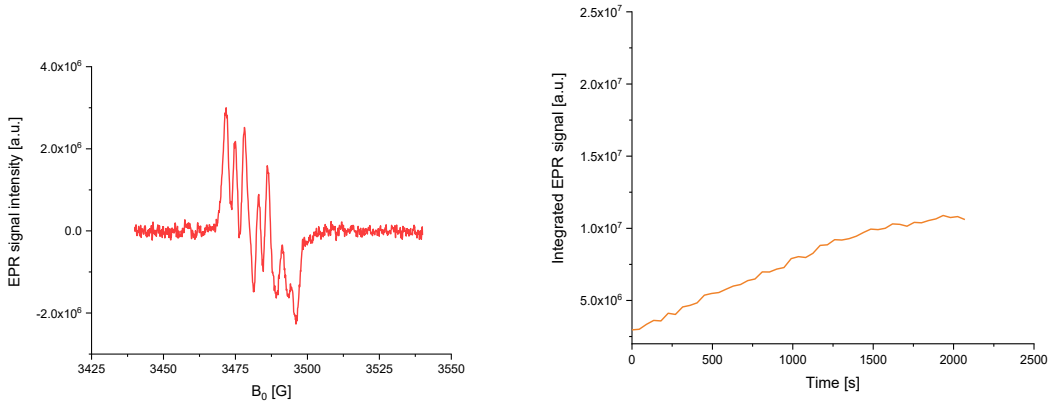

Figure 5.9: EPR spectrum of stilbene (2.5), benzylamine (2.13) and PrPPT (left, reaction condition mimic) and radical accumulation (right).

5.3.2.2.5 EPR-experiment Nr.5: d_2-2.5 & PrPPT

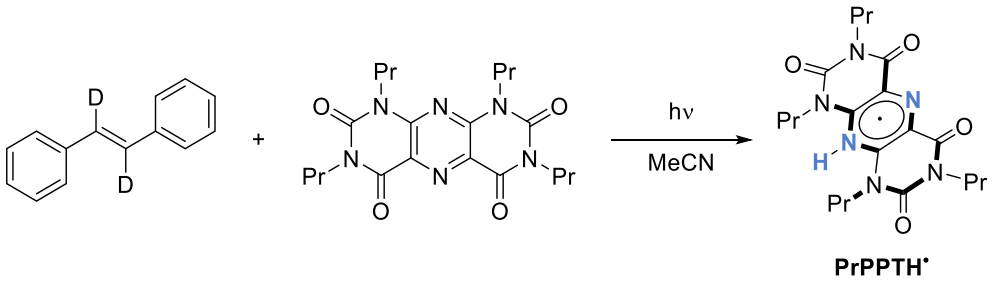

The reaction was performed under Schlenk conditions using a septum sealed EPR-flatcell. The photocatalyst PrPPT (54 mg, 0.130 mmol) and stilbene (**d_2-2.5**, 23 mg, 0.132 mmol, 1.02 equiv.) were solved in dry acetonitrile (1.0 ml). The mixture was irradiated at 396 nm (1x30 W, ONFURO LED) without stirring while operando EPR-spectroscopy.

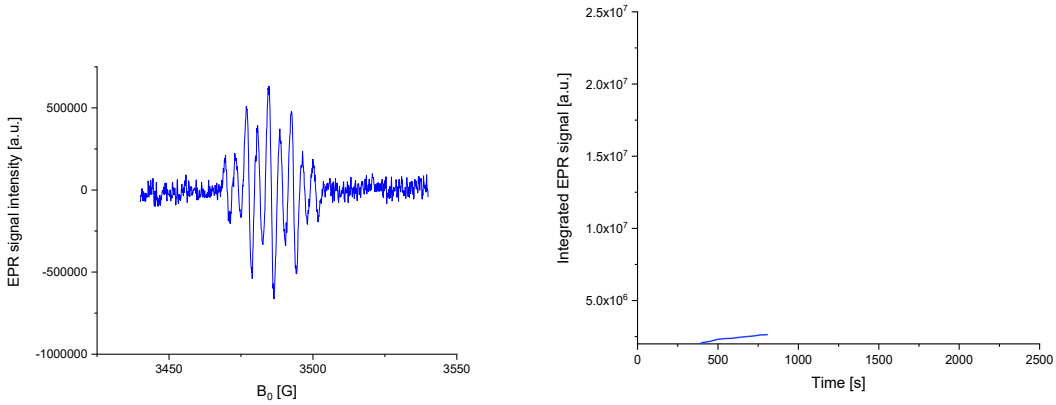

Figure 5.10: EPR spectrum of d_2-stilbene (d_2-2.5) and PrPPT (left) and radical accumulation (right).

5.3.2.2.6 EPR-experiment Nr.6: 2.5, 2.13 & PrPPT (1:1:1)

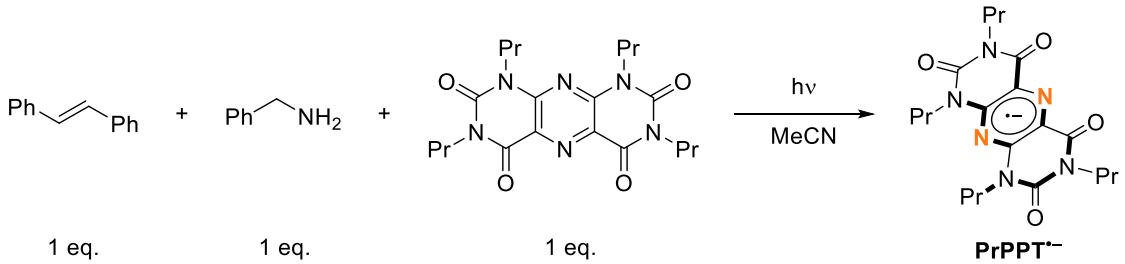

The reaction was performed under Schlenk conditions using a septum sealed EPR-flatcell. The photocatalyst PrPPT (60 mg, 0.144 mmol), benzylamine (**2.13**, 15 mg, 0.140 mmol, 1.0 equiv.) and stilbene (**2.5**, 26 mg, 0.142 mmol, 1.0 equiv.) were solved in dry acetonitrile (1.0 ml). The mixture was irradiated at 396 nm (1x30 W, ONFURO LED) without stirring while operando EPR-spectroscopy.

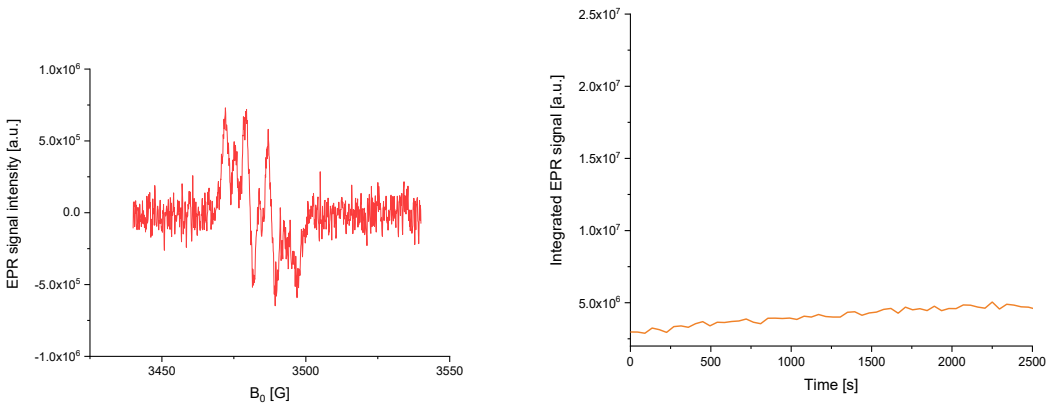

Figure 5.11: EPR spectrum of stilbene (2.5), benzylamine (2.13) and PrPPT (left, 1:1 ratio) and radical accumulation (right).

5.3.2.3 UV-vis experiments

The reactions was performed with dry solvents using a argon flushed standard fluorescence cuvette. Separately, the photocatalyst PrPPT (20.1 mg, 0.048 mmol) and benzylamine (10.2 mg, 0.095 mmol, 1.9 equiv.) were dissolved in dry acetonitrile (0.6 ml). The solution were mixed in the cuvette and 2 ml of dry acetonitrile was added. The UV-vis spectra of this mixture was set as “background” and the mixture was irradiated (1x30 W) without stirring in the reaction set up. After the described time the UV-vis spectra were recorded, during this time the irradiation was stopped for approximately 1 min.

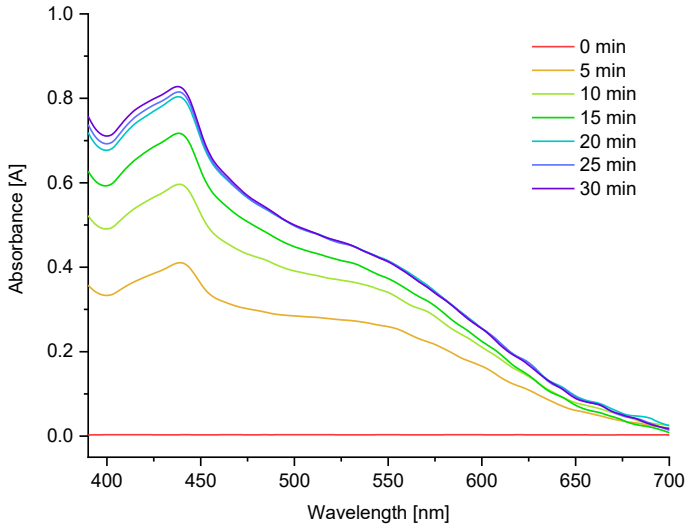

Figure 5.12: Differential UV-vis absorption spectra of a solution containing benzylamine (31 mM) and PrPPT (15 mM). Irradiated at 396 nm for the indicated time.

5.3.2.4 NMR-Results

The reactions was performed under Schlenk conditions using a J. Young-valve NMR-tube. The photocatalyst PrPPT (20.1 mg, 0.048 mmol) was added and the tube was backfilled with argon. Dry benzylamine (9.4 mg, 0.088 mmol, 1.8 equiv.) and dry deuterated acetonitrile (0.6 ml, 0.8 M) was added. The mixture was irradiated at 396 nm (1x30 W, ONFURO LED) without stirring. After the described time the NMR-spectra was recorded, during this time the irradiation was stopped for approximately 2-3 min. Samples were measured after irradiation for the indicated time (Figure 5.13). Eventually, the tube was quenched with air and the sample was recorded again.

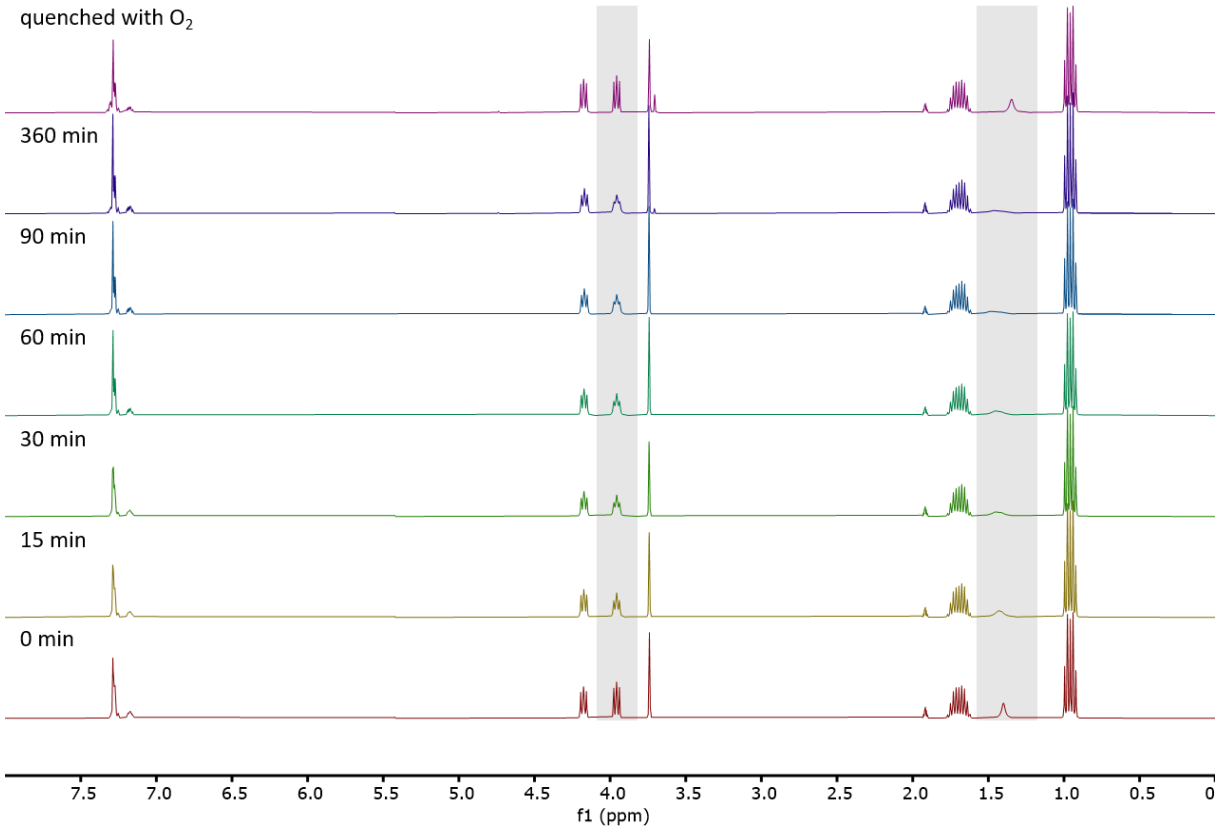

Figure 5.13: ^{1}H NMR spectra of PrPPT (1.6) and benzylamine (2.13) under irradiation at 396 nm. Irradiation time as indicated and after quenching with oxygen.

5.3.2.5 Stern Volmer experiments

Stern-Volmer quenching experiments were run with freshly prepared solutions of **PrPPT** (0.02 mM in dry MeCN) at room temperature under an inert atmosphere. The solutions were degassed by "freeze-pump-thaw" technique and then flushed with argon directly before measurement. The solutions were irradiated at 350 nm or 375 nm and luminescence was measured at 385 nm.

Table 5.1: Fluorescence quenching data of PrPPT* with (*E*)-stilbene (2.5).

I_x [a.u.]	$I_0/I_x - 1$ [a.u.]	Q [mM]
I_0 = 961.5422	0	0
I_1 = 823.6488	0.1674	2.8574
I_2 = 723.4052	0.3292	5.4550
I_3 = 645.9644	0.4885	7.8268
I_4 = 588.0695	0.6351	10.0009
I_5 = 538.9952	0.7840	12.0011
I_6 = 502.9805	0.9117	13.5474

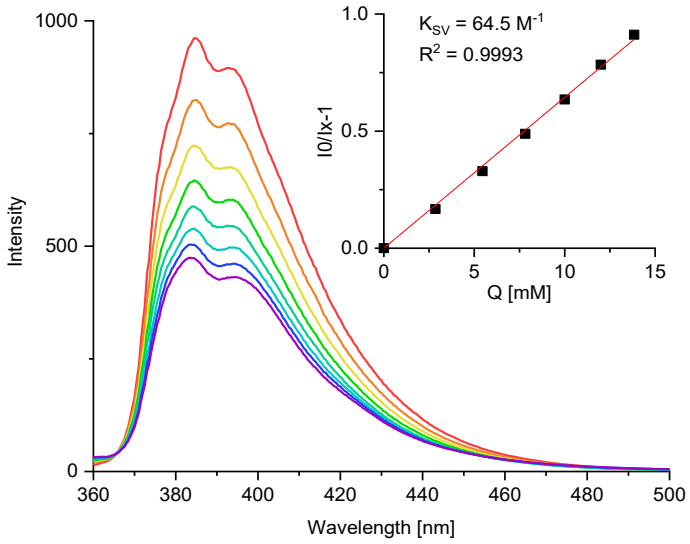

Figure 5.14: Quenching of luminescence and Stern-Volmer plot (inset) of PrPPT with varying concentrations of (*E*)-stilbene (2.5).

Table 5.2: Fluorescence quenching data of PrPPT* with (*Z*)-stilbene (2.6).

I_x [a.u.]	$I_0/I_x - 1$ [a.u.]	Q [mM]
I_0 = 484.5554	0	0
I_1 = 417.6843	0.1601	2.9166
I_2 = 366.1409	0.3234	5.5680
I_3 = 329.9178	0.4687	7.9889
I_4 = 301.3432	0.6080	10.2080
I_5 = 278.5020	0.7399	12.2497
I_6 = 258.2646	0.8762	14.1342
I_7 = 241.6800	1.0049	15.8792

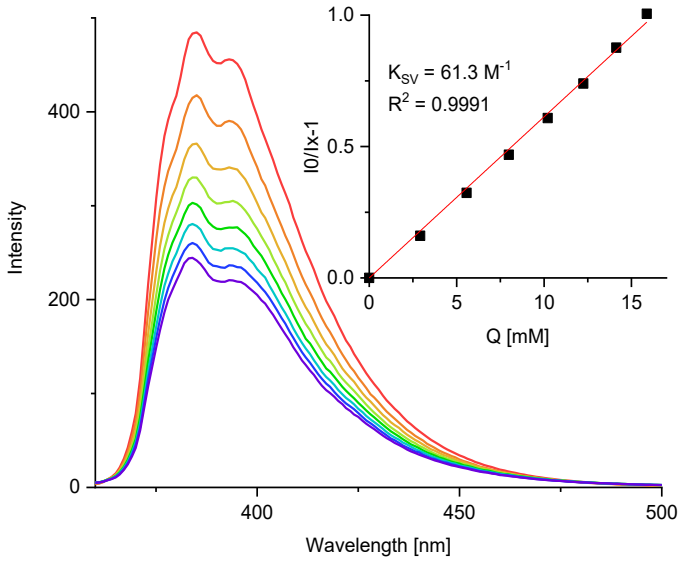

Figure 5.15: Quenching of luminescence and Stern-Volmer plot (inset) of PrPPT with varying concentrations of (*Z*)-stilbene (2.6).

Table 5.3: Fluorescence quenching data of PrPPT* with (*E*)-methoxystilbene (2.15).

I_x [a.u.]	$I_0/I_x - 1$ [a.u.]	Q [mM]
I_0 = 939.1526	0	0
I_1 = 773.5023	0.2142	2.8760
I_2 = 652.0507	0.4403	5.4905
I_3 = 542.5369	0.7310	7.8777
I_4 = 473.9391	0.9816	10.0659
I_5 = 424.0188	1.2149	12.0791
I_6 = 371.4589	1.5283	13.9375

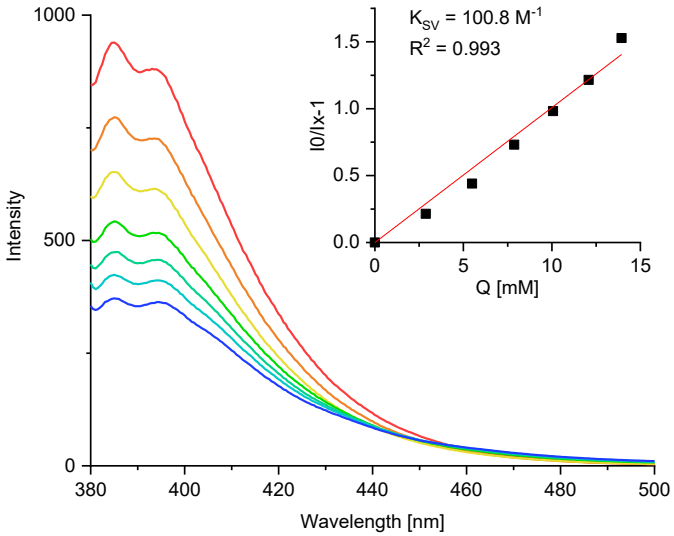

Figure 5.16: Quenching of luminescence and Stern-Volmer plot (inset) of PrPPT with varying concentrations of (*E*)-methoxystilbene (2.15).

Table 5.4: Fluorescence quenching data of PrPPT* with (*E*)-trifluromethylstilbene (2.1).

I_x [a.u.]	$I_0/I_x - 1$ [a.u.]	Q [mM]
I_0 = 913.5665	0	0
I_1 = 807.6686	0.1311	2.8523
I_2 = 725.1946	0.2598	5.4454
I_3 = 651.1423	0.4030	7.8130
I_4 = 590.6799	0.5466	9.9832
I_5 = 529.7399	0.7246	11.9799
I_6 = 485.7741	0.8806	13.8229

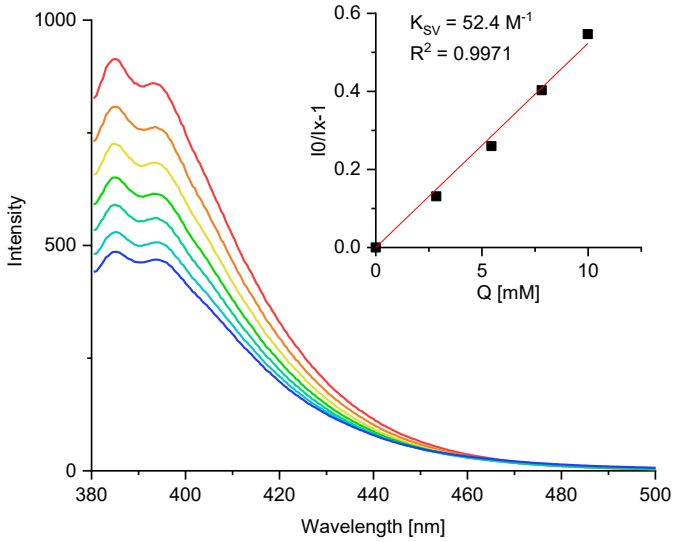

Figure 5.17: Quenching of luminescence and Stern-Volmer plot (inset) of PrPPT with varying concentrations of (*E*)-trifluromethylstilbene (2.1).

Table 5.5: Fluorescence quenching data of PrPPT* with benzylamine (2.13).

I_x [a.u.]	$I_0/I_x - 1$ [a.u.]	Q [mM]
I_0 = 493.6455	0	0
I_1 = 440.2701	0.1212	3.1035
I_2 = 408.6491	0.2080	5.9249
I_3 = 383.1306	0.2885	8.5009
I_4 = 361.7695	0.3645	10.8623
I_5 = 344.3997	0.4334	13.0347
I_6 = 329.0381	0.5003	15.0401
I_7 = 315.1751	0.5663	16.8969
I_8 = 306.7914	0.6091	18.6210
I_9 = 297.0331	0.6619	20.2263
I_{10} = 289.3639	0.7060	21.7245

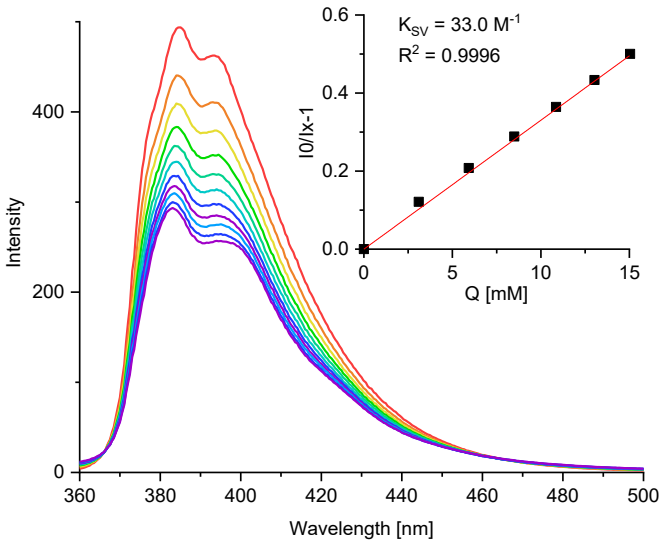

Figure 5.18: Quenching of luminescence and Stern-Volmer plot (inset) of PrPPT with varying concentrations of benzylamine (2.13).

Table 5.6: Fluorescence quenching data of PrPPT* with dibutylamine (2.17).

I_x [a.u.]	$I_0/I_x - 1$ [a.u.]	Q [mM]
I_0 = 517.1000	0	0
I_1 = 487.9067	0.0598	1.1230
I_2 = 470.1379	0.0999	2.1438
I_3 = 444.7845	0.1626	3.0759
I_4 = 426.7958	0.2116	3.9304
I_5 = 413.2624	0.2513	4.7164
I_6 = 382.1855	0.3530	5.4420
I_7 = 364.1885	0.4199	6.1139

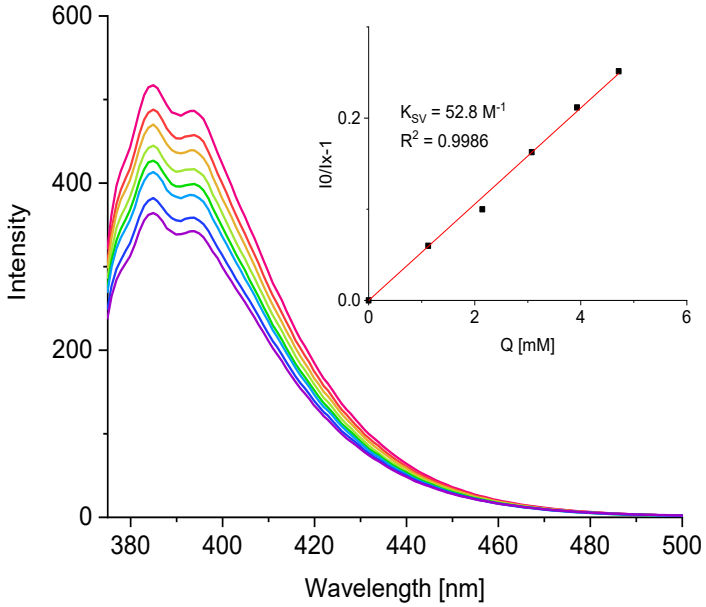

Figure 5.19: Quenching of luminescence and Stern-Volmer plot (inset) of PrPPT with varying concentrations of dibenzylamin (2.17).

5.3.2.6 Competitive Stern Volmer Experiments

Stern-Volmer quenching experiments were run with freshly prepared solutions of **PrPPT** (0.02 mM in dry MeCN) at room temperature under an inert atmosphere. The solutions were degassed by "freeze-pump-thaw" technique and then flushed with argon directly before measurement. The solutions were irradiated at 350 nm and luminescence was measured at 385 nm. In this competitive experiment, the fluorescence quenching of a quencher up to a concentration of 10 mM was measured. Subsequently, the influence of the second quenchers is examined.

Table 5.7: Fluorescence quenching data from a solution of PrPPT first with benzylamine (2.13; Q_1) and then (*E*)-stilbene (2.5; Q_2).

I_x [a.u.]	Q_1: $I_0/I_x - 1$ [a.u.]	Q_2: $I_0/I_x - 1$ [a.u.]	Q_1 [mM]	Q_2 [mM]
$I_{0'}$ = 504.4574	0	-	0	0
$I_{1'}$ = 463.3353	0.0888	-	2.8661	0
$I_{2'}$ = 425.2285	0.1863	-	5.4908	0
$I_{3'}$ = 397.8763	0.2679	-	7.9033	0
$I_{4'}$ = 376.6942	0.3392	-	10.1283	0
I_0 = 377.4438	0.3392	0	10.1283	0
I_1 = 354.4338	0.3392	0.0649	9.9189	1.2408
I_2 = 339.5746	0.3392	0.1115	9.7179	2.4313
I_3 = 325.0934	0.3392	0.1610	9.5250	3.5746
I_4 = 313.0285	0.3392	0.2058	9.3395	4.6733
I_5 = 301.9561	0.3392	0.2500	9.1611	5.7301
I_6 = 291.3434	0.3392	0.2955	8.9895	6.7473
I_7 = 283.1437	0.3392	0.3330	8.8241	7.7270
I_8 = 275.2831	0.3392	0.3711	8.6647	8.6713
I_9 = 267.4177	0.3392	0.4114	8.5110	9.5821
I_{10} = 260.6298	0.3392	0.4482	8.3626	10.4612
I_{11} = 254.2239	0.3392	0.4847	8.2193	11.3102
I_{12} = 248.7989	0.3392	0.5171	8.0808	12.1305

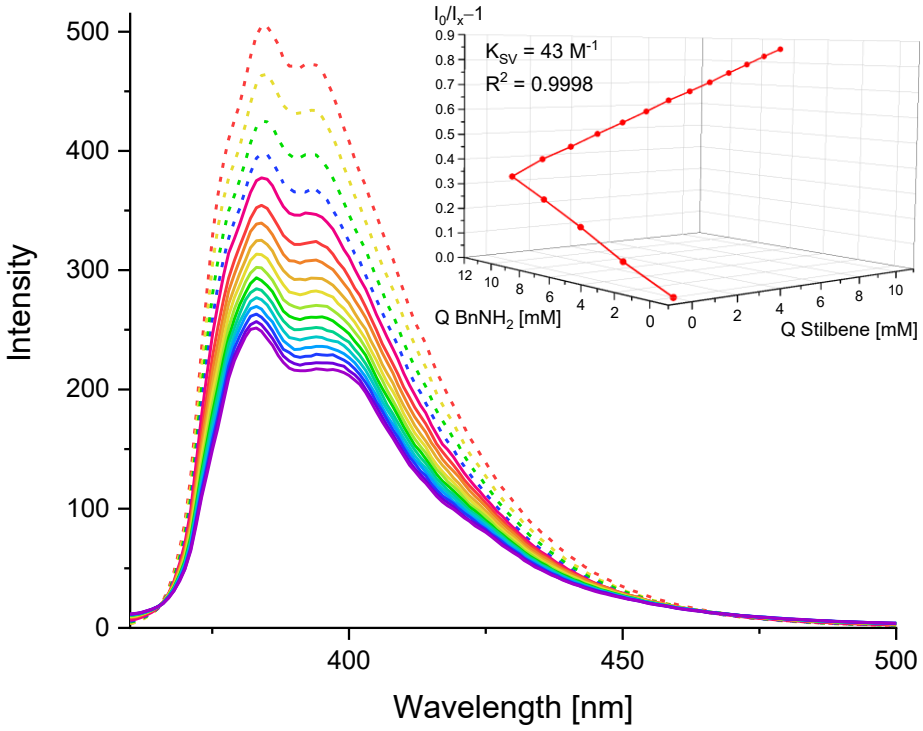

Figure 5.20: Quenching of luminescence and Stern-Volmer plot (inset) of PrPPT variation of the concentration of benzylamine (2.13) (dotted lines) and subsequent variation of the concentration of *E*-stilbene (2.5) (solid lines).

Table 5.8: Fluorescence quenching data from a solution of PrPPT first with benzylamine (2.13; Q_1) and then (*Z*)-stilbene (2.6; Q_2).

I_x [a.u.]	Q_1: $I_0/I_x - 1$ [a.u.]	Q_2: $I_0/I_x - 1$ [a.u.]	Q_1 [mM]	Q_2 [mM]
$I_{0'}$ = 494.2883	0	-	0	0
$I_{1'}$ = 447.7521	0.1039	-	2.8661	0
$I_{2'}$ = 411.2444	0.2019	-	5.4908	0
$I_{3'}$ = 385.7421	0.2814	-	7.9033	0
$I_{4'}$ = 363.9764	0.3580	-	10.1283	0
I_0 = 366.4317	0.3580	0	10.1283	0
I_1 = 348.2160	0.3580	0.0523	9.9189	1.2665
I_2 = 332.0264	0.3580	0.1036	9.7179	2.4817
I_3 = 317.8150	0.3580	0.1530	9.5250	3.6486
I_4 = 307.7310	0.3580	0.1908	9.3395	4.7701
I_5 = 297.1721	0.3580	0.2331	9.1611	5.8488
I_6 = 287.2294	0.3580	0.2757	8.9895	6.8870
I_7 = 276.4632	0.3580	0.3254	8.8241	7.8870
I_8 = 268.6963	0.3580	0.3637	8.6647	8.8509
I_9 = 261.3752	0.3580	0.4019	8.5110	9.7806
I_{10} = 254.9919	0.3580	0.4370	8.3626	10.6779
I_{11} = 247.2670	0.3580	0.4819	8.2193	11.5444
I_{12} = 240.7931	0.3580	0.5218	8.0808	12.3817

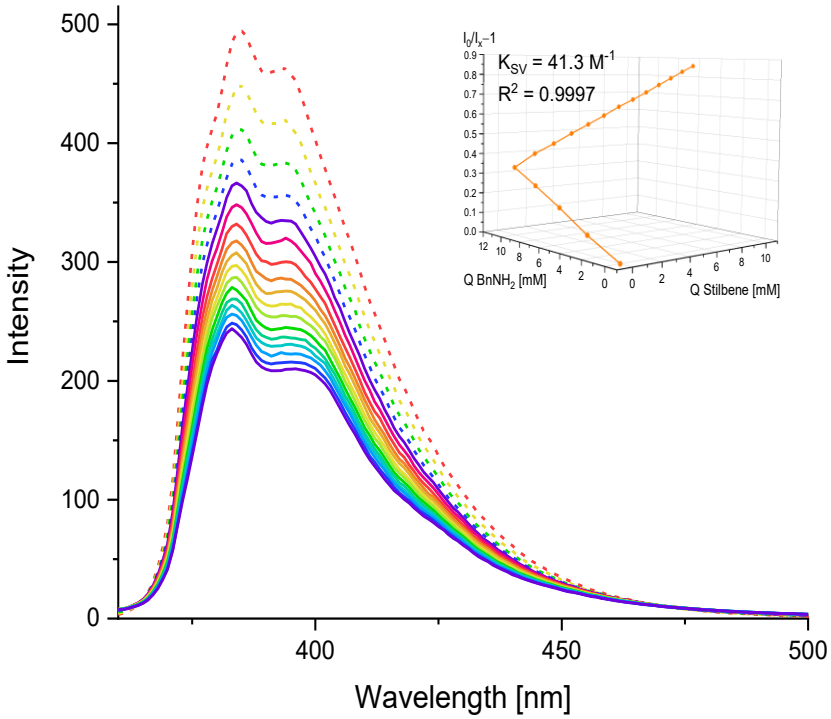

Figure 5.21: Quenching of luminescence and Stern-Volmer plot (inset) of PrPPT variation of the concentration of benzylamine (2.13) (dotted lines) and subsequent variation of the concentration of *Z*-stilbene (2.6) (solid lines).

Table 5.9: Fluorescence quenching data from a solution of PrPPT first with (*E*)-stilbene (2.5; Q_1) and then benzylamine (2.13; Q_2).

I_x [a.u.]	Q_1: $I_0/I_x - 1$ [a.u.]	Q_2: $I_0/I_x - 1$ [a.u.]	Q_1 [mM]	Q_2 [mM]
$I_{0'}$ = 492.0147	0	-	0	0
$I_{1'}$ = 409.9788	0.0888	-	2.8574	0
$I_{2'}$ = 362.5087	0.1863	-	5.455	0
$I_{3'}$ = 325.2377	0.2679	-	7.8268	0
$I_{4'}$ = 298.8894	0.3392	-	10.0009	0
I_0 = 952.931	0.3392	0	10.0009	0
I_1 = 943.986	0.3392	0.0095	9.8370	1.0684
I_2 = 939.3539	0.3392	0.0145	9.6783	2.1024
I_3 = 934.3158	0.3392	0.0199	9.5247	3.1035
I_4 = 933.3154	0.3392	0.0210	9.3759	4.0733
I_5 = 927.1115	0.3392	0.0278	9.2316	5.0134
I_6 = 926.1149	0.3392	0.0290	9.0917	5.9249
I_7 = 922.0298	0.3392	0.0335	8.9561	6.8092
I_8 = 919.6316	0.3392	0.0362	8.8243	7.6675
I_9 = 915.1237	0.3392	0.0413	8.6965	8.5009
I_{10} = 910.3328	0.3392	0.0468	8.5722	9.3105
I_{11} = 905.7416	0.3392	0.0521	8.4515	10.0973
I_{12} = 903.2186	0.3392	0.0550	8.3341	10.8623

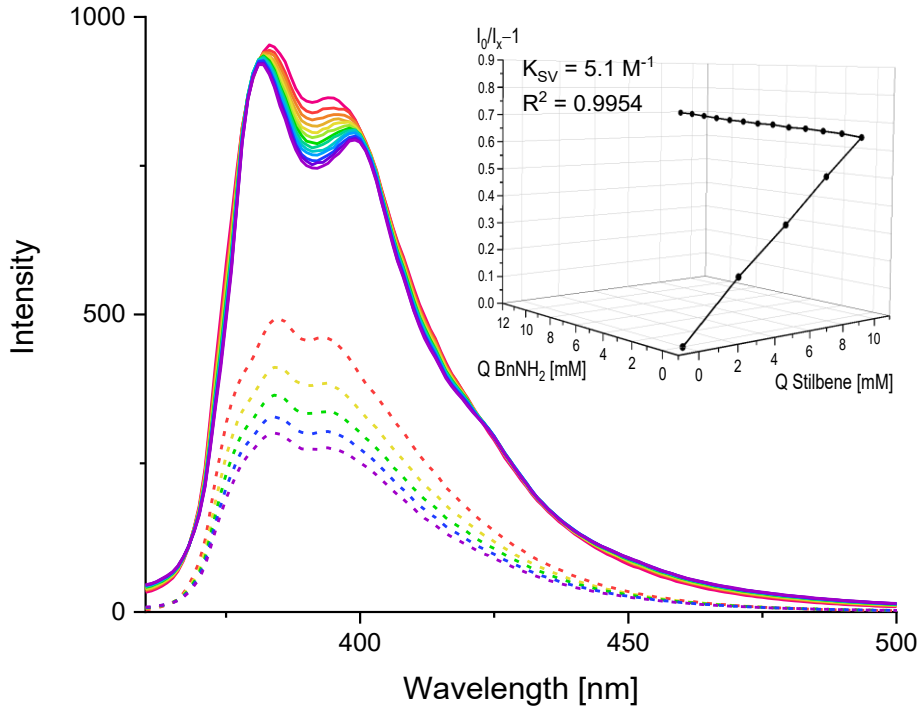

Figure 5.22: Quenching of luminescence and Stern-Volmer plot (inset) of PrPPT first varying the concentration of *E*-stilbene (2.5) (dotted lines) and subsequent benzylamine (2.13) (solid lines). Change in intensity due to the enlargement of the emission slot.

5.3.2.7 Computational methods and models

All calculations were carried out using Gaussian 16 program. [44] Geometry optimization was carried out in gas phase at the B3PW91[45] level with the all-electron TZVP[46] under the consideration of solvation effect of acetonitrile as solvent based on solute electron density (SMD[47]) and van der Waals dispersion (GD3BJ[48]). All optimized structures were further characterized at the same level either as energy minimums without imaginary frequencies or transition states with only one imaginary frequency by frequency calculations, which provided zero-point vibrational energies and thermal corrections to enthalpy and Gibbs free energy at 298.15 K under 1 atmosphere. 1,3,7,9-tetramethylpyrimido[5,4-g]pteridine-2,4,6,8(1*H*,3*H*,7*H*,9*H*)-tetraone **MePPT** was used as model catalyst. The final Gibbs free energies for discussion include the thermal corrections to enthalpies and Gibbs free energies.

Table 5.10: Computed Gibbs free energies of selected compounds concerning the proton transfer from $PPTH^{\bullet-}$ to benzylamine.

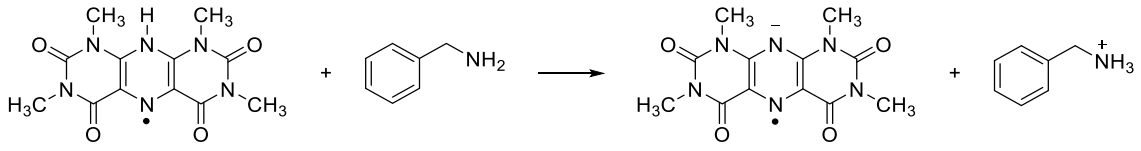

PPTH• **$BnNH_2$** **$PPT^{\bullet-}$** **$BnNH_3^+$**

Entry	Compound	G [Hartree]	G [kcal·mol^{-1}]
1	**PPTH•**	1094.413940	686755.262513
2	**$BnNH_2$**	326.821509	205083.63701
3	**$PPT^{\bullet-}$**	1093.963957	686472.893857
4	**$BnNH_3^+$**	327.280673	205371.76683

$$(\Delta G(PT) = (-686472.893857) + (-205371.76683) - (-686755.262513) - (-205083.63701) = -5.76\ kcal/mol$$

The deprotonation of the protonated catalyst **PPTH•** by benzylamine (**2.13**) is exergonic by −5.76 kcal/mol.

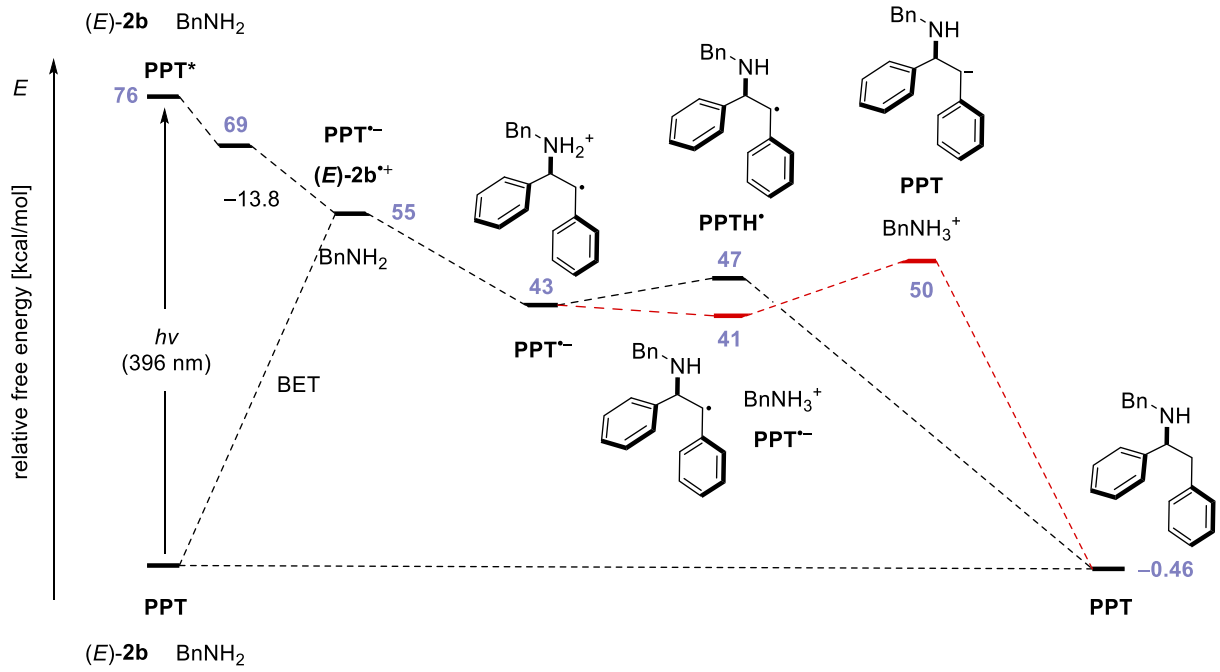

Figure 5.23: Calculation of free energy values in the proposed energy profile.

1. The excited-state energy of **PPT** was measured to be 76 kcal/mol.[115]
   Note: A discrepancy of 7 kcal/mol is noticed, potentially attributed to a proton transfer as evident by EPR experiments.
2. The excited-state reduction potential of **PPT** was calculated to be (E^*[**MePPT***/**MePPT**$^{\bullet-}$] = +1.75 V vs Fc^+/Fc in MeCN).[11] The oxidation potential of *E*-stilbene ((*E*)-**2b**) was measured by cyclic voltammetry ($E_{1/2}^{ox}$ = +1.15 V vs Fc^+/Fc in MeCN).

$$\Delta G = (1.15 - 1.75) * 23.06 \frac{kcal}{mol} = -13.8\ kcal/mol$$

3. The nucleophilic attack of benzyl amine to the radical cation of stilbene is exergonic by $-11.6\ kcal/mol$.

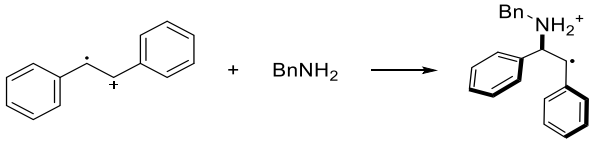

$$\Delta G = (-867.198057) - (-540.358067 - 326.821509) * 627.51 \frac{kcal}{mol} = -11.6 \frac{kcal}{mol}$$

4. The proton transfer (PT) from the seminal adduct of the stilbene radical cation and benzylamine was calculated from the Gibbs free energies of the products and substrates.

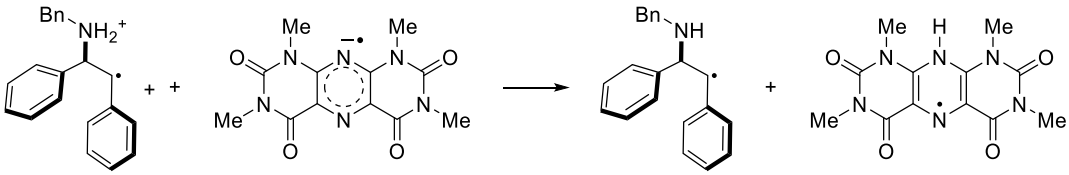

$$\Delta G = (-866{,}742472 - 1094{,}41394) - (-867{,}198057 - 1093{,}963957) * 627.51 \frac{kcal}{mol}$$
$$= 3.52\ kcal/mol$$

5. The HAT from the protonated radical catalyst **PPTH•** was calculated from the Gibbs free energies of the products and substrates.

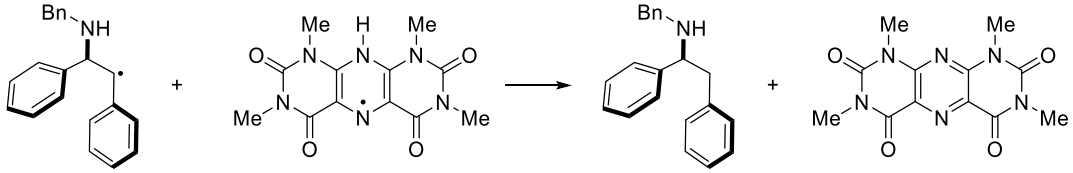

$$\Delta G = (-867{,}381022 - 1093{,}850848) - (-866{,}74247 - 1094{,}41394) * 627.51 \frac{kcal}{mol}$$
$$= -47.4\ kcal/mol$$

6. The overall free energy difference of the addition of benzylamine across (*E*)-stilbene can be calculated from the standard Gibbs free energy equation and Boltzmann's entropy formula.

$$\Delta G = \Delta H - T\Delta S = -0.46\ kcal/mol$$

Table 5.11: B3PW91 computed total electronic energy (HF, au), zero-point vibrational energies (ZPOE, au), number of imaginary frequencies (NImag), thermal corrected enthalpies (Htot, au) and Gibbs free energies (Gtot, au) under the consideration of van der Waals dispersion correction (GD3BJ) and solvation effect (SMD) of acetonitrile as solvent as well as the optimized coordinates of the equilibrium geometries (B3PW91-SMD-GD3BH//TZVP)

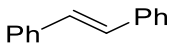	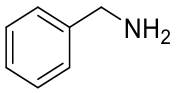
HF=-540.7367133 ZPE= 0.213504 NImag=0 Htot= -540.512425 Gtot= -540.558785	HF=-326.9350375 ZPE=0.145704 NImag=0 Htot=-326.781119 Gtot= -326.821509
C,0,0.0000000023,-0.1386885332,0.8933111153 C,0,0.0000000057,0.1973055109,3.6837745062 C,0,0.0000000033,-1.2434083118,1.7559916194 C,0,0.0000000031,1.1428534263,1.4642575122 C,0,0.0000000048,1.3057658592,2.8399280208	H,0,-0.1908641546,0.1104189789,-0.0205400722 C,0,-0.1124248,0.0751935254,1.0616292666 C,0,0.0911262529,-0.0138306801,3.82643033 C,0,0.0059777175,-1.1587310566,1.6962204036 C,0,-0.1321908475,1.2565216026,1.7975109491

C,0,0.000000005,-1.0790800401,3.1341861657 H,0,0.0000000027,-2.2418960077,1.33070568 H,0,0.0000000024,2.0210994232,0.8292074613 H,0,0.0000000053,2.3058111538,3.2598362213 H,0,0.0000000057,-1.9503052774,3.7801137938 H,0,0.000000007,0.3300943749,4.7597959969 C,0,-0.0000000023,0.3161530692,-2.9485826613 C,0,-0.0000000057,-0.019840975,-5.7390460522 C,0,-0.0000000033,1.4208728477,-3.8112631654 C,0,-0.0000000031,-0.9653888903,-3.5195290582 C,0,-0.0000000048,-1.1283013232,-4.8951995668 C,0,-0.000000005,1.2565445761,-5.1894577117 H,0,-0.0000000027,2.4193605437,-3.3859772261 H,0,-0.0000000024,-1.8436348872,-2.8844790073 H,0,-0.0000000053,-2.1283466178,-5.3151077673 H,0,-0.0000000057,2.1277698133,-5.8353853398 H,0,-0.000000007,-0.1526298389,-6.815067543 C,0,0.0000000006,-0.3783458312,-0.5459646504 H,0,0.0000000002,-1.4288628067,-0.8245975715 C,0,-0.0000000006,0.5558103672,-1.5093068957 H,0,-0.0000000002,1.6063273427,-1.2306739745	C,0,-0.0301996121,1.2146487898,3.1820333168 C,0,0.1093084713,-1.1891227243,3.0882053614 H,0,-0.2255839021,2.2091119888,1.2871678892 H,0,-0.045282129,2.13312393,3.7585481105 H,0,0.2060327141,-2.1446527526,3.5934453722 H,0,0.1675956145,-0.0535201793,4.9077819352 C,0,0.0476094361,-2.4349933957,0.8996842592 H,0,-0.2492777524,-2.2138419098,-0.1339938999 H,0,-0.6890848497,-3.1363384224,1.3025184718 N,0,1.3652571972,-3.0711621461,1.0002933533 H,0,1.3552086924,-3.9489766918,0.4905329443 H,0,2.0576276653,-2.4842592867,0.5448068748
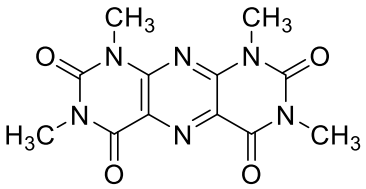	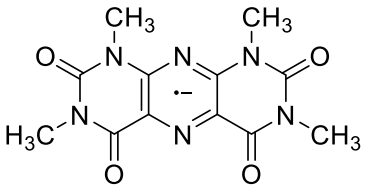
HF=-1094.0543315 ZPE=0.253986 NImag=0 Htot=-1093.779532	HF=-1094.1653212 ZPE=0.251072 NImag=0 Htot=-1093.893340

Gtot=-1093.850848	Gtot=-1093.963957
C,0,0.0430205681,-1.1406626907,1.0371580091	C,0,0.0442245144,-1.1597505472,1.072505924
C,0,-0.0492883827,-1.1281858799,-0.3701942386	C,0,-0.0468468719,-1.130569018,-0.3198034524
N,0,-0.0689044406,0.0060586894,-1.057810965	N,0,-0.0679400055,0.0059241625,-1.0315585335
C,0,0.0023711528,1.1323557809,-0.3606110391	C,0,0.0052356597,1.1341899786,-0.3102271667
N,0,0.1134682379,-0.0098663827,1.7156075213	N,0,0.1187862587,-0.0103724184,1.8070349116
C,0,0.0951979267,1.1286691921,1.0467574796	C,0,0.0973639077,1.1473831987,1.082255847
N,0,-0.0165175395,2.3097426278,-1.0463085068	N,0,-0.0153165659,2.3115357981,-1.027059732
N,0,-0.1215581228,-2.2976338144,-1.0658566695	N,0,-0.1212311329,-2.2996274123,-1.0465656526
C,0,0.1729147119,2.3924654251,1.7900755581	C,0,0.172222189,2.4051577192,1.780282985
C,0,0.0619846626,-2.4129254276,1.7697756708	C,0,0.0607505591,-2.4254846189,1.7598821934
O,0,0.140173208,-2.4962341277,2.9794509265	O,0,0.1380485794,-2.56583759,2.9794636518
O,0,0.254680375,2.4618594559,3.0003923354	O,0,0.2558420001,2.5314907469,3.0009796757
C,0,0.0534679349,3.5392801034,-0.4022016185	C,0,0.0528773737,3.5499708773,-0.4184828018
C,0,-0.1088442535,-3.5344787276,-0.4321471733	C,0,-0.110076005,-3.5449895475,-0.4484964275
O,0,0.0362565376,4.5863323925,-1.0167160437	O,0,0.0343827013,4.5951502182,-1.0587736428
O,0,-0.1739311152,-4.5744018448,-1.0554981529	O,0,-0.1762858388,-4.5827685075,-1.0976073856
N,0,0.1449097811,3.5264717228,0.9836947748	N,0,0.1437004253,3.5509560942,0.9541286338
N,0,-0.0183210291,-3.5375800319,0.9538637877	N,0,-0.0203627012,-3.5617340487,0.9240859364
C,0,0.2164614941,4.8376392439,1.6207700143	C,0,0.2150998643,4.8610688473,1.5833004172
H,0,-0.6768082701,5.4152804838,1.3860317666	H,0,-0.6766363747,5.4437444397,1.3501983645
H,0,1.0961898543,5.3753617395,1.2691229082	H,0,1.0929865128,5.4040557134,1.231913729
H,0,0.2835920838,4.6800468981,2.6923192028	H,0,0.2831488529,4.7035024084,2.6552751275
C,0,-0.1133559469,2.2826774297,-2.5027782636	C,0,-0.1122696679,2.2559250812,-2.4794512404
H,0,-1.0351331136,1.785188935,-2.8022055749	H,0,-1.0320523775,1.7523844363,-2.7764220218
H,0,0.7387656766,1.7468798714,-2.919501932	H,0,0.7373659585,1.712939978,-2.8930357895
H,0,-0.1144181127,3.3086844214,-2.85405457	H,0,-0.1138488173,3.2763799196,-2.8485952451
C,0,-0.2159642356,-2.2538486523,-2.5220798643	C,0,-0.2149209916,-2.2273522525,-2.498437753
H,0,-1.1144873954,-1.7133699381,-2.817687254	H,0,-1.1103177279,-1.6793322773,-2.7911410978
H,0,-0.2623158765,-3.27575648,-2.882138483	H,0,-0.263526243,-3.2434950775,-2.8761800397

H,0,0.6594641493,-1.7528836967,-2.9337696683 C,0,-0.0079730257,-4.8559718203,1.5798663407 H,0,-0.9259707683,-5.3903716837,1.3382699544 H,0,0.0635755224,-4.7106369532,2.6528608934 H,0,0.8472978052,-5.4301861008,1.2255429796	H,0,0.6590762858,-1.7207705085,-2.9074343076 C,0,-0.0096979664,-4.8790073349,1.542168674 H,0,-0.9263062455,-5.4187229347,1.3022934694 H,0,0.0629458571,-4.7337481481,2.6155789925 H,0,0.8435780874,-5.4581972158,1.1879238627
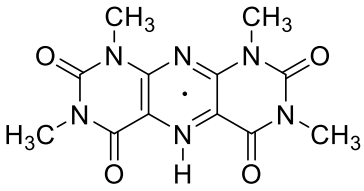	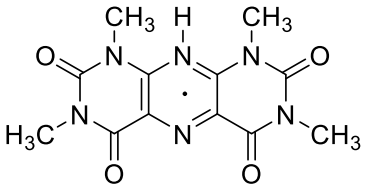
HF=-1094.6512968 ZPE=0.264545 NImag=0 Htot=-1094.365424 Gtot= -1094.436681	HF=-1094.6265578 ZPE=0.263953 NImag=0 Htot=-1094.341155 Gtot= -1094.413940
C,0,0.040557869,-1.1902144832,1.0282255751 C,0,-0.0491510062,-1.1349160827,-0.3565473142 N,0,-0.0690996153,0.006064728,-1.0573327382 C,0,0.0032294415,1.1389578232,-0.346940139 N,0,0.1127396552,-0.0098278737,1.7129251422 C,0,0.0950933491,1.1783709669,1.0382345416 N,0,-0.0152884006,2.3214323909,-1.0375513522 N,0,-0.1219818239,-2.3094085858,-1.0571139544 C,0,0.1695166518,2.4030989837,1.7720854278 C,0,0.0583778581,-2.4232236366,1.7516927007 O,0,0.1367045528,-2.4820686399,2.9755580452 O,0,0.2501974481,2.4479384159,2.9963909036 C,0,0.0527138042,3.5562764857,-0.4047897095 C,0,-0.1104046341,-3.5513892862,-0.4348556552	C,0,0.052937162,-1.16087329,1.037213029 C,0,-0.0394852606,-1.1830063753,-0.3384251904 N,0,-0.051223917,0.0054987208,-1.0191889442 C,0,0.0157451372,1.1863826155,-0.3284289837 N,0,0.1298362395,-0.0104444542,1.7594941584 C,0,0.1062154482,1.1483798241,1.046988065 N,0,-0.010355097,2.3417028668,-1.0463429465 N,0,-0.1196026611,-2.329754728,-1.0660191653 C,0,0.1769614383,2.4088742575,1.7677358115 C,0,0.0666422699,-2.4293845092,1.7471627676 O,0,0.1461095936,-2.5335917281,2.9606385692 O,0,0.2598000739,2.4990045366,2.9821169712 C,0,0.0530523545,3.5796484748,-0.4129925002 C,0,-0.1115590955,-3.574669859,-0.4433069869

O,0,0.0353944148,4.6029831692,-1.0273813274 O,0,-0.1758842285,-4.5908912458,-1.0662523746 N,0,0.1421529593,3.5479346022,0.9767560129 N,0,-0.0213459122,-3.5588318733,0.9467181251 C,0,0.2127674231,4.8513360147,1.6243001654 H,0,-0.6798816245,5.4326045282,1.3947799803 H,0,1.0927807492,5.3937725344,1.279759308 H,0,0.2785067515,4.6832938119,2.6948587872 C,0,-0.110939844,2.286518097,-2.4931084798 H,0,-1.0340616028,1.7920079886,-2.7933422459 H,0,0.738717896,1.7458301892,-2.9083694472 H,0,-0.1073802216,3.3114155961,-2.8481069225 C,0,-0.2157618719,-2.2578365484,-2.5122978642 H,0,-1.1143106176,-1.7174978556,-2.8080136222 H,0,-0.2609092451,-3.2787450419,-2.8758352627 H,0,0.658658898,-1.7547229219,-2.9233923647 C,0,-0.0108895706,-4.8695248881,1.5832129984 H,0,-0.9285718766,-5.4077597577,1.3475964421 H,0,0.0606525442,-4.7136956078,2.6552460707 H,0,0.8442174334,-5.4483736869,1.2351912013 H,0,0.1761566964,-0.0155658104,2.7249565465	O,0,0.0292832945,4.6222374442,-1.0432906238 O,0,-0.1808301498,-4.6097250455,-1.0825951722 N,0,0.1434286361,3.5580372502,0.9605293303 N,0,-0.0212928576,-3.5688563226,0.930379292 C,0,0.2086383261,4.8632467372,1.6078393276 H,0,-0.6880549273,5.4391461388,1.380167776 H,0,1.084118819,5.4105422315,1.2593483061 H,0,0.2788375999,4.6956464525,2.6777277445 C,0,-0.1093437886,2.3137469526,-2.502462869 H,0,-1.0394301617,1.8327410559,-2.8106133652 H,0,0.7513115738,1.797803085,-2.9317381919 H,0,-0.1126848117,3.3416414087,-2.8484579412 C,0,-0.217289911,-2.284975098,-2.5218073348 H,0,-1.1218262639,-1.7547782864,-2.8252328944 H,0,-0.2732468922,-3.3085196083,-2.876095342 H,0,0.6683050742,-1.8100220974,-2.9476707813 C,0,-0.0155940716,-4.8811152122,1.5665892867 H,0,-0.931111373,-5.418952877,1.3219227475 H,0,0.0473280883,-4.7256031416,2.6387663165 H,0,0.8422815131,-5.4597590724,1.2246509178 H,0,-0.1290558023,0.0115570526,-2.0253611839
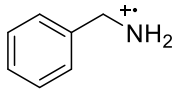	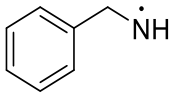
HF=-326.7192894 ZPE=0.143316 NImag=0 Htot=-326.567560 Gtot= -326.608526	HF=-326.2654655 ZPE=0.130612 NImag=0 Htot=-326.126750 Gtot= -326.167621

H,0,-0.4690100001,0.1899244561,-0.0294202539 C,0,-0.2628000473,0.1341283087,1.0337744145 C,0,0.283579542,-0.0196610176,3.758333239 C,0,0.0663581754,-1.0925212524,1.6096737965 C,0,-0.3181068795,1.2766263374,1.8177196367 C,0,-0.0424139547,1.2022399291,3.1797271053 C,0,0.3333085725,-1.1659065901,2.979176178 H,0,-0.5732833798,2.2283052137,1.3660388399 H,0,-0.089239492,2.0959437994,3.7915648771 H,0,0.559437304,-2.1230499889,3.4379123423 H,0,0.4866629513,-0.0819753023,4.8211817898 C,0,0.0973163228,-2.323241615,0.769966666 H,0,0.1062159306,-2.0794157997,-0.3133242984 H,0,-0.8232844253,-2.9245303607,0.863173277 N,0,1.1866858522,-3.174520229,1.01022325 H,0,1.1687566675,-4.1400505811,0.6870944652 H,0,2.0206525744,-2.8527057377,1.4994595411	H,0,-0.3301433976,0.1397530012,-0.0104160074 C,0,-0.1870589569,0.0943354558,1.064820089 C,0,0.1964283823,-0.0140850606,3.8093687621 C,0,0.0933174016,-1.1304573464,1.6676847333 C,0,-0.2766848848,1.2551562929,1.8243127305 C,0,-0.0852590831,1.2042892854,3.2003854175 C,0,0.2822620649,-1.1732868854,3.0478789188 H,0,-0.4917198151,2.2014205894,1.33970479 H,0,-0.1523987566,2.1088701238,3.7947500025 H,0,0.5047420817,-2.1215982946,3.5244733114 H,0,0.3472672507,-0.0621828207,4.8824934457 C,0,0.1497761758,-2.3865899112,0.8406980047 H,0,0.3503953306,-2.1342431679,-0.2130295645 H,0,-0.8517996422,-2.852801437,0.8140183751 N,0,1.1007559194,-3.3469726616,1.3047354994 H,0,1.0243039295,-4.1541111631,0.6780464919
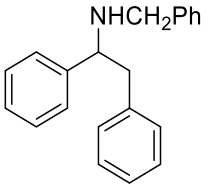	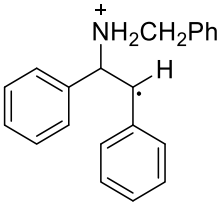
HF=-867.6951069 ZPE= 0.364601 NImag=0 Htot= -867.310821 Gtot= -867.381022	HF=-867.512873 ZPE= 0.366691 NImag=0 Htot= -867.126404 Gtot= -867.198057

C,0,-0.5770433693,-0.1751617971,1.1453594199	H,0,-1.8286111368,-2.7369509112,0.224444562
C,0,-1.0701018726,-0.5717704286,3.8754900697	C,0,-0.7773971089,-3.0003956437,0.2643107642
C,0,-1.8765499678,-0.3702602595,1.6141004186	C,0,1.9198422911,-3.6614139743,0.3475356491
C,0,0.4703473013,-0.1777930325,2.0657769755	C,0,0.1826835253,-1.9941734017,0.2428181773
C,0,0.2284693213,-0.3739290596,3.4202270325	C,0,-0.3914019608,-4.3337155816,0.332091491
C,0,-2.1235355669,-0.5668972982,2.9671599023	C,0,0.9569724226,-4.6658952246,0.3705578121
H,0,-2.7019069849,-0.3703760458,0.9090463853	C,0,1.5354657275,-2.3295167189,0.2927430355
H,0,1.4861018477,-0.0339621134,1.7129221319	H,0,-1.1454099391,-5.1125726777,0.3496186955
H,0,1.0563369506,-0.3748180617,4.121138359	H,0,1.2593068506,-5.705924147,0.4196489255
H,0,-3.140484478,-0.715776872,3.3141454831	H,0,2.2912446862,-1.5507716809,0.286902775
H,0,-1.2610081223,-0.7259389746,4.9318271245	H,0,2.9729061137,-3.9171631762,0.379261235
C,0,-0.3090367994,-0.0445062101,-0.3243535498	C,0,-0.2550962311,-0.547982672,0.1919394694
H,0,0.6677902109,0.4157174802,-0.4911432101	H,0,-1.3429233735,-0.509809985,0.1349388573
H,0,-1.0652021489,0.5948839787,-0.790518952	C,0,0.2584314831,0.2428220618,1.3434495594
C,0,-0.3314910801,-1.4063500979,-1.0401363744	H,0,1.2433255159,0.6882101059,1.2415026079
H,0,-1.325988217,-1.8520142425,-0.8790543687	C,0,-0.3940460208,0.3335098808,2.5869705503
C,0,0.6860174824,-2.3419241703,-0.4323317352	C,0,-1.6188643045,0.5636590464,5.1144685924
C,0,2.5747566207,-3.9836439381,0.8172275066	C,0,-1.646581122,-0.2761295242,2.8524314295
C,0,0.2825122174,-3.3533822558,0.4340253913	C,0,0.2214653589,1.0571959481,3.6415398097
C,0,2.0474817332,-2.1631984735,-0.6715025391	C,0,-0.3833347772,1.1689099551,4.8764051045
C,0,2.9860917171,-2.9786328287,-0.0535350616	C,0,-2.2401292727,-0.1569490446,4.0941407368
C,0,1.2190414953,-4.1699714235,1.0584966326	H,0,-2.1463305297,-0.846952317,2.0795778656
H,0,-0.7760472995,-3.4976515786,0.6244353792	H,0,1.1828898541,1.5256911099,3.4595490816
H,0,2.3663012569,-1.379985463,-1.3499866605	H,0,0.106042034,1.7282725406,5.6661485196
H,0,4.0427827227,-2.8293127334,-0.2483316291	H,0,-3.1978905056,-0.6321144582,4.2760875862
H,0,0.8887667947,-4.9525090362,1.7330922216	H,0,-2.0914541033,0.6512097989,6.0859352866
H,0,3.3078796791,-4.6195743669,1.3012950121	N,0,0.2249485708,0.0961687313,-1.0846344508
N,0,-0.0701106252,-1.1907516946,-2.4578615819	H,0,-0.0659508289,1.0777886865,-1.080211144
H,0,-0.663903983,-0.4345067918,-2.7846413794	C,0,-0.2729994434,-0.5541373079,-2.3401456236
C,0,-0.3308368924,-2.3764527206,-3.2702082453	H,0,-1.3582139674,-0.4700520562,-2.3225880138
H,0,0.3316928315,-3.17288272,-2.9192198188	H,0,0.0090028992,-1.6030806422,-2.2806632596

H,0,-1.3626643739,-2.7401118907,-3.1521189118 C,0,-0.0600257141,-2.0965960344,-4.7208048735 C,0,0.452871216,-1.5157051507,-7.4098953265 C,0,1.2482232241,-1.9088135973,-5.1698567395 C,0,-1.1052431318,-1.985721927,-5.634320218 C,0,-0.8528341099,-1.6988436253,-6.9725019714 C,0,1.504603545,-1.6218173773,-6.5035749071 H,0,2.068732956,-1.9921339973,-4.4646414098 H,0,-2.1259140909,-2.1273872204,-5.2931056869 H,0,-1.6774736397,-1.6177121604,-7.6724543182 H,0,2.5265046869,-1.483867139,-6.8402510906 H,0,0.6527909428,-1.2928969763,-8.4522504112	C,0,0.3282943385,0.1120060206,-3.5382410578 C,0,1.4908691849,1.3915436319,-5.7233843709 C,0,1.5768114911,-0.2941629039,-4.0075535142 C,0,-0.3343396822,1.1618306817,-4.1705842687 C,0,0.244668091,1.7988540547,-5.2608335391 C,0,2.1566583402,0.3441656802,-5.0956901 H,0,2.0916505962,-1.1148281034,-3.5185416127 H,0,-1.3077518631,1.4764817658,-3.8090731913 H,0,-0.2785044221,2.6119248458,-5.7513607956 H,0,3.1263159079,0.0212327585,-5.4574952718 H,0,1.9420765983,1.8878728634,-6.5752911207 H,0,1.2493382117,0.1061603843,-1.0946999445
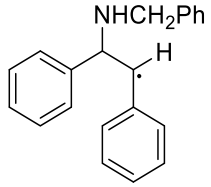	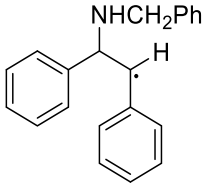
HF=-867.0418815 ZPE=0.350837 NImag=0 Htot=-866.671322 Gtot= -866.742295	HF=-867.0430621 ZPE= 0.350851 NImag=0 Htot= -866.672644 Gtot= -866.742472
H,0,-1.7895401914,-2.7335212389,0.6740172624 C,0,-0.7500210432,-3.0146070922,0.5421216828 C,0,1.9059361459,-3.7312320188,0.178790384 C,0,0.1859849866,-2.0363837322,0.2205404218 C,0,-0.3635995455,-4.3430817535,0.6855558259 C,0,0.9657598007,-4.7050749175,0.5050685739 C,0,1.519009215,-2.4054906513,0.041110708 H,0,-1.1039697855,-5.0963863175,0.932331679	C,0,-0.3226621437,0.358673417,2.5860047136 C,0,0.3017188919,0.1646957639,1.339258273 C,0,-0.2036033171,-0.7184838706,0.2479793399 N,0,0.2817764008,-0.2237669198,-1.0441934645 C,0,-0.6201700251,-0.5189274531,-2.1543574297 C,0,-0.7208089009,-1.9932105215,-2.4456458776 C,0,-1.9564756832,-2.6321431654,-2.4279752919 C,0,-2.0543737832,-4.0016435388,-2.6530758948

H,0,1.2687606897,-5.7406699928,0.6136008037	C,0,-0.9091578384,-4.7485208423,-2.8947301394
H,0,2.2477971392,-1.6468475971,-0.2203822651	C,0,0.331240325,-4.1158109981,-2.9234874927
H,0,2.9445554526,-4.0080018712,0.0323766185	C,0,0.4218620579,-2.7490457009,-2.7063854428
C,0,-0.2303914849,-0.5775758191,0.1142635027	C,0,0.2641060261,-2.1433285979,0.5106934124
H,0,-1.3297864382,-0.5573783783,0.0956653382	C,0,1.6243015263,-2.4486559965,0.4881359248
C,0,0.270642526,0.1527689006,1.3150136824	C,0,2.059750916,-3.7436491533,0.727675246
H,0,1.2823176593,0.54255322,1.2463818253	C,0,1.1388233781,-4.7519683933,1.0005350723
C,0,-0.4062291161,0.2794348982,2.5427778126	C,0,-0.2171612464,-4.4516147791,1.0353730132
C,0,-1.6804424752,0.5787905017,5.0462098365	C,0,-0.6493807479,-3.1512441279,0.7965725652
C,0,-1.7119661544,-0.2283250435,2.7705445611	C,0,-1.5658760996,-0.2315792155,2.9323487253
C,0,0.2318680569,0.9413527351,3.6259221552	C,0,-2.1357698212,-0.0094646674,4.1715384495
C,0,-0.3946312974,1.0865975492,4.8466073873	C,0,-1.501521595,0.8003566475,5.1142587377
C,0,-2.3276539892,-0.0770533453,3.9984689545	C,0,-0.2761096233,1.3908802666,4.7970238333
H,0,-2.234795632,-0.7419830451,1.9736315511	C,0,0.3043522969,1.1762254191,3.5637296296
H,0,1.2319160594,1.3352079109,3.4766715047	H,0,-1.7092584032,-2.9210751693,0.8073954654
H,0,0.1164956151,1.5972809159,5.6556975626	H,0,-0.9424491841,-5.2319607757,1.2390814553
H,0,-3.3260648896,-0.4744977562,4.1470989971	H,0,1.4778793309,-5.7661707764,1.1807402403
H,0,-2.1707515381,0.6924095384,6.0062415915	H,0,2.3403047093,-1.6684728928,0.2550915968
N,0,0.3298122912,0.0346273983,-1.0886937063	H,0,3.1199653417,-3.9714084596,0.6974426899
H,0,0.1859229362,1.0384684629,-1.0350718681	H,0,-1.3028542922,-0.729875908,0.2648405447
C,0,-0.2898076199,-0.4675682603,-2.3127670662	H,0,1.2738911528,0.6230694658,1.1794854567
H,0,-1.379361031,-0.314315295,-2.3174344986	H,0,-2.0763705648,-0.8650904454,2.2179588489
H,0,-0.1170580088,-1.5468257593,-2.3538710183	H,0,1.2575324305,1.6354639336,3.322937737
C,0,0.3169239935,0.1878602262,-3.520037233	H,0,0.2245203186,2.020917147,5.5244034097
C,0,1.4809893367,1.4484870205,-5.7304474866	H,0,-3.0866461032,-0.4727731438,4.4124112229
C,0,1.619604161,-0.1252784717,-3.9115130145	H,0,-1.9553723534,0.9688739598,6.0841212538
C,0,-0.3913816375,1.1414452044,-4.2468958881	H,0,0.3904856151,0.7824765628,-0.9846711054
C,0,0.184518515,1.7684929554,-5.3476237997	H,0,-0.2317598754,0.0041938272,-3.0334522895
C,0,2.1982505789,0.4982525386,-5.0084593234	H,0,-1.6348511482,-0.136331409,-1.9676276975
H,0,2.1794283559,-0.8660615153,-3.3499216135	H,0,-2.8498015756,-2.0537564639,-2.214606777
H,0,-1.4042021112,1.3929274926,-3.9483519784	H,0,1.3908245139,-2.2625369409,-2.7103916033

H,0,-0.3806324006,2.5076793863,-5.9050047573 H,0,3.2095130135,0.2415787137,-5.3051811221 H,0,1.9319834591,1.9348154257,-6.5884915546	H,0,1.2300523245,-4.6933563068,-3.1106899228 H,0,-3.0246901862,-4.4856615977,-2.6260588665 H,0,-0.9788050451,-5.8184576794,-3.057487662
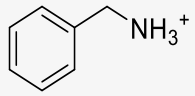	
HF=-327.4077265 ZPE= 0.160784 NImag=0 Htot= -327.238474 Gtot= -327.280673	
C,0,-0.0154801715,0.0000000269,1.0624391718 C,0,0.0238100127,0.0000000309,3.8488399733 C,0,-0.0069877082,-1.2038782706,1.7646232562 C,0,-0.0069877247,1.2038783265,1.7646232531 C,0,0.0129571416,1.2040247904,3.153330976 C,0,0.0129571581,-1.2040247306,3.1533309791 H,0,-0.0195470485,-2.1417314681,1.2189891509 H,0,-0.0195470779,2.1417315224,1.2189891452 H,0,0.0158327743,2.1442605091,3.6930841108 H,0,0.0158328038,-2.1442604479,3.6930841165 H,0,0.0364971543,0.0000000324,4.9330610786 C,0,-0.0006600705,0.0000000251,-0.4354775096 H,0,-0.4779615973,0.8879683769,-0.8448696993 H,0,-0.4779615851,-0.8879683344,-0.8448696969 N,0,1.4095806909,0.0000000341,-0.9479206597 H,0,1.9188083421,-0.8248210158,-0.6224642075 H,0,1.9188083308,0.8248210918,-0.6224642097 H,0,1.4338094057,0.0000000329,-1.9699820398	

5.3.2.8 Characterization of hydroamination products

5.3.2.8.1 Synthesis of *N*-benzyl-2-phenyl-1-(4-(trifluoromethyl)phenyl)ethan-1-amine and *N*-benzyl-1-phenyl-2-(4-(trifluoromethyl)phenyl)ethan-1-amine (2.19)

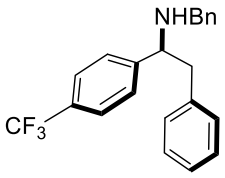

2.19a

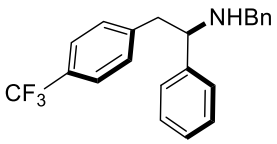

2.19b

Compounds **2.19a** and **2.19b** were prepared following general procedure 2.A, with a reaction time of 24 h. Purification by column chromatography (*n*-pentane:EtOAc = 20:1) yielded the title compound (76 mg, 0.214 mmol, 43%, **23a**:**23b** = 62:38) as colorless oil.

2.19a:

R_f = 0.2 (*n*-pentane:EtOAc = 10:1, $KMnO_4$).

^{1}H NMR (300 MHz, $CDCl_3$) δ 7.61 (d, *J* = 8.1 Hz, 2H), 7.50 (d, *J* = 8.1 Hz, 2H), 7.27 (dqt, *J* = 5.5, 3.8, 1.9 Hz, 6H), 7.18 – 7.02 (m, 4H), 3.97 (dd, *J* = 8.4, 5.7 Hz, 1H), 3.66 (d, *J* = 13.5 Hz, 1H), 3.47 (d, *J* = 13.6 Hz, 1H), 3.05 – 2.81 (m, 2H).

^{13}C NMR (75 MHz, $CDCl_3$) δ 148.1, 140.2, 138.2, 129.4, 129.3, 128.7, 128.5, 128.0, 127.9, 127.0, 126.8, 125.5, 125.5, 63.4, 51.5, 45.3.

^{19}F NMR (282 MHz, $CDCl_3$) δ -62.30.

MS (EI): *m*/*z* (relative intensity) 354 (1), 265 (12), 264 (75), 92 (15), 91 (100), 65 (36).

2.19b:

R_f = 0.1 (n-pentane:EtOAc = 10:1, $KMnO_4$).

^{1}H NMR (300 MHz, $CDCl_3$) δ 7.53 – 7.45 (m, 2H), 7.38 – 7.21 (m, 9H), 7.15 (dddd, *J* = 9.5, 7.6, 1.8, 1.1 Hz, 4H), 3.88 (t, *J* = 7.0 Hz, 1H), 3.67 (d, *J* = 13.4 Hz, 1H), 3.49 (d, *J* = 13.4 Hz, 1H), 2.99 (d, *J* = 7.0 Hz, 2H).

^{13}C NMR (75 MHz, $CDCl_3$) δ 143.1, 140.4, 129.8, 128.6, 128.5, 128.1, 127.5, 127.5, 127.0, 125.3, 125.3 (q, *J* = 3.8 Hz), 63.5, 51.5, 45.1.

^{19}F NMR (282 MHz, $CDCl_3$) δ -62.30.

MS (EI): *m*/*z* (relative intensity) 354 (1), 196 (50), 91 (100), 65 (10).

The analytical data is in accordance with those reported in the literature.[16b, 51]

5.3.2.8.2 Synthesis of ethyl -4-(1-(benzylamino)-2-phenylethyl)benzoate and ethyl 4-(2-(benzylamino)-2-phenylethyl)benzoate (2.20)

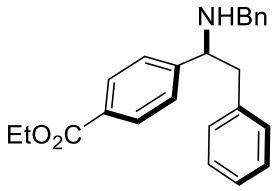

2.20a

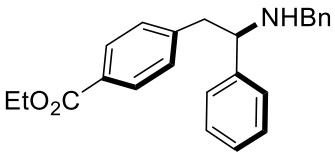

2.20b

Compounds **2.20a** and **2.20b** were prepared following general procedure A with a reaction time of 24 h. Purification by column chromatography (*n*-pentane:EtOAc = 9:1) yielded the title compounds ((86 mg, 0.239 mmol, 49%, **2.20a**:**2.20b** = 55:45) as a colorless oil.

2.20a:

R_f = 0.4 (*n*-pentane:EtOAc = 5:1, UV).

^{1}H NMR (300 MHz, $CDCl_3$) δ 8.11 – 8.01 (m, 2H), 7.51 – 7.41 (m, 2H), 7.33 – 7.20 (m, 6H), 7.17 – 7.05 (m, 4H), 4.42 (q, *J* = 7.1 Hz, 2H), 3.99 (dd, *J* = 7.9, 6.2 Hz, 1H), 3.68 (d, *J* = 13.5 Hz, 1H), 3.49 (d, *J* = 13.5 Hz, 1H), 3.04 – 2.89 (m, 2H), 1.91 (s, 1H), 1.44 (t, *J* = 7.1 Hz, 3H).

^{13}C NMR (75 MHz, $CDCl_3$) δ 168.3, 148.8, 141.3, 138.3, 129.9, 129.6, 129.4, 128.6, 128.5, 128.1, 127.6, 127.0, 126.7, 63.1, 58.4, 50.8, 43.2, 13.5.

MS (EI): *m*/*z* (relative intensity) 358 (1), 314 (1), 268 (42), 91 (100), 65 (9).

2.20b:

R_f = 0.3 (*n*-pentane:EtOAc = 5:1, $KMnO_4$).

^{1}H NMR (400 MHz, CD_2Cl_2) δ 7.93 – 7.86 (m, 2H), 7.38 – 7.10 (m, 12H), 4.34 (q, *J* = 7.1 Hz, 2H), 3.93 (dd, *J* = 7.4, 6.7 Hz, 1H), 3.64 (d, *J* = 13.4 Hz, 1H), 3.49 (d, *J* = 13.4 Hz, 1H), 3.07 – 2.94 (m, 2H), 1.68 (s, 1H), 1.37 (t, *J* = 7.1 Hz, 3H).

^{13}C NMR (101 MHz, CD_2Cl_2) δ 166.7, 144.8, 143.8, 141.0, 129.9, 129.7, 129.7, 129.1, 128.7, 128.6, 128.3, 127.8, 127.6, 127.1, 64.0, 51.7, 45.5, 14.5.

MS (EI): *m*/*z* (relative intensity) 358 (1), 314 (1), 197 (11), 196 (72), 91 (100), 65 (9).

The analytical data is in accordance with those reported in the literature.[16b, 51]

5.3.2.8.3 Synthesis of 4-(1-(benzylamino)-2-phenylethyl)benzonitrile and 4-(2-(benzylamino)-2-phenylethyl)benzonitrile (2.21)

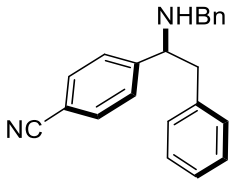

2.21a

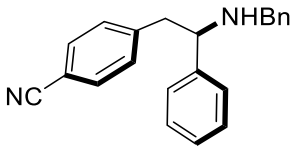

2.21b

Compounds **2.21a** and **2.21b** were prepared following general procedure a with a reaction time of 24 h. Purification by column chromatography (*n*-pentane:EtOAc = 10:1) yielded the title compounds (70 mg, 0.224 mmol, 45%, **2.21a**:**2.21b** = 60:40) as a colorless oil.

2.21a:

R_f = 0.3 (*n*-pentane:EtOAc = 9:1, UV).

^{1}H NMR (400 MHz, $CDCl_3$) δ 7.65 (d, *J* = 8.4 Hz, 2H), 7.50 (d, *J* = 8.3 Hz, 2H), 7.36 – 7.16 (m, 7H), 7.11 (ddt, *J* = 14.0, 5.5, 1.7 Hz, 4H), 3.98 (dd, *J* = 8.2, 6.0 Hz, 1H), 3.66 (d, *J* = 13.5 Hz, 1H), 3.49 (d, *J* = 13.5 Hz, 1H), 3.00 – 2.85 (m, 2H), 1.80 (s, 1H).

^{13}C NMR (101 MHz, $CDCl_3$) δ 149.6, 140.0, 137.8, 132.4, 129.3, 128.7, 128.5, 128.3, 127.9, 127.1, 126.9, 119.2, 111.0, 63.6, 51.6, 45.2.

MS (EI): *m*/*z* (relative intensity) 222 (16), 221 (82), 92 (15), 91 (100), 65 (24).

2.21b:

R_f = 0.1 (*n*-pentane:EtOAc = 9:1, $KMnO_4$).

^{1}H NMR (400 MHz, $CDCl_3$) δ 7.41 (d, *J* = 8.3 Hz, 1H), 7.30 – 7.09 (m, 11H), 7.09 – 6.99 (m, 4H), 3.78 (dd, *J* = 7.0 Hz, 1H), 3.73 (s, 1H), 3.58 (d, *J* = 13.4 Hz, 1H), 3.41 (d, *J* = 13.3 Hz, 1H), 3.00 – 2.83 (m, 2H).

^{13}C NMR (101 MHz, $CDCl_3$) δ 144.6, 142.7, 140.4, 140.3, 132.1, 130.3, 128.7, 128.5, 128.5, 128.3, 128.1, 127.6, 127.4, 127.1, 119.1, 110.3, 63.4, 53.3, 51.4, 45.2.

MS (EI): *m*/*z* (relative intensity) 221 (1), 197 (9), 196 (59), 116 (10), 91 (100), 89 (11), 65 (13).

The analytical data is in accordance with those reported in the literature.[16b, 51]

5.3.3 Analytical data of chapter 3

5.3.3.1 Characterization of heterocyclic aromatic *N*-oxides

5.3.3.1.1 Synthesis of 4-cyanopyridine 1-oxide (3.2b):

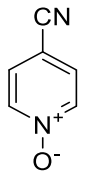

Following modified general procedure A, *m*-CPBA (70%, 2.47 g, 10.0 mmol, 1.0 eq.) was added portion-wise to a stirred solution of 4-cyanopyridine (1.33 g, 10.0 mmol, 1.0 eq.) in CH_2Cl_2 (20 mL) at 0 °C. After complete addition, the reaction mixture was stirred overnight for 16 h at 20°C. Subsequently, the reaction was quenched with sodium thiosulfate (3.16 g, 20.0 mmol, 2.0 eq.) and stirred for 10 min to eliminate any unreacted *m*-CPBA. Silica was added to the solution and the solvent was evaporated under reduced pressure. The mixture was purified by column chromatography (dry loading, CH_2Cl_2:EtOAc:NEt_3 = 4:1:1, isocratic) affording the crude colorless to yellowish/brown product. Recrystallization from a mixture of DCM/hexane yielded analytically pure product **3.2b** (0.94 g, 7.78 mmol, 78%.) as colorless crystals. Further product can be isolated from the mother liquor.

R_f = 0.22 (CH_2Cl_2:EtOAc:NEt_3 = 4:1:1, UV).

m.p. = 226 – 227 °C.

^{1}H NMR (300 MHz, Chloroform-*d*) δ = 8.28 – 8.17 (m, 2H), 7.57 – 7.47 (m, 2H).

^{13}C NMR (75 MHz, Chloroform-*d*) δ = 140.4, 129.0, 115.9, 107.7.

GCMS (EI): *m*/*z* (relative intensity) 120 (100) [M], 104 (20), 103 (14), 93 (20), 77 (23), 76 (31), 75 (13), 65 (62), 54 (86), 63 (41), 62 (22), 61 (12), 60 (10), 5 (22), 51 (31), 50 (43), 49 (12), 42 (14), 41 (27), 39 (39), 38 (69), 37 (54), 30 (41).

HRMS (EI-TOF, *m*/*z*): calcd. for $C_6H_4N_2O_1$ [M] 120.0318; found 120.0320.

IR (ATR, neat, cm^{-1}): 3098(w), 3080(w), 3035(w), 3008(w), 2227(w), 1608(w), 1477(m), 1444(w), 1275(m), 1208(w), 1170(m), 1125(w), 1030(m), 950(w), 849(s), 744(m), 708(s), 672(m), 666(m), 544(s), 461(s), 419(s).

UV-Vis (max. abs., [nm], MeCN): 297.

Luminescence (max. abs., [nm], MeCN): 412.

The analytical data is in accordance with those reported in the literature.[116]

5.3.3.1.2 Synthesis of 4-(trifluoromethyl)pyridine 1-oxide (3.2e):

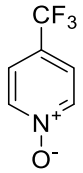

Following general procedure 4.B, using 4-(trifluoromethyl)pyridine afforded the title compound **3.2e** (1.20g, 7.36 mmol, 92%) as an analytically pure white solid after purification by column chromatography (dry loading, *n*-pentane EtOAc 5:1, isocratic).

R_f = 0.06 (*n*-pentane EtOAc 5:1, UV).

m.p. = 173 – 177 °C.

^{1}H NMR (300 MHz, Chloroform-*d*) δ = 8.32 – 8.21 (m, 2H), 7.55 – 7.44 (m, 2H).

^{13}C NMR (75 MHz, Chloroform-*d*) δ = 140.0, 127.9, 127.0, 124.3, 123.1 (q, *J* = 3.7 Hz), 120.7.

^{19}F NMR (282 MHz, Chloroform-*d*) δ = -63.7.

GCMS (EI): *m*/*z* (relative intensity) 163 (100) [M], 144 (28), 127 (10), 107 (11), 88 (16), 69 (11), 63 (14). 57 (14), 51 (11), 50 (10), 39 (15).

HRMS (EI-TOF, *m*/*z*): calcd. for $C_6H_4NOF_3$ [M] 163.0240; found 163.0239.

IR (ATR, neat, cm^{-1}): 3096(w), 3068(w), 3025(m), 1628(w), 1503(w), 1453(w), 1324(m), 1250(m), 1220(m), 1172(s), 1111(s), 1080(s), 1036(m), 978(w), 873(s), 846(m), 757(w), 616(s), 601(s), 518(w), 484(s).

UV-Vis (max. abs., [nm], MeCN): 283.

Luminescence (max. abs., [nm], MeCN): 391, 476.

The analytical data is in accordance with those reported in the literature.[110b]

5.3.3.1.3 Synthesis of 4-(methoxycarbonyl)pyridine 1-oxide (3.2c):

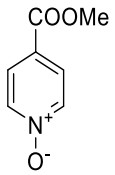

Following modified general procedure B, a mixture of 4-(methoxycarbonyl)pyridine (1.00 g, 8.0 mmol, 1.0 eq.) and $MeReO_3$ (10.0 mg, 40.0 µmol, 0.5 mol%) in CH_2Cl_2 (20 mL) was treated with 30% aqueous H_2O_2 (1.90 g, 16.8 mmol, 2.1 eq.) after which the solution turned light yellow/green. After complete addition, the reaction mixture was stirred overnight for 16.5 h at 20 °C. Silica was added to the solution and the solvent was evaporated under reduced

pressure. The mixture was then purified by column chromatography (dry loading, EtOAc, isocratic) affording product **3.2c** (1.13g, 7.38 mmol, 92%) as analytically pure white solid.

R_f = 0.23 (EtOAc, UV).

m.p. = 119 – 120 °C.

^{1}H NMR (300 MHz, Chloroform-*d*) δ = 8.26 – 8.16 (m, 2H), 7.92 – 7.82 (m, 2H), 3.94 (s, 3H).

^{13}C NMR (75 MHz, Chloroform-*d*) δ = 164.0, 139.6, 126.6, 126.5, 53.0.

GCMS (EI): *m*/*z* (relative intensity) 153 (72) [M^+], 137 (11), 122 (100), 106 (13), 94 (19), 78 (13), 63 (14). 51 (15), 50 (10), 39 (21).

HRMS (EI-TOF, *m*/*z*): calcd. for $C_7H_7NO_3$ [M] 153.0420; found 153.0419.

IR (ATR, neat, cm^{-1}): 3119(w), 3050(w), 2952(w), 2924(w), 1713(s), 1673(w), 1608(m), 1482(w), 1431(m), 1296(m), 1259(s), 1189(m), 1161(m), 1117(m), 1091(m), 1023(m), 975(w), 954(m), 912(w), 856(s), 826(w), 810(m), 767(s), 680(s), 655(w), 632(s), 516(m), 445(m).

UV-Vis (max. abs., [nm], MeCN): 301.

Luminescence (max. abs., [nm], MeCN): 413.

The analytical data is in accordance with those reported in the literature.[117]

5.3.3.1.4 Synthesis of 4-(ethoxycarbonyl)pyridine 1-oxide (3.2d):

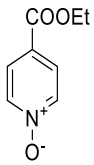

Following general procedure B, using 4-(ethoxycarbonyl)pyridine afforded the title compound **3.2d** (1.31g, 7.81 mmol, 98%) as an analytically pure white solid after purification by column chromatography (dry loading, EtOAc, isocratic).

R_f = 0.38 (EtOAc, UV).

m.p. = 63 – 66 °C.

^{1}H NMR (300 MHz, Chloroform-*d*) δ = 8.26 – 8.16 (m, 2H), 7.93 – 7.83 (m, 2H), 4.40 (q, *J* = 7.1 Hz, 2H), 1.40 (t, *J* = 7.1 Hz, 3H).

^{13}C NMR (75 MHz, Chloroform-*d*) δ = 163.5, 139.6, 127.0, 126.5, 62.1, 14.4.

GCMS (EI): *m*/*z* (relative intensity) 167 (41) [M], 139 (40), 123 (30), 122 (100), 106 (34), 95 (17), 94 (24). 78 (38), 64 (14), 63 (41), 62 (12), 53 (14), 52 (10), 51 (67), 50 (40), 45 (14). 40 (10), 39 (89), 38 (22), 29 (57).

HRMS (EI-TOF, *m*/*z*): calcd. for $C_8H_9NO_3$ [M] 167.0577; found 167.0575.

IR (ATR, neat, cm^{-1}): 3080(w), 3052(w), 2982(w), 1717(s), 1610(m), 1473(m), 1443(m), 1393(w), 1368(w), 1308(w), 1280(m), 1250(s), 1161(s), 1127(m), 1106(s), 1092(s), 1015(s), 911(w), 869(s), 861(s), 832(m), 823(m), 768(s), 683(s), 632(s), 513(m), 456(s).

UV-Vis (max. abs., [nm], MeCN): 301.

Luminescence (max. abs., [nm], MeCN): 406.

The analytical data is in accordance with those reported in the literature.[118]

5.3.3.1.5 Synthesis of 4-chloropyridine 1-oxide (3.2t):

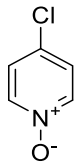

Following a modified literature procedure[78], a stirred mixture of 4-nitropyridine 1-oxide (**3.2s**, 2.10 g, 15.0 mmol, 1.0 eq.) in acetic acid (2.5 mL) was treated dropwise with acetyl chloride (16.5 g, 210.0 mmol, 14.0 eq.). After complete addition the reaction mixture was stirred for 1 h at 50 °C under reflux. The reaction was allowed to cool to room temperature and a saturated solution of aq. $NaHCO_3$ was added to liberate the acetylated *N*-oxide. The mixture was extracted with CH_2Cl_2 several times (10 x 60 mL), the organic phase dried over Na_2SO_4, filtered and solvents removed under reduced pressure to afford crude white to pale yellow product. Recrystallization from acetone, removal of leftover water by addition of toluene and removal of solvents using reduced pressure afforded product **9b** (0.50 g, 3.86 mmol, 26%) as analytically pure white solid. Further product can be isolated from the mother liquor.

R_f = 0.54 (CH_2Cl_2:MeOH = 10:1, UV).

m.p. = 150 – 154 °C (decomposition).

^{1}H NMR (300 MHz, Chloroform-*d*) δ = 8.18 – 8.07 (m, 2H), 7.31 – 7.20 (m, 2H).

^{13}C NMR (75 MHz, Chloroform-*d*) δ = 140.2, 132.0, 126.5.

GCMS (EI): *m*/*z* (relative intensity) 131 (22), 129 (66) [M], 113 (18), 102 (10), 78 (28), 76 (19), 75 (19), 74 (12). 73 (44), 67 (15), 66 (18), 64 (11), 63 (42), 62 (28), 61 (16), 51 (47), 50 (54), 49 (22), 39 (100), 38 (45), 37 (24), 30 (20).

HRMS (EI-TOF, *m*/*z*): calcd. for C_5H_4ONCl [M^+] 128.9976; found 128.9979.

IR (ATR, neat, cm^{-1}): 3080(w), 3024(w), 3000(w), 1473(w), 1445(m), 1242(m), 1188(m), 1114(w), 1039(w), 864(s), 828(m), 668(m), 516(s), 481(s).

UV-Vis (max. abs., [nm], MeCN): 282.

Luminescence (max. abs., [nm], MeCN): 375.

The analytical data is in accordance with those reported in the literature.[119]

5.3.3.1.6 Synthesis of 4-methoxypyridine 1-oxide (3.2u):

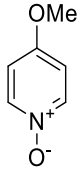

Following a modified literature procedure[79], a stirred mixture of 4-methoxypyridine (1.15 g, 10.5 mmol, 1.0 eq.) and aqueous hydrogen peroxide (3.0 ml, 29.4 mmol (*c* = 30 wt), 2.8 eq.) was refluxed in acetic acid (10.0 mL) for 24 h. The reaction was cooled to room temperature and concentrated in vacuo. The tile product **9b** (0.72 g, 5.75 mmol, 55%) was isolated as white solid after purification by column chromatography (dry loading, EtOAc, isocratic).

^{1}H NMR (400 MHz, Chloroform-*d*) δ 8.01 (s, 2H), 6.72 (s, 2H), 3.75 (s, 3H).

^{13}C NMR (101 MHz, Chloroform-*d*) δ 157. 9, 140.0, 111.7 (2 C-nuclei), 56.1.

IR (ATR, neat, cm-1): 1600 (w), 1573 (w), 1478 (s), 1455 (s), 1301 (w), 1254 (s), 1215 (m), 1201 (m), 1185 (m), 1157 (w), 1118 (m), 1096 (m), 1034 (w), 975 (w), 948 (w), 904 (w), 883 (w), 867 (w), 835 (w), 815 (w), 779 (w), 752 (s), 676 (m), 635 (w), 586 (m), 541 (w), 528 (w), 512 (m), 477 (w), 418 (w).

UV-Vis (max. abs., [nm], MeCN): 283.

Luminescence (max. abs., [nm], MeCN): 383.

5.3.3.1.7 Synthesis of pyridine 1-oxide (3.2a).

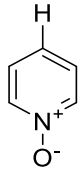

Following modified general procedure A, *m*-CPBA (70%, 3.95 g, 16.0 mmol, 1.0 eq.) was added portion-wise to a stirring solution of pyridine (1.27 g, 16.0 mmol, 1.0 eq.) in CH_2Cl_2 (20 mL) at 0 °C. After complete addition, the reaction mixture was stirred overnight for 16 h at 20°C. Subsequently, the reaction was quenched with sodium thiosulfate (5.06 g, 32.0 mol, 2.0 eq.) and stirred for 10 min to eliminate any unreacted *m*-CPBA. Silica was added to the solution and the solvent was evaporated under reduced pressure. The mixture was purified by column chromatography (dry loading, CH_2Cl_2:MeOH = 10:1, isocratic) affording the product **3.2a** (1.51 g, 15.8 mmol, 99%) as a colorless to brownish solid. Pyridine *N*-oxide is highly

hygroscopic and should be stored under inert atmosphere immediately after isolation. Recrystallization from MeOH, distillation or sublimation before use is highly recommended.

R_f = 0.24 (*n*-pentane:EtOAc:MeOH = 2:1:0.1, UV).

m.p. = 65 – 66 °C.

^{1}H NMR (400 MHz, Chloroform-*d*) δ = 8.28 – 8.18 (m, 2H), 7.31 – 7.27 (m, 3H).

^{13}C NMR (101 MHz, Chloroform-*d*) δ = 139.6, 126.3, 126.2.

GCMS (EI): *m*/*z* (relative intensity) 95 (100) [M^+], 79 (12), 78 (11), 68 (12), 52 (13), 51 (16). 50 (12), 40 (12), 39 (44), 38 (10).

HRMS (ESI-TOF, *m*/*z*): calcd. for C_5H_5NO [M+H] 96.0449; found 96.0453.

UV-Vis (max. abs., [nm], MeCN): 276.

Luminescence (max. abs., [nm], MeCN): 321.

The analytical data is in accordance with those reported in the literature.[116]

5.3.3.1.8 Synthesis of 4-(tert-butyl)pyridine 1-oxide (3.2f).

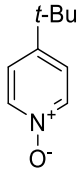

Following modified general procedure B, a mixture of 4-(*tert*-butyl)pyridine (1.08 g, 8.0 mmol, 1.0 eq.) and $MeReO_3$ (10.0 mg, 40.0 µmol, 0.5 mol%) in CH_2Cl_2 (10 mL) was treated with 30% aqueous H_2O_2 (1.81 g, 16.0 mmol, 2.0 eq.) after which the solution turned light yellow/green. After complete addition, the reaction mixture was stirred overnight for 16 h at 20 °C. Silica was added to the solution and the solvent was evaporated under reduced pressure. The mixture was then purified by column chromatography (dry loading, EtOAc:MeOH = 4:1, isocratic) affording the crude product. Toluene (5 ml) was added and evaporated under reduced pressure to remove any leftover H_2O and the mixture then dried on the Schlenk-line to crystallize product **3.2f** (1.15g, 7.62 mmol, 95%) as analytically pure white solid.

R_f = 0.35 (EtOAc:MeOH = 4:1, UV).

m.p. = 86 – 90 °C.

^{1}H NMR (300 MHz, Chloroform-*d*) δ = 8.20 – 8.10 (m, 2H), 7.31 – 7.22 (m, 2H), 1.33 (s, 9H).

^{13}C NMR (75 MHz, Chloroform-*d*) δ = 150.9, 138.7, 123.2, 34.7, 30.6.

GCMS (EI): *m*/*z* (relative intensity) 151 (10) [M^+], 136 (34), 135 (41), 121 (11), 120 (100), 118 (10), 108 (11). 92 (43), 65 (10), 51 (12), 39 (10).

HRMS (ESI-TOF, *m*/*z*): calcd. for $C_9H_{13}NO$ [M] 152.1075; found 152.1077.

IR (ATR, neat, cm^{-1}): 3045(w), 2954(m), 2909(w), 2867(w), 1489(s), 1474(m), 1449(w), 1437(m), 1395(w), 1363(w), 1278(w), 1243(s), 1180(s), 1120(w), 1106(m), 1040(w), 1029(w), 976(w), 937(w), 908(w), 860(m), 843(s), 826(s), 816(s), 732(w), 679(m), 661(m), 555(s), 511(m), 493(m), 438(s).

UV-Vis (max. abs., [nm], MeCN): 278.

Luminescence (max. abs., [nm], MeCN): 361.

The analytical data is in accordance with those reported in the literature.[110b]

5.3.3.1.9 Synthesis of [4,4'-bipyridine] 1-oxide (3.2g) and [4,4'-bipyridine] 1,1'-dioxide (3.2h):

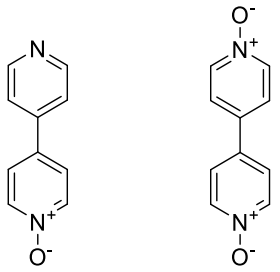

Following general procedure B, using 4,4'-bipyridine afforded the title compound **3.2g** (36.6 mg, 213 µmol, 34%) as analytically pure white to slightly brown solid and title compounds **3.2h** (62.0 mg, 329 µmol, 53%) as analytically pure light yellow solid after purification by column chromatography (dry loading, EtOAc:MeOH 1:1, isocratic).

Compound 3.2g:

R_f = 0.43 (EtOAc:MeOH 1:1, UV).

m.p. = 165 – 170 °C (decomposition).

^{1}H NMR (300 MHz, DMSO-d_6) δ = 8.74 – 8.63 (m, 2H), 8.38 – 8.25 (m, 2H), 7.97 – 7.86 (m, 2H), 7.90 – 7.75 (m, 2H).

^{13}C NMR (75 MHz, DMSO-d_6) δ = 150.6, 142.6, 139.3, 133.1, 124.1, 120.5.

GCMS (EI): *m*/*z* (relative intensity) 172 (79) [M], 157 (11), 156 (100), 155 (50), 129 (13), 128 (17), 116 (24). 103 (16), 102 (18), 101 (12), 90 (25), 89 (36), 86 (10), 78 (18), 77 (13), 76 (31). 75 (29), 74 (21), 64 (12), 63 (47), 62 (22), 52 (21), 51 (73), 50 (55), 39 (21), 38 (11).

HRMS (EI-TOF, *m*/*z*): calcd. for $C_{10}H_8N_2O$ [M] 172.0631; found 172.0630.

IR (ATR, neat, cm^{-1}): 3188(w), 3119(w), 3085(w), 3049(w), 3030(w), 1603(w), 1514(w), 1481(w), 1464(w), 1409(w), 1251(w), 1227(m), 1190(m), 1126(w), 1098(w), 1075(w), 1029(w),

1002(w), 865(w), 850(w), 820(m), 682(m), 645(m), 578(s), 549(m), 520(m), 488(s), 422(w), 403(w).

UV-Vis (max. abs., [nm], MeCN): 314.

Luminescence (max. abs., [nm], MeCN): 451.

The analytical data is in accordance with those reported in the literature.[120]

Compound 3.2h:

R_f = 0.14 (EtOAc:MeOH 1:1, UV).

m.p. = 299 – 301 °C (decomposition).

^{1}H NMR (300 MHz, DMSO-d_6) δ = 8.34 – 8.24 (m, 4H), 7.93 – 7.84 (m, 4H).

^{13}C NMR (75 MHz, DMSO-d_6) δ = 139.2, 131.7, 123.4.

MS (EI): *m*/*z* (relative intensity) 188 (53) [M], 173 (16), 172 (100), 171 (10), 157 (13), 156 (99), 155 (63), 129 (13), 128 (15), 117 (11), 116 (24), 103 (10), 102 (11), 90 (20). 89 (20), 78 (10), 77 (10), 76 (11), 63 (14), 57 (12), 51 (18), 50 (12). 44 (35), 43 (14), 41 (10).

HRMS (ESI-TOF, *m*/*z*): calcd. for $C_{10}H_8N_2O_2$ [M+H] 189.0664; found 189.0659.

IR (ATR, neat, cm^{-1}): 3184(w), 3104(w), 3071(w), 3027(w), 1474(w), 1463(w), 1427(w), 1235(m), 1177(m), 1124(w), 1098(w), 1020(m), 961(w), 835(s), 743(w), 701(m), 680(m), 619(m), 545(s), 507(s), 466(s).

UV-Vis (max. abs., [nm], MeCN): 345.

Luminescence (max. abs., [nm], MeCN): 427.

The analytical data is in accordance with those reported in the literature.[121]

5.3.3.1.10 Synthesis of [3,3'-bipyridine] 1-oxide (3.2i) and [3,3'-bipyridine] 1,1'-doxide (3.2j).

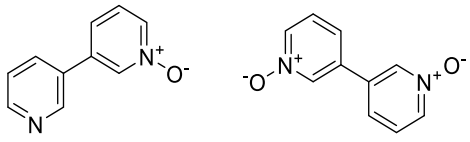

Following modified general procedure B, a mixture of 3,3'-bipyridine (171 mg, 1.10 mmol, 1.0 eq.) and $MeReO_3$ (1.37 mg, 5.49 µmol, 0.5 mol%) in CH_2Cl_2 (15 mL) was treated with 30% aqueous H_2O_2 (249 mg, 2.19 mmol, 2.0 eq.). After complete addition, the reaction mixture was stirred overnight for 16 h at 20 °C after which a white precipitate had formed. MeOH was added until the solid was fully dissolved, then silica was added to the solution and the solvent was evaporated under reduced pressure. The mixture was then purified by column chromatography (dry loading, EtOAc:MeOH 1:1, isocratic) affording a main fraction of title compound **3.2i** (96.0

mg, 558 µmol, 51%) as analytically pure white solid. The mixed fractions of compound **3.2i** and compound **3.2j** were again purified by column chromatography twice (dry loading, EtOAc:MeOH 2:1, isocratic; dry loading, EtOAc:MeOH 1:1 → acetone 100%) affording title compound **3.2j** (86.5 mg, 460 µmol, 42%) as analytically pure off-white solid.

Compound 3.2i:

R_f = 0.32 (EtOAc:MeOH 1:1, UV).

m.p. = 150 – 151 °C.

^{1}H NMR (400 MHz, DMSO-d_6) δ = 8.96 (dd, *J* = 2.5 Hz, 0.9 Hz, 1H), 8.69 (td, *J* = 1.8 Hz, 0.6 Hz, 1H), 8.65 (dd, *J* = 4.8 Hz, 1.6 Hz, 1H), 8.27 (ddd, *J* = 6.4, 1.8 Hz, 1.0 Hz, 1H), 8.17 (ddd, *J* = 8.0 Hz, 2.5 Hz, 1.6 Hz, 1H), 7.72 (ddd, *J* = 8.0 Hz, 1.7 Hz, 1.0 Hz, 1H), 7.57 – 7.49 (m, 2H).

^{13}C NMR 101 MHz, DMSO-d_6) δ = 150.0, 147.8, 138.0, 136.7, 136.3, 134.6, 130.6, 126.7, 124.0, 123.6.

GCMS (EI): *m*/*z* (relative intensity) 173 (12), 172 (100) [M], 156 (14), 155 (11), 145 (18), 117 (25), 116 (38). 90 (40), 89 (44), 78 (12), 76 (16), 75 (17), 74 (13), 64 (11), 63 (35). 62 (14), 51 (19), 50 (20), 39 (17).

HRMS (ESI-TOF, *m*/*z*): calcd. for $C_{10}H_8N_2O$ [M+H] 173.0715; found 173.0711.

IR (ATR, neat, cm^{-1}): 3077(w), 3023(w), 1601(w), 1573(w), 1557(w), 1471(w), 1433(m), 1398(m), 1315(m), 1215(s), 1188(m), 1163(m), 1128(w), 1105(w), 1091(w), 1071(w), 1025(w), 1011(s), 918(w), 899(s), 815(w), 788(s), 740(w), 726(w), 707(s), 680(s), 648(m), 624(w), 611(m), 553(s), 530(m), 481(m), 436(s), 401(s).

UV-Vis (max. abs., [nm], MeCN): 278.

Luminescence (max. abs., [nm], MeCN): 392.

The analytical data is in accordance with those reported in the literature.[122]

Compound 3.2j:

R_f = 0.11 (EtOAc:MeOH 1:1, UV).

m.p. = 305 – 306 °C (decomposition).

^{1}H NMR (400 MHz, DMSO-d_6) δ = 8.69 (t, *J* = 1.7 Hz, 2H), 8.29 (ddd, *J* = 6.5 Hz, 1.8 Hz, 0.9 Hz, 2H), 7.72 (ddd, *J* = 8.1 Hz, 1.7 Hz, 0.9 Hz, 2H), 7.53 (dd, *J* = 8.1 Hz, 6.4 Hz, 2H). **^{1}H NMR** (400 MHz, Chloroform-*d*) δ = 8.43 (td, *J* = 1.6 Hz, 0.7 Hz, 2H), 8.29 (dt, *J* = 6.0 Hz, 1.6 Hz, 2H), 7.44 – 7.37 (m, 4H).

^{13}C NMR (101 MHz, DMSO-d_6) δ = 138.8, 137.0, 134.3, 126.7, 123.7.

^{13}C NMR (101 MHz, Chloroform-*d*) δ = 139.6, 137.7, 135.0, 126.7, 124.0

MS (EI): *m*/*z* (relative intensity) 189 (12), 188 (100) [M], 173 (10), 172 (88), 171 (13), 156 (73), 155 (31). 145 (10), 128 (10), 117 (14), 116 (29), 90 (15), 89 (18), 78 (12), 77 (11). 76 (11), 63 (13), 57 (13), 51 (13), 50 (11), 44 (15), 43 (10), 39 (11).

HRMS (ESI-TOF, *m*/*z*): calcd. for $C_{10}H_8N_2O_2$ [M+H] 189.0664; found 189.0665.

IR (ATR, neat, cm^{-1}): 3069(w), 3044(w), 1596(w), 1555(w), 1469(w), 1442(w), 1415(w), 1392(m), 1321(w), 1233(m), 1189(m), 1176(m), 1156(w), 1091(w), 1070(w), 1017(w), 1005(m), 956(m), 926(w), 882(m), 846(s), 791(s), 723(m), 677(s), 640(m), 582(w), 556(s), 543(m), 512(m), 495(m), 479(m), 461(m), 428(s).

UV-Vis (max. abs., [nm], MeCN): 282, 327.

Luminescence (max. abs., [nm], MeCN): 404.

The analytical data is in accordance with those reported in the literature.[123]

5.3.3.1.11 Synthesis of [2,2'-bipyridine] 1-oxide (3.2k):

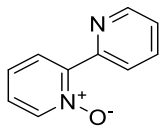

Following a modified general procedure A, to a stirred solution of *m*-CPBA (70%, 4.62 mmol, 1.2 eq.) in CH_2Cl_2 (20 mL) was added portion-wise a solution of 2,2'-bipyridine (625 mg, 4.0 mmol, 1.0 eq.) in CH_2Cl_2 (10 mL). Following completion of the addition, the reaction mixture was stirred 2 h at 20 °C and then filled to 50 mL with CH_2Cl_2. The mixture was then washed with saturated aq. Na_2SO_4 (2 x 15 mL) and 15% aq. NaOH (2 x 10 mL). The combined aq. phases were extracted with CH_2Cl_2 (3 x 10 mL) and the combined organic phases again washed with 20% aq. NaOH (10 mL) to remove the majority of formed dioxide before being filtered over dry Na_2SO_4. Silica was added to the solution and the solvent was evaporated under reduced pressure. The mixture was then purified by column chromatography (dry loading, EtOAc:MeOH:NEt_3 2:1:0.04, isocratic) affording the crude product as a brown oil. After drying on the Schlenk for several hours title compound **3.2k** (496 mg, 2.88 mmol, 72%) was obtained as an analytically pure brown solid.

R_f = 0.56 (EtOAc:MeOH:NEt_3 2:1:0.04, UV, $KMnO_4$).

m.p. = 53 – 56 °C.

^{1}H NMR (300 MHz, Chloroform-*d*) δ = 8.89 (dt, *J* = 8.1 Hz, 1.1 Hz, 1H), 8.72 (ddd, *J* = 4.8 Hz, 1.9 Hz, 1.0 Hz, 1H), 8.31 (ddd, *J* = 6.4 Hz, 1.3 Hz, 0.6 Hz, 1H), 8.17 (ddd, *J* = 8.0 Hz, 2.3 Hz, 0.6 Hz, 1H), 7.82 (ddd, *J* = 8.1 Hz, 7.6 Hz, 1.8 Hz, 1H), 7.42 – 7.30 (m, 2H), 7.30 – 7.20 (m, 1H).

^{13}C NMR (75 MHz, DMSO-d_6) δ = 149.5, 149.4, 146.1, 140.5, 136.3, 127.5, 126.2, 125.4, 124.9, 124.4.

GCMS (EI): *m*/*z* (relative intensity) 172 (49) [M], 171 (40), 156 (23), 155 (16), 129 (10), 128 (20), 118 (56). 117 (42), 116 (18), 105 (26), 104 (24), 91 (13), 90 (21), 89 (25), 79 (25). 78 (100), 77 (14), 76 (20), 75 (20), 74 (16), 68 (11), 66 (10), 64 (18), 63 (35), 62 (18), 52 (41), 51 (86), 50 (44), 40 (13), 39 (69), 38 (17).

HRMS (ESI-TOF, *m*/*z*): calcd. for $C_{10}H_8N_2O$ [M+H] 173.0715; found 173.0716.

IR (ATR, neat, cm^{-1}): 3068(w), 3043(w), 1579(w), 1566(w), 1461(w), 1442(m), 1416(m), 1315(w), 1250(m), 1233(m), 1154(w), 1118(w), 1097(w), 1060(w), 1031(m), 990(w), 953(w), 875(w), 848(m), 793(w), 760(s), 746(m), 737(s), 720(s), 667(w), 643(w), 618(m), 574(m), 544(m), 513(w), 458(m), 447(w), 403(m).

UV-Vis (max. abs., [nm], MeCN): 279, 329.

Luminescence (max. abs., [nm], MeCN): 431.

The analytical data is in accordance with those reported in the literature.[124]

5.3.3.1.12 Synthesis of [2,2'-bipyridine] 1,1'-dioxide (3.2l):

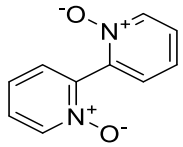

Following modified general procedure B, a mixture of 2,2'-bipyridine (1.25 g, 8.0 mmol, 1.0 eq.) and $MeReO_3$ (10.0 mg, 40.0 µmol, 0.5 mol%) in CH_2Cl_2 (20 mL) was treated with 30% aqueous H_2O_2 (1.81 g, 16.0 mmol, 2.0 eq.) after which the solution turned bright yellow. After complete addition, the reaction mixture was stirred overnight for 19 h at 20 °C after which a white precipitate suddenly crashed out. Silica was added to the solution and the solvent was evaporated under reduced pressure. The mixture was then purified by column chromatography (dry loading, EtOAc:MeOH:NEt_3 2:1:0.04, isocratic) affording product **3.2l** (382 mg, 2.03 mmol, 25%) as analytically pure white solid.

R_f = 0.24 (EtOAc:MeOH:NEt_3 2:1:0.04, UV, $KMnO_4$).

m.p. = 309 – 310 °C (decomposition).

^{1}H NMR (400 MHz, DMSO-d_6) δ = 8.34 (d, *J* = 6.4 Hz, 2H), 7.63 (dd, *J* = 7.7 Hz, 2.1 Hz, 2H), 7.52 (ddd, *J* = 7.7 Hz, 6.5 Hz, 2.2 Hz, 2H), 7.41 (td, *J* = 7.7 Hz, 1.2 Hz, 2H).

^{13}C NMR (^{13}C NMR (101 MHz, DMSO-d_6) δ = 139.2, 132.2, 128.4, 127.0, 124.5.

GCMS (EI): *m*/*z* (relative intensity) 188 (37) [M], 172 (27), 171 (58), 156 (21), 155 (16), 144 (24), 143 (31), 142 (13), 129 (10), 128 (16), 118 (21), 117 (24), 116 (30). 105 (21),

104 (20), 91 (14), 90 (14), 89 (16), 79 (39), 78 (100), 77 (17). 76 (16), 75 (11), 74 (14), 64 (17), 63 (29), 62 (15), 52 (38), 51 (80), 50 (31), 40 (11), 39 (76), 38 (14), 30 (14).

HRMS (ESI-TOF, *m*/*z*): calcd. for $C_{10}H_8N_2O_2$ [M+H] 189.0664; found 189.0664.

IR (ATR, neat, cm^{-1}): 3037(w), 3005(w), 2975(w), 1472(w), 1425(m), 1297(w), 1247(s), 1145(m), 1116(w), 1096(w), 1061(w), 1032(w), 1019(m), 982(w), 958(m), 892(w), 849(m), 836(m), 762(s), 722(m), 667(w), 631(w), 579(s), 540(m), 525(s), 515(s), 464(s).

UV-Vis (max. abs., [nm], MeCN): 278.

Luminescence (max. abs., [nm], MeCN): 389.

The analytical data is in accordance with those reported in the literature.[125]

5.3.3.1.13 Synthesis of 1,4-diazine 1-oxide (3.2m):

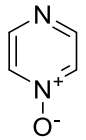

Following general procedure B, using pyrazine afforded the title compound **3.2m** (1.00 g, 10.5 mmol, 70%) as an analytically pure white solid after purification by column chromatography (dry loading, EtOAc, isocratic) and recrystallization from acetone. Further product can be isolated from mother liquor.

R_f = 0.18 (EtOAc = 10:1, UV).

m.p. = 110 – 112 °C (decomposition).

^{1}H NMR (400 MHz, Chloroform-*d*) δ = 8.46 (d, *J* = 4.9 Hz, 2H), 8.10 (d, *J* = 4.9 Hz, 2H).

^{13}C NMR (101 MHz, Chloroform-*d*) δ = 148.0, 134.3.

GCMS (EI): *m*/*z* (relative intensity) 96 (100) [M], 80 (11), 53 (31), 52 (35), 51 (18), 41 (59), 40 (52). 39 (42), 38 (17), 30 (34).

HRMS (EI-TOF, *m*/*z*): calcd. for $C_4H_4N_2O$ [M] 96.0318; found 96.0319.

IR (ATR, neat, cm^{-1}): 3120(w), 3078(m), 3025(w), 3005(w), 2890(w), 1649(w), 1591(s), 1546(w), 1467(s), 1429(s), 1307(s), 1210(s), 1168(m), 1074(m), 1001(s), 846(s), 835(s), 714(m), 679(w), 538(s), 473(s).

UV-Vis (max. abs., [nm], MeCN): 273.

Luminescence (max. abs., [nm], MeCN): 412.

The analytical data is in accordance with those reported in the literature.[126]

5.3.3.1.14 Synthesis of 1,3-diazine 1-oxide (3.2n):

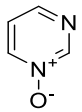

Following general procedure B, using pyrimidine afforded the title compound **3.2n** (1.30 g, 13.53 mmol, 90%) as an analytically pure white solid after purification by column chromatography (dry loading, EtOAc:MeOH 10:1 → MeOH 100%) and recrystallization from MeOH.

R_f = 0.17 (EtOAc = 10:1, UV).

m.p. = 90 – 92 °C.

^{1}H NMR (400 MHz, Chloroform-*d*) δ = 9.00 – 8.95 (m, 1H), 8.37 (dt, *J* = 6.6 Hz, 1.8 Hz, 1H), 8.23 (dd, *J* = 4.7 Hz, 1.5 Hz, 1H), 7.34 – 7.27 (m, 1H).

^{13}C NMR (101 MHz, Chloroform-*d*) δ = 150.1, 144.4, 143.7, 121.3.

GCMS (EI): *m*/*z* (relative intensity) 96 (63) [M], 80 (100), 69 (11), 66 (24), 53 (41), 52 (25), 51 (17). 40 (10), 39 (45), 38 (17).

HRMS (EI-TOF, *m*/*z*): calcd. for $C_4H_4N_2O$ [M] 96.0318; found 96.0318.

IR (ATR, neat, cm^{-1}): 3032(w), 2985(w), 2949(w), 1535(m), 1467(m), 1412(s), 1252(s), 1222(s), 1209(m), 1121(m), 1095(m), 1050(m), 1028(s), 982(w), 957(w), 918(w), 843(m), 817(s), 690(s), 635(m), 562(s), 520(m), 461(s), 411(s).

UV-Vis (max. abs., [nm], MeCN): 277, 323.

Luminescence (max. abs., [nm], MeCN): ,375.

The analytical data is in accordance with those reported in the literature.[127]

5.3.3.1.15 Synthesis of 1,2-diazine 1-oxide (3.2o):

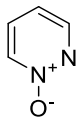

Following general procedure B, using pyridazine afforded the title compound **3.2o** (1.32 g, 13.7 mmol, 92%) as an analytically pure brown oil after purification by column chromatography twice (dry loading, EtOAc → MeOH 100%; dry loading, EtOAc 100%, isocratic).

R_f = 0.08 (EtOAc 100%, UV).

^{1}H NMR (300 MHz, DMSO-d_6) δ = 8.62 – 8.53 (m, 1H), 8.32 (dt, *J* = 6.4 Hz, 1.0 Hz, 1H), 7.88 (ddd, *J* = 7.8 Hz, 6.4 Hz, 2.5 Hz, 1H), 7.25 (ddd, *J* = 7.8 Hz, 5.4 Hz, 0.9 Hz, 1H).

^{13}C NMR (75 MHz, DMSO-d_6) δ = 151.0, 135.3, 134.4, 116.6.

GCMS (EI): *m*/*z* (relative intensity) 96 (53) [M], 66 (18), 52 (10), 51 (21), 50 (14), 40 (19), 39 (100). 38 (26), 37 (15), 30 (16).

HRMS (EI-TOF, *m*/*z*): calcd. for $C_4H_4N_2O$ [M] 96.0318; found 96.0317.

IR (ATR, neat, cm^{-1}): 3437(w), 3106(w), 3065(w), 3013(w), 1709(w), 1642(w), 1581(m), 1544(m), 1495(w), 1455(w), 1400(s), 1309(s), 1143(m), 1084(w), 1043(w), 978(s), 909(w), 845(s), 779(s), 713(m), 650(m), 576(s), 524(m), 500(s), 409(s).

UV-Vis (max. abs., [nm], MeCN): 322.

Luminescence (max. abs., [nm], MeCN): 419.

5.3.3.1.16 Synthesis of phthalazine 2-oxide (3.2p):

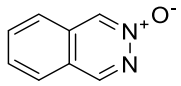

Following modified general procedure B, a mixture of phthalazine (1.01 g, 7.74 mmol, 1.0 eq.) and $MeReO_3$ (12.2 mg, 50.0 µmol, 0.6 mol%) in CH_2Cl_2 (25 mL) was treated with 30% aqueous H_2O_2 (1.83 g, 16.1 mmol, 2.1 eq.) after which the solution turned bright yellow. After complete addition, the reaction mixture was stirred overnight for 16 h at 20 °C after which a white precipitate had formed. Silica was added to the solution and the solvent was evaporated under reduced pressure. The mixture was then purified by column chromatography (dry loading, EtOAc:MeOH: 10:1, isocratic) affording crude product. Toluene (3 x 10 ml) and pentane (3 x 15 mL) were added and removed under reduced pressure to remove leftover H_2O and H_2O_2 and the mixture was dried on Schlenk for 5 h (< 0.1 mbar) and then for 2 h at 80 °C. The crude pre-dried mixture was then purified by column chromatography twice (dry loading, EtOAc:MeOH 5:1, isocratic; dry loading, EtOAc:MeOH 2:1 → MeOH 100%) to afford title compound **3.2p** (1.08 g, 7.39 mmol, 96%) as analytically pure white to pale yellow solid.

R_f = 0.21 (EtOAc:MeOH 10:1, UV), 0.3 (EtOAc:MeOH 5:1, UV), 0.6 (EtOAc:MeOH 2:1, UV).

m.p. = 135 – 140 °C.

^{1}H NMR (300 MHz, DMSO-d_6) δ = 9.37 (s, 1H), 8.91 – 8.85 (m, 1H), 8.11 (dq, *J* = 8.2 Hz, 1.0 Hz, 1H), 7.96 – 7.82 (m, 2H), 7.73 (ddd, *J* = 8.2 Hz, 6.0 Hz, 2.1 Hz, 1H).

^{1}H NMR (400 MHz, Chloroform-*d*) δ = 9.07 (s, 1H), 8.57 (t, *J* = 1.0 Hz, 1H), 7.92 (dq, *J* = 8.2 Hz, 1.0 Hz, 1H), 7.82 (ddd, *J* = 8.2 Hz, 7.0 Hz, 1.2 Hz, 1H), 7.73 – 7.63 (m, 2H).

^{13}C NMR (75 MHz, DMSO-d_6) δ = 153.4, 134.0, 132.6, 129.3, 127.4, 126.9, 123.5, 120.3.

^{13}C NMR (101 MHz, Chloroform-*d*) δ = 152.8, 134.2, 133.0, 132.6, 129.8, 127.6, 127.3, 123.5, 121.1.

GCMS (EI): *m*/*z* (relative intensity) 146 (37) [M], 116 (23), 90 (32), 89 (100), 76 (21), 75 (14), 74 (13), 64 (16), 63 (58), 62 (29), 61 (10), 51 (14), 50 (31). 39 (27), 38 (13), 30 (14).

HRMS (ESI-TOF, *m*/*z*): calcd. for $C_8H_6N_2O$ [M+H] 147.0558; found 147.0562.

IR (ATR, neat, cm^{-1}): 3366(w), 3052(w), 2987(w), 1618(w), 1565(m), 1438(m), 1333(s), 1273(m), 1243(w), 1179(s), 1118(m), 1052(w), 1014(m), 975(w), 932(m), 883(m), 785(w), 751(s), 669(m), 630(s), 562(m), 527(m), 499(m), 461(s), 446(s), 412(s).

UV-Vis (max. abs., [nm], MeCN): 298, 310, 371.

Luminescence (max. abs., [nm], MeCN): 430.

The analytical data is in accordance with those reported in the literature.[128]

5.3.3.1.17 Synthesis of phenazine 5-oxide (3.2q) and synthesis of phenazine 5,10-dioxide (3.2r):

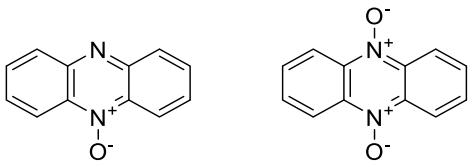

Following modified general procedure B + modified literature procedure for phenazine 5,10-dioxide[129], a mixture of phenazine (100 mg, 555 µmol, 1.0 eq.) and $MeReO_3$ (1.45 mg, 5.82 µmol, 1.0 mol%) in CH_2Cl_2 (20 mL) was treated with 30% aqueous H_2O_2 (126 mg, 1.11 mmol, 2.0 eq.) after which the solution turned yellow. After complete addition, the reaction mixture was stirred overnight for 16 h at 20 °C after which an orange/red crystalline solid had precipitated. Excess CH_2Cl_2 was added to solve the solid, then silica was added to the solution and the solvent was evaporated under reduced pressure. The mixture was then purified by column chromatography (dry loading, *n*-pentane:EtOAc 2:1, isocratic) affording a main fraction of pure compound **3.2q**. The mixed fractions of compound **3.2q** and compound **3.2r** were again purified by column chromatography (dry loading, *n*-pentane:EtOAc 1:1, isocratic). The combined respective fractions afforded title compound **3.2q** (70.0 mg, 357 µmol, 64%) as analytically pure bright yellow solid and title compound **3.2r** (32.2 mg, 175 µmol, 32%) as analytically pure bright red solid. This reaction was also performed on 0.85 g (4.72 mmol) scale using 0.3 mol% $MeReO_3$ yielding comparable results (**3.2q:** 524 mg, 2.67 mmol 57%, **3.2r**: 243 mg, 1.15 mmol, 24%). Furthermore, unreacted starting material was easily re-isolated (120 mg, 0.67 mmol, 14%). Isolation of the main fraction of pure title compound **3.2r** can more easily be achieved by column chromatography (dry loading) using toluene:EtOAc 7:3 → EtOAc 100% as eluent.[129]

Compound 3.2q:

R_f = 0.33 (*n*-pentane:EtOAc 2:1, UV), 0.5 (toluene:EtOAc 7:3, UV).

m.p. = 214 – 217 °C (decomposition).

^{1}H NMR (300 MHz, Chloroform-*d*) δ = 8.66 (ddd, *J* = 8.8 Hz, 1.6 Hz, 0.7 Hz, 2H), 8.17 (ddd, *J* = 8.7 Hz, 1.4 Hz, 0.7 Hz, 2H), 7.76 (dddd, *J* = 23.9 Hz, 8.8 Hz, 6.7 Hz, 1.4 Hz, 4H).

^{13}C NMR (75 MHz, Chloroform-*d*) δ = 145.6, 134.9, 131.3, 130.5, 130.2, 119.2.

GCMS (EI): *m*/*z* (relative intensity) 197 (14), 196 (100) [M], 195 (15), 180 (22), 179 (24), 170 (31), 168 (10). 152 (12), 140 (12), 102 (20), 77 (18), 76 (27), 75 (24), 74 (14), 64 (16), 63 (26). 52 (11), 51 (23), 50 (36), 39 (18).

HRMS (EI-TOF, *m*/*z*): calcd. for $C_{12}H_8N_2O$ [M] 196.0631; found 196.0627.

IR (ATR, neat, cm^{-1}): 3114(w), 3076(w), 3027(w), 1602(w), 1588(w), 1505(w), 1462(w), 1344(m), 1297(w), 1282(m), 1269(m), 1256(m), 1197(w), 1171(w), 1151(w), 1116(m), 1097(m), 1018(w), 1003(w), 960(w), 935(w), 866(m), 854(m), 748(s), 680(m), 644(m), 632(s), 609(s), 569(w), 544(w), 518(w), 466(m), 443(w), 420(w), 403(w).

UV-Vis (max. abs., [nm], MeCN): 361, 380, 395, 418.

Luminescence (max. abs., [nm], MeCN): 459.

The analytical data is in accordance with those reported in the literature[130].

Compound 3.2r:

R_f = 0.09 (*n*-pentane:EtOAc, 2:1, UV), 0.22 (toluene:EtOAc 7:3, UV).

m.p. = 183 – 189 °C (decomposition).

^{1}H NMR (300 MHz, Chloroform-*d*) δ = 8.79 – 8.67 (m, 4H), 7.89 – 7.75 (m, 4H).

^{13}C NMR (75 MHz, Chloroform-*d*) δ = 136.2, 131.4, 120.4.

MS (EI): *m*/*z* (relative intensity) 212 (17) [M], 197 (12), 196 (91), 195 (12), 181 (11), 180 (100), 179 (37), 170 (20), 152 (11), 144 (14), 90 (10), 76 (11), 59 (10).

HRMS (ESI-TOF, *m*/*z*): calcd. for $C_{12}H_8N_2O_2$ [M+H] 213.0664; found 213.0666.

IR (ATR, neat, cm^{-1}): 3110(w), 3077(w), 3028(w), 2920(w), 2850(w), 1604(w), 1589(w), 1461(w), 1429(w), 1341(s), 1283(w), 1266(m), 1208(w), 1171(w), 1124(w), 1086(s), 1020(m), 1009(m), 961(m), 918(w), 856(m), 804(w), 763(s), 749(s), 707(w), 681(w), 646(w), 616(s), 605(s), 519(m), 465(m).

UV-Vis (max. abs., [nm], MeCN): 458, 487.

Luminescence (max. abs., [nm], MeCN): 510.

The analytical data is in accordance with those reported in the literature.[131]

5.3.3.2 Characterization of oxygen atom transfer products

5.3.3.2.1 Synthesis of 9H-xanthen-9-ol (3.4):

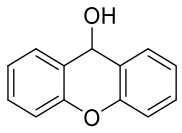

The following procedure was carried out under argon. Xanthen (91.1 mg, 0.5 mmol, 1.0 eq.) and 4-nitropyridine-*N*-oxide (140.1 mg, 1.0 mmol, 2.0 eq.) were transferred into a pre-heated 8 mL tube and dissolved in acetonitrile (5.0 mL, 50 mM). The flask was sealed with a septum and irradiated for 16 h (398 nm). Afterwards, the reaction and quenched with water. The mixture was extracted 3 times with CH_2Cl_2 and dried over anhydrous Na_2SO_4. The crude product was then purified by column chromatography to furnish the tile product **3.4** (36 mg, 0.18 mmol, 36%).

R_f = 0.65 (*n*-pentan:EtOAc = 10:1, UV).

^{1}H NMR (400 MHz, Chloroform-*d*) δ 7.22 (t, *J* = 7.7 Hz, 2H), 6.94 (t, *J* = 7.4 Hz, 2H), 6.89 (d, *J* = 8.1 Hz, 2H), 6.67 (d, *J* = 7.5 Hz, 2H), 4.21 (s, 1H).

^{13}C NMR (101 MHz, Chloroform-*d*) δ 153.2, 129.3, 128.2, 122.8, 122.0, 116.0, 49.7.

IR (ATR, neat, cm-1): 3351 (w), 3105 (w), 3079 (w), 3023 (w), 1618 (w), 1559 (w), 1490 (s), 1438 (m), 1293 (m), 1209 (s), 1180 (m), 1109 (w), 1016 (s), 855 (s), 834 (m), 809 (w), 752 (s), 658 (w), 542 (m), 525 (s), 458 (s), 421 (m), 405 (m).

The analytical data is in accordance with those reported in the literature.[132]

5.3.3.2.2 Synthesis of 1-((methylsulfonyl)oxy)pyridin-1-ium methanesulfonate (3.14):

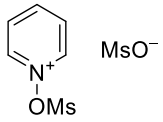

Following a modified literature procedure[71], a stirred mixture of pyridine 1-oxide (3.00 g, 31.55 mmol, 1.0 eq.) in DCM (100 mL) was treated dropwise with solution containing methanesulfonic anhydride (7.13 g, 37.9 mmol, 1.3 eq.) at −30 °C. After complete addition the reaction mixture was stirred for 2 h and allowed to warm to room temperature. The white precipitate was filtered and washed with fresh DCM. Additional drying in vacuo yields the tile product (6.40 g, 23.8 mmol, 75%).

^{1}H NMR (400 MHz, Acetonitrile-d_3) δ 8.72 (s, 2H), 8.09 (s, 1H), 7.85 (s, 2H), 3.46 (s, 2H), 2.61 (s, 3H).

^{13}C NMR (101 MHz, Acetonitrile-d_3) δ 140.62, 129.10, 41.78, 39.65.

IR (ATR, neat, cm-1): 3108 (w), 3013 (w), 2986 (w), 2943 (w), 1606 (w), 1479 (w), 1428 (w), 1381 (m), 1330 (w), 1315 (w), 1289 (w), 1182 (s), 1163 (s), 1144 (m), 1040 (s), 1002 (m), 984 (s), 818 (m), 789 (s), 762 (s), 672 (m), 655 (s), 602 (w), 554 (s), 520 (s), 507 (s), 489 (m), 456 (m), 421 (m).

5.3.3.3 Electrochemical Properties

Cyclic Voltammetry and Differential Pulse Voltammetry

All electrochemical investigations were performed at room temperature in dried acetonitrile p.A. (VWR) under an Argon atmosphere with 0.1 M tetrabutylammonium hexafluorophosphate (Fluka) as conducting salt using an Autolab (PGSTAT 204, Metrohm). A glassy carbon disk electrode (d = 2 mm) was used as working electrode, a glassy carbon electrode as the counter electrode and an Ag/AgCl/LiCl sat. in EtOH-system as the reference electrode (all electrodes: Metrohm). All potentials mentioned in this paper were measured with respect to this reference system and were checked by using the ferrocenium/ferrocene-internal reference system (potential of Fc^+/Fc: 0.54 V [vs. Ag/AgCl/LiCl sat. in EtOH]. The potentials reported relative to the Fc^+/Fc redox couple was converted to SCE by adding 0.38 V.[21] The CV scans were done three times at a scan rate of 40 mV s^{-1}. The measurements were performed with 5 μM compound dissolved in the electrolyte.

Differential pulse voltammetry was measured using a step potential of 5 mV, modulation amplitude of 25 mV, modulation time 0.05 s, interval time 0.05 s.

Redox potentials from DPV-peak:

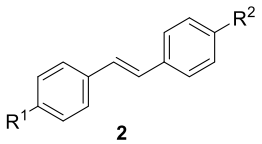

2

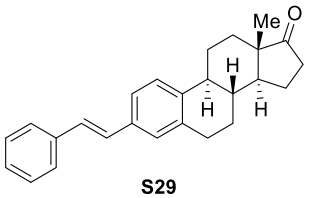

S29

entry	R^1	R^2	note	$E^{red}_{1/2}$ (V vs SCE)	$E^{ox}_{1/2}$ (V vs SCE)
1	NMe_2	H		-2.43	0.52
2	OMe	H		-2.38	1.14
3	OMe	CF_3		-2.10	1.22
4			benzylamine (**1a**)	--	1.29
5			**S29**	-2.34	1.32
6	Me	H		-2.33	1.33
7	Me	F		-2.35	1.34
8	F	H		-2.29	1.44
9	OAc	H		-2.24	1.44
10	Br	Br		-1.96	1.49
11	H	H	*trans*-stilbene	-2.28	1.53
12	H	H	*cis*-stilbene	-2.30	1.56
13			phenanthrene	-2.54	1.58
14	CN	H		-1.83	1.63
15	CO_2Et	H		-1.86	1.65
16	CF_3	H		-2.57	1.69

5.3.3.3.1 Redox potentials of heteroarene *N*-oxide

5.3.3.3.1.1 4-nitropyridine 1-oxide:

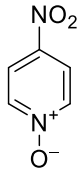

Cyclovoltammogram

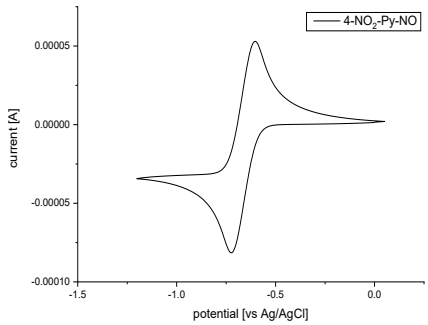

Differential pulse voltammetry

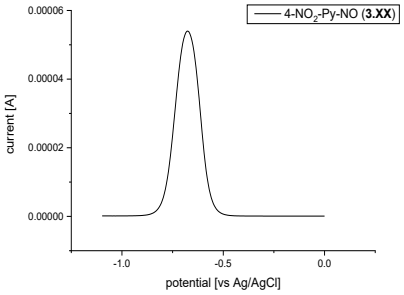

$E_{1/2}^{ox}(Fc^+/Fc) = +0.52\,V\ vs\ Ag/AgCl$

5.3.3.3.1.2 4-cyanopyridine 1-oxide:

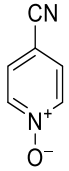

Cyclovoltammogram

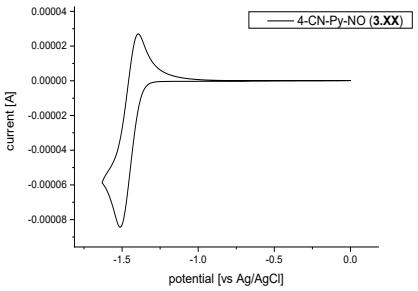

Differential pulse voltammetry

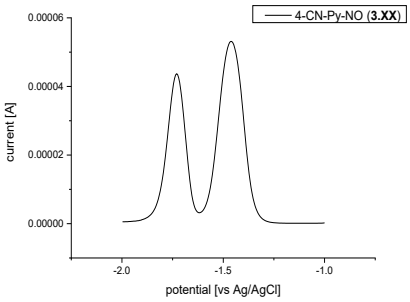

$E_{1/2}^{ox}(Fc^+/Fc) = +0.53\,V\ vs\ Ag/AgCl$

5.3.3.3.1.3 4-(trifluoromethyl)pyridine 1-oxide:

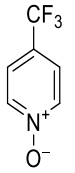

Cyclovoltammogram

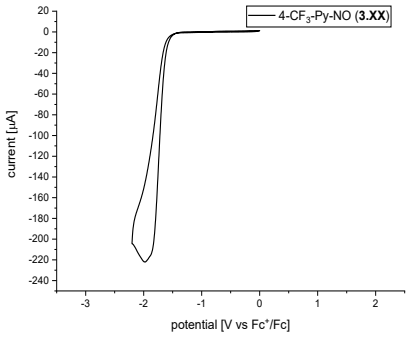

Differential pulse voltammetry

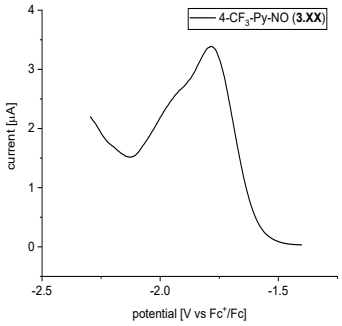

5.3.3.3.1.4 4-(methoxycarbonyl)pyridine 1-oxide:

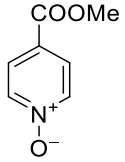

Cyclovoltammogram

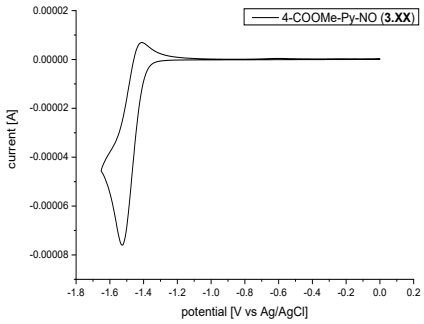

Differential pulse voltammetry

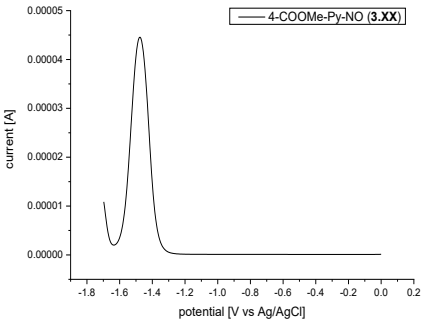

$E_{1/2}^{ox}(Fc^{+}/Fc) = +0.55\ V\ vs\ Ag/AgCl$

5.3.3.3.1.5 4-(ethoxycarbonyl)pyridine 1-oxide:

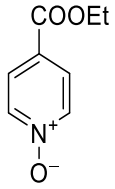

Cyclovoltammogram

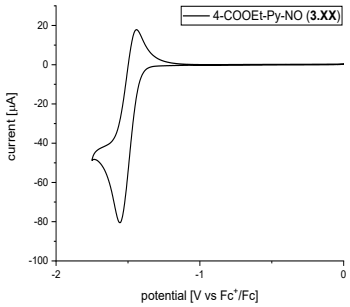

Differential pulse voltammetry

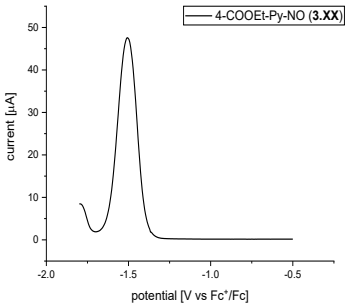

5.3.3.3.1.6 4-chloropyridine 1-oxide:

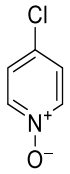

Cyclovoltammogram

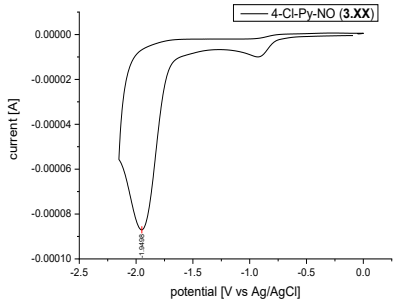

Differential pulse voltammetry

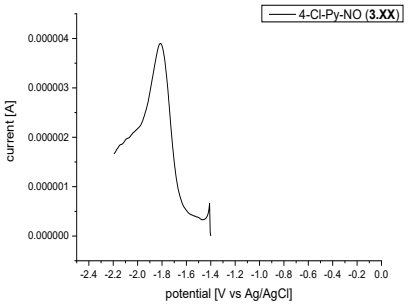

$E_{1/2}^{ox}(Fc^{+}/Fc) = +0.55\ V\ vs\ Ag/AgCl$

5.3.3.3.1.7 pyridine 1-oxide:

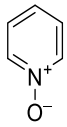

Cyclovoltammogram

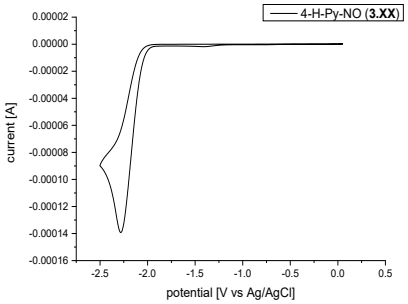

Differential pulse voltammetry

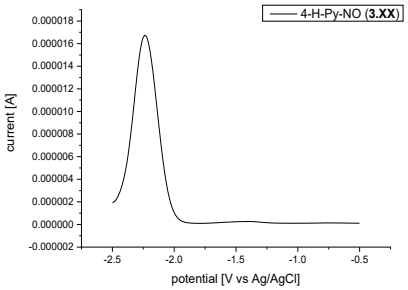

$E_{1/2}^{ox}(Fc^+/Fc) = +0.54\ V\ vs\ Ag/AgCl$

5.3.3.3.1.8 4-phenylpyridine 1-oxide:

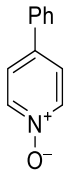

Cyclovoltammogram

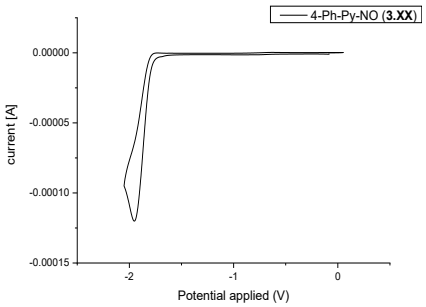

Differential pulse voltammetry

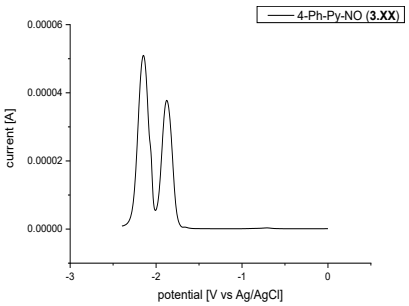

$E_{1/2}^{ox}(Fc^+/Fc) = +0.53\ V\ vs\ Ag/AgCl$

5.3.3.3.1.9 4-(tert-butyl)pyridine 1-oxide:

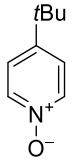

Cyclovoltammogram

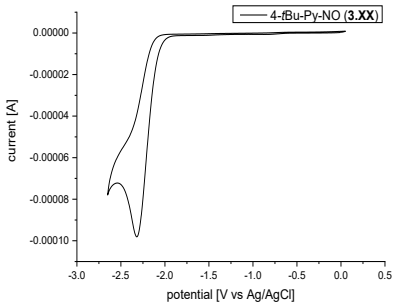

Differential pulse voltammetry

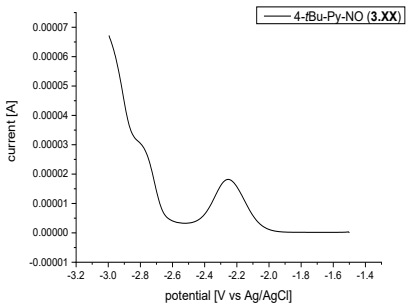

$E_{1/2}^{ox}(Fc^+/Fc) = +0.54\,V\ vs\ Ag/AgCl$

5.3.3.3.1.10 4-methoxypyridine 1-oxide:

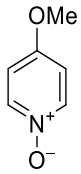

Cyclovoltammogram

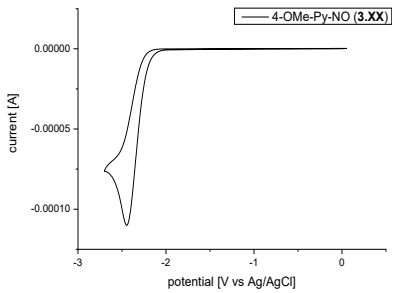

Differential pulse voltammetry

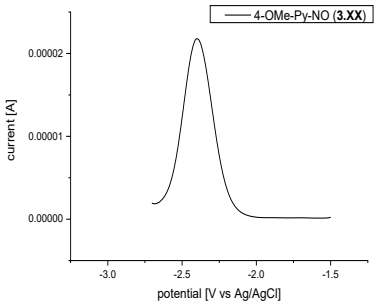

$E_{1/2}^{ox}(Fc^+/Fc) = +0.53\,V\ vs\ Ag/AgCl$

5.3.3.3.1.11 [4,4'-bipyridine] 1-oxide:

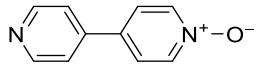

Cyclovoltammogram

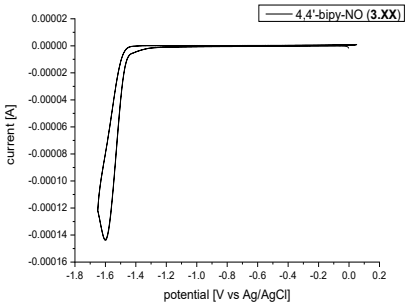

Differential pulse voltammetry

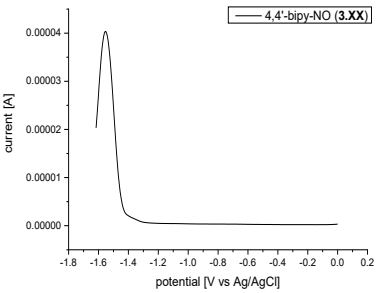

$E_{1/2}^{ox}(Fc^+/Fc) = +0.53\ V\ vs\ Ag/AgCl$

5.3.3.3.1.12 [4,4'-bipyridine] 1,1'-dioxide:

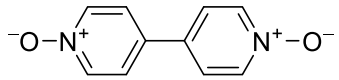

Cyclovoltammogram

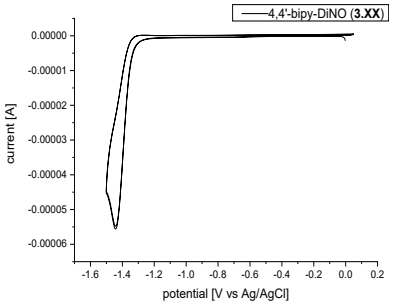

Differential pulse voltammetry

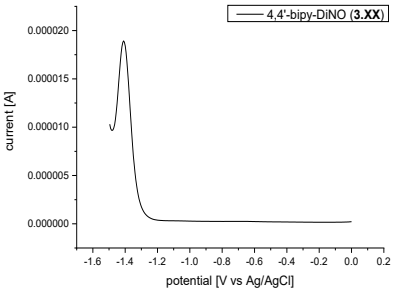

$E_{1/2}^{ox}(Fc^+/Fc) = +0.54\ V\ vs\ Ag/AgCl$

5.3.3.3.1.13 [3,3'-bipyridine] 1-oxide:

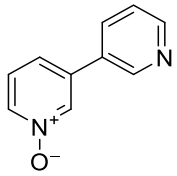

Cyclovoltammogram

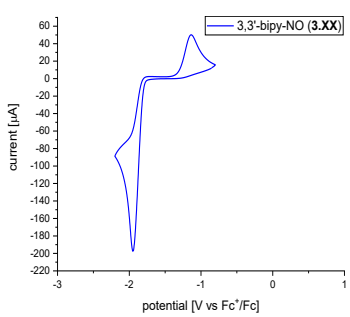

Differential pulse voltammetry

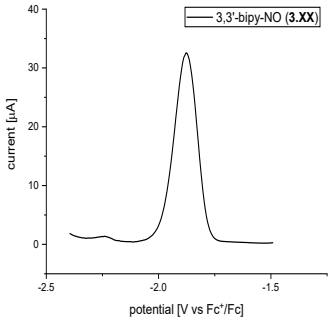

5.3.3.3.1.14 [3,3'-bipyridine] 1,1'-dioxide:

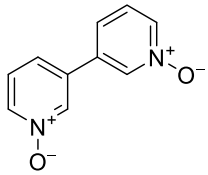

Cyclovoltammogram

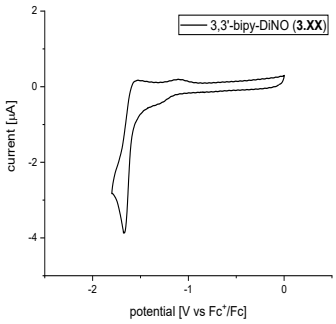

Differential pulse voltammetry

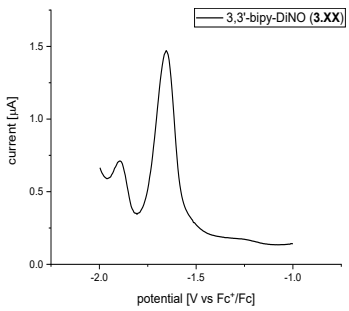

5.3.3.3.1.15 [2,2'-bipyridine] 1-oxide:

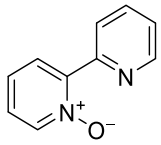

Cyclovoltammogram

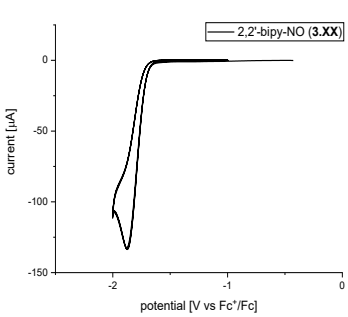

Differential pulse voltammetry

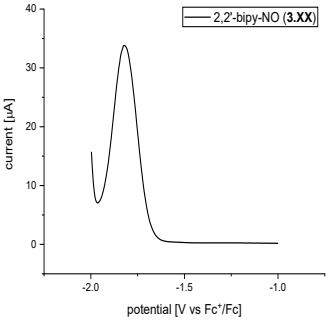

5.3.3.3.1.16 [2,2'-bipyridine] 1,1'-dioxide:

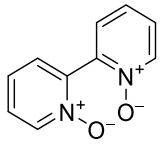

Cyclovoltammogram

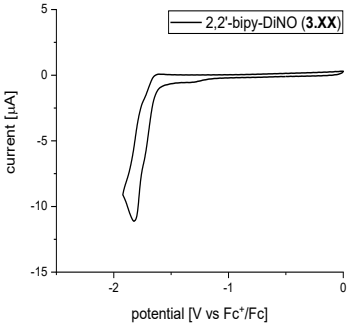

Differential pulse voltammetry

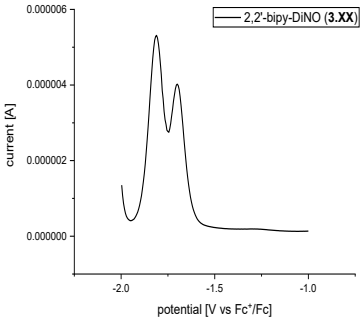

5.3.3.3.1.17 1,4-diazine-NO (pyrazine 1-oxide):

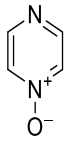

Cyclovoltammogram

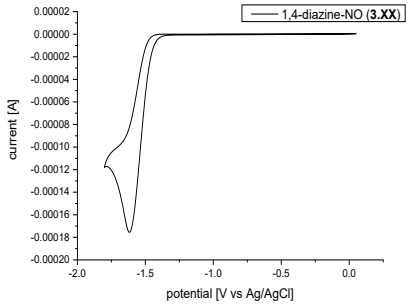

Differential pulse voltammetry

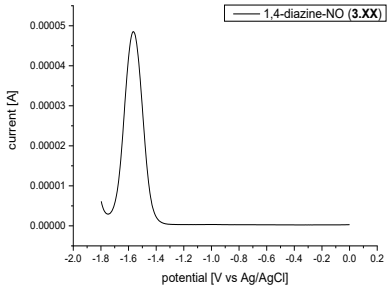

$E_{1/2}^{ox}(Fc^+/Fc) = +0.53\,V\ vs\ Ag/AgCl$

5.3.3.3.1.18 1,3-diazine-NO (pyrimidine 1-oxide):

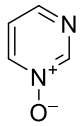

Cyclovoltammogram

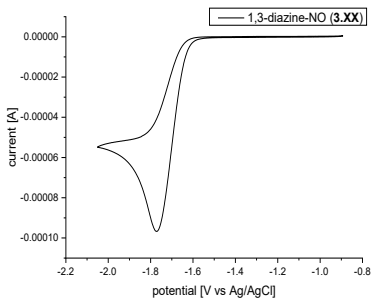

Differential pulse voltammetry

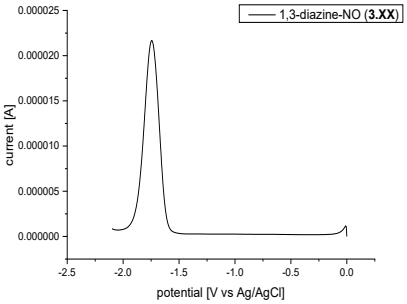

$E_{1/2}^{ox}(Fc^+/Fc) = +0.53\,V\ vs\ Ag/AgCl$

5.3.3.3.1.19 1,2-diazine-NO (pyridazine 1-oxide):

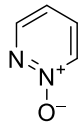

Cyclovoltammogram

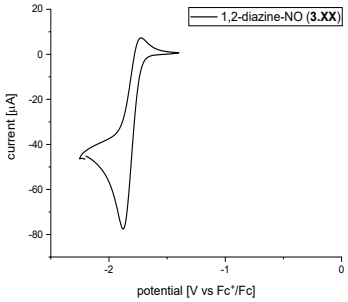

Differential pulse voltammetry

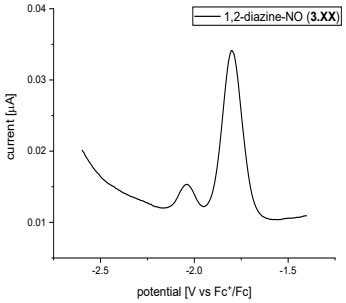

5.3.3.3.1.20 phthalazine 2-oxide:

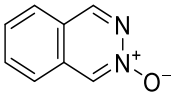

Cyclovoltammogram

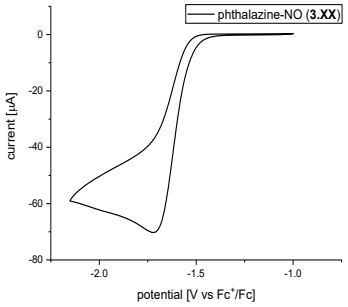

Differential pulse voltammetry

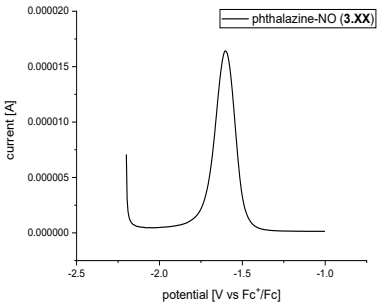

5.3.3.3.1.21 phenazine 5-oxide:

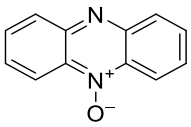

Cyclovoltammogram

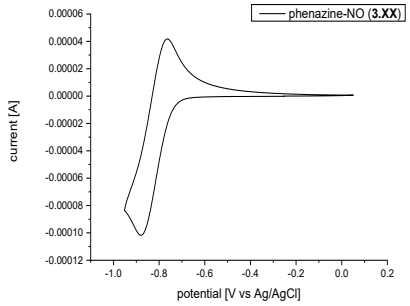

Differential pulse voltammetry

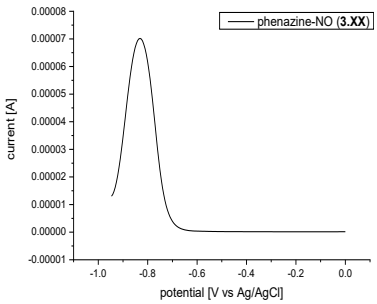

$E_{1/2}^{ox}(Fc^+/Fc) = +0.53\,V\ vs\ Ag/AgCl$

5.3.3.3.1.22 phenazine 5,10-dioxide:

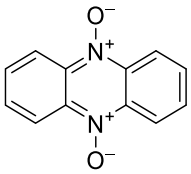

Cyclovoltammogram

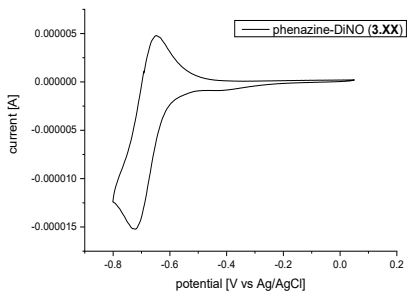

Differential pulse voltammetry

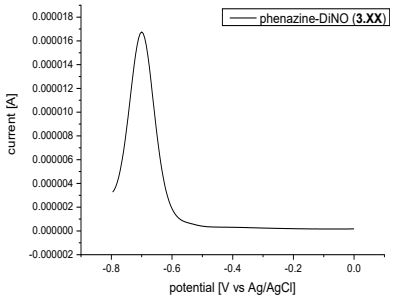

$E_{1/2}^{ox}(Fc^+/Fc) = +0.54\,V\ vs\ Ag/AgCl$

5.3.3.3.1.23 9-chloroacridine 10-oxide:

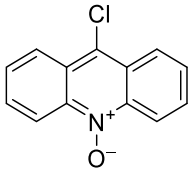

Cyclovoltammogram

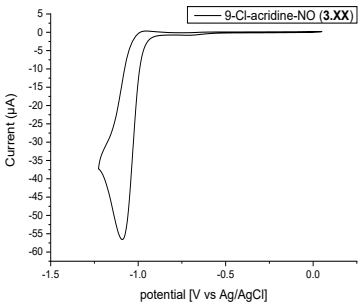

Differential pulse voltammetry

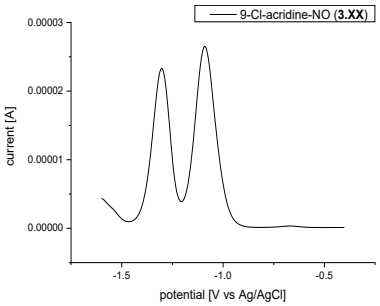

$E_{1/2}^{ox}(Fc^{+}/Fc) = +0.53\ V\ vs\ Ag/AgCl$

5.3.4 Analytical data of chapter 4

5.3.4.1 Characterization of *N,N*-dimethylaniline scope

5.3.4.1.1 Synthesis of 4-(*tert*-butyl)phenyl trifluoromethanesulfonate (4.1a):

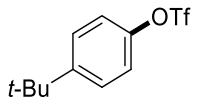

4.1a

Following general procedure A, using 20 mmol 4-(*tert*-butyl)phenol at 0 °C instead of −78 °C with pyridine as the base afforded the title compound **4.1a** (5.65 g, 19.24 mmol, 96%) as a clear colorless oil after purification via column chromatography (pure *n*-pentane).

R_f = 0.40 (*n*-pentane)

^{1}H NMR (300 MHz, Chloroform-*d*) δ 7.49 – 7.41 (m, 2H), 7.22 – 7.16 (m, 2H), 1.33 (s, 9H).

^{13}C NMR (75 MHz, Chloroform-*d*) δ 151.8, 147.6, 127.3, 120.8, 118.9 (q, *J* = 320.7 Hz), 34.9, 31.4.

^{19}F NMR (282 MHz, Chloroform-d) δ -72.97.

MS (EI): m/z (relative intensity) 282 (11), 269 (10), 268 (15), 267 (100), 175 (17), 134 (12), 109 (11), 106 (10), 79 (10), 78 (10), 77 (13), 41 (13).

HR-MS (EI) m/z calcd for $C_{11}H_{13}O_3F_3S_1^+$ $[M]^+$ 282.0532, found 282.0530.

IR (ATR, neat, cm-1): 2966 (w), 2909 (w), 2873 (w), 1648 (w), 1596 (w), 1504 (m), 1466 (w), 1422 (s), 1366 (w), 1310 (w), 1268 (w), 1249 (m), 1205 (s), 1138 (s), 1111 (m), 1015 (m), 942 (w), 886 (s), 837 (s), 780 (m), 756 (m), 730 (m), 664 (m), 637 (m), 609 (s), 582 (m), 552 (m), 531 (m), 509 (s), 414 (m).

The analytical data is in accordance with those reported in the literature.[133]

5.3.4.1.2 Synthesis of 4-(*tert*-butyl)-*N,N*-dimethylaniline hydrochloride (4.3a·HCl):

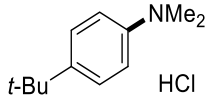

4.3a·HCl

Following general procedure B, using 4-(*tert*-butyl)phenyl trifluoromethanesulfonate (**4.1a**) afforded the title compound **4.3a** (106 mg, 0.497 mmol, 99%) as a white crystalline solid after purification via column chromatography (pure *n*-pentane) and treatment with HCl (2.0 M in Et_2O).

R_f = 0.21 (*n*-pentane, UV) free base

^{1}H NMR (300 MHz, Chloroform-*d*) δ 14.14 (s, 1H), 7.69 – 7.62 (m, 2H), 7.46 – 7.39 (m, 2H), 3.13 (s, 6H), 1.24 (s, 9H).

^{13}C NMR (75 MHz, Chloroform-*d*) δ 153.4, 140.3, 127.3, 120.2, 46.4, 34.8, 31.1.

MS (EI): m/z (relative intensity) 177 (24), 163 (13), 162 (100), 147 (15).

HRMS (ESI-TOF, *m*/*z*): calcd. for $C_{12}H_{19}N$ $[M+H]^+$ 178.1595, found 178.1598.

IR (ATR, neat, cm-1): 3020 (w), 2957 (m), 2901 (w), 2865 (w), 2488 (w), 2351 (m), 1599 (w), 1513 (m), 1484 (m), 1451 (m), 1417 (w), 1396 (w), 1362 (w), 1269 (w), 1205 (w), 1188 (w), 1143 (m), 1120 (w), 1018 (w), 991 (m), 898 (m), 837 (m), 741 (w), 656 (w), 573 (s), 544 (w), 461 (w).

The analytical data is in accordance with those reported in the literature.[134]

5.3.4.1.3 Synthesis of 4-isopropylphenyl trifluoromethanesulfonate (4.1b):

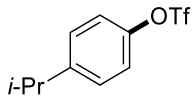

4.1b

Following general procedure 3.A, using 2 mmol 4-isopropylphenol at 0 °C instead of −78 °C and pyridine as the base afforded the title compound **4.1b** (389 mg, 1.45 mmol 72%) as a clear colorless oil after purification via column chromatography (pure *n*-pentane).

Rf = 0.50 (*n*-pentane, UV)

^{1}H NMR (300 MHz, Chloroform-d) δ 7.32 – 7.26 (m, 2H), 7.22 – 7.16 (m, 2H), 2.95 (sept, *J* = 6.9 Hz, 1H), 1.26 (d, *J* = 6.9 Hz, 6H).

^{13}C NMR (75 MHz, Chloroform-d) δ 149.5, 147.8, 128.3, 121.2, 118.9 (q, *J* = 320.7 Hz), 33.8, 24.0.

^{19}F NMR (282 MHz, Chloroform-d) δ -72.95.

MS (EI): m/z (relative intensity) 268 (48), 254 (11), 253 (100), 135 (42), 107 (29), 103 (32), 92 (14), 91 (60), 79 (13), 77 (16), 69 (23), 65 (16).

HRMS (EI, *m*/*z*): calcd. for $C_{10}H_{11}O_3F_3S_1$ $[M]^+$ 268.0376, found 268.0375.

IR (ATR, neat, cm-1): 2966 (s), 2933 (s), 2876 (s), 1597 (s), 1502 (s), 1465 (s), 1419 (s), 1367 (s), 1339 (s), 1302 (s), 1281 (s), 1249 (s), 1204 (s), 1181 (s), 1134 (s), 1057 (s), 1017 (s), 942 (s), 883 (s), 837 (s), 787 (s), 763 (s), 730 (s), 684 (s), 637 (s), 608 (s), 588 (s), 564 (s), 537 (s), 511 (s), 472 (w).

5.3.4.1.4 Synthesis of 4-isopropyl-*N,N*-dimethylaniline hydrochloride (4.3b·HCl):

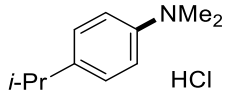

4.3b·HCl

Following general procedure 3.B, using 0.524 mmol 4-isopropylphenyl trifluoromethanesulfonate (**4.1b**) afforded the title compound **4.3b** (91 mg, 0.456 mmol, 90%) as a white crystalline solid after purification via column chromatography (pure *n*-pentane) and treatment with HCl (2.0 M in Et_2O).

Rf = 0.17 (*n*-pentane, UV) free base

^{1}H NMR (300 MHz, Chloroform-*d*) δ 14.22 (s, 1H), 7.66 (d, *J* = 8.2 Hz, 2H), 7.30 (d, *J* = 8.0 Hz, 2H), 3.14 (s, 6H), 2.91 (sept, *J* = 7.1 Hz, 1H), 1.20 (d, *J* = 6.8 Hz, 6H).

^{13}C NMR (75 MHz, Chloroform-*d*) δ 151.4, 140.5, 128.5, 120.6, 46.7, 33.9, 23.8.

MS (EI): m/z (relative intensity) 163 (29), 149 (11), 148 (100).

HRMS (EI, *m*/*z*): calcd. for $C_{11}H_{17}N$ $[M+H]^+$ 164.1439, found 164.1442.

IR (ATR, neat, cm-1): 3408 (w), 3006 (w), 2957 (m), 2932 (w), 2869 (w), 2492 (w), 2296 (s), 1940 (w), 1810 (w), 1662 (w), 1600 (w), 1511 (s), 1482 (s), 1461 (m), 1413 (m), 1384 (w), 1363 (w), 1311 (w), 1287 (w), 1251 (w), 1190 (m), 1133 (m), 1057 (m), 1019 (m), 1000 (m), 963 (w), 900 (m), 848 (s), 834 (s), 740 (w), 677 (w), 638 (w), 582 (s), 557 (m), 456 (w), 410 (w).

The analytical data is in accordance with those reported in the literature.[135]

5.3.4.1.5 Synthesis of *p*-tolyl trifluoromethanesulfonate (4.1c):

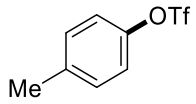

4.1c

Following general procedure 3.A, using *p*-cresol (9.25 mmol) at 0 °C instead of −78 °C with NEt_3 as the base afforded the title compound **4.1c** (2.18 g, 9.07 mmol, 98%) as a clear colorless oil after purification via column chromatography (pure *n*-pentane).

Rf = 0.36 (*n*-pentane, UV)

^{1}H NMR (300 MHz, Chloroform-d) δ 7.27 – 7.20 (m, 2H), 7.18 – 7.12 (m, 2H), 2.38 (s, 3H).

^{13}C NMR (75 MHz, Chloroform-*d*) δ 147.6, 138.5, 130.7, 121.0, 118.8 (q, *J* = 320.7 Hz), 20.9.

^{19}F NMR (282 MHz, Chloroform-d) δ -72.91.

MS (EI): m/z (relative intensity) 240 (65), 175 (11), 107 (100), 91 (12), 79 (24), 78 (14), 77 (60), 69 (18), 51 (11).

HRMS (EI, *m*/*z*): calcd. for $C_8H_{11}N$ $[M]^+$ 240.0063, found 240.0061.

IR (ATR, neat, cm-1): 1600 (w), 1501 (m), 1420 (s), 1249 (m), 1203 (s), 1178 (m), 1132 (s), 1044 (w), 1018 (w), 938 (w), 881 (s), 821 (s), 770 (w), 714 (w), 691 (m), 639 (m), 606 (s), 583 (m), 561 (w), 542 (w), 502 (s), 485 (m), 417 (w).

The analytical data is in accordance with those reported in the literature.[133]

5.3.4.1.6 Synthesis of *N,N,*4-trimethylaniline hydrochloride (4.3c·HCl):

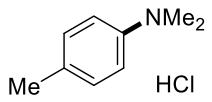

4.3c·HCl

Following general procedure 3.B, using *p*-tolyl trifluoromethanesulfonate (**4.1c**) afforded the title compound **4.3c** (78 mg, 0.454 mmol, 90%) as a white crystalline solid after purification via column chromatography (pure *n*-pentane) and treatment with HCl (2.0 M in Et_2O).

Rf = 0.20 (*n*-pentane, UV) free base

^{1}H NMR (300 MHz, Chloroform-*d*) δ 13.86 (s, 1H), 7.60 (d, *J* = 6.1 Hz, 2H), 7.21 – 7.09 (m, 2H), 3.09 (s, 6H), 2.24 (s, 3H).

^{13}C NMR (75 MHz, Chloroform-*d*) δ 140.2, 130.7, 120.4, 46.5, 20.9.

MS (EI): m/z (relative intensity) 135 (66), 134 (100), 119 (14), 118 (14), 91 (18).

HRMS (EI, *m*/*z*): calcd. for $C_9H_{13}N$ $[M]^+$ 135.1046, found 135.1046.

IR (ATR, neat, cm-1): 3031 (w), 2922 (w), 2627 (w), 2536 (w), 2498 (w), 2422 (m), 2405 (m), 1611 (w), 1501 (s), 1485 (s), 1462 (m), 1440 (m), 1423 (m), 1362 (w), 1267 (w), 1249 (s), 1231 (m), 1173 (m), 1128 (m), 1094 (w), 1027 (s), 987 (m), 944 (w), 919 (s), 878 (w), 854 (m), 815 (m), 724 (w), 697 (w), 634 (s), 554 (w), 448 (m), 423 (m).

The analytical data is in accordance with those reported in the literature.[136]

5.3.4.1.7 Synthesis of phenyl trifluoromethanesulfonate (4.1d):

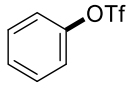

4.1d

Following general procedure 3.A, using 2.13 mmol phenol at 0 °C instead of −78 °C with triethylamine as the base afforded the title compound **4.1d** (365 mg, 1.61 mmol, 76%) as a clear colorless oil after purification via column chromatography (pure *n*-pentane).

R_f = 0.45 (*n*-pentane, UV)

^{1}H NMR (300 MHz, Chloroform-*d*) δ 7.43 – 7.27 (m, 3H), 7.24 – 7.15 (m, 2H).

^{13}C NMR (75 MHz, Chloroform-*d*) δ 149.8, 130.4, 128.5, 121.5, 118.9 (q, *J* = 320.7 Hz).

^{19}F NMR (282 MHz, Chloroform-*d*) δ -72.96.

MS (EI): m/z (relative intensity) 226 (19), 96 (12), 93 (28), 69 (100), 65 (95), 64 (16), 63 (18), 50 (10), 48 (12), 39 (58), 38 (11).

HRMS (EI, *m*/*z*): calcd. for $C_7H_5O_3F_3S$ $[M]^+$ 225.9906, found 225.9905.

IR (ATR, neat, cm-1): 1603 (w), 1587 (w), 1487 (m), 1459 (w), 1420 (s), 1287 (w), 1249 (m), 1203 (s), 1175 (m), 1129 (s), 1073 (w), 1024 (w), 912 (m), 879 (s), 826 (w), 779 (m), 764 (s), 735 (m), 685 (m), 621 (m), 600 (s), 567 (m), 515 (s), 475 (m), 405 (w).

The analytical data is in accordance with those reported in the literature.[133]

5.3.4.1.8 Synthesis of N,N-dimethylaniline hydrochloride (4.3d·HCl):

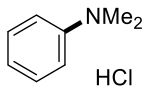

4.3d·HCl

Following general procedure 3.B, using phenyl trifluoromethanesulfonate (**4.1d**) afforded the title compound **4.3d** (78 mg, 0.496 mmol, 99%) as a colorless waxy solid after purification via column chromatography (pure *n*-pentane) and treatment with HCl (2.0 M in Et_2O).

R_f = 0.15 (*n*-pentane, UV) free-base

^{1}H NMR (300 MHz, Chloroform-*d*) δ 14.05 (s, 1H), 7.81 – 7.62 (m, 2H), 7.46 – 7.28 (m, 2H), 3.10 (s, 6H).

^{13}C NMR (75 MHz, Chloroform-*d*) δ 142.7, 130.3, 130.1, 120.7, 46.4.

MS (EI): m/z (relative intensity) 121 (71), 120 (100), 105 (12), 104 (13), 77 (22), 51 (11).

HRMS (ESI-TOF, *m*/*z*): calcd. for $C_8H_{11}N$ $[M+H]^+$ 122.0969, found 122.0969.

IR (ATR, neat, cm-1): 3045 (w), 3012 (w), 2952 (w), 2929 (w), 2853 (w), 2629 (w), 2529 (w), 2495 (m), 2381 (s), 2127 (w), 1598 (m), 1494 (s), 1468 (m), 1421 (m), 1403 (w), 1345 (w), 1326 (w), 1196 (m), 1185 (w), 1158 (w), 1136 (m), 1127 (m), 1079 (w), 1063 (w), 1026 (w), 995 (m), 928 (w), 899 (m), 853 (w), 764 (s), 696 (s), 616 (w), 575 (m), 542 (s), 480 (w).

The analytical data is in accordance with those reported in the literature.[137]

5.3.4.1.9 Synthesis of 4-methoxyphenyl trifluoromethanesulfonate (4.1e):

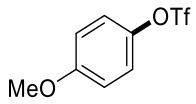

4.1e

Following general procedure 3.A, using 4-methoxyphenol (2.00 mmol) at 0 °C instead of −78 °C and triethylamine as the base afforded the title compound **4.1e** (456 mg, 1.78 mmol, 89%) as a clear colorless oil after purification via column chromatography (pure *n*-pentane).

Rf = 0.13 (*n*-pentane, UV)

^{1}H NMR (400 MHz, Chloroform-d) δ 7.24 – 7.16 (m, 2H), 6.96 – 6.88 (m, 2H), 3.81 (s, 3H).

^{13}C NMR (101 MHz, CDCl3) δ 159.2, 143.2, 122.5, 118.9 (q, *J* = 320.9 Hz), 115.2, 55.8.

^{19}F NMR (282 MHz, Chloroform-d) δ -72.87.

MS (EI): m/z (relative intensity) 256 (13), 123 (100), 95 (37), 69 (27).

HRMS (EI, *m*/*z*): calcd. for $C_{20}H_{26}O_3$ $[M+H]^+$ 256.0012, found 256.0005.

IR (ATR, neat, cm-1): 2953 (w), 2843 (w), 1597 (w), 1501 (s), 1465 (w), 1417 (s), 1300 (w), 1248 (m), 1203 (s), 1168 (s), 1133 (s), 1105 (m), 1032 (m), 1008 (m), 928 (w), 881 (s), 832 (s), 808 (s), 769 (w), 721 (w), 694 (m), 636 (m), 606 (s), 561 (m), 518 (s), 503 (m), 469 (m).

The analytical data is in accordance with those reported in the literature.[133]

5.3.4.1.10 Synthesis of 4-methoxy-*N,N*-dimethylaniline hydrochloride (4.3e·HCl):

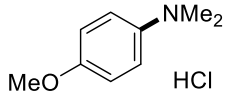

4.3e·HCl

Following general procedure 3.B, using 4-methoxyphenyl trifluoromethanesulfonate (**4.1e**, 0.332 mmol) afforded the title compound **4.3e** (57 mg, 0.304 mmol, 92%) as a white crystalline solid after purification via column chromatography (*n*-pentane:EtOAc = 10:1) and treatment with HCl (2.0 M in Et_2O).

Rf = 0.27 (*n*-pentane:EtOAc = 10:1) free base

^{1}H NMR (300 MHz, Chloroform-*d*) δ 14.07 (s, 1H), 7.72 – 7.63 (m, 2H), 6.92 – 6.84 (m, 2H), 3.74 (s, 3H), 3.10 (s, 6H).

^{13}C NMR (75 MHz, Chloroform-*d*) δ 160.3, 135.6, 122.1, 115.4, 55.7, 46.9.

MS (EI): m/z (relative intensity) 151 (56), 136 (100), 108 (11).

HRMS (EI, *m*/*z*): calcd. for $C_{14}H_{16}N$ $[M+H]^+$ 152.1075, found 152.1078.

IR (ATR, neat, cm-1): 3126 (w), 3074 (w), 3056 (w), 3006 (w), 2974 (w), 2943 (w), 2913 (w), 2844 (w), 2621 (w), 2531 (w), 2498 (m), 2427 (m), 2407 (m), 2150 (w), 2120 (w), 2036 (w), 1954 (w), 1921 (w), 1885 (w), 1700 (w), 1616 (w), 1605 (m), 1519 (s), 1492 (m), 1458 (s), 1447 (m), 1425 (w), 1404 (w), 1314 (m), 1266 (s), 1242 (m), 1181 (s), 1158 (m), 1141 (m), 1119 (m), 1023 (s), 995 (m), 979 (m), 900 (m), 849 (s), 823 (m), 813 (m), 724 (w), 700 (m), 636 (w), 565 (s), 552 (s), 486 (w), 438 (w), 418 (w).

The analytical data is in accordance with those reported in the literature.[136]

5.3.4.1.11 Synthesis of 4-methoxyphenyl trifluoromethanesulfonate (4.1f)

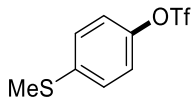

4.1f

Following general procedure 3.A, using 4-(methylthio)phenol (4.00 mmol) and NEt*i*Pr$_2$ as the base afforded the title compound **4.1f** (0.981 g, 3.60 mmol, 90%) as a clear colorless oil after purification via column chromatography (*n*-pentane:EtOAc = 50:1, UV).

Rf = 0.35 (*n*-pentane:EtOAc = 50:1, UV)

^{1}H NMR (300 MHz, Chloroform-d) δ 7.32 – 7.26 (m, 1H), 7.24 – 7.17 (m, 1H), 2.50 (s, 1H).

^{13}C NMR (75 MHz, Chloroform-d) δ 147.0, 139.9, 127.6, 121.8, 118.8 (d, *J* = 320.9 Hz), 15.7.

^{19}F NMR (282 MHz, Chloroform-d) δ -72.89.

MS (EI): m/z (relative intensity) 272 (33), 139 (100), 111 (14), 69 (18).

HRMS (EI, *m*/*z*): calcd. for $C_8H_7O_3F_3S_2$ $[M]^+$ 271.9783, found 271.9790.

IR (ATR, neat, cm-1): 2178 (w), 2152 (w), 1983 (w), 1486 (m), 1418 (m), 1399 (m), 1248 (w), 1201 (s), 1183 (m), 1131 (s), 1090 (m), 1011 (m), 970 (w), 944 (w), 885 (s), 828 (s), 782 (m), 756 (m), 720 (w), 648 (w), 632 (m), 604 (s), 575 (m), 556 (w), 525 (m), 490 (m), 472 (w), 456 (m), 437 (w), 427 (w), 420 (m), 401 (m).

The analytical data is in accordance with those reported in the literature.[138]

5.3.4.1.12 Synthesis of *N,N*-dimethyl-4-(methylthio)aniline hydrochloride (4.3f):

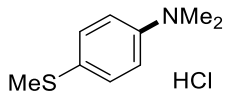

4.3f·HCl

Following general procedure 3.B, using 4-(methylthio)phenyl trifluoromethanesulfonate (**4.1f**) afforded the title compound **4.3f** (100 mg, 0.492 mmol, 99%) as a white crystalline solid after purification via column chromatography (*n*-pentane:EtOAc = 50:1) and treatment with 2 M HCl in Et_2O.

Rf = 0.29 (*n*-pentane:EtOAc = 50:1, UV) free base

^{1}H NMR (300 MHz, Chloroform-*d*) δ 7.70 – 7.63 (m, 2H), 7.25 – 7.18 (m, 2H), 3.11 (s, 6H), 2.40 (s, 3H).

^{13}C NMR (75 MHz, Chloroform-*d*) δ 142.0, 139.5, 127.2, 121.2, 46.6, 15.3.

MS (EI): m/z (relative intensity) 167 (68), 153 (12), 152 (100), 136 (19), 119 (13), 108 (16), 77 (11), 69 (17), 63 (12), 51 (12), 47 (23), 45 (37), 42 (22).

HRMS (EI, *m*/*z*): calcd. for $C_8H_7O_3F_3S_2$ $[M]^+$ 167.0763, found 167.0757.

IR (ATR, neat, cm-1): 3482 (w), 3042 (w), 3008 (w), 2974 (w), 2914(w), 2535 (w), 2497 (m), 2394 (s), 1925 (w), 1656 (w), 1590 (w), 1486 (s), 1464 (m), 1426 (m), 1395 (m), 1321 (w), 1286 (w), 1187 (m), 1157 (w), 1138 (m), 1096 (m), 1016 (w), 992 (m), 981 (w), 956 (m), 897 (m), 825 (s), 776 (w), 715 (w), 635 (w), 539 (s), 520 (m), 413 (w).

The analytical data is in accordance with those reported in the literature.[139]

5.3.4.1.13 Synthesis of benzo[d][1,3]dioxol-5-yl trifluoromethanesulfonate (4.1g):

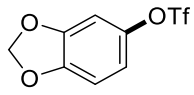

4.1g

Following general procedure 3.A, using benzo[d][1,3]dioxol-5-ol (4.00 mmol) and pyridine as the base afforded the title compound **4.1g** (1.01 g, 3.74 mmol, 93%) as a clear colorless oil after purification via column chromatography (*n*-pentane:EtOAc = 50:1).

Rf = 0.34 (*n*-pentane:EtOAc = 50:1, UV)

^{1}H NMR (300 MHz, Chloroform-*d*) δ 6.83 – 6.71 (m, 3H), 6.03 (s, 2H).

^{13}C NMR (75 MHz, Chloroform-*d*) δ 148.7, 147.6, 143.6, 118.9 (q, *J* = 320.8 Hz), 114.5, 108.3, 103.5, 102.6.

^{19}F NMR (282 MHz, Chloroform-*d*) δ -72.84.

MS (EI): m/z (relative intensity) 270 (19), 137 (100), 107 (43), 79 (44), 69 (64), 53 (35), 51 (20), 50 (14).

HRMS (EI, *m*/*z*): calcd. for $C_8H_5O_5F_3S_1$ $[M]^+$ 269.9804, found 269.9806.

IR (ATR, neat, cm-1): 2908 (w), 1638 (w), 1610 (w), 1505 (m), 1481 (s), 1418 (s), 1366 (w), 1245 (s), 1202 (s), 1163 (m), 1136 (s), 1108 (s), 1087 (s), 1036 (s), 940 (s), 928 (s), 859 (s), 843 (s), 804 (s), 772 (w), 733 (m), 713 (m), 652 (m), 606 (s), 589 (s), 559 (m), 534 (w), 504 (s), 452 (m), 426 (m).

The analytical data is in accordance with those reported in the literature.[138]

5.3.4.1.14 Synthesis of *N,N*-dimethylbenzo[d][1,3]dioxol-5-amine hydrochloride (4.3g·HCl):

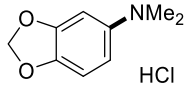

4.3g·HCl

Following general procedure 3.B, using benzo[d][1,3]dioxol-5-yl trifluoromethanesulfonate **4.1g** (0.529 mmol) afforded the title compound **4.3g** (103 mg, 0.501 mmol, 95%) as a white crystalline solid after purification via column chromatography (*n*-pentane:EtOAc = 10:1) and treatment with 2 M HCl in Et_2O.

Rf = 0.4 (*n*-pentane:EtOAc = 10:1, UV) free base

^{1}H NMR (300 MHz, Chloroform-*d*) δ 14.48 (s, 1H), 7.31 (dd, *J* = 8.4, 2.4 Hz, 1H), 7.24 (d, *J* = 2.3 Hz, 1H), 6.84 (d, *J* = 8.3 Hz, 1H), 6.05 (s, 2H), 3.12 (s, 6H).

^{13}C NMR (75 MHz, Chloroform-*d*) δ 149.1, 148.9, 136.9, 114.6, 109.1, 102.6, 102.0, 47.0.

MS (EI): m/z (relative intensity) 166 (10), 165 (100), 164 (61), 149 (14), 136 (12), 107 (13), 92 (37), 82 (13), 65 (11).

HRMS (EI, *m*/*z*): calcd. for $C_9H_{11}O_2N$ $[M]^+$ 165.0784, found 165.0782.

IR (ATR, neat, cm-1): 3031 (w), 2923 (w), 2536 (w), 2498 (w), 2422 (m), 2405 (m), 1651 (w), 1612 (w), 1501 (s), 1462 (m), 1440 (m), 1423 (m), 1362 (w), 1267 (w), 1249 (s), 1231 (m), 1173 (m), 1129 (m), 1094 (m), 1028 (s), 987 (m), 944 (w), 919 (s), 878 (w), 854 (m), 815 (m), 762 (w), 723 (w), 696 (w), 634 (s), 554 (w), 528 (w), 479 (w), 447 (m), 422 (m).

The analytical data is in accordance with those reported in the literature.[140]

5.3.4.1.15 Synthesis of 4-nitrophenyl trifluoromethanesulfonate (4.1h):

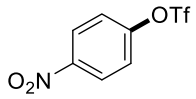

4.1h

Following general procedure 3.A, using 4-nitrophenol (3.59 mmol) and pyridine as the base afforded the title compound **4.1h** (940 mg, 3.47 mmol, 96%) as a clear white solid after purification via column chromatography (Pure *n*-pentane).

Rf = 0.24 (*n*-pentane, UV)

^{1}H NMR (300 MHz, Chloroform-*d*) δ 8.42 – 8.29 (m, 2H), 7.56 – 7.41 (m, 2H).

^{13}C NMR (75 MHz, Chloroform-*d*) δ 153.1, 147.1, 126.0, 122.5, 118.6 (q, *J* = 320.9 Hz).

^{19}F NMR (282 MHz, Chloroform-*d*) δ -72.73.

MS (EI): m/z (relative intensity) 271 (62), 177 (41), 161 (16), 149 (18), 95 (59), 92 (21), 75 (11), 69 (100), 64 (37), 63 (43), 62 (11), 38 (11), 30 (25).

HRMS (EI, *m*/*z*): calcd. for $C_7H_4O_5NF_3S$ $[M]^+$ 270.9757, found 270.9752.

IR (ATR, neat, cm-1): 3124 (w), 1622 (w), 1589 (w), 1534 (s), 1485 (m), 1420 (s), 1381 (w), 1347 (s), 1318 (w), 1291 (w), 1250 (m), 1210 (s), 1174 (m), 1129 (s), 1011 (m), 892 (s), 859 (s), 779 (m), 757 (m), 740 (s), 689 (m), 629 (m), 608 (s), 572 (s), 524 (s), 472 (m), 444 (s).

The analytical data is in accordance with those reported in the literature.[141]

5.3.4.1.16 Synthesis of *N,N*-dimethyl-4-nitroaniline hydrochloride (4.3h·HCl):

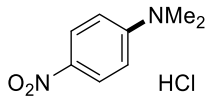

4.3h·HCl

Following general procedure 3.B, using 4-nitrophenyl trifluoromethanesulfonate (**4.1h**) afforded the title compound **4.3h** (65 mg, 0.391 mmol, 71%, freebase) as a yellow crystalline solid after purification via column chromatography (*n*-pentane: EtOAc = 10:1).

Rf = 0.20 (*n*-pentane: EtOAc = 10:1, UV) free base

^{1}H NMR (300 MHz, Chloroform-*d*) δ 8.14 – 8.03 (m, 2H), 6.63 – 6.53 (m, 2H), 3.09 (s, 6H).

^{13}C NMR (75 MHz, Chloroform-*d*) δ 154.2, 136.8, 126.1, 110.2, 40.3.

MS (EI): m/z (relative intensity) 166 (63), 165 (15), 136 (57), 120 (15), 119 (26), 118 (20), 108 (15), 105 (19), 104 (21), 92 (11), 91 (11), 79 (15), 78 (18), 77 (39), 76 (17), 65 (18), 64 (12), 63 (17), 51 (19), 50 (22), 46 (47), 42 (52), 39 (14), 30 (100).

HRMS (EI, *m*/*z*): calcd. for $C_9H_{11}O_2N$ $[M]^+$ 166.0737, found 166.0736.

IR (ATR, neat, cm-1): 2918(w), 1915(w), 1580(s), 1526(m), 1481(s), 1449(m), 1382(w), 1284(s), 1231(s), 1196(s), 1112(s), 1066(s), 938(m), 819(s), 748(s), 695(s), 629(m), 604(m), 539(s), 505(s), 491(s).

The analytical data is in accordance with those reported in the literature.[136]

5.3.4.1.17 Synthesis of naphthalen-2-yl trifluoromethanesulfonate (4.1i):

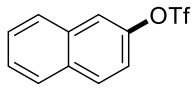

4.1i

Following general procedure 3.A, using naphthalen-2-ol (4.00 mmol) and pyridine as the base afforded the title compound **4.1i** (1.00 g, 3.62 mmol, 91%) as a clear colorless oil after purification via column chromatography (*n*-pentane).

Rf = 0.50 (*n*-pentane, UV)

^{1}H NMR (300 MHz, Chloroform-*d*) δ 7.96 – 7.83 (m, 3H), 7.78 (d, *J* = 2.5 Hz, 1H), 7.65 – 7.53 (m, 2H), 7.39 (dd, *J* = 9.0, 2.5 Hz, 1H).

^{13}C NMR (75 MHz, Chloroform-*d*) δ 147.2, 133.4, 132.5, 130.7, 128.1, 128.0, 127.7, 127.3, 119.6, 119.3, 119.0 (q, *J* = 320.8 Hz).

^{19}F NMR (282 MHz, Chloroform-*d*) δ -72.82.

MS (EI): m/z (relative intensity) 276 (41), 143 (42), 115 (100).

HRMS (EI, *m*/*z*): calcd. for $C_{11}H_7O_3F_3S$ $[M]^+$ 276.0063, found 276.0061.

IR (ATR, neat, cm-1): 3063 (w), 1633 (w), 1600 (w), 1582 (w), 1511 (w), 1461 (w), 1419 (s), 1356 (w), 1250 (m), 1233 (m), 1201 (s), 1135 (s), 1104 (s), 955 (s), 911 (s), 884 (m), 859 (s), 831 (s), 807 (s), 766 (m), 748 (s), 697 (m), 643 (s), 620 (m), 603 (s), 577 (m), 542 (w), 522 (w), 495 (s), 471 (s), 430 (m).

The analytical data is in accordance with those reported in the literature.[142]

5.3.4.1.18 Synthesis of *N,N*-dimethylnaphthalen-2-amine hydrochloride (4.3i·HCl):

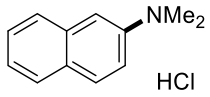

4.3i·HCl

Following general procedure 3.B, using naphthalen-2-yl trifluoromethanesulfonate (**4.1i**) afforded the title compound **4.3i** (102 mg, 0.491 mmol, 95%) as a white crystaline solid after purification via column chromatography (pure *n*-pentane) and treatment with 2 M HCl in Et_2O.

Rf = 0.13 (*n*-pentane, UV) free base

^{1}H NMR (300 MHz, Chloroform-*d*) δ 14.49 (s, 1H), 8.34 (d, *J* = 2.4 Hz, 1H), 7.94 (d, *J* = 8.9 Hz, 1H), 7.90 – 7.79 (m, 2H), 7.76 (dd, *J* = 8.9, 2.4 Hz, 1H), 7.59 – 7.44 (m, 2H), 3.25 (s, 6H).

^{13}C NMR (75 MHz, Chloroform-*d*) δ 139.9, 133.2, 132.8, 131.2, 128.4, 128.0, 127.9, 120.2, 117.4, 46.7.

MS (EI): m/z (relative intensity) 172 (12), 171 (100), 170 (87), 155 (19), 128 (27), 127 (24), 77 (11).

HRMS (ESY-TOF, *m*/*z*): calcd. for $C_{12}H_{13}N$ $[M+H]^+$ 172.1126, found 172.1126.

IR (ATR, neat, cm-1): 3465 (w), 3405 (w), 3011 (w), 2506 (w), 2305 (m), 1634 (w), 1603 (w), 1515 (m), 1486 (m), 1470 (m), 1422 (w), 1361 (w), 1271 (w), 1181 (m), 1135 (m), 1109 (m), 990 (w), 954 (m), 922 (w), 909 (w), 870 (m), 843 (m), 816 (s), 755 (s), 693 (w), 655 (m), 616 (w), 566 (m), 545 (m), 483 (s), 474 (s).

The analytical data is in accordance with those reported in the literature.[143]

5.3.4.1.19 Synthesis of [1,1'-biphenyl]-4-yl trifluoromethanesulfonate (4.1j):

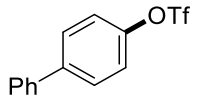

4.1j

Following general procedure 3.A, using [1,1'-biphenyl]-4-ol (2.10 mmol) at 0 °C instead of −78 °C and triethylamine as the base afforded the title compound **4.1j** (0.510 g, 1.69 mmol, 80%) as a clear colorless oil after purification via column chromatography (pure *n*-pentane).

Rf = 0.36 (*n*-pentane, UV)

^{1}H NMR (400 MHz, Chloroform-d) δ 7.70 – 7.62 (m, 2H), 7.61 – 7.54 (m, 2H), 7.52 – 7.40 (m, 3H), 7.40 – 7.32 (m, 2H).

^{13}C NMR (75 MHz, Chloroform-d) δ 149.1, 141.8, 139.4, 129.1, 129.0, 128.2, 127.3, 121.8, 118.9 (q, *J* = 320.8 Hz).

^{19}F NMR (282 MHz, Chloroform-d) δ -72.79.

MS (EI): m/z (relative intensity) 302 (46), 170 (13), 169 (100), 141 (51), 139 (13), 115 (36).

HRMS (EI, *m*/*z*): calcd. for $C_{13}H_9F_3O_3S$ $[M+H]^+$ 302.0219, found 302.0225.

IR (ATR, neat, cm-1): 3061 (w), 1595 (w), 1483 (m), 1454 (w), 1425 (s), 1342 (s), 1250 (m), 1213 (s), 1179 (m), 1226 (s), 1016 (m), 1006 (m), 945 (w), 876 (m), 844 (s), 787 (m), 758 (s), 720 (m), 687 (s), 640 (m), 599 (m), 569 (s), 541 (m), 513 (s), 475 (m), 419 (m).

The analytical data is in accordance with those reported in the literature.[142]

5.3.4.1.20 Synthesis of *N,N*-dimethyl-[1,1'-biphenyl]-4-amine hydrochloride (4.3j·HCl):

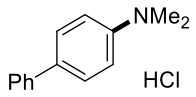

4.3j·HCl

Following general procedure 3.B, using [1,1'-biphenyl]-4-yl trifluoromethanesulfonate (**4.1j**) afforded the title compound **4.3j** (122 mg, 0.522 mmol, 99%) as a white crystalline solid after purification via column chromatography (*n*-pentane:EtOAc = 50:1) and treatment with 2 M HCl in Et_2O.

Rf = 0.38 (*n*-pentane:EtOAc = 20:1, UV) free base

m.p. = 160 °C

^{1}H NMR (300 MHz, Chloroform-d) δ 14.49 (s, 1H), 7.85 (ddd, *J* = 8.8, 2.5, 2.1 Hz, 2H), 7.66 (dt, *J* = 9.0, 2.1 Hz, 2H), 7.53 – 7.47 (m, 2H), 7.47 – 7.32 (m, 3H), 3.21 (s, 6H).

^{13}C NMR (75 MHz, CDCl3) δ 143.3, 141.9, 139.0, 129.1, 129.1, 128.4, 127.2, 121.2, 46.6.

MS (EI): m/z (relative intensity) 198 (16), 197 (100), 196 (78), 181 (14), 180 (10), 153 (12), 152 (21), 98 (13).

HRMS (ESY-TOF, *m*/*z*): calcd. for $C_{14}H_{16}N$ $[M+H]^+$ 198.1283, found 198.1283.

IR (ATR, neat, cm-1): 3505 (w), 3367 (w), 3014 (w), 2957 (w), 2548 (w), 2498 (w), 2453 (w), 1631 (w), 1599 (w), 1577 (w), 1522 (w), 1484 (m), 1441 (w), 1418 (w), 1396 (w), 1337 (w), 1273 (w), 1246 (w), 1211 (w), 1186 (w), 1154 (w), 1137 (m), 1077 (w), 1062 (w), 1041 (w), 1019 (w), 1005 (w), 994 (w), 899 (w), 837 (m), 765 (s), 720 (m), 691 (s), 638 (w), 583 (m), 557 (m), 503 (s).

The analytical data is in accordance with those reported in the literature.[144]

5.3.4.1.21 Synthesis of [1,1'-biphenyl]-3-yl trifluoromethanesulfonate (4.1k):

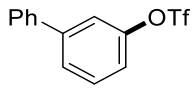

4.1k

Following general procedure 3.A, using [1,1'-biphenyl]-3-ol (2.94 mmol) and pyridine as the base afforded the title compound **4.1k** (0.886 g, 2.93 mmol, 80%) as a clear colorless oil after purification via column chromatography (pure *n*-pentane).

Rf = 0.29 (*n*-pentane, UV)

^{1}H NMR (300 MHz, Chloroform-*d*) δ 7.67 – 7.57 (m, 3H), 7.57 – 7.41 (m, 6H), 7.29 (dd, *J* = 8.3, 2.5 Hz, 1H).

^{13}C NMR (75 MHz, Chloroform-*d*) δ 150.2, 144.1, 139.1, 130.6, 128.5, 127.3, 127.2, 120.1, 119.9, 118.9 (q, *J* = 320.6 Hz).

^{19}F NMR (282 MHz, Chloroform-*d*) δ -72.83.

MS (EI): m/z (relative intensity) 303 (11), 302 (74), 238 (12), 141 (100), 115 (37), 66 (14).

HRMS (EI, *m*/*z*): calcd. for $C_{13}H_9O_3F_3S_2$ $[M]^+$ 302.0224, found 302.0219.

IR (ATR, neat, cm-1): 3067 (w), 3037 (w), 1608 (w), 1571 (w), 1477 (m), 1418 (s), 1244 (m), 1204 (s), 1126 (s), 1087 (w), 1048 (w), 1025 (w), 1000 (w), 897 (s), 806 (s), 755 (s), 690 (s), 613 (m), 599 (s), 574 (s), 511 (s), 452 (w), 420 (w).

The analytical data is in accordance with those reported in the literature.[145]

5.3.4.1.22 Synthesis of *N,N*-dimethyl-[1,1'-biphenyl]-3-amine hydrochloride (4.3k·HCl):

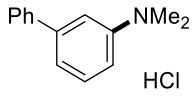

4.3k·HCl

Following general procedure 3.B, using [1,1'-biphenyl]-3-yl trifluoromethanesulfonate (**4.1k**) afforded the title compound **4.3k** (70 mg, 0.408 mmol, 77%) as a white crystalline solid after purification via column chromatography (*n*-pentane:EtOAc = 10:1).

Rf = 0.22 (*n*-pentane:EtOAc = 10:1, UV) free base

^{1}H NMR (300 MHz, Chloroform-*d*) δ 14.42 (s, 1H), 7.99 (s, 1H), 7.74 (d, *J* = 8.3 Hz, 1H), 7.64 (d, *J* = 7.7 Hz, 1H), 7.59 – 7.47 (m, 3H), 7.45 – 7.30 (m, 3H), 3.20 (s, 6H).

^{13}C NMR (75 MHz, Chloroform-*d*) δ 143.9, 143.5, 138.8, 130.9, 129.1, 128.8, 128.5, 127.2, 119.4, 119.3, 46.6.

MS (EI): m/z (relative intensity) 197 (94), 196 (100), 153 (12), 152 (22), 98 (12).

HRMS (ESY-TOF, *m*/*z*): calcd. for $C_{14}H_{15}N$ $[M+H]^+$ 198.1283, found 198.1283.

IR (ATR, neat, cm-1): 3017 (w), 2925 (w), 2852 (w), 2496 (w), 2380 (m), 1609 (w), 1594 (w), 1573 (w), 1514 (w), 1480 (m), 1462 (m), 1442 (m), 1419 (w), 1403 (w), 1321 (w), 1294 (w), 1270 (w), 1192 (m), 1156 (w), 1135 (m), 1096 (w), 1073 (w), 1052 (w), 1025 (w), 995 (m), 913 (m), 803 (m), 757 (s), 696 (s), 634 (m), 614 (w), 585 (m), 527 (w), 489 (w), 464 (w).

The analytical data is in accordance with those reported in the literature.[146]

5.3.4.1.23 Synthesis of 4-(1,3-dioxolan-2-yl)-N,N-dimethylaniline (4.3n):

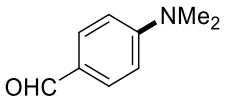

4.3n

Following general procedure B, using 4-(1,3-dioxolan-2-yl)phenyl trifluoromethane-sulfonate (**1l** ,523 mmol) afforded the title compound **4.3n** (77 mg, 0.516 mmol, 99%, free base) as a white solid after purification via column chromatography (*n*-pentane:EtOAc = 10:1).

Rf = 0.16 (*n*-pentane:EtOAc = 10:1, UV)

^{1}H NMR (300 MHz, Chloroform-*d*) δ 9.72 (s, 1H), 7.79 – 7.65 (m, 2H), 6.77 – 6.60 (m, 2H), 3.13 – 2.99 (m, 6H).

^{13}C NMR (75 MHz, Chloroform-*d*) δ 190.3, 154.3, 132.0, 125.1, 111.0, 40.1.

MS (EI): m/z (relative intensity) 149 (80), 148 (100), 132 (11), 77 (52).

HRMS (ESI-TOF, *m*/*z*): calcd. for $C_9H_{11}NO$ $[M+H]^+$ 150.0919, found 150.0921.

IR (ATR, neat, cm-1): 2918 (w), 2795 (w), 2713 (w), 1656 (w), 1589 (m), 1546 (m), 1529 (m), 1459 (w), 1431 (w), 1367 (m), 1311 (w), 1230 (s), 1161 (m), 1065 (m), 999 (w), 937 (w), 824 (m), 811 (s), 726 (m), 632 (w), 594 (m), 508 (m), 472 (w).

The analytical data is in accordance with those reported in the literature.[147]

5.3.4.1.24 Synthesis of *tert*-butyl 6-(((trifluoromethyl)sulfonyl)oxy)-1*H*-indole-1-carboxylate (4.1l):

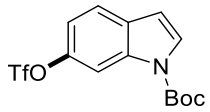

4.1l

Following general procedure A, using *tert*-butyl 6-hydroxy-1*H*-indole-1-carboxylate (2.23 mmol) and pyridine as the base afforded the title compound **4.1l** (675 mg, 1.85 mmol, 82%) as a clear colorless oil after purification via column chromatography (*n*-pentane:EtOAc = 50:1).

Rf = 0.50 (*n*-pentane:EtOAc = 10:1, UV)

^{1}H NMR (300 MHz, Chloroform-d) δ 8.15 (s, 1H), 7.69 (d, *J* = 3.8 Hz, 1H), 7.57 (d, *J* = 8.6 Hz, 1H), 7.15 (dd, *J* = 8.6, 2.4 Hz, 1H), 6.59 (dd, *J* = 3.7, 0.8 Hz, 1H), 1.69 (s, 9H).

^{13}C NMR (75 MHz, Chloroform-d) δ 149.1, 146.6, 134.8, 130.2, 128.0, 121.8, 118.9 (d, *J* = 320.9 Hz), 116.0, 108.9, 106.9, 84.8, 28.0.

^{19}F NMR (282 MHz, Chloroform-d) δ -72.82.

MS (EI): m/z (relative intensity) 365 (7), 309 (22), 292 (13), 265 (17), 200 (7), 176 (18), 132 (80), 104 (12), 103 (13), 69 (15), 57 (100), 41 (20).

HRMS (EI, *m*/*z*): calcd. for $C_{14}H_{14}O_5NF_3S$ $[M]^+$ 187.1235, found 187.1236.

IR (ATR, neat, cm-1): 2982 (w), 1738 (s), 1616 (w), 1534 (w), 1470 (w), 1445 (m), 1420 (s), 1372 (m), 1334 (s), 1291 (w), 1244 (s), 1202 (s), 1139 (s), 1121 (s), 1074 (m), 1040 (w), 1024 (m), 932 (s), 880 (s), 836 (s), 814 (s), 789 (m), 762 (m), 739 (w), 723 (m), 661 (w), 622 (m), 598 (s), 576 (m), 500 (s), 432 (m).

The analytical data is in accordance with those reported in the literature.[148]

5.3.4.1.25 Synthesis of *tert*-butyl 6-(dimethylamino)-1*H*-indole-1-carboxylate (4.3l):

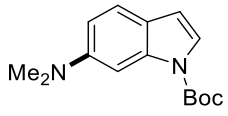

4.3l

Following general procedure B, using *tert*-butyl 6-(((trifluoromethyl)sulfonyl)oxy)-1H-indole-1-carboxylate (**4.1l**) afforded the title compound **4.3l** (89 mg, 0.342 mmol, 67%, free base) as a white solid after purification via column chromatography (*n*-pentane:EtOAc =10:1).

Rf = 0.36 (*n*-pentane:EtOAc = 10:1, UV) free base

^{1}H NMR (300 MHz, Chloroform-*d*) δ 7.60 (s, 1H), 7.46 = 7.32 (m, 2H), 6.80 (dd, *J* = 8.6, 2.3 Hz, 1H), 6.50 = 6.38 (m, 1H), 3.02 (s, 6H), 1.68 (s, 9H).

13C NMR (75 MHz, Chloroform-d) δ 150.2, 149.1, 137.0, 123.6, 121.8, 121.1, 110.7, 107.3, 99.7, 83.1, 41.7, 28.4.

MS (EI): m/z (relative intensity) 260 (20), 205 (13), 204 (100), 160 (46), 159 (61), 176 (18), 132 (80), 104 (12), 103 (13), 69 (15), 57 (100), 41 (20).

HRMS (ESY-TOF, *m*/*z*): calcd. for $C_{15}H_{20}N_2O_2$ $[M+H]^+$ 261.1603, found 261.1598.

IR (ATR, neat, cm-1): 2977 (w), 2930 (w), 2799 (w), 1724 (s), 1619 (m), 1575 (w), 1531 (m), 1500 (m), 1461 (w), 1440 (m), 1380 (s), 1368 (m), 1333 (s), 1288 (m), 1248 (s), 1222 (m), 1184 (m), 1161 (s), 1144 (s), 1132 (s), 1075 (m), 1038 (m), 1018 (s), 962 (s), 895 (m), 846 (s), 795 (m), 768 (s), 755 (m), 705 (m), 634 (m), 614 (m), 575 (m), 469 (w), 442 (w).

5.3.4.1.26 Synthesis of *N,N*-dimethyl-4-(2-methyl-1,3-dioxolan-2-yl)aniline (4.3o):

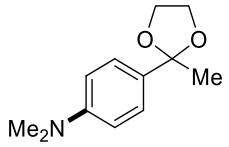

4.3o

Following general procedure B, using 4-(2-methyl-1,3-dioxolan-2-yl)phenyl trifluoromethanesulfonate (0.447 mmol) afforded the title compound **4.3o** (93 mg, 0.446 mmol, 99%, freebase) as a white solid after purification via column chromatography (*n*-pentane:EtOAc = 20:1).

Rf = 0.18 (*n*-pentane:EtOAc = 20:1, UV) free base

MS (EI): m/z (relative intensity) 207 (20), 193 (12), 192 (100), 148 (52).

^{1}H NMR (400 MHz, Chloroform-*d*) δ 7.28 – 7.22 (m, 2H), 6.63 – 6.58 (m, 2H), 3.99 – 3.84 (m, 2H), 3.77 – 3.63 (m, 2H), 2.85 (s, 6H), 1.56 (s, 3H).

^{13}C NMR (101 MHz, Chloroform-*d*) δ 149.1, 129.9, 125.1, 111.1, 108.0, 63.3, 39.5, 26.6.

MS (EI): m/z (relative intensity) 207 (20), 193 (12), 192 (100), 148 (52).

HRMS (ESY-TOF, *m*/*z*): calcd. for $C_9H_{13}N$ $[M+H]^+$ 208.1337, found 208.1339.

IR (ATR, neat, cm-1): 2995 (w), 2943 (w), 2890 (w), 2801 (w), 1611 (m), 1519 (m), 1445 (w), 1426 (w), 1373 (w), 1344 (m), 1257 (w), 1221 (m), 1198 (m), 1182 (s), 1137 (m), 1100 (m), 1078 (m), 1028 (s), 947 (m), 888 (m), 861 (s), 817 (s), 761 (w), 694 (w), 621 (w), 604 (w), 568 (m), 523 (m), 505 (m).

5.3.4.1.27 Synthesis of 4-(1H-pyrrol-1-yl)phenyl trifluoromethanesulfonate (4.1m):

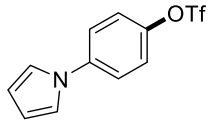

4.1m

Following general procedure A, using benzo[d][1,3]dioxol-5-ol (3.14 mmol) and pyridine as the base afforded the title compound **4.1m** (350 mg, 1.20 mmol, 38%) as a clear colorless oil after purification via column chromatography (*n*-pentane:EtOAc 50:1).

Rf = 0.08 (*n*-pentane, UV)

^{1}H NMR (300 MHz, Chloroform-*d*) δ 7.51 – 7.40 (m, 2H), 7.41 – 7.30 (m, 2H), 7.11 – 7.03 (m, 2H), 6.43 – 6.35 (m, 2H).

^{13}C NMR (75 MHz, Chloroform-*d*) δ 146.7, 140.6, 122.7, 121.7, 119.3, 118.8 (q, *J* = 320.9 Hz), 111.4.

^{19}F NMR (282 MHz, Chloroform-*d*) δ -72.69.

MS (EI): m/z (relative intensity) 291 (46), 159 (12), 158 (100), 130 (38), 103 (15), 77 (20), 69 (12) 69(18).

HRMS (ESY-TOF, *m*/*z*): calcd. for $C_{14}H_{15}N$ $[M+H]^+$ 292.0255, found 292.0251.

IR (ATR, neat, cm-1): 3137 (w), 3094 (w), 1603 (w), 1514 (s), 1425 (s), 1412 (s), 1329 (m), 1250 (m), 1207 (s), 1191 (s), 1133 (s), 1070 (s), 1012 (m), 938 (w), 921 (w), 881 (s), 832 (s), 781 (m), 753 (m), 723 (s), 645 (m), 632 (m), 604 (s), 571 (s), 527 (s), 503 (s), 441 (m).

The analytical data is in accordance with those reported in the literature.[149]

5.3.4.1.28 Synthesis of *N,N*-dimethyl-4-(1H-pyrrol-1-yl)aniline hydrochloride (4.3m·HCl):

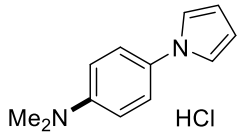

4.3m·HCl

Following general procedure B, using 4-(1H-pyrrol-1-yl)phenyl trifluoromethanesulfonate (**4.1m**) afforded the title compound **4.3m** (111 mg, 0.498 mmol, 99%) as a white crystalline solid after purification via column chromatography (*n*-pentane:EtOAc - 20:1) and treatment with 2 M HCl in Et_2O.

R_f = 0.44 (*n*-pentane:EtOAc - 10:1, UV) free base

^{1}H NMR (300 MHz, Chloroform-*d*) δ 14.34 (br. s, 1H), 7.87 (d, *J* = 8.9 Hz, 2H), 7.54 – 7.41 (m, 2H), 7.12 – 7.00 (m, 2H), 6.40 – 6.29 (m, 2H), 3.20 (s, 6H), 2.02 (br. s, 1H).

^{13}C NMR (75 MHz, Chloroform-*d*) δ 141.8, 139.7, 122.4, 121.5, 119.1, 111.7, 46.7.

MS (EI): m/z (relative intensity) 187 (13), 186 (100), 185 (44), 171 (32), 170 (26), 143 (12), 115 (16).

HRMS (EI, *m*/*z*): calcd. for $C_{12}H_{14}N_2$ $[M]^+$ 187.1235, found 187.1236.

IR (ATR, neat, cm-1): 3479 (w), 3410 (w), 3054 (w), 3011 (w), 2498 (w), 2347 (w), 1612 (w), 1523 (m), 1489 (w), 1473 (w), 1413 (w), 1329 (m), 1253 (w), 1203 (w), 1188 (w), 1159 (w), 1141 (m), 1123 (w), 1074 (w), 1060 (w), 1013 (w), 996 (w), 919 (w), 899 (w), 869 (w), 851 (w), 830 (m), 770 (w), 733 (s), 638 (w), 608 (w), 548 (m), 510 (m), 484 (m).

The analytical data is in accordance with those reported in the literature.[150]

5.3.4.1.29 Synthesis of (8R,9S,13S)-13-methyl-6,7,8,9,11,12,13,14,15,16-decahydrospiro [cyclopenta [a]phenanthrene- 17,2'-[1,3]dioxolan]-3-yl trifluoromethane-sulfonate (4.1p):

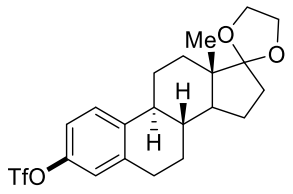

4.1p

Following general procedure A, using carbonyl protected estrogen (3.28 mmol) and NEt_3 as the base afforded the title compound **4.1p** (1.44 g, 3.23 mmol, 99%) as a clear colorless oil after purification via column chromatography (*n*-pentan:EtOAc = 50:1).

R_f = 0.70 (*n*-pentan:EtOAc = 10:1, UV)

^{1}H NMR (300 MHz, Chloroform-d) δ 7.33 (d, *J* = 8.6 Hz, 1H), 7.01 (dd, *J* = 8.6, 2.8 Hz, 1H), 6.96 (d, *J* = 2.7 Hz, 1H), 4.01 – 3.83 (m, 4H), 2.92 – 2.84 (m, 2H), 2.38 – 2.18 (m, 2H), 2.09 – 1.71 (m, 5H), 1.70 – 1.22 (m, 6H), 0.88 (s, 3H).

^{13}C NMR (75 MHz, Chloroform-d) δ 147.6, 141.1, 139.7, 127.3, 121.2, 119.4, 118.9 (q, *J* = 320.7 Hz), 118.2, 65.4, 64.7, 49.4, 46.1, 43.9, 38.6, 34.3, 30.7, 29.6, 26.7, 26.0, 22.5, 14.4.

^{19}F NMR (282 MHz, Chloroform-d) δ -72.97.

MS (EI): m/z (relative intensity) 446 (6), 384 (15), 99 (100), 86 (12), 84 (10), 28 (35).

HRMS (EI, *m*/*z*): calcd. for $C_{21}H_{25}O_5F_3S_1[M]^+$ 446.1369, found 446.1370.

IR (ATR, neat, cm-1): 2973 (w), 2938 (w), 2872 (w), 1739 (w), 1606 (w), 1583 (w), 1489 (m), 1456 (w), 1418 (s), 1381 (w), 1339 (w), 1308 (w), 1274 (w), 1248 (m), 1204 (s), 1182 (m), 1163 (m), 1139 (s), 1118 (s), 1105 (m), 1075 (w), 1060 (m), 1044 (m), 1032 (m), 1013 (m), 984 (w), 963 (m), 948 (m), 915 (s), 882 (m), 849 (m), 836 (m), 818 (m), 780 (m), 765 (w), 751 (w), 718 (w), 704 (w), 657 (w), 603 (s), 565 (m), 548 (w), 535 (w), 511 (m), 491 (w), 477 (w), 453 (w), 422 (w), 404 (w).

The analytical data is in accordance with those reported in the literature.[151]

5.3.4.1.30 Synthesis of (8R,9S,13S,14S)-*N,N,*13-trimethyl-6,7,8,9,11,12,13,14,15,16-decahydrospiro [cyclopenta[a] phenanthrene-17,2'-[1,3]dioxolan]-3-amine (4.3p):

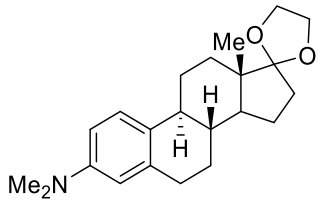

4.3p

Following general procedure B, using (8R,9S,13S,14S)-13-methyl-6,7,8,9,11,12,13,14,-15,16-decahydrospiro [cyclopenta[a]phenanthrene-17,2'-[1,3]dioxolan]-3-yl trifluoromethane-sulfonate (**4.1p**, 0.365 mmol) afforded the title compound **4.3p** (110 mg, 0.322 mmol, 88%, Freebase) as a white solid after purification via column chromatography (*n*-pentane:EtOAc = 4:1).

Rf = 0.08 (*n*-pentane:EtOAc = 8:1, UV) free base

m.p. = 90.3 °C

^{1}H NMR (400 MHz, Chloroform-d) δ 7.19 (d, *J* = 8.6 Hz, 1H), 6.64 (d, *J* = 7.4 Hz, 1H), 6.53 (s, 1H), 4.02 – 3.84 (m, 4H), 2.91 (s, 6H), 2.89 – 2.77 (m, 2H), 2.37 – 2.17 (m, 2H), 2.09 – 1.98 (m, 1H), 1.94 – 1.71 (m, 4H), 1.69 – 1.59 (m, 1H), 1.57 – 1.26 (m, 5H), 0.88 (s, 3H).

^{13}C NMR (101 MHz, CDCl3) δ 137.5, 126.2, 119.6, 113.7, 111.4, 77.4, 65.4, 64.7, 49.5, 46.4, 43.7, 41.3, 39.4, 34.4, 30.9, 30.2, 27.3, 26.3, 22.5, 14.5.

MS (EI): m/z (relative intensity) 341 (49), 240 (17), 186 (12), 172 (19), 158 (17), 129 (12), 99 (100), 86 (14), 55 (15), 43 (16).

HRMS (EI, *m*/*z*): calcd. for $C_{20}H_{26}O_3[M]^+$ 341.2349, found 341.2368.

IR (ATR, neat, cm-1): 2972 (w), 2921 (m), 2870 (m), 2808 (m), 1610 (m), 1561 (w), 1509 (s), 1469 (m), 1458 (m), 1436 (m), 1409 (w), 1376 (m), 1354 (m), 1337 (m), 1299 (m), 1275 (m), 1224 (s), 1195 (m), 1180 (m), 1157 (s), 1120 (s), 1103 (s), 1074 (m), 1059 (s), 1045 (s),

1031 (s), 1010 (m), 1001 (m), 985 (m), 955 (s), 934 (m), 918 (m), 884 (m), 856 (m), 836 (m), 803 (m), 773 (s), 747 (m), 713 (m), 696 (m), 650 (m), 629 (m), 587 (m), 572 (m), 525 (m), 511 (m), 483 (m), 443 (m), 420 (m), 406 (m).

5.3.4.1.31 Synthesis of (8R,9S,13S)-13-methyl-17-oxo-7,8,9,11,12,13,14,15,16,17-decahydro-6H-cyclopenta[a]phenanthren-3-yl trifluoromethanesulfonate (4.1q):

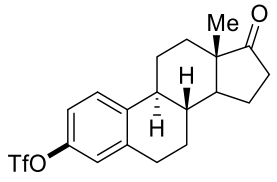

4.1q

Following general procedure A, using estrogen (3.70 mmol) and NEt_3 as the base afforded the title compound **4.1q** (1.46 g, 19.24 mmol, 98%) as a white solid after purification via column chromatography (*n*-pentane:EtOAc = 5:1).

R_f = 0.30 (*n*-pentane:EtOAc = 5:1, UV)

m.p. = 91.3 °C

^{1}H NMR (300 MHz, Chloroform-d) δ 7.34 (d, *J* = 8.5 Hz, 1H), 7.03 (dd, *J* = 8.6, 2.8 Hz, 1H), 6.99 (d, *J* = 2.6 Hz, 1H), 2.94 (dd, *J* = 8.7, 4.3 Hz, 2H), 2.59 – 2.46 (m, 1H), 2.45 – 2.36 (m, 1H), 2.30 (td, *J* = 10.4, 9.9, 4.1 Hz, 1H), 2.23 – 1.91 (m, 4H), 1.73 – 1.38 (m, 6H), 0.92 (s, 3H).

^{13}C NMR (75 MHz, Chloroform-d) δ 220.5, 147.7, 140.4, 139.4, 127.3, 121.4, 118.9 (q, *J* = 320.8 Hz), 118.4, 50.5, 48.0, 44.2, 37.9, 35.9, 31.6, 29.5, 26.2, 25.8, 21.7, 13.9.

^{19}F NMR (282 MHz, Chloroform-d) δ -72.97.

MS (EI): m/z (relative intensity) 402 (60), 358 (35), 345 (22), 292 (11), 251 (17), 225 (22), 213 (35), 185 (14), 157 (17), 129 (24), 128 (23), 115 (39), 91 (22), 69 (100), 55 (24), 41 (24).

HRMS (EI, *m*/*z*): calcd. for $C_{21}H_{25}O_5F_3S_1[M]^+$ 402.1107, found 402.1105.

IR (ATR, neat, cm-1): 2966 (w), 2931 (w), 2869 (w), 1736 (s), 1604 (w), 1488 (w), 1455 (w), 1418 (s), 1405 (m), 1373 (w), 1338 (w), 1275 (w), 1249 (m), 1207 (s), 1137 (s), 1085 (m), 1054 (m), 1007 (m), 983 (w), 951 (w), 916 (s), 901 (m), 879 (m), 848 (m), 836 (s), 820 (m), 785 (m), 766 (w), 723 (w), 714 (w), 702 (m), 654 (w), 639 (w), 620 (m), 605 (s), 578 (m), 548 (m), 506 (m), 487 (w), 475 (w), 443 (m).

The analytical data is in accordance with those reported in the literature.[152]

5.3.4.1.32 Synthesis of (8*R*,9*S*,13*S*,14*S*)-3-(dimethylamino)-13-methyl-6,7,8,9,11,12,13,14,15,16-decahydro-17*H*-cyclopenta[*a*]phenanthren-17-one (4.3q):

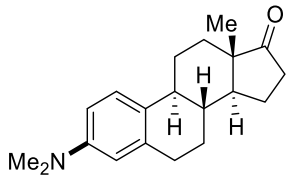

4.3q

Following general procedure B, using (8*R*,9*S*,13*S*,14*S*)-13-methyl-17-oxo-7,8,9,11,12,13,14,15,16,17-decahydro-6*H*-cyclopenta[a]phenanthren-3-yl trifluoromethanesulfonate (**4.1q**, 0.532 mmol) afforded the title compound **4.3q** (87%, 138 mg, 0.463 mmol, freebase) as a white solid after purification via column chromatography (*n*-pentane:EtOAc = 20:1).

Rf = 0.44 (*n*-pentane:EtOAc = 10:1, UV) free base

^{1}H NMR (300 MHz, Chloroform-d) δ 7.19 (d, *J* = 8.7 Hz, 1H), 6.63 (dd, *J* = 8.6, 2.8 Hz, 1H), 6.52 (d, *J* = 2.8 Hz, 1H), 2.98 – 2.88 (m, 7H), 2.59 – 1.89 (m, 7H), 1.74 – 1.37 (m, 6H), 1.28 (s, 1H), 0.92 (s, 3H).

^{13}C NMR (75 MHz, Chloroform-d) δ 221.2, 149.0, 137.0, 128.3, 126.0, 113.2, 111.1, 50.4, 48.1, 44.0, 40.9, 38.6, 35.9, 31.7, 30.0, 26.8, 26.0, 21.6, 13.9.

MS (EI): m/z (relative intensity) 298 (22), 297 (100), 296 (12), 212 (20), 173 (38), 172 (12).

HRMS (EI, *m*/*z*): calcd. for $C_{20}H_{27}NO$ $[M]^+$ 298.2171, found 298.2167.

IR (ATR, neat, cm-1): 2972 (w), 2921 (m), 2870 (m), 2808 (m), 1610 (m), 1561 (w), 1509 (s), 1469 (m), 1458 (m), 1436 (m), 1409 (w), 1376 (m), 1354 (m), 1337 (m), 1299 (m), 1275 (m), 1224 (s), 1195 (m), 1180 (m), 1157 (s), 1120 (s), 1103 (s), 1074 (m), 1059 (s), 1045 (s), 1031 (s), 1010 (m), 1001 (m), 985 (m), 955 (s), 934 (m), 918 (m), 884 (m), 856 (m), 836 (m), 803 (m), 773 (s), 747 (m), 713 (m), 696 (m), 650 (m), 629 (m), 587 (m), 572 (m), 525 (m), 511 (m), 483 (m), 443 (m), 420 (m), 406 (m).

Crystal data of CCDC1981523: $C_{20}H_{27}NO$, *M* = 297.42, orthorhombic, space group $P2_12_12_1$, $\bar{1}a$ = 8.2340(2), *b* = 12.4121(4), *c* = 16.2533(5) Å, *V* = 1661.11(8) Å^3, *T* = 150(2) K, *Z* = 4, 9416 reflections measured, 2923 independent reflections (R_{int} = 0.0317), final *R* values ($I > 2\sigma(I)$): R_1 = 0.0442, wR_2 = 0.1217, final *R* values (all data): R_1 = 0.0453, wR_2 = 0.1234, 202 parameters.

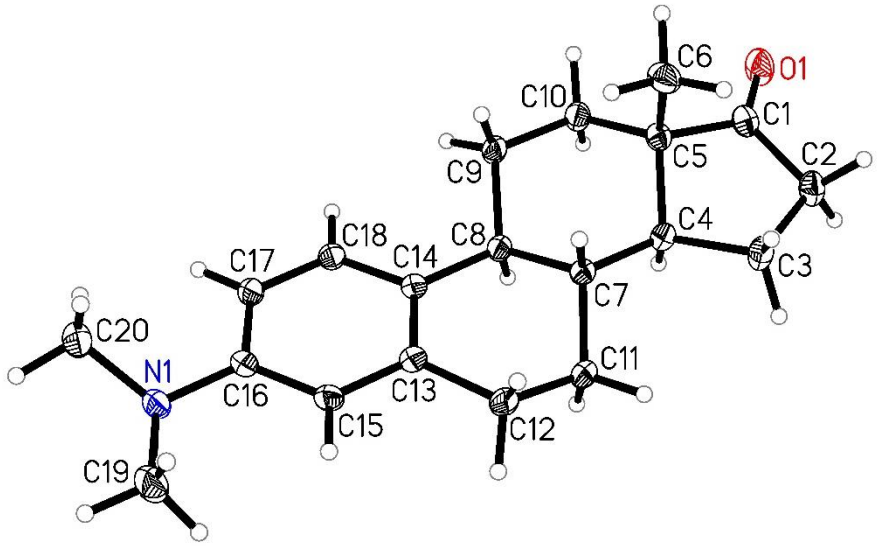

Figure 5.24. Molecular structure of CCDC1981523. Displacement ellipsoids correspond to 30% probability.

5.3.4.1.33 Synthesis of 4-allyl-2-methoxyphenyl trifluoromethanesulfonate (4.1s):

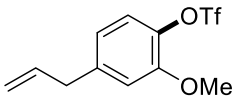

4.1s

Following general procedure A, using 4-allyl-2-methoxyphenol (3.50 mmol) and 2,6-dimethylpyridine as the base afforded the title compound **4.1s** (830 mg, 2.67 mmol; 76%) as a colorless oil after purification via column chromatography (*n*-pentane:EtOAc = 20:1).

Rf = 0.45 (*n*-pentane:EtOAc = 20:1, UV)

^{1}H NMR (300 MHz, Chloroform-*d*) 7.14 (d, *J* = 8.3 Hz, 1H), 6.87 (d, *J* = 2.0 Hz, 1H), 6.80 (dd, *J* = 8.3, 2.0 Hz, 1H), 6.07 – 5.80 (m, 1H), 5.21 – 5.04 (m, 2H), 3.90 (s, 3H), 3.40 (d, *J* = 6.8 Hz, 1H).

^{13}C NMR (75 MHz, Chloroform-*d*) 151.3, 142.0, 137.2, 136.4, 122.2, 120.9, 118.9 (q, *J* = 320.5 Hz), 116.9, 113.5, 56.2, 40.1.

^{19}F NMR (282 MHz, Chloroform-*d*) δ -74.00.

MS (EI): m/z (relative intensity) 296 (34), 164 (11), 163 (100), 107 (19), 105 (12), 103 (40), 91 (38), 79 (16), 77 (19), 69 (19), 65 (13), 41 (18), 39 (10).

HRMS (ESffI-TOF, *m*/*z*): calcd. for $C_{11}H_{11}O_4F_3S$ $[M]^+$ 296.0325, found 296.0318.

IR (ATR, neat, cm-1): 3082 (w), 3012 (w), 2980 (w), 2944 (w), 2916 (w), 2847 (w), 1640 (w), 1606 (m), 1503 (m), 1465 (w), 1417 (s), 1291 (w), 1270 (m), 1248 (m), 1201 (s), 1175 (m), 1137 (s), 1105 (s), 1032 (m), 995 (w), 903 (m), 873 (s), 815 (m), 774 (w), 751 (m), 708 (m), 616 (s), 571 (m), 546 (w), 500 (s), 456 (w).

The analytical data is in accordance with those reported in the literature.[117]

5.3.4.1.34 Synthesis of 4-allyl-2-methoxy-*N,N*-dimethylaniline hydrochloride (4.3s·HCl):

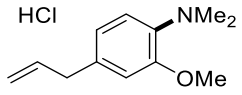

4.3s·HCl

Following general procedure B, using 4-allyl-2-methoxyphenyl trifluoromethanesulfonate (**4.1s**, 0.526 mmol) afforded the title compound **4.3s** (35 mg, 0.154 mmol, 29%) as a white solid after purification via column chromatography (*n*-pentane:EtOAc = 20:1) and treatment with 2 M HCl in Et_2O.

Rf = 0.36 (*n*-pentane:EtOAc = 20:1, UV) free base

^{1}H NMR (300 MHz, Chloroform-*d*) δ 13.76 (s, 1H), 7.95 (d, *J* = 8.0 Hz, 1H), 6.81 (d, *J* = 1.6 Hz, 1H), 6.77 (dd, *J* = 8.2, 1.6 Hz, 1H), 5.94 – 5.75 (m, 1H), 5.03 (dd, *J* = 8.3, 1.5 Hz, 1H), 3.92 (s, 3H), 3.33 (d, *J* = 6.8 Hz, 1H).

^{13}C NMR (75 MHz, Chloroform-*d*) δ 152.3, 144.1, 135.9, 128.4, 123.7, 121.7, 117.1, 113.3, 56.0, 44.8, 40.00.

MS (EI): m/z (relative intensity) 192 (13), 191 (100), 177 (10), 176 (81), 174 (11), 160 (13), 91 (10), 42 (24).

HRMS (ESI-TOF, *m*/*z*): calcd. for $C_{12}H_{17}NO$ $[M]^+$ 192.1388, found 192.1393.

5.3.4.1.35 Synthesis of 2-methoxy-4-propylphenyl trifluoromethanesulfonate (4.1t):

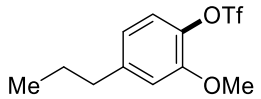

4.1t

Following general procedure A, using 2-methoxy-4-propylphenol (3.17 mmol) and pyridine as the base afforded the title compound **4.1t** (830 mg, 2.78 mmol, 88%) as a colorless oil after purification via column chromatography (*n*-pentane:EtOAc = 20:1).

Rf = 0.45 (*n*-pentane:EtOAc = 20:1, UV)

1H NMR (300 MHz, Chloroform-d) δ 7.12 (d, *J* = 8.3 Hz, 1H), 6.86 (d, *J* = 2.0 Hz, 1H), 6.78 (dd, *J* = 8.3, 1.9 Hz, 1H), 3.89 (s, 3H), 2.67 – 2.54 (m, 2H), 1.87 – 1.51 (m, 2H), 0.97 (t, *J* = 7.3 Hz, 3H).

^{13}C NMR (75 MHz, Chloroform-*d*) 151.0, 144.5, 136.8, 121.9, 120.6, 118.8 (q, *J* = 320.4 Hz), 113.2, 56.0, 37.9, 24.4, 13.7.

^{19}F NMR (282 MHz, Chloroform-*d*) δ -74.13.

MS (EI): m/z (relative intensity) 298 (25), 166 (11), 165 (100), 109 (11), 107 (10), 105 (11), 95 (27), 79 (10), 77 (19), 69 (15), 65 (10), 43 (20).

HRMS (EI, *m*/*z*): calcd. for $C_{11}H_{13}O_4F_3S$ $[M]^+$ 298.0481, found 298.0484.

IR (ATR, neat, cm-1): 2964 (w), 2937 (w), 2874 (w), 1605 (m), 1504 (m), 1465 (w), 1417 (s), 1291 (m), 1268 (m), 1248 (m), 1202 (s), 1179 (s), 1138 (s), 1107 (s), 1032 (m), 936 (w), 876 (s), 815 (m), 788 (w), 740 (m), 704 (w), 612 (s), 546 (w), 504 (s), 458 (s).

The analytical data is in accordance with those reported in the literature.[153]

5.3.4.1.36 Synthesis of 2-methoxy-*N,N*-dimethyl-4-propylaniline hydrochloride (4.3t·HCl):

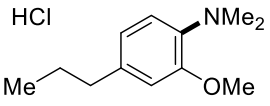

4.3t·HCl

Following general procedure 3.B, using 2-methoxy-4-propylphenyl trifluoromethanesulfonate (**4.1t**) afforded the title compound **4.3t** (40 mg, 0.170 mmol, 34%) as a white solid after purification via column chromatography (*n*-pentane:EtOAc = 20:1) and treatment with 2 M HCl in Et_2O.

Rf = 0.40 (*n*-pentane:EtOAc = 20:1, UV) free base

^{1}H NMR (300 MHz, Chloroform-*d*) δ 7.92 (d, *J* = 8.1 Hz, 1H), 6.78 (d, *J* = 1.6 Hz, 1H), 6.74 (dd, *J* = 8.1, 1.6 Hz, 1H), 3.91 (s, 3H), 2.58 – 2.44 (m, 2H), 3.17 (s, 7H), 2.56 – 2.48 (m, 2H), 1.65 – 1.48 (m, 2H), 0.87 (t, *J* = 7.3 Hz, 3H).

^{13}C NMR (75 MHz, Chloroform-*d*) δ 152.1, 146.7, 127.9, 123.5, 121.4, 113.2, 55.9, 44.7, 37.9, 24.3, 13.7.

MS (EI): m/z (relative intensity) 193 (49), 178 (23), 165 (11), 164 (100), 149 (16), 134 (15).

HRMS (ESI-TOF, *m*/*z*): calcd. for $C_{12}H_{19}NO$ $[M]^+$ 194.1545, found 194.1548.

5.3.4.1.37 Synthesis of 4-formyl-2-methoxyphenyl trifluoromethanesulfonate (4.1u):

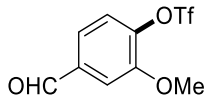

4.1u

Following general procedure 3.A, using 2-methoxy-4-propylphenol (3.17 mmol) and pyridine as the base afforded the title compound **4.1u** (1.080 g, 3.80 mmol, 76%) as a colorless oil after purification via column chromatography (*n*-pentane:EtOAc = 20:1).

Rf = 0.33 (*n*-pentane:EtOAc = 5:1)

^{1}H NMR (300 MHz, Chloroform-*d*) δ 9.97 (s, 1H), 7.58 – 7.54 (m, 1H), 7.53 – 7.45 (m, 1H), 7.40 (dd, *J* = 8.2, 0.9 Hz, 1H), 3.99 (s, 3H).

^{13}C NMR (75 MHz, Chloroform-*d*) δ 190.4, 152.2, 142.7, 136.8, 124.1, 123.2, 118.7 (q, *J* = 320.5 Hz), 111.8, 56.5.

^{19}F NMR (282 MHz, Chloroform-*d*) δ -73.79.

MS (EI): m/z (relative intensity) 284 (77), 151 (100), 95 (71), 80 (14), 79 (29), 77 (36), 69 (32), 67 (15), 65 (22), 52 (17), 51 (28), 50 (11).

HRMS (EI, *m*/*z*): calcd. for $C_9H_7O_5F_{3S}$ $[M]^+$ 283.9961, found 283.9964.

IR (ATR, neat, cm-1): 2857 (w), 2842 (w), 2736 (w), 1704 (m), 1605 (m), 1499 (m), 1466 (w), 1420 (s), 1388 (m), 1318 (w), 1278 (m), 1248 (m), 1203 (s), 1134 (s), 1101 (s), 1027 (m), 957 (w), 931 (w), 868 (s), 820 (m), 778 (m), 733 (m), 711 (m), 611 (s), 590 (s), 569 (m), 539 (m), 509 (m), 467 (m), 451 (m).

The analytical data is in accordance with those reported in the literature.[154]

5.3.4.1.38 Synthesis of 4-(dimethylamino)-3-methoxybenzaldehyde hydrochloride (4.3u·HCl):

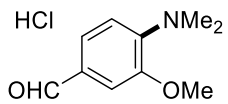

4.3u·HCl

Following general procedure B, using 4-formyl-2-methoxyphenyl trifluoromethanesulfonate (**4.1u**) afforded the title compound **4.3u** (16 mg, 0.074 mmol, 15%) as a white solid after purification via column chromatography (*n*-pentane:EtOAc = 5:1) and treatment with 2 M HCl in Et_2O.

Rf = 0.26 (*n*-pentane:EtOAc = 5:1) free base

^{1}H NMR (300 MHz, Chloroform-*d*) δ 9.81 (s, 1H), 7.40 (dd, *J* = 8.0, 1.8 Hz, 1H), 7.36 (d, *J* = 1.8 Hz, 1H), 6.94 (d, *J* = 8.4 Hz, 1H), 3.93 (s, 3H), 2.95 (s, 6H).

^{13}C NMR (75 MHz, Chloroform-*d*) δ 191.0, 151.8, 126.9, 116.7, 109.3, 77.4, 55.8, 42.8, 29.8.

MS (EI): m/z (relative intensity) 180 (11), 179 (100), 178 (14), 164 (67), 162 (20), 148 (20), 108 (10), 92 (14), 65 (13), 42 (19).

HRMS (ESI-TOF, *m*/*z*): calcd. for $C_{12}H_{13}NO_2$ $[M]^+$ 180.1024, found 180.1026.

The analytical data is in accordance with those reported in the literature.[155]

5.3.4.1.39 Synthesis of [1,1'-biphenyl]-2-yl trifluoromethanesulfonate (4.1v):

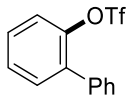

4.1v

Following general procedure A, using [1,1'-biphenyl]-2-ol (2.94 mmol) and pyridine as the base afforded the title compound **4.1v** (875 mg, 2.89 mmol, 95%) as a clear colorless oil after purification via column chromatography (*n*-pentane:EtOAc = 50:1).

Rf = 0.55 (*n*-Pentan:EtOAc = 20:1, UV)

^{1}H NMR (300 MHz, Chloroform-*d*) δ 7.54 – 7.41 (m, 9H).

^{13}C NMR (75 MHz, Chloroform-*d*) δ 146.9, 135.6, 132.0, 129.4, 129.0, 128.6, 128.5, 128.4, 122.1, 118.4 (q, *J* = 320.5 Hz).

^{19}F NMR (282 MHz, Chloroform-*d*) δ -74.09.

MS (EI): m/z (relative intensity) 302 (47), 170 (13), 169 (100), 141 (33), 139 (14), 115 (29).

HRMS (EI, *m*/*z*): calcd. for $C_{13}H_9O_3F_3S$ $[M]^+$ 302.0219, found 302.0221.

IR (ATR, neat, cm-1): 3066 (w), 3035 (w), 1504 (w), 1476 (m), 1419 (s), 1360 (w), 1246 (m), 1202 (m), 1135 (s), 1099 (s), 1076 (w), 1046 (m), 1011 (w), 948 (w), 881 (s), 783 (s), 763 (s), 751 (s), 731 (s), 697 (s), 646 (m), 624 (s), 593 (s), 570 (s) , 462 (m) , 436 (m).

The analytical data is in accordance with those reported in the literature.[145]

5.3.4.1.40 Synthesis of 4-acetylphenyl trifluoromethanesulfonate (4.1r):

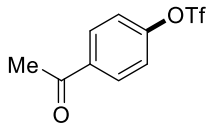

4.1r

Following general procedure 3.A, using 1-(4-hydroxyphenyl)ethan-1-one (11.02 mmol) at 0 °C instead of −78 °C and triethylamine as the base afforded the title compound **4.1r** (2.82 g, 10.51 mmol, 95%) as a clear colorless oil after purification via column chromatography (*n*-pentane:EtOAc = 5:1).

Rf = 0.27 (*n*-Pentan:EtOAc = 5:1, UV)

^{1}H NMR (300 MHz, Chloroform-*d*) δ 8.04 (d, *J* = 8.9 Hz, 2H), 7.36 (d, *J* = 8.8 Hz, 2H), 2.61 (s, 3H).

^{13}C NMR (75 MHz, Chloroform-*d*) δ 196.1, 152.5, 136.9, 130.6, 121.7, 118.7 (q, *J* = 320.8 Hz), 26.7.

^{19}F NMR (282 MHz, Chloroform-*d*) δ -73.03 (dd, *J* = 10.0, 4.8 Hz).

MS (EI): m/z (relative intensity) 268 (17), 253 (100), 95 (12).

HRMS (EI, *m*/*z*): calcd. for $C_9H_7O_4F_3S$ $[M]^+$ 268.0012, found 268.0005.

IR (ATR, neat, cm-1): 1690 (m), 1594 (w), 1497 (w), 1423 (m), 1409 (m), 1360 (w), 1301 (w), 1263 (m), 1250 (m), 1205 (s), 1132 (s), 1077 (w), 1014 (w), 960 (w), 879 (s), 842 (s), 787 (m), 762 (w), 672 (m), 632 (m), 607 (s), 585 (s), 571 (m), 524 (m), 471 (w), 422 (w).

The analytical data is in accordance with those reported in the literature.[156]

5.3.4.1.41 Synthesis of 1-(4-(dimethylamino)phenyl)ethan-1-one hydrochloride (4.3r·HCl):

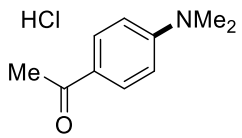

4.3r·HCl

Following general procedure 3.B, using 4-formyl-2-methoxyphenyl trifluoromethanesulfonate (**4.1r**) afforded the title compound **4.3r** (15 mg, 0.092 mmol, 18%) as a white solid after purification via column chromatography (*n*-pentane:EtOAc = 10:1) and treatment with 2 M HCl in Et_2O.

Rf = 0.20 (*n*-pentane:EtOAc = 5:1, UV) free base

^{1}H NMR (300 MHz, Chloroform-*d*) δ 7.94 – 7.84 (m, 1H), 6.73 – 6.59 (m, 1H), 3.07 (s, 3H), 2.52 (s, 2H).

^{13}C NMR (75 MHz, Chloroform-*d*) δ 196.4, 153.4, 130.5, 125.4, 110.7, 40.1, 26.0.

MS (EI): m/z (relative intensity) 163 (30), 148 (100), 118 (10), 104 (12), 91 (11), 78 (10), 77 (23), 74 (13), 63 (13), 51 (13), 50 (11), 43 (29), 42 (39).

HRMS (ESI-TOF, *m*/*z*): calcd. for $C_{10}H_{13}NO$ $[M+H]^+$ 164.1075, found 164.1075.

IR (ATR, neat, cm-1): 2901 (w), 2822 (w), 2651 (w), 1649 (m), 1586 (m), 1547 (w), 1522 (w), 1429 (m), 1413 (m), 1356 (m), 1313 (m), 1282 (m), 1229 (m), 1187 (m), 1130 (m), 1067 (m), 1018 (m), 943 (m), 814 (s), 654 (m), 592 (m), 560 (m), 498 (m).

The analytical data is in accordance with those reported in the literature.[157]

5.3.4.1.42 2-isopropylphenyl trifluoromethanesulfonate (4.1x):

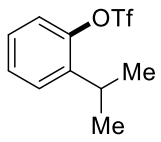

4.1x

Following general procedure A, using 2-isopropylphenol (7.34 mmol) with pyridine as the base afforded the title compound **4.1x** (1.96 g, 7.34 mmol, 99%) as a clear colorless oil after purification via column chromatography (*n*-pentane:EtOAc = 50:1).

Rf = 0.35 (n-Pentan:EtOAc = 50:1, UV);

^{1}H NMR (300 MHz, Chloroform-d) δ 7.45 – 7.39 (m, 1H), 7.38 – 7.30 (m, 1H), 7.29 – 7.22 (m, 2H), 3.33 (hept, *J* = 6.9 Hz, 1H), 1.28 (d, *J* = 6.9 Hz, 6H).

^{13}C NMR (75 MHz, CDCl3) δ 147.15, 141.23, 128.60, 127.83, 127.42, 121.18, 118.67 (q, *J* = 319.9 Hz), 27.12, 23.04;

^{19}F NMR (282 MHz, CDCl3) δ -74.07;

MS (EI): m/z (relative intensity) 268 (81), 254 (10), 253 (100), 135 (27), 134 (14), 120 (48), 119 (21), 118 (15), 107 (43), 103 (36), 95 (23), 92 (11), 91 (74), 77 (20), 69 (23), 65 (15), 39 (11);

HRMS (EI, m/z): calcd. for $C_{10}H_{11}O_3F_3S$ [M]+ 268.0376, found 268.0370.

5.3.4.1.43 2-isopropyl-*N*,*N*-dimethylaniline hydrochloride (4.3x·HCl):

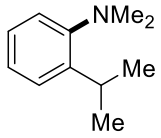

4.3x

Following general procedure B, using 2-isopropylphenyl trifluoromethanesulfonate (**4.1x**) afforded the title compound **4.3x** (24 mg, 0.120 mmol, 24%) as a white solid after purification via column chromatography (*n*-pentane:EtOAc = 10:1) and treatment with 2 M HCl in Et_2O.

R_f = 0.54 (*n*-pentane:EtOAc = 10:1, UV) free base.

^{1}H NMR (400 MHz, Chloroform-d) δ 7.29 (m, 1H), 7.21 – 7.13 (m, 2H), 7.10 (m, 1H), 3.58 (hept, *J* = 6.9 Hz, 1H), 2.71 (s, 6H), 1.26 (d, *J* = 6.9 Hz, 6H).

^{13}C NMR (75 MHz, CDCl3) δ 152.0, 144.3, 126.6, 126.3, 124.1, 119.7, 46.0, 26.8, 24.3.

MS (EI): m/z (relative intensity) 163 (71), 162 (11), 149 (13), 148 (100), 134 (18), 133 (45), 132 (34), 118 (38), 117 (20), 91 (11), 77 (12).

HRMS (ESI-TOF, *m*/*z*): calcd. for $C_{11}H_{17}N$ $[M+H]^+$ 164.1439, found 164.1440.

The analytical data is in accordance with those reported in the literature.[88d]

5.3.4.1.44 Synthesis of *o*-tolyl trifluoromethanesulfonate (4.1w):

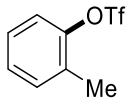

4.1w

Following general procedure 3A, using *o*-cresol (9.25 mmol) at 0 °C instead of −78 °C with triethylamine as the base afforded the title compound **4.1w** (1.97 g, 8.18 mmol, 88%) as a clear colorless oil after purification via column chromatography (pure *n*-pentane).

Rf = 0.52 (*n*-pentane:EtOAc = 20:1, UV)

^{1}H NMR (300 MHz, Chloroform-*d*) δ 8.00 (dd, *J* = 8.8, 1.9 Hz, 2H), 7.33 (dd, *J* = 8.7, 1.8 Hz, 2H), 2.57 (s, 3H).

^{13}C NMR (75 MHz, Chloroform-*d*) δ 196.1, 152.5, 136.9, 130.6, 121.6, 118.7 (q, *J* = 320.7 Hz), 26.5.

^{19}F NMR (282 MHz, Chloroform-*d*) δ -73.03.

MS (EI): m/z (relative intensity) 240 (58), 107 (100), 91 (12), 79 (24), 78 (14), 77 (60), 69 (18), 51 (11).

HRMS (ESI-TOF, *m*/*z*): calcd. for $C_{12}H_{13}NO_2$ $[M]^+$ 240.006, found 240.006.

IR (ATR, neat, cm-1): 1582 (w), 1491 (w), 1462 (w), 1417 (s), 1293 (w), 1249 (m), 1203 (s), 1136 (s), 1086 (s), 1043 (w), 990 (w), 942 (w), 887 (s), 800 (s), 760 (s), 726 (w), 702 (m), 646 (m), 626 (m), 602 (s), 572 (m), 546 (w), 520 (s), 493 (m), 442 (m).

The analytical data is in accordance with those reported in the literature.[156]

5.3.4.1.45 Synthesis of *N,N*,2-trimethylaniline hydrochloride (4.3w·HCl):

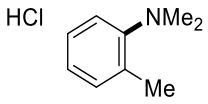

4.3w·HCl

Following general procedure 3.B, using o-tolyl trifluoromethanesulfonate (**4.1w**) afforded the title compound **4.3x** (70 mg, 0.408 mmol, 77%) as a white crystalline solid after purification via column chromatography (*n*-pentane:EtOAc = 20:1) and treatment with 2 M HCl in Et_2O.

R_f = 0.24 (*n*-pentane:EtOAc = 20:1, UV) free base

^{1}H NMR (300 MHz, Chloroform-*d*) δ 13.00 (s, 1H), 7.62 – 7.45 (m, 1H), 7.36 – 7.23 (m, 3H), 3.23 (s, 6H), 2.84 – 2.63 (m, 3H).

^{13}C NMR (75 MHz, Chloroform-*d*) δ 141.0, 133.3, 133., 130.1, 128.1, 120.0, 46.6, 19.3.

MS (EI): m/z (relative intensity) 135 (100), 134 (87), 120 (73), 119 (13), 118 (34), 104 (20), 91 (37), 77 (12), 67 (10), 65 (20).

HRMS (ESI-TOF, *m*/*z*): calcd. for $C_9H_{13}N$ $[M+H]^+$ 136.1126, found 136.1126.

IR (ATR, neat, cm-1): 3378 (w), 3038 (w), 2954 (w), 2495 (m), 2442 (m), 1995 (w), 1813 (w), 1495 (m), 1461 (s), 1381 (s), 1210 (w), 1180 (m), 1140 (m), 1116 (m), 1098 (m), 1051 (m), 983 (m), 895 (m), 804 (w), 770 (s), 715 (s), 597 (s), 556 (m), 499 (m), 455 (s).

The analytical data is in accordance with those reported in the literature.[158]

5.3.4.2 Characterization of *N*-*N*-Dialkylaniline scope

5.3.4.2.1 Experimental Procedures and Characterization for Products

Synthesis of 4-(tert-butyl)-*N,N*-diethylaniline hydrochloride (4.4b·HCl):

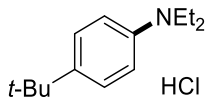

4.4b·HCl

Following general procedure B, using 4-(tert-butyl)phenyl trifluoromethanesulfonate (**4.1a**) and diethylamine solution (2 M THF, 1 ml) afforded the title compound **4.4b** (116 mg, 0.480 mmol, 95%) as a white crystalline solid after purification via column chromatography (pure *n*-pentane) and treatment with 2 M HCl in Et_2O.

R_f = 0.67 (*n*-pentane:EtOAc = 10:1, UV) free base

^{1}H NMR (300 MHz, Chloroform-*d*) δ 13.35 (s, 1H), 7.60 (d, *J* = 8.4 Hz, 2H), 7.42 (d, *J* = 8.4 Hz, 2H), 3.68 – 3.20 (m, 4H), 1.24 (s, 9H), 1.17 (t, *J* = 7.0 Hz, 6H).

^{13}C NMR (101 MHz, DMSO-d_6) δ 153.4, 134.4, 127.1, 122.4, 53.5, 34.8, 31.1, 10.3.

MS (EI): m/z (relative intensity) 205 (22), 191 (15), 190 (100).

HRMS (EI, *m*/*z*): calcd. for $C_{14}H_{23}N$ $[M]^+$ 205.1825, found 205.1831.

IR (ATR, neat, cm-1): 2950 (m), 2863 (w), 2330 (m), 1736 (w), 1596 (w), 1509 (m), 1462 (m), 1381 (m), 1373 (m), 1327 (w), 1307 (w), 1264 (m), 1191 (w), 1157 (m), 1122 (m), 1107 (w), 1066 (w), 1026 (m), 1011 (m), 926 (w), 875 (w), 853 (s), 838 (m), 799 (w), 767 (w), 740 (w), 650 (w), 593 (s), 542 (m), 516 (w), 480 (w), 455 (w).

The analytical data is in accordance with those reported in the literature.[159]

5.3.4.2.2 Synthesis of 4-(tert-butyl)-*N,N*-dipropylaniline hydrochloride (4.4c·HCl):

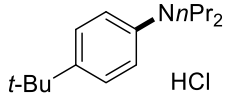

4.4c·HCl

Following general procedure B, using 4-(tert-butyl)phenyl trifluoromethanesulfonate (**4.1a**) and dipropylamine solution (2 M THF, 1 ml) afforded the title compound **4.4c** (132 mg, 0.489 mmol, 95%) as a white crystalline solid after purification via column chromatography (pure *n*-pentane) and treatment with 2 M HCl in Et_2O.

R_f = 0.76 (*n*-pentane:EtOAc = 10:1, UV) free base

^{1}H NMR (300 MHz, Chloroform-*d*) δ 13.46 (s, 1H), 7.52 (d, *J* = 8.7 Hz, 2H), 7.34 (d, *J* = 8.8 Hz, 2H), 3.40 – 3.20 (m, 2H), 3.16 – 2.96 (m, 2H), 1.99 – 1.77 (m, 2H), 1.18 (s, 9H), 1.27 – 1.09 (m, 2H), 0.74 (t, *J* = 7.4 Hz, 6H).

^{13}C NMR (101 MHz, DMSO-d_6) δ 153.4, 135.6, 127.2, 122.2, 60.4, 34.9, 31.3, 18.3, 11.0.

MS (EI): m/z (relative intensity) 233 (20), 218 (14), 205 (16), 204 (100), 162 (18), 146 (10).

HRMS (EI, *m*/*z*): calcd. for $C_{16}H_{27}N$ $[M]^+$ 233.2168, found 233.2136.

IR (ATR, neat, cm-1): 3042 (w), 2960 (s), 2933 (s), 2874 (m), 2848 (m), 2542 (w), 2421 (m), 1607 (w), 1570 (w), 1516 (m), 1461 (m), 1446 (m), 1398 (w), 1380 (w), 1361 (w), 1338 (w), 1315 (w), 1268 (m), 1193 (w), 1159 (w), 1110 (w), 1070 (w), 1054 (w), 1025 (w), 997 (s), 969 (w), 875 (w), 847 (s), 783 (w), 761 (m), 740 (m), 700 (w), 652 (w), 603 (s), 589 (w), 544 (w), 516 (w), 506 (w), 480 (w), 462 (w), 425 (w), 411 (w).

5.3.4.2.3 Synthesis of 4-(tert-butyl)-*N,N*-dibutylaniline hydrochloride (4.4d·HCl):

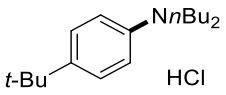

4.4d·HCl

Following general procedure B, using 4-(tert-butyl)phenyl trifluoromethanesulfonate (**4.1a**) and dibutylamine solution (2 M THF, 1 ml) afforded the title compound **4.4d** (150 mg, 0.504 mmol, 97%) as a white crystalline solid after purification via column chromatography (pure *n*-pentane) and treatment with 2 M HCl in Et_2O.

R_f = 0.79 (*n*-pentane:EtOAc = 10:1, UV) free base

^{1}H NMR (300 MHz, Chloroform-*d*) δ 13.53 (d, *J* = 8.7 Hz, 1H), 7.60 (d, *J* = 8.3 Hz, 2H), 7.42 (d, *J* = 8.3 Hz, 2H), 3.52 – 3.30 (m, 2H), 3.27 – 3.07 (m, 2H), 2.05 – 1.82 (m, 2H), 1.26 (d, *J* = 0.6 Hz, 6H), 1.24 – 1.09 (m, 1H), 0.79 (t, *J* = 6.9 Hz, 6H).

^{13}C NMR (101 MHz, DMSO-d_6) δ 148.5, 130.8, 122.4, 117.3, 53.9, 30.1, 26.4, 21.7, 15.1, 8.7.

MS (EI): m/z (relative intensity) 261 (25), 246 (15), 219 (16), 218 (100), 176 (43), 162 (12), 146 (10).

HRMS (EI, *m*/*z*): calcd. for $C_{16}H_{27}N$ $[M]^+$ 261.2451, found 261.2452.

IR (ATR, neat, cm-1): 3040 (w), 2961 (s), 2935 (m), 2871 (m), 2656 (w), 2402 (m), 1599 (w), 1515 (m), 1463 (m), 1430 (m), 1402 (w), 1379 (w), 1364 (w), 1339 (w), 1316 (w), 1267 (m), 1236 (w), 1202 (w), 1183 (w), 1160 (w), 1127 (w), 1108 (w), 1018 (w), 987 (w), 966 (w), 949

(w), 936 (w), 876 (w), 848 (s), 793 (w), 767 (w), 742 (w), 652 (w), 636 (w), 602 (s), 551 (w), 461 (w).

The analytical data is in accordance with those reported in the literature.[160]

5.3.4.2.4 Synthesis of tert-butyl 3-(2-((tert-butoxycarbonyl)amino)ethyl)-1H-indole-1-carboxylate hydrochloride (4.4i·HCl):

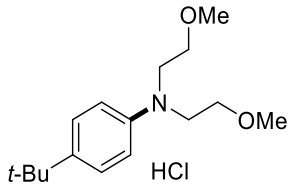

4.4i·HCl

Following general procedure C, using bis(2-methoxyethyl)amine (1.05 mmol) afforded the title compound **4.4i** (100 mg, 0.331 mmol, 65%) as a red oil after purification via column chromatography (*n*-pentane:EtOAc = 10:1 and treatment with HCl (2.0 M in Et2O).

R_f = 0.34 (*n*-pentane:EtOAc = 10:1, UV) free base

^{1}H NMR (400 MHz, Chloroform-*d*) δ 7.40 – 7.11 (m, 2H), 6.86 – 6.49 (m, 2H), 3.56 (s, 8H), 3.36 (s, 6H), 1.30 (s, 9H). Free base

^{13}C NMR (101 MHz, Chloroform-*d*) δ 126.1, 126.1, 113.6, 111.8, 70.1, 59.0, 51.3, 33.8, 31.6. Free base

MS (EI): m/z (relative intensity) 265 (11), 221 (16), 220 (100), 59 (20).

HRMS (EI, *m*/*z*): calcd. for $C_{16}H_{27}NO_2$ $[M+H]^+$ 266.2120, found 266.2121.

IR (ATR, neat, cm-1): 3405 (w), 2958 (m), 2873 (w), 2373 (w), 1614 (w), 1519 (s), 1460 (m), 1393 (w), 1363 (m), 1269 (m), 1196 (m), 1113 (s), 1016 (m), 959 (w), 925 (w), 813 (m), 548 (m), 463 (w).

5.3.4.2.5 Synthesis of *N*-benzyl-4-(tert-butyl)aniline hydrochloride (4.4l·HCl):

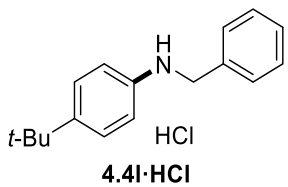

4.4l·HCl

Following general procedure C, using benzylamine (0.999 mmol) afforded the title compound **4.4l** (123 mg, 0.446 mmol, 87%) as a white crystalline solid after purification via column chromatography (*n*-pentane:EtOAc = 20:1) and treatment with HCl (2.0 M in Et_2O).

R_f = 0.45 (*n*-pentane:EtOAc = 10:1, UV) free base

^{1}H NMR (400 MHz, Chloroform-*d*) δ 11.73 (s, 2H), 7.43 – 7.36 (m, 2H), 7.33 – 7.26 (m, 3H), 7.25 – 7.19 (m, 2H), 4.29 (s, 2H), 1.25 (s, 4H).

^{13}C NMR (101 MHz, Chloroform-*d*) δ 152.5, 131.7, 131.1, 129.6, 129.3, 128.6, 126.6, 123.4, 56.0, 34.7, 31.2.

MS (EI): m/z (relative intensity) 239 (31), 225 (18), 224 (100), 91 (47).

HRMS (EI, *m*/*z*): calcd. for $C_{17}H_{21}N$ $[M]^+$ 240.1752, found 240.1753.

IR (ATR, neat, cm-1): 3061 (w), 3005 (w), 2960 (w), 2855 (w), 2658 (w), 2604 (w), 2520 (m), 2384 (w), 1509 (m), 1476 (w), 1447 (w), 1416 (m), 1388 (w), 1362 (w), 1321 (w), 1269 (w), 1229 (w), 1205 (w), 1188 (w), 1127 (w), 1108 (w), 1032 (w), 1018 (w), 976 (m), 956 (w), 926 (w), 876 (w), 833 (m), 750 (s), 703 (s), 678 (w), 639 (w), 590 (w), 558 (s), 496 (m), 470 (w), 435 (w), 406 (s).

The analytical data is in accordance with those reported in the literature.[161]

5.3.4.2.6 Synthesis of 4-(tert-butyl)-N-methyl-N-phenylaniline hydrochloride (4.4g·HCl):

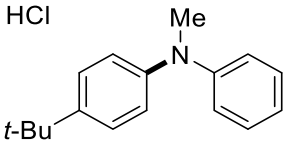

4.4g·HCl

Following general procedure C, using *N*-methylaniline (0.784 mmol) afforded the title compound **4.4g** (131 mg, 0.475 mmol, 93%) as a white crystalline solid after purification via column chromatography (pure *n*-pentane) and treatment with HCl (2.0 M in Et_2O).

R_f = 0.70 (*n*-pentane:EtOAc = 10:1, UV) free base

^{1}H NMR (300 MHz, Chloroform-*d*) δ 7.43 – 7.27 (m, 4H), 7.13 – 7.02 (m, 4H), 7.00 – 6.92 (m, 1H), 3.37 (d, *J* = 0.6 Hz, 3H), 1.40 (s, 9H).

^{13}C NMR (75 MHz, Chloroform-*d*) δ 149.3, 146.5, 144.9, 129.1, 126.2, 121.3, 120.3, 119.1, 40.3, 34.3, 31.6.

MS (EI): m/z (relative intensity) 239 (33), 225 (17), 224 (100).

HRMS (ESI-TOF, *m*/*z*): calcd. for $C_{17}H_{21}N$ $[M]^+$ 240.1752, found 240.1755.

IR (ATR, neat, cm-1): 3035 (w), 2959 (m), 2902 (w), 2866 (w), 2809 (w), 1594 (s), 1511 (s), 1494 (s), 1393 (w), 1362 (m), 1340 (m), 1267 (m), 1254 (m), 1200 (w), 1132 (m), 1087 (w), 1067 (w), 1026 (w), 991 (w), 870 (w), 823 (m), 746 (s), 693 (s), 593 (m), 542 (m), 483 (w), 408 (w).

The analytical data is in accordance with those reported in the literature.[162]

5.3.4.2.7 Synthesis of 4-(tert-butyl)-*N,N*-dibutylaniline hydrochloride (4.4f·HCl):

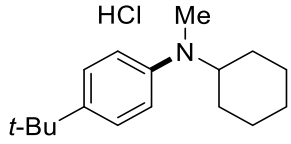

4.4f·HCl

Following general procedure C, using *N*-methylcyclohexanamine (0.765 mmol) afforded the title compound **4.4f** (138 mg, 0.504 mmol, 96%) as a white crystalline solid after purification via column chromatography (*n*-pentane:EtOAc = 50:1) and treatment with HCl (2.0 M in Et_2O).

R_f = 0.58 (*n*-pentane:EtOAc = 10:1, UV) free base

^{1}H NMR (300 MHz, Chloroform-*d*) δ 13.59 (s, 1H), 7.68 – 7.54 (m, 2H), 7.43 (d, *J* = 8.3 Hz, 2H), 3.37 – 3.19 (m, 1H), 3.10 (d, *J* = 4.9 Hz, 3H), 2.36 – 2.22 (m, 1H), 1.94 – 1.46 (m, 6H), 1.30 – 1.25 (m, 9H), 1.33 – 1.00 (m, 3H).

^{13}C NMR (75 MHz, Chloroform-*d*) δ 153.2, 137.5, 126.9, 122.2, 68.4, 41.2, 34.8, 31.1, 27.9, 27.7, 25.0, 24.5.

MS (EI): m/z (relative intensity) 245 (41), 230 (29), 203 (15), 202 (100), 174 (13), 148 (13), 146 (29), 144 (11), 132 (13), 91 (10), 55 (17), 42 (10), 41 (17).

HRMS (EI, *m*/*z*): calcd. for $C_{17}H_{27}N$ $[M]^+$ 246.2222, found 246.2225.

IR (ATR, neat, cm-1): 3036 (w), 2942 (w), 2859 (w), 2304 (m), 1513 (m), 1466 (m), 1452 (m), 1414 (w), 1364 (w), 1311 (w), 1272 (w), 1204 (w), 1165 (w), 1140 (w), 1111 (m), 1093 (w), 1058 (w), 1011 (m), 927 (w), 903 (m), 857 (s), 795 (w), 679 (w), 637 (w), 594 (s), 556 (m), 434 (w).

The analytical data is in accordance with those reported in the literature.[160]

5.3.4.2.8 Synthesis of N-benzyl-4-(tert-butyl)-*N*-methylaniline hydrochloride (4.4k·HCl):

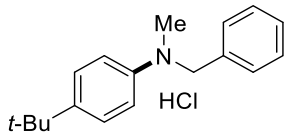

4.4k·HCl

Following general procedure C, using *N*-methylbenzylamine (0.770 mmol) afforded the title compound **4.4k** (126 mg, 0.504 mmol, 87%) as a white crystalline solid after purification via column chromatography (pure *n*-pentane) and treatment with HCl (2.0 M in Et_2O).

R_f = 0.61 (*n*-pentane:EtOAc = 10:1, UV) free base

NMR (300 MHz, Chloroform-*d*) δ 7.46 – 7.38 (m, 2H), 7.37 – 7.30 (m, 4H), 7.31 – 7.17 (m, 4H), 4.53 (s, 2H), 3.16 (s, 3H), 1.24 (s, 9H).

^{13}C NMR (75 MHz, Chloroform-*d*) δ 131.5, 129.8, 128.7, 127.0, 126.8, 122.3, 121.5, 63.8, 43.0, 34.8, 31.1.

MS (EI): m/z (relative intensity) 253 (31), 239 (18), 238 (90), 146 (19), 91 (100), 65 (15).

HRMS (ESI-TOF, *m*/*z*): calcd. for $C_{18}H_{23}N$ $[M+H]^+$ 254.1908, found 254.1913.

IR (ATR, neat, cm-1): 2957 (w), 2400 (w), 1511 (w), 1455 (w), 1403 (m), 1363 (w), 1268 (w), 1242 (w), 1215 (w), 1152 (w), 1132 (w), 1117 (w), 1012 (w), 936 (w), 909 (w), 845 (m), 830 (w), 779 (w), 749 (s), 700 (s), 653 (w), 633 (w), 608 (m), 573 (s), 543 (w), 512 (w).

The analytical data is in accordance with those reported in the literature.[163]

5.3.4.2.9 Synthesis of 4-(tert-butyl)-*N*-(2-((tert-butyldimethylsilyl)oxy)ethyl)-*N*-methylaniline (4.4h):

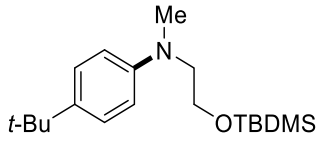

4.4h

Following general procedure C, with *N*-methylbenzylamine (0.908 mmol) afforded the title compound **4.4h** (160 mg, 0.504 mmol, 94%, freebase) as a yellow oil after purification via column chromatography (*n*-pentane:EtOAc = 50:1).

R_f = 0.70 (*n*-pentane:EtOAc = 10:1, UV) free base

^{1}H NMR (300 MHz, Chloroform-*d*) δ 7.32 – 7.20 (m, 2H), 6.67 (d, *J* = 8.3 Hz, 2H), 3.78 (t, *J* = 6.5 Hz, 2H), 3.44 (t, *J* = 6.5 Hz, 2H), 2.97 (s, 3H), 1.30 (s, 9H), 0.90 (s, 9H), 0.05 (s, 6H).

^{13}C NMR (75 MHz, Chloroform-*d*) δ 125.9, 111.6, 60.6, 55.1, 39.1, 33.7, 31.6, 25.9, 18.3, -5.3.

MS (EI): m/z (relative intensity) 321 (16), 177 (18), 176 (100).

HRMS (EI, *m*/*z*): calcd. for $C_{19}H_{35}NOSi$ $[M]^+$ 321.2482, found 321.2481.

IR (ATR, neat, cm-1): 2953 (w), 2857 (w), 1614 (w), 1519 (s), 1462 (w), 1362 (m), 1250 (m), 1205 (m), 1097 (s), 1006 (w), 987 (w), 927 (w), 834 (s), 810 (s), 774 (s), 731 (w), 664 (w), 551 (w).

5.3.4.2.10 Synthesis of N-methyl-2-(1-methyl-1H-indol-3-yl)ethan-1-amine (2l):

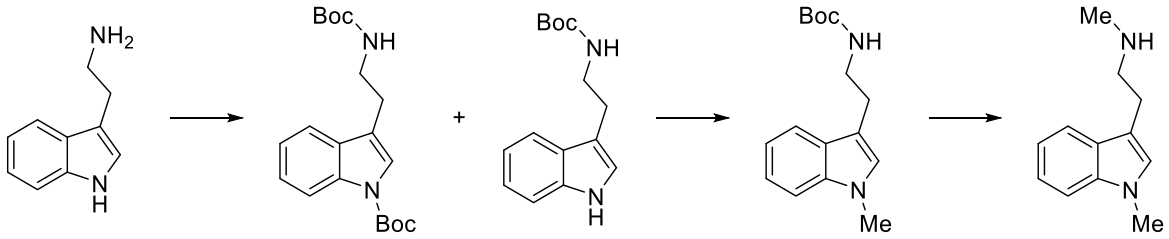

5.3.4.2.11 Synthesis of tert-butyl 3-(2-((tert-butoxycarbonyl)amino)ethyl)-1H-indole-1-carboxylate (4.2j-S1):

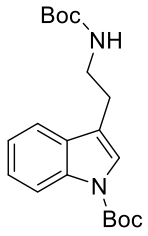

4.2j-S1

A solution of tryptamine hydrochloride (993 mg, 6.20 mmol, 1.0 equiv.), 4-dimethylaminopyridine (1.55 g, 12.69 mmol, 2.0 equiv.) and di-tert-butyl dicarbonate (2.90 g, 13.29 mmol, 2.1 equiv.) in acetonitrile (20 mL) was stirred at rt under argon. After 16 h, water was added, and the aqueous phase was extracted with CH_2Cl_2. The combined organic layers were dried over Na_2SO_4, filtered and the solvent was removed under reduced pressure. The crude product was purified by column chromatography (*n*-pentane:EtOAc = 10:1) yielding the title compound **4.2j-S1** (1.11 g, 3.08 mmol, 50%).

R_f = 0.24 (*n*-pentane:EtOAc = 10:1, UV)

^{1}H NMR (300 MHz, Chloroform-*d*) δ 8.13 (d, *J* = 8.0 Hz, 1H), 7.58 – 7.50 (m, 1H), 7.42 (s, 1H), 7.32 (ddd, *J* = 8.4, 7.2, 1.4 Hz, 1H), 7.30 – 7.18 (m, 1H), 4.66 (s, 1H), 3.46 (q, *J* = 6.7 Hz, 2H), 2.89 (t, *J* = 7.0 Hz, 2H), 1.67 (s, 9H), 1.44 (s, 9H).

^{13}C NMR (75 MHz, Chloroform-*d*) δ 155.9, 149.7, 135.6, 130.5, 124.5, 123.2, 122.5, 119.0, 117.8, 115.3, 83.5, 79.3, 40.2, 28.4, 28.2, 25.6.

HRMS (ESI-TOF, *m*/*z*): calcd. for $C_{20}H_{28}N_2O_4$ $[M+Na]^+$ 383.1941, found 383.1952.

HRMS (EI, *m*/*z*): calcd. for $C_{20}H_{28}N_2O_4$ $[M]^+$ 360.2044, found 360.2041.

IR (ATR, neat, cm-1): 3410 (w), 2979 (w), 2934 (w), 1808 (w), 1713 (m), 1510 (w), 1477 (w), 1453 (m), 1369 (s), 1308 (m), 1251 (s), 1211 (m), 1157 (s), 1114 (s), 1061 (s), 1017 (m), 956 (w), 844 (m), 768 (m), 745 (s), 663 (w), 592 (w), 521 (w), 462 (w), 424 (w).

The analytical data is in accordance with those reported in the literature.[164]

5.3.4.2.12 Synthesis of tert-butyl (2-(1H-indol-3-yl)ethyl)carbamate (4.2j-S2):

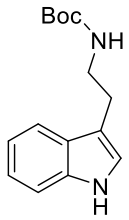

4.2j-S2

A solution of di-tert-butyl dicarbonate (6.13 g, 28.09 mmol, 3.0 equiv.) in 1,4-dioxane (5 mL) was added to a mixture of tryptamine (1.52 g, 9.47 mmol, 1.0 equiv.) and triethylamine (2.84 g, 28.09 mmol, 3.0 equiv.) in 1,4-Dioxane (10 mL) and the reaction was stirred at rt. After 16 h, water was added and the aqueous phase was extracted with CH_2Cl_2. The combined organic layers were dried over Na_2SO_4, filtered and the solvent was removed under reduced pressure. The crude product was purified by column chromatography (*n*-pentane:EtOAc =5:1) yielding to title compound **S2I-2** (1.55 g, 5.94 mmol, 63%). Additionally, **S2I-1** was re-isolated in 37% yield.

R_f = 0.10 (*n*-pentane:EtOAc = 10:1, UV)

^{1}H NMR (400 MHz, Chloroform-*d*) δ 8.36 (s, 1H), 7.62 (d, *J* = 7.7 Hz, 1H), 7.37 (d, *J* = 8.1 Hz, 1H), 7.22 (t, *J* = 7.5 Hz, 1H), 7.14 (t, *J* = 7.6 Hz, 1H), 6.99 (s, 1H), 4.67 (s, 1H), 3.47 (s, 2H), 2.96 (t, *J* = 6.8 Hz, 2H), 1.48 (s, 9H).

^{13}C NMR (101 MHz, Chloroform-*d*) δ 156.2, 136.5, 127.4, 122.1, 119.4, 118.9, 113.0, 111.3, 79.3, 41.1, 28.5, 25.9.

MS (EI): m/z (relative intensity) 260 (6), 143 (32), 131 (14), 130 (100), 103 (10), 77 (14), 59 (12), 57 (43), 41 (28), 39 (11), 29 (13).

HRMS (EI, *m*/*z*): calcd. for $C_{15}H_{20}N_2O_2$ $[M]^+$ 260.1519, found 260.1516.

IR (ATR, neat, cm-1): 3434 (w), 3313 (m), 3062 (w), 3002 (w), 2974 (w), 2936 (w), 1686 (s), 1619 (w), 1521 (s), 1452 (m), 1436 (w), 1390 (m), 1366 (s), 1351 (m), 1284 (m), 1270 (m),

1248 (m), 1229 (m), 1163 (s), 1131 (m), 1107 (m), 1079 (m), 1038 (m), 1008 (w), 954 (m), 867 (m), 809 (m), 773 (m), 736 (s), 684 (m), 623 (m), 588 (m), 562 (m), 492 (s), 465 (m), 419 (s).

The analytical data is in accordance with those reported in the literature.[165]

5.3.4.2.13 Synthesis of tert-butyl (2-(1-methyl-1H-indol-3-yl)ethyl)carbamate (4.2j-S3):

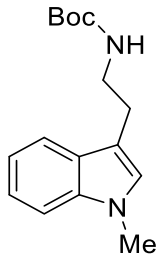

4.2j-S3

A solution of tert-butyl (2-(1H-indol-3-yl)ethyl)carbamate (1.00 g, 3.85 mmol, 1.0 equiv.) in DMF (5 ml) was added dropwise to a stirred mixture of mineral oil suspended NaH (169 mg, 4.04 mmol, 60 %wt, 1.05 equiv.) in DMF (5 mL) at -30 °C. The reaction was allowed to warm to room temperature over the period of one hour. Afterwards the reaction was cooled again to -30°C and MeI (598mg, 4.21 mmol, 1.09 equiv.) was added dropwise. After 16 h, water was added, and the aqueous phase was extracted with CH_2Cl_2. The combined organic layers were dried over Na_2SO_4, filtered and the solvent was removed under reduced pressure. The crude product was purified by column chromatography yielding the title compound **4.2j-S3** (1.03 g, 3.76 mmol, 98%).

R_f = 0.25 (*n*-pentane:EtOAc = 20:1, UV)

^{1}H NMR (300 MHz, Chloroform-d) δ 7.61 (d, *J* = 7.9 Hz, 1H), 7.36 – 7.19 (m, 2H), 7.19 – 7.07 (m, 1H), 6.89 (s, 1H), 4.67 (s, 1H), 3.75 (s, 3H), 3.60 – 3.33 (m, 2H), 3.07 – 2.79 (m, 2H), 1.46 (s, 9H).

^{13}C NMR (101 MHz, Chloroform-*d*) δ 156.1, 137.2, 127.9, 126.9, 121.7, 119.0, 118.9, 111.6, 109.3, 79.2, 41.2, 32.7, 28.5, 25.8.

MS (EI): m/z (relative intensity) 274 (16), 157 (26), 145 (13), 144 (100).

HRMS (EI, *m*/*z*): calcd. for $C_{16}H_{22}N_2O_2$ $[M]^+$ 274.1676, found 274.1676.

IR (ATR, neat, cm-1): 3351 (w), 2974 (w), 2930 (w), 1691 (s), 1615 (w), 1505 (m), 1473 (m), 1390 (m), 1364 (m), 1326 (m), 1246 (s), 1158 (s), 1071 (w), 1048 (w), 1012 (w), 958 (w), 869 (w), 780 (w), 736 (s), 602 (w), 541 (w), 462 (w), 427 (m).

The analytical data is in accordance with those reported in the literature.[166]

5.3.4.2.14 Synthesis of N-methyl-2-(1-methyl-1H-indol-3-yl)ethan-1-amine (4.2j):

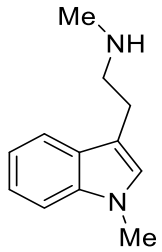

4.2j

A solution of tert-butyl (2-(1-methyl-1H-indol-3-yl)ethyl)carbamate (**4.2j-S3**, 750 mg, 2.73 mmol) in THF (5.0 ml) was added dropwise to a stirred suspension of $LiAlH_4$ (1.08 g, 28.4 mmol, 10 equiv.) in THF (10 mL) at -78 °C. The reaction was then heated to 50 °C. After 16 h, water was added, and the mixture was filtered through a small pad of ceolite. The aqueous phase was extracted with CH_2Cl_2. The combined organic layers were dried over Na_2SO_4, filtered and the solvent was removed under reduced pressure. The crude product was purified by column chromatography (*n*-pentane:EtOAc = 10:1) yielding the title compound **4.2j** (366 mg, 1.94 mmol, 71%).

R_f = 0.31 (*n*-pentane:EtOAc = 10:1, UV)

^{1}H NMR (400 MHz, Chloroform-*d*) δ 7.64 (d, *J* = 8.0 Hz, 1H), 7.31 (d, *J* = 8.2 Hz, 1H), 7.28 – 7.20 (m, 1H), 7.17 – 7.08 (m, 1H), 6.91 (s, 1H), 3.75 (s, 3H), 3.04 – 2.97 (m, 2H), 2.97 – 2.89 (m, 2H), 2.46 (s, 3H), 2.12 (s, 1H).

^{13}C NMR (101 MHz, Chloroform-*d*) δ 137.2, 127.9, 126.9, 121.7, 119.1, 118.8, 112.4, 109.3, 52.2, 36.3, 32.7, 25.5.

MS (EI): m/z (relative intensity) 188 (4), 146 (12), 145 (88), 144 (100), 129 (10), 128 (13), 115 (17), 102 (15), 77 (17), 44 (67).

HRMS (EI, *m*/*z*): calcd. for $C_{12}H_{26}N_2$ $[M]^+$ 188.1308, found 188.1308.

IR (ATR, neat, cm-1): 3052 (w), 2927 (w), 2842 (w), 2787 (w), 1614 (w), 1552 (w), 1470 (m), 1442 (w), 1424 (w), 1376 (m), 1325 (m), 1248 (w), 1154 (w), 1129 (m), 1064 (w), 1011 (w), 922 (w), 734 (s), 663 (w), 601 (w), 564 (w), 426 (m).

The analytical data is in accordance with those reported in the literature.

5.3.4.2.15 Synthesis of 4-(tert-butyl)-*N*-methyl-*N*-(2-(1-methyl-1H-indol-3-yl)ethyl)aniline (4.4j):

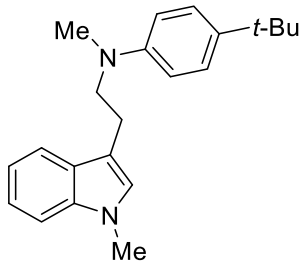

4.4j

Following general procedure C, using 0.781 mmol *N*-methyl-2-(1-methyl-1*H*-indol-3-yl)ethan-1-amine (**2l**) afforded the title compound **4.4j** (141 mg, 0.440 mmol, 85%, freebase) as a clear colorless oil after purification via column chromatography (*n*-pentane:EtOAc = 20:1).

R_f = 0.24 (*n*-pentane:EtOAc = 20:1, UV)

^{1}H NMR (300 MHz, Chloroform-*d*) δ 7.67 (d, *J* = 7.8 Hz, 1H), 7.34 (d, *J* = 8.9 Hz, 3H), 7.28 (ddd, *J* = 8.2, 6.8, 1.2 Hz, 1H), 7.17 (ddd, *J* = 8.0, 6.8, 1.3 Hz, 1H), 6.91 (s, 1H), 6.81 (d, *J* = 8.0 Hz, 2H), 3.78 (s, 3H), 3.71 – 3.59 (m, 2H), 3.06 (dd, *J* = 9.8, 6.0 Hz, 2H), 3.00 (s, 3H), 1.36 (s, 9H).

^{13}C NMR (75 MHz, Chloroform-*d*) δ 137.2, 128.0, 126.7, 126.2, 121.7, 119.0, 118.9, 112.5, 112.1, 109.4, 54.1, 38.6, 33.9, 32.7, 31.7, 22.4.

HRMS (ESI-TOF, *m*/*z*): calcd. for $C_{22}H_{28}N_2$ $[M+H]^+$ 321.2331, found 321.2333.

IR (ATR, neat, cm-1): 3050 (w), 2951 (m), 2864 (w), 1613 (m), 1518 (s), 1472 (m), 1424 (w), 1361 (m), 1325 (m), 1298 (w), 1270 (m), 1247 (m), 1225 (w), 1203 (m), 1184 (m), 1156 (w), 1128 (w), 1100 (w), 1063 (w), 1012 (w), 956 (w), 812 (s), 734 (s), 630 (w), 607 (w), 550 (m), 498 (w).

5.3.4.3 Comparison of different Electrophiles and intramolecular competition experiments

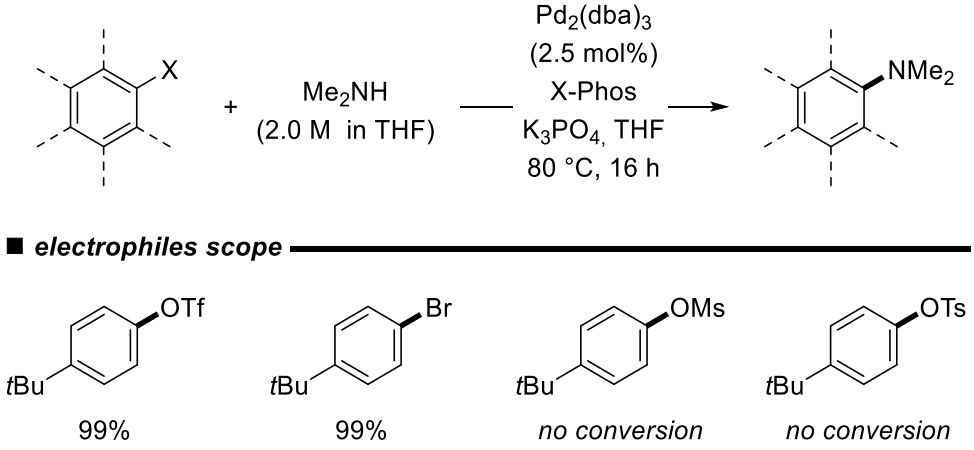

All reactions were carried out in septum sealed 4 ml Vials. Subsequently, $Pd_2(dba)_3$ (2.5 mol%), XPhos (1.5 eq of the metal), K_3PO_4 (1.2 eq) and 4-(tert-butyl)phenyl (pseudo)halide (0.5 mmol) were added and the vial was sealed. The mixture was 3 times securated under vacuo and flushed with argon. Afterwards 1 ml THF was added and the suspension was stirred at 80 °C in a block of aluminum. After 5 min an appropriate dimethylamine solution (2 M THF, 1 ml) was added through the septum in one portion. After 16h the reaction was quenched with water and extracted 3 times with DCM. Subsequently, the solvent was removed in vacuo (500 mbar) and the desired dimethylaniline was purified with column chromatography. In order to avoid a loss of yields due to volatility of the desired amines, the fraction was treated with an HCl solution (Diethyl ether) to form the corresponding hydrochloride salts.

5.3.4.3.1 Synthesis of 4-bromophenyl trifluoromethanesulfonate (4.1y):

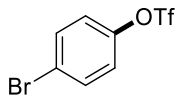

4.1y

Following general procedure A, using 4-bromophenol (3.03 mmol) at 0 °C instead of −78 °C and triethylamine as the base afforded the title compound **4.1y** (0.635 g, 2.08 mmol, 69%) as a clear colorless oil after purification via column chromatography (pure *n*-pentane).

R_f = 0.78 (*n*-pentane, UV)

^{1}H NMR (300 MHz, Chloroform-d) δ 7.64 – 7.52 (m, 2H), 7.20 – 7.13 (m, 2H).

^{13}C NMR (75 MHz, Chloroform-*d*) δ 148.6, 133.5, 123.2, 122.2, 118.8 (q, *J* = 320.9 Hz).

^{19}F NMR (282 MHz, Chloroform-*d*) δ -72.71.

MS (EI): m/z (relative intensity) 306 (82), 304 (79), 242 (29), 242 (30), 173 (98), 171 (100), 145 (92), 143 (17), 119 (16), 117 (17), 92 (22), 69 (59), 64 (36), 63 (59), 62 (14), 38 (14).

HRMS (EI, *m*/*z*): calcd. for $C_7H_4O_3BrF_3S$ $[M]^+$ 303.9011, found 303.9011.

IR (ATR, neat, cm-1): 1480 (m), 1423 (s), 1400 (m), 1296 (w), 1250 (m), 1205 (s), 1173 (m), 1134 (s), 1099 (m), 1069 (s), 1012 (s), 939 (w), 877 (s), 829 (s), 779 (m), 748 (s), 700 (w), 639 (m), 627 (m), 602 (s), 572 (m), 522 (s), 483 (s), 422 (m).

The analytical data is in accordance with those reported in the literature.[141]

5.3.4.3.2 Synthesis of 4-bromophenyl trifluoromethanesulfonate hydrochloride (4.4y·HCl):

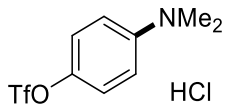

4.4y·HCl

Following general procedure B, using 4-bromophenyl trifluoromethanesulfonate (**4.1y**, 0.515 mmol) afforded the title compound **4.4y** (100 mg, 0.497 mmol, 99%) as a white crystalline solid after purification via column chromatography (*n*-pentane:EtOAc = 50:1) and treatment with HCl (2.0 M in Et_2O).

R_f = 0.16 (*n*-pentane:EtOAc = 50:1, UV) free base

^{1}H NMR (300 MHz, Chloroform-*d*) δ 13.16 (s, 1H), 8.04 – 7.94 (m, 2H), 7.48 – 7.37 (m, 2H), 3.20 (s, 6H).

^{13}C NMR (75 MHz, Chloroform-*d*) δ 149.6, 142.7, 123.7, 123.4, 118.6 (q, *J* = 320.9 Hz), 46.5.

^{19}F NMR (282 MHz, Chloroform-*d*) δ -72.60.

MS (EI): m/z (relative intensity) 269 (5), 136 (100), 108 (16), 69 (33), 67 (12), 66 (12), 65 (19), 42 (10).

HRMS (ESI-TOF, *m*/*z*): calcd. for $C_9H_{10}F_3NO_3S$ $[M]^+$ 270.041, found 270.041.

IR (ATR, neat, cm-1): 3019 (w), 2489 (w), 2355 (m), 1619 (w), 1504 (m), 1451 (w), 1415 (s), 1326 (w), 1237 (m), 1202 (s), 1130 (s), 1017 (m), 990 (m), 881 (s), 850 (s), 794 (m), 767 (m), 734 (w), 691 (w), 624 (s), 581 (s), 556 (m), 536 (s), 515 (m), 488 (m), 415 (w).

5.3.4.3.3 Synthesis of 4-(tert-butyl)phenyl 4-methylbenzenesulfonate (4.1ad)

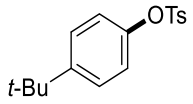

4.1ad

Following general procedure A, using 4-(tert-butyl)phenol (20 mmol) at 0 °C instead of −78 °C and NEt_3 as the base and 4-methylbenzenesulfonyl chloride as the sulfonating agent afforded the title compound **4.1ad** (5.63 g, 18.49 mmol, 92%) as a white solid after purification via column chromatography (pure *n*-pentane).

R_f = 0.51 (*n*-pentane:EtOAc = 18:1, UV)

^{1}H NMR (300 MHz, Chloroform-*d*) δ 7.75 – 7.69 (m, 2H), 7.32 (t, *J* = 0.7 Hz, 1H), 7.31 – 7.28 (m, 2H), 7.26 (s, 1H), 6.92 – 6.86 (m, 2H), 2.45 (d, *J* = 0.8 Hz, 3H), 1.27 (s, 9H).

^{13}C NMR (75 MHz, Chloroform-*d*) δ 150.2, 147.4, 145.3, 132.9, 129.8, 128.6, 126.6, 121.8, 34.7, 31.4, 21.8.

MS (EI): m/z (relative intensity) 304 (25), 290 (18), 289 (100), 155 (26), 109 (10), 91 (54), 65 (12).

HRMS (EI, *m*/*z*): calcd. for $C_{17}H_{20}O_3S$ $[M]^+$ 304.1128, found 304.1131.

IR (ATR, neat, cm-1): 3062 (w), 2962 (w), 2868 (w), 1596 (w), 1504 (m), 1475 (w), 1457 (w), 1395 (w), 1363 (s), 1307 (w), 1297 (w), 1266 (w), 1202 (m), 1178 (s), 1156 (s), 1112 (w), 1092 (s), 1040 (w), 1017 (m), 963 (w), 948 (w), 924 (w), 866 (s), 846 (s), 835 (s), 817 (s), 759 (s), 734 (m), 705 (w), 682 (s), 649 (m), 584 (s), 552 (s), 543 (s), 531 (s), 430 (w).

5.3.4.3.4 Synthesis of 4-(tert-butyl)phenyl methanesulfonate (4.1ac):

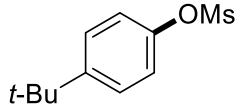

4.1ac

Following general procedure A, using 4-(tert-butyl)phenol (20 mmol) at 0 °C instead of −78 °C with NEt_3 as the base and 4-methylbenzenesulfonyl chloride as the sulfonating agent afforded the title compound **4.1ac** (5.63 g, 18.49 mmol, 92%) as a white solid after purification via column chromatography (*n*-pentane:EtOAc = 18:1, UV).

R_f = 0.26 (*n*-pentane:EtOAc = 18:1, UV)

^{1}H NMR (300 MHz, Chloroform-*d*) δ 7.45 – 7.39 (m, 2H), 7.23 – 7.17 (m, 2H), 3.11 (s, 3H), 1.32 (s, 9H).

^{13}C NMR (75 MHz, Chloroform-*d*) δ 150.5, 147.0, 126.9, 121.4, 37.2, 34.6, 31.3.

MS (EI): m/z (relative intensity) 228 (19), 214 (10), 213 (100), 135 (44).

HRMS (EI, *m*/*z*): calcd. for $C_{11}H_{16}O_3S$ $[M]^+$ 228.0815, found 228.0813.

IR (ATR, neat, cm-1): 3030 (w), 3014 (w), 2962 (w), 2952 (w), 2936 (w), 2906 (w), 2870 (w), 1591 (w), 1501 (m), 1478 (w), 1466 (w), 1411 (w), 1396 (w), 1352 (s), 1337 (s), 1267 (w), 1204 (m), 1174 (m), 1153 (s), 1108 (m), 1015 (w), 969 (s), 947 (w), 924 (w), 870 (s), 851 (s), 836 (s), 822 (m), 790 (s), 741 (w), 726 (m), 656 (w), 639 (w), 573 (s), 530 (s), 509 (s), 471 (w), 431 (w), 404 (m).

5.3.4.4 Derivatization of *N*,*N*-dimethylanilines

5.3.4.4.1 Synthesis of 4-(tert-butyl)-*N,N*-dimethylaniline oxide (4.5):

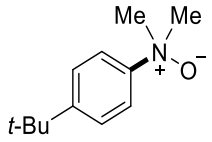

4.5

4-(tert-butyl)-*N*,*N*-dimethylaniline (**4.3a**) (539 mg, 2.52 mmol) was dissolved in CH_2Cl_2 (0.5 M) and cooled to 0 °C Afterwards, *meta*-chloroperoxybenzoic acid (70%, 1.0 eq) was added in one portion and the mixture was allowed to warm to room temperature. After 16 h the reaction was quenched with saturated K_2CO_3-solution and extracted 3 times with CH_2Cl_2. Removal of the solvent afforded the title compound **4.5** (82%, 400 mg, 2.07 mmol) as a white crystalline solid.

R_f = 0.00 (EtOAc, UV)

^{1}H NMR (300 MHz, Chloroform-*d*) δ 7.78 – 7.71 (m, 2H), 7.38 – 7.32 (m, 2H), 3.47 (s, 6H), 1.22 (s, 9H).

^{13}C NMR (75 MHz, Chloroform-*d*) δ 152.0, 151.6, 126.0, 119.4, 63.1, 34.6, 31.2.

MS (EI): m/z (relative intensity) 193 (44), 179 (13), 178 (100), 148 (23), 147 (44), 146 (29), 132 (17), 118 (10).

HRMS (ESI-TOF, *m*/*z*): calcd. for $C_{12}H_{19}NO$ $[M+H]^+$ 194.1545, found 194.1541.

IR (ATR, neat, cm-1): 3391 (w), 3129 (w), 3058 (w), 3021 (w), 2952 (m), 2902 (w), 2865 (w), 1654 (w), 1560 (w), 1503 (w), 1463 (w), 1401 (w), 1362 (w), 1267 (w), 1249 (w), 1186 (w),

1138 (w), 1101 (w), 1012 (w), 971 (m), 875 (m), 838 (s), 760 (w), 749 (w), 709 (m), 636 (m), 584 (s), 546 (w), 508 (m), 461 (w), 422 (w).

5.3.4.4.2 Synthesis of 5-(tert-butyl)-2-(dimethylamino)phenol (4.6)

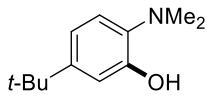

4.6

4-(*tert*-butyl)-*N,N*-dimethylaniline oxide (**4.5**, 96mg, 0.5 mmol) was dissolved in CH_2Cl_2 (5 ml, 0.1 M) and cooled to −78 °C. Afterwards, trifluroacertic anhydride was added dropwise via a syringe over a period of 15 min. The resultant solution was stirred for 1 h whereupon triethylamine (150mg, 3.00 equiv) was added. Subsequently, the mixture was allowed to warm to room temperature and quenched with saturated $NaHCO_3$ solution. Afterwards the aqueous phase was extracted with DCM. The combined organic layers were dried with Na_2SO_4 and the solvent was evaporated in vacuum. The crude product was further purified with column chromatography (*n*-pentane:EtOAc = 20:1) yielding the title compound **4.6** (88 mg, 0.455 mmol, 91%).

R_f = 0.38 (*n*-pentane:EtOAc = 20:1, UV)

^{1}H NMR (300 MHz, Chloroform-*d*) δ 7.10 (d, *J* = 8.3 Hz, 1H), 7.00 (d, *J* = 2.2 Hz, 1H), 6.89 (dd, *J* = 8.3, 2.2 Hz, 1H), 2.65 (s, 6H), 1.31 (s, 9H).

^{13}C NMR (75 MHz, Chloroform-*d*) δ 151.0, 149.5, 137.9, 120.1, 116.8, 111.4, 45.4, 34.6, 31.5.

MS (EI): m/z (relative intensity) 193 (34), 179 (12), 178 (100).

HRMS (ESI-TOF, *m*/*z*): calcd. for $C_{12}H_{19}NO$ $[M+H]^+$ 194.1545, found 194.1550.

IR (ATR, neat, cm-1): 3053 (w), 2957 (s), 2867 (m), 2834 (m), 2791 (m), 1746 (w), 1568 (m), 1503 (s), 1478 (m), 1454 (m), 1441 (m), 1430 (m), 1393 (w), 1363 (w), 1308 (m), 1288 (s), 1271 (s), 1236 (m), 1202 (s), 1168 (s), 1125 (s), 1087 (m), 1035 (m), 1024 (m), 947 (s), 917 (s), 873 (m), 809 (s), 724 (s), 648 (s), 543 (w), 510 (m), 497 (m), 459 (m), 439 (m), 416 (s).

Synthesis of 5-(tert-butyl)-2-(dimethylamino)phenol (4.8)

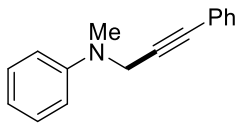

4.8

A mixture of CuBr (40.0 mg, 0.28 mmol, 7.0 mol%), *N*,*N*-dimethylaniline (974 mg, 8.0 mmol, 2.0 equiv.), phenylacetylene (412 mg, 4.0 mmol, 1.0 equiv.) and tert-butyl hydroperoxide (0.8 mL, 5-6M in decane) was heated to 100 °C under argon. After 16 h water was added, and the aqueous phase was extracted with DCM. The combined organic layers were dryed with Na_2SO_4 and the solvent was evaporated in vacuum. The crude product was further purified with column chromatography yielding the title compound **4.8** (469 mg, 2.26 mmol, 56%).

$\mathbf{R_f}$ = 0.57 (*n*-pentane:EtOAc = 10:1, UV)

^{1}H NMR (400 MHz, Chloroform-d) δ 7.45 – 7.39 (m, 2H), 7.38 – 7.28 (m, 5H), 7.02 – 6.92 (m, 2H), 6.87 (td, *J* = 7.3, 1.3 Hz, 1H), 4.30 (d, *J* = 1.2 Hz, 2H), 3.15 – 3.03 (m, 3H).

^{13}C NMR (101 MHz, Chloroform-*d*) δ 149.4, 131.8, 129.1, 128.2, 128.1, 123.1, 118.2, 114.4, 85.1, 84.2, 43.4, 38.8.

MS (EI): m/z (relative intensity) 222 (15), 221 (93), 220 (91), 144 (18), 116 (11), 115 (100), 104 (14), 89 (13), 77 (25).

HRMS (EI, *m*/*z*): calcd. for $C_{16}H_{14}N$ $[M]^+$ 221.1199, found 221.1192.

IR (ATR, neat, cm-1): 3057 (w), 1597 (s), 1503 (m), 1489 (m), 1442 (w), 1423 (w), 1365 (w), 1333 (m), 1241 (w), 1200 (w), 1110 (w), 1029 (w), 995 (m), 920 (m), 867 (w), 750 (s), 687 (s), 597 (m), 526 (m), 489 (w), 446 (m).

5.3.4.4.3 Synthesis of 5-(tert-butyl)-2-(dimethylamino)phenol (4.7)

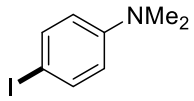

4.7

N,*N*-Dimethylaniline (**4.3d**, 122 mg, 1.00 mmol) was dissolved in 1,4-dioxane (5 ml) and pyridine (5 ml) and the mixture was cooled to 0 °C. Iodine (761 mg, 3 mmol, 3.0 equiv.) was add in one portion. After 2 h water was added, and the aqueous phase was extracted with DCM. The combined organic layers were dryed with Na_2SO_4 and the solvent was evaporated in vacuum. The crude product was further purified with column chromatography (*n*-pentane:EtOAc = 20:1) yielding the title compound **4.7** (220 mg, 0.89 mmol, 89%).

R_f = 0.29 (*n*-pentane:EtOAc = 20:1, UV)

^{1}H NMR (300 MHz, Chloroform-*d*) δ 7.53 – 7.42 (m, 1H), 6.55 – 6.44 (m, 1H), 2.92 (s, 3H).

^{13}C NMR (75 MHz, Chloroform-*d*) δ 150.0, 137.6, 114.7, 77.5, 40.4.

MS (EI): m/z (relative intensity) 247 (100), 246 (54), 119 (15), 77 (11).

HRMS (EI, *m*/*z*): calcd. for C_8H_9NI $[M]^+$ 245.9774, found 245.9773.

IR (ATR, neat, cm-1): 2881 (w), 2800 (w), 1868 (w), 1733 (w), 1582 (w), 1443 (m), 1346 (m), 1312 (m), 1227 (m), 1191 (m), 1164 (m), 1125 (m), 1062 (m), 983 (w), 943 (w), 799 (s), 743 (m), 691 (m), 566 (w), 505 (s), 476 (m).

The analytical data is in accordance with those reported in the literature.[136]

6 References

[1] I. Pérez-Juste, O. Nieto Faza, in *Structure Elucidation in Organic Chemistry*, **2015**, pp. 1-26.

[2] a) E. Schrödinger, *Ann. Phys. (Berl.)* **1926**, *384*, 361-376; b) P. A. Hanle, *Isis* **1977**, *68*, 606-609.

[3] a) J. Franck, E. G. Dymond, *Trans. Faraday Society* **1926**, *21*, 536-542; b) E. Condon, *Phys. Rev.* **1926**, *28*, 1182-1201.

[4] M. Kasha, *Discuss Faraday Soc* **1950**, *9*, 14-19.

[5] N. A. Romero, D. A. Nicewicz, *Chem. Rev.* **2016**, *116*, 10075-10166.

[6] H. G. Roth, N. A. Romero, D. A. Nicewicz, *Synlett* **2016**, *27*, 714-723.

[7] a) B. König, *Eur. J. Org. Chem.* **2017**, *2017*, 1979-1981; b) G. E. M. Crisenza, P. Melchiorre, *Nat. Commun.* **2020**, *11*, 803; c) T. P. Nicholls, D. Leonori, A. C. Bissember, *Nat. Prod. Rep.* **2016**, *33*, 1248-1254; d) J. J. Douglas, M. J. Sevrin, C. R. J. Stephenson, *Org. Process Res. Dev.* **2016**, *20*, 1134-1147; e) R. C. McAtee, E. J. McClain, C. R. J. Stephenson, *Trends Chem.* **2019**, *1*, 111-125; f) D. Petzold, M. Giedyk, A. Chatterjee, B. König, *Eur. J. Org. Chem.* **2020**, *2020*, 1193-1244.

[8] a) E. Speckmeier, T. G. Fischer, K. Zeitler, *J. Am. Chem. Soc.* **2018**, *140*, 15353-15365; b) Y. Lee, M. S. Kwon, *Eur. J. Org. Chem.* **2020**, *2020*, 6028-6043.

[9] J.-H. Shon, T. S. Teets, *Comments Inorg. Chem.* **2020**, *40*, 53-85.

[10] C. K. Prier, D. A. Rankic, D. W. C. MacMillan, *Chem. Rev.* **2013**, *113*, 5322-5363.

[11] M. Sako, K. Shimada, K. Hirota, Y. Maki, *J. Am. Chem. Soc.* **1986**, *108*, 6039 - 6041.

[12] a) M. Sako, S. Ohara, K. Hirota, Y. Maki, *J. Chem. Soc., Perkin Trans. 1* **1990**, 3339-3344; b) M. Sako, K. Hirota, Y. Maki, *Chem. Pharm. Bull.* **1990**, *38*, 2069-2071; c) M. Sako, S. Ohara, K. Shimada, K. Hirota, Y. Maki, *J. Chem. Soc., Perkin Trans. 1* **1990**, 863-868.

[13] a) M. Sako, K. Shimada, K. Hirota, Y. Maki, *Tetrahedron Lett.* **1986**, *27*, 3877-3880; b) Y. Maki, M. Sako, I. Oyabu, T. Murase, Y. Kitade, K. Hirota, *J. Chem. Soc., Chem. Commun.* **1989**, 1780-1782; c) Y. Maki, I. Oyabu, S. Ohara, M. Sako, Y. Kitade, K. Hirota, *Chem. Pharm. Bull.* **1989**, *37*, 3239-3242.

[14] A. Petrosyan, R. Hauptmann, J. Pospech, *Eur. J. Org. Chem.* **2018**, *2018*, 5237-5252.

[15] R. Hauptmann, A. Petrosyan, F. Fennel, M. A. Argüello Cordero, A.-E. Surkus, J. Pospech, *Chem. Eur. J.* **2019**, *25*, 4325-4329.

[16] a) F. El-Hage, C. Schöll, J. Pospech, *J. Org. Chem.* **2020**, *85*, 13853-13867; b) T. Taeufer, R. Hauptmann, F. El-Hage, T. S. Mayer, H. Jiao, J. Rabeah, J. Pospech, *ACS Catal.* **2021**, *11*, 4862-4869.

[17] a) D. H. Waldeck, *Chem. Rev.* **1991**, *91*, 415-436; b) N. Minezawa, M. S. Gordon, *J. Phys. Chem. A* **2011**, *115*, 7901-7911.

[18] D. J. Pietrzyk, C. W. Frank, in *Anal. Chem.* (Eds.: D. J. Pietrzyk, C. W. Frank), Academic Press, **1979**, pp. 410-424.

[19] L. O'Neill, H. J. Byrne, *J. Phys. Chem. B* **2005**, *109*, 12685-12690.

[20] E. V. Anslyn, D. A. Dougherty, *Modern physical organic chemistry*, University Science Books, Sausalito, CA, **2005**.

[21] V. V. Pavlishchuk, A. W. Addison, *Inorg. Chim. Acta* **2000**, *298*, 97-102.

[22] Z. Stojek, in *Electroanalytical Methods: Guide to Experiments and Applications* (Ed.: F. Scholz), Springer, **2010**, p. 107.

[23] T. Morack, J. B. Metternich, R. Gilmour, *Org. Lett.* **2018**, *20*, 1316-1319.

[24] F. El-Hage, Dissertation thesis, University of Rostock (Rostock), **2021**.

[25] M. F. Roberts, M. Wink, *Alkaloids : Biochemistry, Ecology, and Medicinal Applications*, Springer US, Boston, MA, **1998**.

[26] C. F. Valenzuela, M. P. Puglia, S. Zucca, *Alcohol research & health : the journal of the National Institute on Alcohol Abuse and Alcoholism* **2011**, *34*, 106-120.

[27] a) E. Symvoulakis, D. Anyfantakis, C. Lionis, *Sao Paulo Med. J.* **2010**, *128*, 167; b) S. P. Cass, *Curr. Sports Med. Rep.* **2017**, *16*.

[28] a) F. D. Lewis, *Acc. Chem. Res.* **1979**, *12*, 152-158; b) J. W. Beatty, C. R. J. Stephenson, *Acc. Chem. Res.* **2015**, *48*, 1474-1484; c) D. Menigaux, P. Belmont, E. Brachet, *Eur. J. Org. Chem.* **2017**, *2017*, 2008-2055; d) I. K. Sideri, E. Voutyritsa, C. G. Kokotos, *Org. Biomol. Chem.* **2018**, *16*, 4596-4614.

[29] B. M. Trost, W. Tang, *J. Am. Chem. Soc.* **2002**, *124*, 14542-14543.

[30] a) S. Z. Zard, *Chem. Soc. Rev.* **2008**, *37*, 1603-1618; b) T. M. Nguyen, D. A. Nicewicz, *J. Am. Chem. Soc.* **2013**, *135*, 9588-9591; cJ.-R. Chen, X.-Q. Hu, L.-Q. Lu, W.-J. Xiao, *Chem. Soc. Rev.* **2016**, *45*, 2044-2056; dT. Xiong, Q. Zhang, *Chem. Soc. Rev.* **2016**, *45*, 3069-3087; eM. D. Kärkäs, *ACS Catal.* **2017**, *7*, 4999-5022; fY.-T. He, D. Kang, I. Kim, S. Hong, *Green Chem.* **2018**, *20*, 5209-5214; gQ. Guo, Q. Peng, H. Chai, Y. Huo, S. Wang, Z. Xu, *Nat. Commun.* **2020**, *11*, 1463; hJ. M. Ganley, P. R. D. Murray, R. R. Knowles, *ACS Catal.* **2020**, *10*, 11712-11738.

[31] S. Yasui, M. Tsujimoto, K. Itoh, A. Ohno, *J. Org. Chem.* **2000**, *65*, 4715-4720.

[32] J. L. Bourdelande, I. Gallardo, G. Guirado, *J. Am. Chem. Soc.* **2007**, *129*, 2817-2821.

[33] A. M. d. P. Nicholas, D. R. Arnold, *Can. J. Chem.* **1982**, *60*, 2165-2179.

[34] a) A. J. Musacchio, B. C. Lainhart, X. Zhang, S. G. Naguib, T. C. Sherwood, R. R. Knowles, *Science* **2017**, *355*, 727-730; b) Q. Zhu, D. E. Graff, R. R. Knowles, *J. Am. Chem. Soc.* **2018**, *140*, 741-747; c) D. C. Miller, J. M. Ganley, A. J. Musacchio, T. C. Sherwood, W. R. Ewing, R. R. Knowles, *J. Am. Chem. Soc.* **2019**, *141*, 16590-16594.

[35] D. D. M. Wayner, D. J. McPhee, D. Griller, *J. Am. Chem. Soc.* **1988**, *110*, 132-137.

[36] a) K. A. Margrey, D. A. Nicewicz, *Acc. Chem. Res.* **2016**, *49*, 1997-2006; b) J. Guin, C. Mück-Lichtenfeld, S. Grimme, A. Studer, *J. Am. Chem. Soc.* **2007**, *129*, 4498-4503; c) D. C. Miller, G. J. Choi, H. S. Orbe, R. R. Knowles, *J. Am. Chem. Soc.* **2015**, *137*, 13492-13495; d) J. M. Mayer, D. A. Hrovat, J. L. Thomas, W. T. Borden, *J. Am. Chem. Soc.* **2002**, *124*, 11142-11147; e) J. M. Mayer, *Acc. Chem. Res.* **2011**, *44*, 36-46; f) L. Capaldo, D. Ravelli, *Eur. J. Org. Chem.* **2017**, *2017*, 2056-2071.

[37] a) T. M. Nguyen, N. Manohar, D. A. Nicewicz, *Angew. Chem. Int. Ed.* **2014**, *53*, 6198-6201; b) J. B. McManus, N. P. R. Onuska, D. A. Nicewicz, *J. Am. Chem. Soc.* **2018**, *140*, 9056-9060.

[38] P. D. Morse, T. M. Nguyen, C. L. Cruz, D. A. Nicewicz, *Tetrahedron* **2018**, *74*, 3266-3272.

[39] a) Y. Lei, L. Yu, M. Shen, S. Luo, Z. Gao, *New J. Chem.* **2019**, *43*, 15700-15705; b) H. Jiang, A. Studer, *Chem. Eur. J.* **2019**, *25*, 7105-7109.

[40] M. Yasuda, T. Yamashita, K. Shima, C. Pac, *J. Org. Chem.* **1987**, *52*, 753-759.

[41] a) M. Yasuda, T. Isami, J. Kubo, M. Mizutani, T. Yamashita, K. Shima, *J. Org. Chem.* **1992**, *57*, 1351-1354; b) M. Yasuda, K. Shiomori, S. Hamasuna, K. Shima, T. Yamashita, *J. Chem. Soc., Perkin Trans.* **1992**, 305-310; c) T. Yamashita, M. Yasuda, T. Isami, K. Tanabe, K. Shima, *Tetrahedron* **1994**, *50*, 9275-9286; d) M. Yasuda, Y. Watanabe, K. Tanabe, K. Shima, *J. Photochem. Photobiol. A* **1994**, *79*, 61-65.
[42] M. Yasuda, Y. Matsuzaki, K. Shima, C. Pac, *Journal of the Chemical Society, Perkin Transactions 2* **1988**, 745-751.
[43] a) O. Stern, M. Volmer, *Z. Phys.* **1919**, *20*, 183-188; b) A. Y. Moon, D. C. Poland, H. A. Scheraga, *J. Phys. Chem. A* **1965**, *69*, 2960-2966.
[44] M. J. Frisch, G. W. Trucks, H. B. Schlegel, G. E. Scuseria, M. A. Robb, J. R. Cheeseman, G. Scalmani, V. Barone, G. A. Petersson, H. Nakatsuji, X. Li, M. Caricato, A. V. Marenich, J. Bloino, B. G. Janesko, R. Gomperts, B. Mennucci, H. P. Hratchian, J. V. Ortiz, A. F. Izmaylov, J. L. Sonnenberg, Williams, F. Ding, F. Lipparini, F. Egidi, J. Goings, B. Peng, A. Petrone, T. Henderson, D. Ranasinghe, V. G. Zakrzewski, J. Gao, N. Rega, G. Zheng, W. Liang, M. Hada, M. Ehara, K. Toyota, R. Fukuda, J. Hasegawa, M. Ishida, T. Nakajima, Y. Honda, O. Kitao, H. Nakai, T. Vreven, K. Throssell, J. A. Montgomery Jr., J. E. Peralta, F. Ogliaro, M. J. Bearpark, J. J. Heyd, E. N. Brothers, K. N. Kudin, V. N. Staroverov, T. A. Keith, R. Kobayashi, J. Normand, K. Raghavachari, A. P. Rendell, J. C. Burant, S. S. Iyengar, J. Tomasi, M. Cossi, J. M. Millam, M. Klene, C. Adamo, R. Cammi, J. W. Ochterski, R. L. Martin, K. Morokuma, O. Farkas, J. B. Foresman, D. J. Fox, Wallingford, CT, **2016**.
[45] A. D. Becke, *J. Chem. Phys.* **1993**, *98*, 5648-5652.
[46] A. Schäfer, C. Huber, R. Ahlrichs, *J. Chem. Phys.* **1994**, *100*, 5829-5835.
[47] A. V. Marenich, C. J. Cramer, D. G. Truhlar, *J. Phys. Chem. B* **2009**, *113*, 6378-6396.
[48] S. Grimme, S. Ehrlich, L. Goerigk, *J. Comput. Chem.* **2011**, *32*, 1456-1465.
[49] a) R. Lesclaux, P. V. Khê, P. Dezauzier, J. C. Soulignac, *Chem. Phys. Lett.* **1975**, *35*, 493-497; b) K. Pham Van, J. C. Soulignac, R. Lesclaux, *J. Phys. Chem. A* **1977**, *81*, 210-214; c) P. Neta, P. Maruthamuthu, P. M. Carton, R. W. Fessenden, *The Journal of Physical Chemistry* **1978**, *82*, 1875-1878.
[50] A. Adenier, M. M. Chehimi, I. Gallardo, J. Pinson, N. Vilà, *Langmuir* **2004**, *20*, 8243-8253.
[51] R. Hauptmann, Dissertation thesis, University of Rostock (Rostock), **2020**.
[52] a) D. D. M. Wayner, J. J. Dannenberg, D. Griller, *Chem. Phys. Lett.* **1986**, *131*, 189-191; b) O. Kei, N. Takashi, F. Shunichi, *Bull. Chem. Soc. Jpn.* **2006**, *79*, 1489-1500.
[53] J. Hioe, D. Šakić, V. Vrček, H. Zipse, *Org. Biomol. Chem.* **2015**, *13*, 157-169.
[54] a) V. H. Parker, J. M. Barnes, F. A. Denz, *Br. J. Ind. Med.* **1951**, *8*, 226; b) J. Cramer, C. P. Sager, B. Ernst, *J. Med. Chem.* **2019**, *62*, 8915-8930.
[55] E. G. Hrycay, S. M. Bandiera, *Monooxygenase, Peroxidase and Peroxygenase Properties and Mechanisms of Cytochrome P450*, Springer International Publishing, Switzerland, **2015**.
[56] Copyright granted by Dr. Jola Pospech.
[57] J. T. Groves, *J. Inorg. Biochem.* **2006**, *100*, 434-447.
[58] T. Peschke, P. Bitterwolf, S. Hansen, J. Gasmi, K. S. Rabe, C. M. Niemeyer, *Catalysts* **2019**, *9*, 164.
[59] R. Irie, *Comprehensive Chirality, Vol. 5*, Elsevier

2012.

[60] C. Yuan, Y. Liang, T. Hernandez, A. Berriochoa, K. N. Houk, D. Siegel, *Nature* **2013**, *499*, 192-196.
[61] a) L. Zou, R. S. Paton, A. Eschenmoser, T. R. Newhouse, P. S. Baran, K. N. Houk, *J. Org. Chem.* **2013**, *78*, 4037-4048; b) K. Chen, P. S. Baran, *Nature* **2009**, *459*, 824-828; c) P. A. Wender, M. K. Hilinski, A. V. W. Mayweg, *Org. Lett.* **2005**, *7*, 79-82.
[62] a) D. D. DesMarteau, A. Donadelli, V. Montanari, V. A. Petrov, G. Resnati, *J. Am. Chem. Soc.* **1993**, *115*, 4897-4898; b) D. D. DesMarteau, V. A. Petrov, V. Montanari, M. Pregnolato, G. Resnati, *J. Fluorine Chem.* **1992**, *58*, 339; c) H. Mikula, D. Svatunek, D. Lumpi, F. Glöcklhofer, C. Hametner, J. Fröhlich, *Org. Process Res. Dev.* **2013**, *17*, 313-316.

[63] S. L. Rössler, B. J. Jelier, E. Magnier, G. Dagousset, E. M. Carreira, A. Togni, *Angew. Chem. Int. Ed.* **2020**, *59*, 9264-9280.
[64] H. Strub, C. Strehler, J. Streith, *Chem. Ber.* **1987**, *120*, 355-363.
[65] a) Y. Ogawa, S. Iwasaki, S. Okuda, *Tetrahedron Lett.* **1981**, *22*, 2277-2280; b) H. J. Xu, S. Q. Lin, S. Y. Shen, L. Li, D. W. Chen, G. Z. Xu, *J. Photochem. Photobiol. A* **1989**, *48*, 53-59.
[66] Copyright granted by Dr. Jola Pospech.
[67] F. A. Souto-Bachiller, E. Perez-Inestrosa, R. Suau, R. Rico-Gómez, L. A. Rodríguez-Rodríguez, M. E. Coronado-Pérez, *Photochem. Photobiol.* **1999**, *70*, 875-881.
[68] D. Collado, E. Perez-Inestrosa, R. Suau, *J. Org. Chem.* **2003**, *68*, 3574-3584.
[69] F.-S. He, S. Ye, J. Wu, *ACS Catal.* **2019**, *9*, 8943-8960.
[70] E. D. Lorance, I. R. Gould, *J. Phys. Chem. A* **2005**, *109*, 2912-2919.
[71] S. L. Rössler, B. J. Jelier, P. F. Tripet, A. Shemet, G. Jeschke, A. Togni, E. M. Carreira, *Angew. Chem. Int. Ed.* **2019**, *58*, 526-531.
[72] Joel W. Beatty, James J. Douglas, R. Miller, Rory C. McAtee, Kevin P. Cole, Corey R. J. Stephenson, *Chem* **2016**, *1*, 456-472.
[73] J. Börgel, L. Tanwar, F. Berger, T. Ritter, *J. Am. Chem. Soc.* **2018**, *140*, 16026-16031.
[74] L. Tanwar, J. Börgel, T. Ritter, *J. Am. Chem. Soc.* **2019**, *141*, 17983-17988.
[75] a) S. N. K. J. J. Mousseau, in *Encyclopedia of Reagents for Organic Synthesis*, **2015**, pp. 1-6; b) A. Albini, S. Pietra, *Heterocyclic N-Oxides*, **2019**; cJ. A. Bull, J. J. Mousseau, G. Pelletier, A. B. Charette, *Chem. Rev.* **2012**, *112*, 2642-2713.
[76] C. Copéret, H. Adolfsson, T.-A. V. Khuong, A. K. Yudin, K. B. Sharpless, *J. Org. Chem.* **1998**, *63*, 1740-1741.
[77] J. F. Christen, Master thesis, University of Rostock (Rostock), **2020**.
[78] J. I. Murray, A. C. Spivey, *Adv. Synth. Catal.* **2015**, *357*, 3825-3830.
[79] H. J. Park, J. N. Kim, H.-J. Yoo, K.-R. Wee, S. O. Kang, D. W. Cho, U. C. Yoon, *J. Org. Chem.* **2013**, *78*, 8054-8064.
[80] Adapted from Mario Frahm's master thesis.
[81] X. Lu, X.-X. Li, Y.-M. Lee, Y. Jang, M. S. Seo, S. Hong, K.-B. Cho, S. Fukuzumi, W. Nam, *J. Am. Chem. Soc.* **2020**, *142*, 3891-3904.
[82] a) W. S. Ham, J. Hillenbrand, J. Jacq, C. Genicot, T. Ritter, *Angew. Chem. Int. Ed.* **2019**, *58*, 532-536; b) I. Kim, B. Park, G. Kang, J. Kim, H. Jung, H. Lee, M.-H. Baik, S. Hong, *Angew. Chem. Int. Ed.* **2018**, *57*, 15517-15522.
[83] J. W. Beatty, J. J. Douglas, K. P. Cole, C. R. J. Stephenson, *Nat. Commun.* **2015**, *6*, 7919.
[84] M. B. Majewski, J. G. Smith, M. O. Wolf, B. O. Patrick, *Eur. J. Inorg. Chem.* **2016**, *2016*, 1470-1479.
[85] A. W. V. Hofmann, J. Clark, *Philos. Trans. R. Soc. London* **1850**, *140*, 93-131.
[86] M. S. Donovan, A. B. Lowe, B. S. Sumerlin, C. L. McCormick, *Macromolecules* **2002**, *35*, 4123-4132.
[87] T. a. M. Gessner, U., in *Ullmann's Encyclopedia of Industrial Chemistry, (Ed.)*. **2000**.
[88] a) X. Hu, D. Martin, M. Melaimi, G. Bertrand, *J. Am. Chem. Soc.* **2014**, *136*, 13594-13597; b) G. Song, G. Luo, J. Oyamada, Y. Luo, Z. Hou, *Chem.* **2016**, *7*, 5265-5270; c) T. S. Bush, G. P. A. Yap, W. J. Chain, *Org. Lett.* **2018**, *20*, 5406-5409; d) R. S. Lewis, M. F. Wisthoff, J. Grissmerson, W. J. Chain, *Org. Lett.* **2014**, *16*, 3832-3835; e) C. Monnereau, E. Blart, F. Odobel, *Tetrahedron Lett.* **2005**, *46*, 5421-5423.
[89] a) Z. Li, C.-J. Li, *J. Am. Chem. Soc.* **2004**, *126*, 11810-11811; b) A. K. Yadav, L. D. S. Yadav, *Tetrahedron Lett.* **2017**, *58*, 552-555.
[90] Z.-C. Cao, S.-J. Xie, H. Fang, Z.-J. Shi, *J. Am. Chem. Soc.* **2018**, *140*, 13575-13579.
[91] R. N. Gaykar, A. Guin, S. Bhattacharjee, A. T. Biju, *Org. Lett.* **2019**, *21*, 9613-9617.
[92] W. Eschweiler, *Ber. Dtsch. Chem. Ges* **1905**, *38*, 880-882.
[93] M. M. Heravi, Z. Kheilkordi, V. Zadsirjan, M. Heydari, M. Malmir, *J. Organomet. Chem.* **2018**, *861*, 17-104.
[94] a) M. J. Cawley, F. G. N. Cloke, R. J. Fitzmaurice, S. E. Pearson, J. S. Scott, S. Caddick, *Org. Biomol. Chem.* **2008**, *6*, 2820-2825; b) R. Dorel, C. P. Grugel, A. M.

Haydl, *Angew. Chem. Int. Ed.* **2019**, *58*, 17118-17129; c) P. Ruiz-Castillo, S. L. Buchwald, *Chem. Rev.* **2016**, *116*, 12564-12649.
[95] a) Y. Ohtsuka, T. Yamamoto, T. Miyazaki, T. Yamakawa, *Adv. Synth. Catal.* **2018**, *360*, 1007-1018; b) S. Tasler, J. Mies, M. Lang, *Adv. Synth. Catal.* **2007**, *349*, 2286-2300.
[96] a) F. Paul, J. Patt, J. F. Hartwig, *J. Am. Chem. Soc.* **1994**, *116*, 5969-5970; b) A. S. Guram, S. L. Buchwald, *J. Am. Chem. Soc.* **1994**, *116*, 7901-7902.
[97] R. Martin, S. L. Buchwald, *Acc. Chem. Res.* **2008**, *41*, 1461-1473.
[98] U. Christmann, R. Vilar, *Angew. Chem. Int. Ed.* **2005**, *44*, 366-374.
[99] a) F. Barrios-Landeros, J. F. Hartwig, *J. Am. Chem. Soc.* **2005**, *127*, 6944-6945; b) J. F. Hartwig, F. Paul, *J. Am. Chem. Soc.* **1995**, *117*, 5373-5374.
[100] E. R. Strieter, S. L. Buchwald, *Angew. Chem. Int. Ed.* **2006**, *45*, 925-928.
[101] J. J. Li, Z. Wang, L. H. Mitchell, *J. Org. Chem.* **2007**, *72*, 3606-3607.
[102] B. K. Lee, M. R. Biscoe, S. L. Buchwald, *Tetrahedron Lett.* **2009**, *50*, 3672-3674.
[103] a) U. Schön, J. Messinger, M. Buchholz, U. Reinecker, H. Thole, M. K. S. Prabhu, A. Konda, *Tetrahedron Lett.* **2005**, *46*, 7111-7115; b) R. J. Lundgren, A. Sappong-Kumankumah, M. Stradiotto, *Chem. Eur. J.* **2010**, *16*, 1983-1991.
[104] J. Barluenga, M. A. Fernández, F. Aznar, C. Valdés, *Chem. Eur. J.* **2004**, *10*, 494-507.
[105] M. C. Willis, G. N. Brace, *Tetrahedron Lett.* **2002**, *43*, 9085-9088.
[106] M. Moir, J. J. Danon, T. A. Reekie, M. Kassiou, *Expert Opinion on Drug Discovery* **2019**, *14*, 1137-1149.
[107] D. E. Frantz, D. G. Weaver, J. P. Carey, M. H. Kress, U. H. Dolling, *Org. Lett.* **2002**, *4*, 4717-4718.
[108] D. S. Surry, S. L. Buchwald, *Angew. Chem. Int. Ed.* **2008**, *47*, 6338-6361.
[109] A. L. S. Thompson, G. W. Kabalka, M. R. Akula, J. W. Huffman, *Synthesis* **2005**, *2005*, 547-550.
[110] a) P. Frei, D. H. Jones, S. T. Kay, J. A. McLellan, B. F. Johnston, A. R. Kennedy, N. C. O. Tomkinson, *J. Org. Chem.* **2018**, *83*, 1510-1517; b) S. Duric, C. C. Tzschucke, *Org. Lett.* **2011**, *13*, 2310-2313.
[111] Z.-W. Zhang, H.-B. Li, J. Li, C.-C. Wang, J. Feng, Y.-H. Yang, S. Liu, *J. Org. Chem.* **2020**, *85*, 537-547.
[112] Z. Zhou, G. Dai, S. Ru, H. Yu, Y. Wei, *Dalton Trans.* **2019**, *48*, 14201-14205.
[113] A. Gini, M. Uygur, T. Rigotti, J. Alemán, O. García Mancheño, *Chem. Eur. J.* **2018**, *24*, 12509-12514.
[114] E. Le Gall, C. Haurena, S. Sengmany, T. Martens, M. Troupel, *J. Org. Chem.* **2009**, *74*, 7970-7973.
[115] M. A. Argüello Cordero, Master‘s Thesis 2018, University of Rostock, Germany.
[116] H. P. Kokatla, P. F. Thomson, S. Bae, V. R. Doddi, M. K. Lakshman, *J. Org. Chem.* **2011**, *76*, 7842-7848.
[117] X. Ma, H. Dang, J. A. Rose, P. Rablen, S. B. Herzon, *J. Am. Chem. Soc.* **2017**, *139*, 5998-6007.
[118] C. S. Sevov, R. E. M. Brooner, E. Chénard, R. S. Assary, J. S. Moore, J. Rodríguez-López, M. S. Sanford, *J. Am. Chem. Soc.* **2015**, *137*, 14465-14472.
[119] J. I. Murray, R. Woscholski, A. C. Spivey, *Chem. Commun.* **2014**, *50*, 13608-13611.
[120] C. B. Aakeröy, K. Epa, S. Forbes, N. Schultheiss, J. Desper, *Chem. Eur. J.* **2013**, *19*, 14998-15003.
[121] R. Puttreddy, N. K. Beyeh, S. M. Taimoory, D. Meister, J. F. Trant, K. Rissanen, *Beilstein J. Org. Chem.* **2018**, *14*, 1723-1733.
[122] Y. Yamamoto, T. Tanaka, M. Yagi, M. Inamoto, *ChemInform* **1996**, *27*.
[123] G. A. Tolstikov, U. M. Dzhemilev, V. P. Yur'ev, M. G. Gaisina, *Chemistry of Heterocyclic Compounds* **1971**, *7*, 945-945.
[124] J. Peng, J. H. Docherty, A. P. Dominey, S. P. Thomas, *Chem. Commun.* **2017**, *53*, 4726-4729.
[125] A. Pannwitz, A. Prescimone, O. S. Wenger, *Eur. J. Inorg. Chem.* **2017**, 609-615.
[126] J.-P. Leclerc, K. Fagnou, *Angew. Chem. Int. Ed.* **2006**, *45*, 7781-7786.
[127] R. A. Aitken, B. Fodi, M. H. Palmer, A. M. Z. Slawin, J. Yang, *Tetrahedron* **2012**, *68*, 5845-5851.

[128] G. Bertuzzi, D. Pecorari, L. Bernardi, M. Fochi, *Chem. Commun.* **2018**, *54*, 3977-3980.
[129] J. Nasielski, S. Heilporn, E. Chauveheid, K. Poppe, R. Nasielski-Hinkens, *Bull. Soc. Chim. Belg.* **1990**, *99*, 783-788.
[130] J. Sheng, R. He, J. Xue, C. Wu, J. Qiao, C. Chen, *Org. Lett.* **2018**, *20*, 4458-4461.
[131] H. P. Siǵǵ, A. Toth, *Helv. Chim. Acta* **1967**, *50*, 716-719.
[132] M. Presset, J. Paul, G. N. Cherif, N. Ratnam, N. Laloi, E. Léonel, C. Gosmini, E. Le Gall, *Chem. Eur. J.* **2019**, *25*, 4491-4495.
[133] R.-D. He, C.-L. Li, Q.-Q. Pan, P. Guo, X.-Y. Liu, X.-Z. Shu, *J. Am. Chem. Soc.* **2019**, *141*, 12481-12486.
[134] (Eds.: G. Dentsply Detrey, F. Szillat, C. Renn, C. Scheufler, J. r. Brenneisen), **2019**.
[135] Q. Wu, S. Han, X. Ren, H. Lu, J. Li, D. Zou, Y. Wu, Y. Wu, *Org. Lett.* **2018**, *20*, 6345-6348.
[136] H. A. Patel, M. Rawat, A. L. Patel, A. V. Bedekar, *Appl. Organomet. Chem.* **2019**, *33*, e4767.
[137] H. Wang, Y. Huang, X. Dai, F. Shi, *Chem. Commun.* **2017**, *53*, 5542-5545.
[138] L. A. Smyth, E. M. Phillips, V. S. Chan, J. G. Napolitano, R. Henry, S. Shekhar, *J. Org. Chem.* **2016**, *81*, 1285-1294.
[139] P. J. A. Joseph, S. Priyadarshini, M. L. Kantam, B. Sreedhar, *Tetrahcdron* **2013**, *69*, 8276-8283.
[140] L. Zhu, L.-S. Wang, B. Li, W. Li, B. Fu, *Catal. Sci. Technol.* **2016**, *6*, 6172-6176.
[141] H. Huang, Y. Wu, W. Zhang, C. Feng, B.-Q. Wang, W.-F. Cai, P. Hu, K.-Q. Zhao, S.-K. Xiang, *J. Org. Chem.* **2017**, *82*, 3094-3101.
[142] D. Rosas Vargas, S. P. Cook, *Tetrahcdron* **2018**, *74*, 3314-3317.
[143] T. Jin, F. Yang, Y. Yamamoto, *Org. Lett.* **2010**, *12*, 388-390.
[144] Y. Iyori, K. Takahashi, K. Yamazaki, Y. Ano, N. Chatani, *Chem. Commun.* **2019**, *55*, 13610-13613.
[145] I. Kalvet, G. Magnin, F. Schoenebeck, *Angew. Chem. Int. Ed.* **2017**, *56*, 1581-1585.
[146] C. Santilli, S. S. Beigbaghlou, A. Ahlburg, G. Antonacci, P. Fristrup, P.-O. Norrby, R. Madsen, *Eur. J. Org. Chem.* **2017**, *2017*, 5269-5274.
[147] K. Natte, A. Dumrath, H. Neumann, M. Beller, *Angew. Chem. Int. Ed.* **2014**, *53*, 10090-10094.
[148] X. Shen, A. M. Hyde, S. L. Buchwald, *J. Am. Chem. Soc.* **2010**, *132*, 14076-14078.
[149] S. M. King, S. L. Buchwald, *Org. Lett.* **2016**, *18*, 4128-4131.
[150] S. Conte, G. G. Rodríguez-Calero, S. E. Burkhardt, M. A. Lowe, H. D. Abruña, *RSC Advances* **2013**, *3*, 1957-1964.
[151] E. V. Vinogradova, N. H. Park, B. P. Fors, S. L. Buchwald, *Org. Lett.* **2013**, *15*, 1394-1397.
[152] Y. Duan, J.-H. Lin, J.-C. Xiao, Y.-C. Gu, *Org. Lett.* **2016**, *18*, 2471-2474.
[153] Q. Hu Thomas, R. Cairns Graham, R. James Brian, in *Holzforschung, Vol. 54*, **2000**, p. 127.
[154] T. Si, B. Li, W. Xiong, B. Xu, W. Tang, *Org. Biomol. Chem.* **2017**, *15*, 9903-9909.
[155] A. Sutter, M. Elhabiri, G. Ulrich, *Chem. Eur. J.* **2018**, *24*, 11119-11130.
[156] S. Onodera, T. Kochi, F. Kakiuchi, *J. Org. Chem.* **2019**, *84*, 6508-6515.
[157] D. Wang, D. Kuang, F. Zhang, C. Yang, X. Zhu, *Adv. Synth. Catal.* **2015**, *357*, 714 - 718.
[158] H. Reed, T. R. Paul, W. J. Chain, *J. Org. Chem.* **2018**, *83*, 11359-11368.
[159] K. Kamikawa, S. Sugimoto, M. Uemura, *J. Org. Chem.* **1998**, *63*, 8407-8410.
[160] P. Y. Choy, K. H. Chung, Q. Yang, C. M. So, R. W.-Y. Sun, F. Y. Kwong, *Chem. Asian J.* **2018**, *13*, 2465-2474.
[161] A. Cho, S. Byun, B. M. Kim, *Adv. Synth. Catal.* **2018**, *360*, 1253-1261.
[162] P. Weber, T. Scherpf, I. Rodstein, D. Lichte, L. T. Scharf, L. J. Gooßen, V. H. Gessner, *Angew. Chem. Int. Ed.* **2019**, *58*, 3203-3207.
[163] N. Purkait, G. Kervefors, E. Linde, B. Olofsson, *Angew. Chem. Int. Ed.* **2018**, *57*, 11427-11431.
[164] K. Liu, H.-J. Jiang, N. Li, H. Li, J. Wang, Z.-Z. Zhang, J. Yu, *J. Org. Chem.* **2018**, *83*, 6815-6823.

[165] F. Du, Q. Zhou, Y. Fu, H. Zhao, Y. Chen, G. Chen, *New J. Chem.* **2019**, *43*, 6549-6554.
[166] H. Wang, D. Liu, H. Chen, J. Li, D. Z. Wang, *Tetrahcdron* **2015**, *71*, 7073-7076.